

Anatomical and Physiological Connectivity of the Basal Ganglia-Thalamocortical Motor Circuit

Doctor of Philosophy (D.Phil.) Thesis
Hilary Term, 2021

Naomi Berry
Wolfson College

MRC Brain Network Dynamics Unit
Nuffield Department of Clinical Neurosciences
University of Oxford
Oxford, UK

Abstract

Anatomical and Physiological Connectivity of the Basal Ganglia-Thalamocortical Motor Circuit

Naomi Berry, Wolfson College

Thesis submitted for the degree of Doctor of Philosophy, Hilary Term, 2021

The motor thalamus is a crucial component of the mammalian motor circuit which links subcortical sensorimotor inputs with cortical regions to facilitate ongoing control of movement and behaviour. Thalamocortical neurons from basal ganglia-recipient thalamus (BZ) and cerebellar-recipient thalamus (CZ) preferentially target different layers of motor cortex in rodents. Higher order BZ, comprised of ventral anterior (VA) and ventral medial (VM) thalamic nuclei innervate layer 1 (L1) of frontal cortical areas including motor cortex, and first order CZ, formed of ventral lateral thalamus (VL), innervates deeper layers. The prevailing assumption has been that pyramidal apical tuft dendrites are the exclusive postsynaptic target of BZ axons in L1. However, recent evidence has suggested that L1 elongated neurogliaform cells (ENGCs), which mainly reside in L1a and can be identified by expression of neuron-derived neurotrophic factor (NDNF), are directly targeted by higher order thalamic nuclei in prefrontal cortex and sensory cortical areas.

Here we test the hypothesis that L1 interneurons also receive BZ innervation in motor cortex. Using an NDNF-Cre mouse, we first confirmed with immunohistochemistry that L1 NDNF-expressing (NDNF+) interneurons in motor cortex were GABAergic, and often co-expressed reelin, consistent with being ENGCs. To find out whether these L1 NDNF+ motor cortical interneurons receive direct thalamocortical input, we developed an injection technique to optimise restriction of viral labelling to L1 and demonstrated with monosynaptic retrograde rabies viral tracing that these NDNF+ neurons receive innervation from several thalamic nuclei, especially VM. The same tracing experiments with retinol-binding protein 4 (RBP4)-Cre mice reveal a greater proportion of VL innervation of L5 pyramidal neurons compared with VM. These results suggest that motor thalamus differs not only in its laminar innervation of cortex, but also of its neuronal targets. To explore the physiological influence of ENGCs on the VM thalamocortical pathway in motor cortex, we recorded from both motor cortex and VM in awake mice while optogenetically stimulating VM and inhibiting L1 NDNF+ neurons. We did not see any significant changes in firing rates of cortical neurons, but there was an increase in cortical synchrony in response to suppressing L1 NDNF+ neurons, especially when combined with an increase in VM firing, indicating that a function of ENGCs in motor cortex may be to regulate VM-evoked cortical synchrony.

In addition to these experiments in mice, we also performed neurochemical parcellation of macaque thalamus. This revealed interesting patterns, including complementary patterns of GAD67 and vGluT2 immunostaining in subnuclei of mediodorsal thalamus.

Acknowledgements

First of all, I would like to thank my primary supervisor, Dr. Andrew Sharott, for his guidance, time and support throughout this project. He has been an excellent mentor who has taught me much scientifically, always with enthusiasm and kindness, for which I am very grateful. I also would like to thank my second supervisor, Dr. Anna Mitchell, for her guidance and input to this project.

I also wish to acknowledge and thank all those who contributed to the work in this thesis: Dr. Rahul Shah, for helping develop injection protocols and developing the head-fixed probe recording experiments, and training me in these techniques, Dr. Colin McNamara for setting up the Intan electronics, Dr. Brook Perry for contributing to the macaque histology and microscopy, Dr. Joram van Rheede for spike-sorting the electrophysiology data and providing code for data analysis. I also thank Jane Westcott and Grace Tennant for animal care, Ben Micklem for microscopy advice, and Lauren Waite, Andreia Madalena, Jess Myatt, and Lisa Conyers for technical support in the lab. In addition, I thank past and present members of the Sharott lab and the wider Unit for their support, advice, and friendship.

Finally, I would like to thank my family, friends, and church, who have all been a constant support and encouragement over many years, and without whom this work would not have been possible.

Table of Contents

Abstract i

Acknowledgements ii

Tables and Figures vii

Abbreviations xi

1 General Introduction

1.1 Thalamus 1

1.1.1 Anatomy of Mammalian Thalamus 1

1.1.2 Anatomy of Motor Thalamus 4

1.1.3 First Order and Higher Order Thalamocortical Circuits 7

1.1.4 Core Physiological Principles of Thalamic Relay Neurons 10

1.2 Basal Ganglia 13

1.2.1 Basal Ganglia Pathways 13

1.2.2 Basal Ganglia Models 16

1.3 Cerebellum 18

1.4 Cortex 20

1.4.1 General Structural Organisation of the Cortex 20

1.4.2 Motor Cortex Divisions 20

1.4.3 Cortical Pyramidal Neurons 21

1.4.4 Cortical Interneurons 24

1.4.5 Cortical L1 Interneurons 29

1.5 Motor thalamocortical circuit 33

1.5.1 Anatomical connectivity of motor thalamocortical neurons 33

1.5.2 Thalamocortical and cortical circuits involving L1 35

1.5.2 Behaviour and motor learning 42

1.6 Aims 45

2 Anatomical connectivity of the mouse thalamocortical circuit

2.1 INTRODUCTION 48

2.1.1 Rodent motor thalamus and thalamocortical connectivity 48

2.1.2 Cortical L1 and elongated neurogliaform cells 52

2.1.3 L5 and cortical output 54

2.1.4 Aims 55

2.2 METHODS 56

2.2.1 Animals 56

2.2.2 Surgery and stereotactic injections 56
2.2.3 Perfusion fixation 57
2.2.4 Histology 57
2.2.5 Microscopy 58
2.2.6 Neurochemical characterisation of L1 NDNF+ neurons 59
2.2.7 Rabies virus tracing of monosynaptic thalamic input to L1 NDNF+ motor cortical neurons 60
2.3 RESULTS 63
2.3.1 NDNF-Cre mouse line preferentially labels L1 cortex 63
2.3.2 Neurochemical characterisation of L1 motor cortical NDNF+ neurons 66
2.3.4 RBP4-Cre mouse line preferentially labels L5 cortex 71
2.3.5 Different thalamic regions preferentially innervate L1 and L5 motor cortical neurons 71
2.4 DISCUSSION 80
2.4.1 Neurochemical characterisation of L1 NDNF+ motor cortical neurons 80
2.4.2 Thalamic innervation of L1 NDNF+ motor cortical neurons 83
2.4.3 Thalamic innervation of L5 RBP4+ motor cortical neurons 85
3 Neurochemical parcellation of the rhesus macaque thalamus
3.1 INTRODUCTION 87
3.1.1 Anatomical and physiological connectivity of primate thalamus 87
3.1.2 Macaque atlases and thalamic nomenclature 88
3.1.3 Immunohistochemical delineation of motor and MD macaque thalamus 92
3.1.4 Aims and justification 95
3.2 METHODS 96
3.2.1 Surgery and tracer injections 96
3.2.2 Tissue Processing 97
3.2.3 Immunohistochemistry 97
3.2.4 Microscopy 99
3.2.5 Fluorescence Intensity Measurements 99
3.3 RESULTS 101
3.3.1 Immunofluorescence labelling in MD 102
3.3.2 Immunofluorescence labelling in VA and VL 107
3.3.3 Immunofluorescence labelling in ATN (AD, AM, AV) and LD 111
3.3.4 Immunofluorescence labelling in other thalamic nuclei 112
3.4 DISCUSSION 113
3.4.1 MD subdivisions and connectivity 113
3.4.2 VA and VL subdivisions and connectivity 114

3.4.3 Significance 115

4 Physiological connectivity of the mouse thalamocortical circuit

4.1 INTRODUCTION 117

4.1.1 VM thalamic input to cortical L1 117

4.1.2 ENGCs in cortical microcircuits 119

4.1.3 Experiment summary 120

4.1.4 Aims 122

4.2 METHODS 122

4.2.1 Animals 122

4.2.2 Surgical procedures 122

4.2.3 *In vivo* optogenetics and probe recordings 124

4.2.4 Perfusion fixation and histology 127

4.2.5 Microscopy 128

4.2.6 Analysis 128

4.3 RESULTS 132

4.3.1 Sustained photostimulation causes modulation of VM thalamic single unit firing rates 132

4.3.2 VM stimulation has little effect on motor cortical single unit firing rates 135

4.3.3 Optogenetic inhibition of L1 NDNF+ neurons partially suppresses motor cortical single unit firing rates with and without VM stimulation 139

4.3.4 Effects of VM stimulation and inhibition of L1 NDNF+ neurons on cortical single unit synchrony 148

4.3.4 Histological verification of injection and probe recording sites 152

4.4 DICSUSSION 153

4.4.1 Firing rates 153

4.4.2 Cortical synchrony 154

4.4.3 Cortical microcircuits and outputs 158

4.4.4 Potential function of L1 NDNF+ neurons 159

5 General Discussion

5.1 Overview 161

5.2 Technical limitations 163

5.3 Function of L1 interneurons in higher order motor thalamocortical circuits 166

5.4 Neurochemical parcellation as a method of nucleus delineation 169

5.5 Translational applications 170

5.5 Outlook 171

5.6 Concluding remarks 174

Supplementary Tables 175

References 1756

Tables and Figures

Table 1.1 Motor thalamic zones and their connectivity in rodent……6

Table 1.2 Some key criteria for identifying drivers and modulators in LGN and cortical L5 drivers……10

Table 2.1 Primary and secondary antibody combinations for each stereology protocol……59

Table 3.1 Variations in nomenclature of select thalamic nuclei and their input structures……90

Table 3.2 Abbreviations of thalamic nuclei according to Paxinos et al., 2000; 2008……91

Table 3.3 Primary and secondary antibodies……98

Table S1 Viruses……175

Table S2 Primary antibodies……176

Table S3 Fluorescent secondary antibodies and stains……177

Figure 1.1 Diagram of motor thalamocortical projections……7

Figure 1.2 Dendritic morphology and long-range axonal projections of cortical excitatory neurons……23

Figure 1.3 Morphology of cortical GABAergic interneurons……30

Figure 2.1 Basal ganglia-recipient motor thalamus mainly innervates L1 cortex……51

Figure 2.2 NDNF-Cre mouse line allows preferential labelling of L1 cortex……65

Figure 2.3 Immunohistochemistry showing L1 specificity of NDNF-Cre mouse line……66

Figure 2.4 NDNF+ neurons in mouse L1 motor cortex mostly co-express COUP-TFII and Reelin……69

Figure 2.5 Most NDNF+ neurons in mouse L1 motor cortex do not express NOS and SOM……69

Figure 2.6 NDNF neurons in mouse L1 motor cortex almost exclusively co-express GAD67, but not VIP and CR……69

Figure 2.7 Distribution of neurochemical markers in L1 NDNF+ motor cortical neurons……70

Figure 2.8 RBP4-Cre mouse line allows preferential labelling of L5 cortex……71

Figure 2.9 Laminar distribution of rabies starter neurons in cortex……73

Figure 2.10 VM thalamocortical neurons innervate L1 NDNF+ motor cortical interneurons……77
Figure 2.11 AM and VA thalamocortical neurons innervate L1 NDNF+ motor cortical interneurons……77
Figure 2.12 VL, CM/PC/CL, VM and Po thalamocortical neurons innervate L5 RBP4+ motor cortical neurons……78
Figure 2.13 CL, Po and VM thalamocortical neurons innervate L5 RBP4+ motor cortical neurons……78
Figure 2.14 Thalamic distribution of monosynaptic inputs to L1 and L5 motor cortical neurons……79
Figure 3.1 Fitting atlas overlay and measuring fluorescence intensity……100
Figure 3.2 Expression profiles of GAD67, vGluT2, PV, CR and CB immunofluorescence at different planes through the rostrocaudal thalamic axis on whole brain coronal sections……102
Figure 3.3 The lateral portion of ventral lateral (VL) thalamus has stronger GAD67 immunostaining than medial VL……104
Figure 3.4 MD has distinct regional GABAergic and subcortical glutamatergic innervation……105
Figure 3.5 MD nuclei have complementary distributions of GAD67 and vGluT2 immunostaining……106
Figure 3.6 MDL has stronger PV immunostaining than other MD nuclei……107
Figure 3.7 Parvalbumin immunostaining is enhanced in the magnocellular portion of ventral anterior thalamus……108
Figure 3.8 GAD67 immunostaining is stronger in the lateral than the medial portion of ventral anterior thalamus……109
Figure 3.9 VA and VL have different distributions of GAD67 and vGluT2 immunostaining……110
Figure 3.10 VAMC and VL have enhanced PV fluorescence within VA and VL……111
Figure 3.11 Distribution of GAD67 and vGluT2 in ATN and LD……112
Figure 4.1 Schematic diagrams of injection and recording sites……127
Figure 4.2 Two example thalamic units with optogenetic stimulation of VM……133

Figure 4.3 Modulation of the firing rates of thalamic single units in response to VM stimulation with and without inhibition of cortical L1 NDNF+ neurons……135
Figure 4.4 Depths of motor cortical units……136
Figure 4.5 Firing rates of single cortical units in one recording session show little response to VM stimulation……137
Figure 4.6 Mean firing rates of all cortical units in an example session during VM stimulation……137
Figure 4.7 Modulation of firing rates of cortical single units in response to VM stimulation……138
Figure 4.8 Relative firing rates of cortical units in response to optogenetic stimulation of VM……139
Figure 4.9 Firing rates of single cortical units display no significant overall change in response to L1 cortical interneuron inhibition……141
Figure 4.10 Mean firing rates of all cortical units in an example session during L1 inhibition……141
Figure 4.11 Modulation of firing rates of cortical single units in response to L1 NDNF+ neurons inhibition……142
Figure 4.12 Relative firing rates of cortical units in response to optogenetic inhibition of L1 NDNF+ ArchT-transfected neurons……143
Figure 4.13 Relative firing rates of cortical units in response to light delivery to opsin-negative GFP-control L1 NDNF+ neurons……144
Figure 4.14 Firing rates of single cortical units in one recording session during optogenetic stimulation of VM and inhibition of L1 cortical NDNF+ neurons……146
Figure 4.15 Mean firing rates of all cortical units in an example session during VM stimulation and L1 NDNF+ IN inhibition……146
Figure 4.16 Modulation of firing rates of cortical single units in response to VM stimulation and L1 inhibition……147
Figure 4.17 Relative firing rates of cortical units in response to optogenetic stimulation of VM and inhibition of L1 NDNF+ neurons……148
Figure 4.18 Synchrony of motor cortical single units in response to optogenetic stimulation of VM and inhibition of cortical L1 NDNF+ neurons……150
Figure 4.19 Unit coupling scores for each optogenetic protocol……151

Figure 4.20 Injection and probe sites in cortex and VM thalamus……152

Abbreviations

	#
5-HT	5-hydroxytryptamine
	A
AAV	adeno-associated virus
ACh	acetylcholine
AD	anterdorsal thalamic nucleus
ALM	anterolateral motor cortex
AM	anteromedial thalamic nucleus
AP	anteroposterior
ArchT	archaerhodopsin from Halorubrum strain TP009
AV	anteroventral thalamic nucleus
	B
bNA2	bursting non-adapting 2
BZ	basal ganglia-recipient zone
	C
CB	calbindin D28K
Cg	cingulate cortex
CGE	caudal ganglionic eminence
ChR2	channelrhodopsin-2
CL	centrolateral thalamic nucleus
CM	central medial thalamic nucleus
COUP-TFII	COUP transcription factor 2
CR	calretinin
CT	corticothalamic
CTIP2	COUP-TF-interacting protein 2
CZ	cerebellar-recipient zone
	D
DAPI	4’,6-diamidino-2-phenylindole
DCN	deep cerebellar nuclei
DLS	dorsolateral striatum
DMS	dorsomedial striatum
DV	dorsoventral
	E
ENGC	elongated neurogliaform cell
EP	entopeduncular nucleus
EPSP	excitatory postsynaptic potential
EZ	excitatory subcortical afferent-dominant zone
	F
FEZF2	FEZ family zinc finger 2
FL	forelimb area
FoxP2	forkhead box protein P2 (N-16)
FrA	frontal association area
	G
GABA	gamma-aminobutyric acid
GAD65	glutamate decarboxylase, 65kDa

GAD67	glutamic acid decarboxylase-67
GAD67	glutamate decarboxylase, 67 kDa
GFP	green fluorescent protein
GPe	globus pallidus, external segment
GPi	globus pallidus, internal segment
	H
HL	hindlimb area
	I
IAM	interanteromedial thalamic nucleus
IN	interneuron
IPSP	inhibitory postsynaptic potential
IS	irregular-spiking
ISI	interspike interval
IT	intratelencephalic
IZ	inhibitory afferent-dominant zone
	L
L1	layer 1
LS	late spiking
LTS	low threshold calcium spike
	M
M1	primary motor cortex
M2	secondary motor cortex
MD	mediodorsal thalamic nucleus
MGE	medial ganglionic eminence
ML	mediolateral
mPFC	medial prefrontal cortex
MSN	medium spiny neuron
MSN	medium spiny neuron
	N
NDNF	neuron-derived neurotrophic factor
Necab1	N-terminal EF-hand calcium binding protein 1
NGF	neurogliaform
NLS	non-late spiking
nNOS	neuronal nitric oxide synthase
NPY	neuropeptide Y
	O
OC	orbital cortex
	P
PBS	phosphate buffered saline
PF	parafasicular
PFC	prefrontal cortex
Po	posterior thalamic nuclear group
PT	pyramidal tract
PV	parvalbumin
	R
RBP4	retinol-binding protein 4
Re	reuniens
Rh	rhomboid

Rt	thalamic reticular nucleus
RV	rabies virus
	S
S1	primary somatosensory cortex
SATB2	special AT-rich sequence-binding protein 2
SBC	single bouquet cell
sCRACM	sub-cellular channelrhodopsin2-assisted circuit mapping
SD	standard deviation
SEM	standard error of the mean
SNc	substantia nigra, pars compacta
SNr	substantia nigra, pars reticulata
SOM	somatostatin
SST	somatostatin
STN	subthalamic nucleus
Sub	submedius thalamic nucleus
	T
TH	tyrosine hydroxylase
TRN	thalamic reticular nucleus
Tx	Triton
	V
V1	primary visual cortex
VA	ventral anterior thalamic nucleus
vGluT1	vesicular glutamate transporter 1
vGluT2	vesicular glutamate transporter 2
VIP	vasoactive intestinal peptide
VL	ventrolateral thalamic nucleus
VM	ventromedial thalamic nucleus
vM1	vibrissal primary motor cortex
VPL	ventral posterolateral thalamic nucleus
VPM	ventral posteromedial thalamic nucleus
vS1	vibrissal primary somatosensory cortex
VTA	ventral tegmental area
	W
WFS1	wolframin

1 General Introduction

1.1 Thalamus

The thalamus is a midline subcortical structure composed of a heterogeneous group of nuclei. A substantial amount of input from other subcortical regions passes through the thalamus before reaching the neocortex. More than just a relay centre, the thalamus is important in controlling the delivery of subcortical sensorimotor input to the cortex, as well as receiving and integrating reciprocal cortical signals. It is also involved in regulating alertness states. There are general principles that are similar across mammalian species as well as notable differences. This introduction will focus on rodent and non-human primate thalamus, as these are the species used in this thesis.

1.1.1 Anatomy of Mammalian Thalamus

The mammalian thalamus is formed from the dorsal and ventral thalamus during development, with dorsal thalamus comprising the main part. All dorsal thalamic nuclei contain excitatory glutamatergic thalamocortical projection neurons, known as relay neurons, which innervate the ipsilateral cortex. Relay neurons from different thalamic nuclei target various cortical areas, with some axons branching to innervate multiple cortical areas or layers, while others are more spatially restricted (Hunnicutt et al., 2014). Most mammalian species have local thalamic inhibitory interneurons, apart from rats and mice which generally lack interneurons within the dorsal thalamus but receive inhibitory afferents from the thalamic reticular nucleus (TRN), similar to other species.

Thalamic nuclei can be segregated based on cytoarchitecture and connectivity. Some of the major dorsal thalamic nuclei and their connectivity are described in brief here. The lateral and

medial parts of the ventral posterior nucleus (VPL and VPM) receive peripheral somatosensory input via the medial lemniscus and send afferents to the somatosensory cortex. Somatosensory input, including whisker-related information in rodents, also travels through the medial posterior nucleus (Po or POm). The medial geniculate nucleus (MGN) receives auditory inputs from the inferior colliculus, and the lateral geniculate nucleus (LGN) receives visual input from the retina. These two thalamic nuclei innervate the auditory and visual cortex, respectively. The pulvinar is involved with visual attention, and its homologue in rodents is known as the lateral posterior nucleus (LP). Anteroventral (AV), anterodorsal (AD), and anteromedial (AM) thalamic nuclei, collectively known as anterior thalamic nuclei (ATN), receive input from the mammillary bodies, and reciprocally innervate retrosplenial and cingulate cortex.

As well as innervating cortex, some thalamic nuclei send significant input to elsewhere in the telencephalon. The intralaminar thalamic nuclei, historically referred to as 'non-specific' nuclei, primarily receive subcortical input from the superior colliculus and strongly innervate striatum along with cortex. The intralaminar thalamus is comprised of the caudal and rostral intralaminar groups. The caudal intralaminar group in primates contains both the central medial nucleus (CM) and parafascicular nucleus (PF), together forming a complex and innervating different regions across the whole striatum, while in rodents PF alone forms the caudal group. The rostral intralaminar group contains CM, paracentral nucleus (PC) and central lateral nucleus (CL) (Groenewegen and Berendse, 1994). Within the caudal intralaminar group in rodents, the lateral PF is analogous to the primate CM and innervates dorsolateral striatum. The rodent medial PF is similar to primate PF, in that it innervates limbic and associative regions of the striatum. CM and PF mainly project to striatum, especially to the striatal matrix, where they target both medium spiny neurons (MSNs) and interneurons,

and send collaterals to the cortex, while other thalamic nuclei project preferentially to the cortex with collaterals to striatum (Smith et al., 2004; Lacey et al., 2007; Smith et al., 2014). Other non-intralaminar nuclei also innervate the striatum: mediodorsal thalamus (MD), pulvinar, lateral and medial Po, ventral motor nuclei, anterior and midline nuclei.

During development, the ventral thalamus mostly forms the thalamic reticular nucleus (TRN or Rt) as well as the ventral lateral geniculate nucleus (vLGN). The TRN is a shell-like structure present in all mammals which migrates from the ventral thalamus during development to border the dorsal thalamus dorsolaterally. It contains GABAergic neurons which innervate the dorsal thalamus, with each TRN neuron generally targeting one thalamic nucleus. However, it has also been shown that axons of single reticular cells occasionally branch to innervate two thalamic nuclei (Pinault et al., 1995). In contrast to other mammalian species, there are no GABAergic interneurons within the mouse or rat thalamus providing intrinsic inhibition, and so the TRN crucially provides the primary source of inhibition to the thalamus in these species, along with extra-thalamic inhibitory afferents. The TRN is topographically organised, with neurons within at least seven functionally distinct sectors projecting to broad thalamic regions, such as sensory or auditory (Jones, 1975; Pinault, 2004; Halassa & Acsády, 2016). The boundaries between TRN sectors are less distinct than those in dorsal thalamus, with less architectonic segregation, and dendrites that span borders. Within each TRN sector, there are afferents from one or more thalamic nuclei and cortical areas. All relay cell axons passing from the dorsal thalamus to the cortex and striatum first pass through the TRN, and branch collaterally there. Similarly, glutamatergic cortical axons innervating the thalamus also pass through the TRN and form branches. The TRN does not have any direct efferent connections with the cortex, but reciprocally innervates the dorsal thalamus with inhibitory GABAergic afferents to the area it receives input from. The crossing over of axons within the TRN gives it

its ‘reticulated’ appearance. The TRN also receives inhibitory afferents from the basal ganglia and brainstem afferents.

1.1.2 Anatomy of Motor Thalamus

The motor thalamus in adult rodents consists of ventral anterior (VA), ventral lateral (VL) and ventral medial (VM) thalamus (Table 1.1). These ventral nuclei are distinct from the developmental ventral thalamus which forms TRN. VA and VL are sometimes considered as a unit, where the VA-VL complex can be divided along the rostroventral-caudodorsal axis into VA and VL, which are indistinguishable by cytoarchitecture alone, both having large sparse cells. However, VA is more like VM than VL in its connectivity with other structures. VA and VM both receive GABAergic input from the basal ganglia, primarily from substantia nigra pars reticulata (SNr), and partly from the internal segment of the globus pallidus (GPi), while VL receives input from the deep nuclei of the cerebellum. VA forms the inhibitory afferent-dominant zone (IZ) of motor thalamus (Kuramoto et al., 2009), and VA and VM together form the basal ganglia-recipient zone (BZ) (Nakamura et al., 2014; Table 1.1). BZ can be identified in the rat by strong immunostaining for glutamate decarboxylase 67 (GAD67) in neuropil, indicating the presence of basal ganglia afferent terminals, and weak vesicular glutamate transporter 2 (vGluT2) neuropil staining (Kuramoto et al., 2009; Nakamura et al., 2014). As VL receives glutamatergic cerebellar input, this region can be delineated immunohistochemically with staining for vGluT2, present in the cerebellar axon terminals, and is thus known as the excitatory subcortical afferent-dominant zone (EZ) or cerebellar-recipient zone (CZ) (Kuramoto et al., 2009; Nakamura et al., 2014; Table 1.1). There is also stronger calbindin (CB) immunoreactivity in somata and neuropil in VA and VM than in VL. These motor thalamic nuclei preferentially innervate different layers and regions of motor and motor-associated

cortex, with BZ innervating layer 1 (L1) and CZ innervating L2-5 (Kuramoto et al., 2009; 2015; Fig. 1.1). MD and intralaminar thalamus also receive basal ganglia input. VA and VM contain both small and large GABAergic terminals, with strong GAD67 immunoreactivity, and VL has small GABAergic terminals only (Kuramoto et al., 2011). Conversely, VL has large vGluT2+ terminals and VA and VM have small vGluT2+ terminals. VM has slightly stronger vGluT2 immunoreactivity than VA. Immunoreactivity for glutamic acid decarboxylase 65kDa (GAD65) and vesicular GABA transporter (VGAT) is similar to that for GAD67 although the border between VA and VL as delineated by these neurochemical markers is less clear than for GAD67.

There are some similarities and differences between the rodent and primate motor thalamus with some variations in nomenclature (Table 3.1). Primate VA receives basal ganglia input, VL receives cerebellar input, and MD receives afferents from both regions. GPi, sometimes known as entopeduncular nucleus (EP) or medial globus pallidus (GPm) in primates, and SNr innervate distinct regions of primate motor thalamus. SNr strongly innervates the magnocellular portion of VA (VAmc) which sends projections to PFC, and also receives inputs from superior colliculus (Kultas-Ilinsky and Ilinsky, 1990; Ilinsky, 1993). VAmc is also known as VAM (medial portion of VA), or Va (ventral anterior). GPi innervates the densocellular and parvocellular VA regions (VAdc and VApc), which then innervate premotor and primary motor cortex. The pallidal-recipient portion of VA can also be known as VAL or Vo (ventral oralis). GPi also innervates the CM portion of intralaminar thalamus and the cerebellum innervates CL intralaminar thalamus. VAdc contains both thalamocortical projection neurons and local GABAergic interneurons. These are arranged in clusters, which are innervated by multiple pallidal fibres to form dense plexuses. Pallidal inputs target both somata and dendrites of projection neurons, with a higher density of terminals on somata. In VAmc, the dendrites of

projection neurons are preferentially innervated over dendrites by nigrothalamic inputs, which unlike VAdc, do not form plexuses. There is a high level of topographical organisation between striatum, GPi and SNr, thalamus and cortex, and reciprocal innervation of thalamus by cortex. Primate VL can be divided into medial and lateral VL (VLM and VLL) or pars caudalis (VLpc), pars medialis (VLpm), and pars oralis (VLpo) regions. The cerebellum also innervates the pars parvicellularis and pars densicellularis regions of MD (MDpc and MDdc). The SNr innervates the pars multiformis and pars magnocelularis regions of MD (MDmf and MDmc) (Kultas-Ilinsky et al., 2011). GPi innervates MDpc and ventral pallidum innervates MDmc. As well as receiving basal ganglia and cerebellar input, MD receives afferents from the olfactory cortex and amygdala, and is highly reciprocally connected with prefrontal and orbital frontal cortex.

Thalamic Zone	**Abbreviation**	**Equivalent Thalamic Nuclei**	**Subcortical Input Sources**	**Cortical Laminar Targets**
Inhibitory Zone	IZ	VA	GPi/SNr	L1
Excitatory Zone	EZ	VL	Cerebellum	L2-5
Basal Ganglia-Recipient Zone	BZ	VA and VM	GPi/SNr	L1
Cerebellar-Recipient Zone	CZ	VL	Cerebellum	L2-5

Table 1.1 Motor thalamic zones and their connectivity in rodent

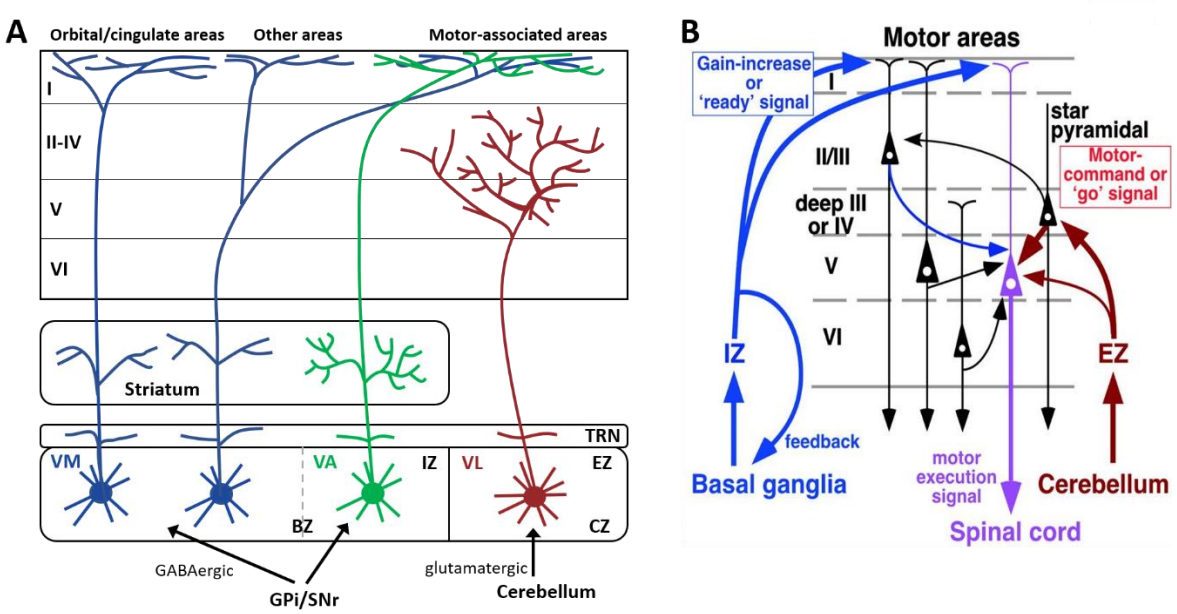


Figure 1.1 Diagram of motor thalamocortical projections
Adapted from Cho et al., 2004 and Kuramoto et al., 2009; 2015. BZ (VA and VM) receives input from GPi and SNr and innervates striatum and cortical L1 of motor and other areas. CZ (VL) receives innervation from the cerebellum and innervates L2-5 of motor cortical areas. L5 pyramidal neurons send motor output signals to spinal cord.

1.1.3 First Order and Higher Order Thalamocortical Circuits

Thalamic nuclei can be functionally divided into 'first order' and 'higher order' nuclei, depending on the nature of subcortical and cortical afferents they receive – whether these are 'drivers' or 'modulators', based on a number of key properties (Guillery, 1995; Sherman and Guillery, 1996; 2002; 2006; Table 1.2). Subcortical or cortical driver inputs to the thalamus relay specific information to their postsynaptic targets by a strong excitatory drive. Characteristic driver features include thick glutamatergic axons with large terminals on proximal dendrites of postsynaptic targets, evoking large EPSPs via ionotropic receptors. In contrast, modulators do not drive thalamic firing but influence the excitability of target neurons. They have thin glutamatergic, GABAergic, or cholinergic axons and form small terminals, converging greatly onto their target and activating metabotropic receptors. Cortical afferents from L5 to thalamus are driver inputs, whereas output from L6 to thalamus is modulatory. Thalamic nuclei that receive driver input from subcortical structures only, and

do not receive cortical driver input but may receive modulatory cortical input, are known as first order nuclei or relays. Some nuclei receive a mixture of subcortical driver and modulator input. Higher order thalamic nuclei receive L5 cortical driver input, such as MD thalamus, which receives both L5 driver input and L6 modulatory input, as well as VA and VM, Po and intralaminar thalamus. Higher order nuclei can receive driver input from one cortical area, and relay it to another cortical area, over multiple iterations.

A classic example of first order and higher order thalamic nuclei is within the mammalian visual system, which includes the LGN and pulvinar. The LGN is a typical first order thalamic relay, receiving driver input from retinal ganglion cells which contribute around 5-10% of total input, modulatory glutamatergic input from cortical L6, cholinergic input from the parabrachial nucleus, and local inhibition from TRN and thalamic interneurons (Sherman and Guillery, 2002; Rovó et al., 2012). The pulvinar is higher order, as it receives driving input from L5 of visual cortical areas and relays information to other visual cortical areas. The LGN is a laminated structure, with six layers differentiated on the basis of relay cell type, function and location of retinal afferents (Sherman and Guillery, 1996; 2006). Within the primate thalamus, the two inner layers 1 and 2 contain large magnocellular (M) cells, which receive input from rods, while layers 3 to 6 contain small parvocellular (P) cells, receiving input from cones. Very small koniocellular (K) cells are situated between layers. Within most primate species, the LGN of each hemisphere receives inputs from both the left and right eyes. In the cat LGN, the laminar distribution is different from primates, and instead of M, P and K cells there are X, Y and W cells. The retinal inputs to LGN have the characteristics of subcortical driver inputs, such as determining the receptive field of the recipient relay cells, the presence of large axon terminals on proximal dendrites, and activation of ionotropic receptors to elicit large EPSPs in the postsynaptic targets (Table 1.2). Other inputs function as modulators to control the effect

of the drivers, including influencing the response mode of the relay cells (Sherman and Guillery, 2002). These modulatory inputs have properties such as not determining the receptive field, thin axons, and small axon terminals, and activate a combination of ionotropic and metabotropic receptors. In the cat LGN, retinal, parabrachial, and interneuron afferents target the proximal dendrites of relay cells, and cortical and reticular inputs target the distal dendrites.

Based on this model, inhibitory input to thalamus, such as that from the TRN or basal ganglia, can be considered non-driver and therefore modulatory, since it is not excitatory (Sherman and Guillery, 2006), although the basal ganglia can also have driver-like effects on BZ (Albin et al., 1989). Within motor cortex, VL is a first order nucleus, as it receives driver input from the deep cerebellar nuclei.

Another classification of thalamocortical cells, mostly used in primates, is based on calcium-binding protein immunoreactivity (Jones, 1998). Calbindin (CB)-expressing neurons are termed ‘matrix’, and parvalbumin (PV)-expressing neurons are referred to as ‘core’. Core cells project to cortical L3 and L4, whereas matrix cells project diffusely to L1. Matrix cells tend to be situated in higher order nuclei, but these two classification systems do not directly correlate with each other.

Criteria	Drivers: Subcortical and Layer 5	Modulators: Layer 6, PRB, TRN and Interneurons
Relay cell receptive field	Determines relay cell receptive field	Does not determine relay cell receptive field
Target receptors	Activates only ionotropic receptors	Activates metabotropic receptors
Post-synaptic potentials	Large EPSPs	Small EPSPs. TRN: Small IPSPs
Terminal size and dendritic location	Large terminals on proximal dendrites	Small terminals on distal (L6, TRN) or proximal (PBR, Int) dendrites
Contacts per terminal	Each terminal forms multiple contacts	Each terminal forms single contact
Convergence onto target	Little convergence onto target	Much convergence onto target
Axon thickness	Often thick axons	Thin axons
Neurotransmitter	Glutamatergic	Glutamatergic, Cholinergic (PBR) or GABAergic (TRN and interneurons)
Paired-pulse ratio	Synapses show paired-pulse depression	Synapses show paired-pulse facilitation

Table 1.2 Some key criteria for identifying drivers and modulators in LGN and cortical L5 drivers (adapted from Table 7.1, Sherman and Guillery, 2006)

1.1.4 Core Physiological Principles of Thalamic Relay Neurons.

Thalamic relay neurons display two main modes of temporally distinct firing in response to afferent input: burst and tonic firing (Sherman and Guillery, 2006). Whether cells fire in burst or tonic mode is determined by their low threshold calcium (Ca^{2+}) conductance. Low threshold Ca^{2+} spikes occur by a similar mechanism to the formation of action potentials, but via T-type Ca^{2+} channels (T channels) rather than Na^{2+} channels. Ca^{2+} spikes have distinct voltage properties and much slower temporal dynamics than action potentials and are not propagated along the axon. Low threshold Ca^{2+} spikes occur when depolarisation activates de-inactivated and deactivated T channels, causing an inward Ca^{2+} current (T current). This triggers a Ca^{2+} spike, lasting for about 50ms. The depolarisation then inactivates T channels, and potassium (K^{+}) channels activate, leading to K^{+} efflux, as a result of which the cell is

repolarised. The T channels are deactivated, and later de-inactivated, requiring about 100ms to change from one activation state to another.

Tonic firing occurs when the T channel is inactivated and is characterised by a steady firing of action potentials that are representative of the input. In contrast, burst firing occurs when the T channel is de-inactivated and consequently can be activated. Action potential firing is 'burst-like', with short periods of rapid firing interspersed with no firing, which is temporally distinct from the afferent input. When relay cells display burst firing, they often demonstrate rhythmic burst firing at around 0.3 – 10Hz, which can characterise individual cells or become synchronised across regions.

There are changes in relay cell bursting mode depending on wakefulness state. For example, in the awake cat, LGN relay cells tend to fire in tonic mode, although not exclusively, with an increase in rhythmic bursting activity of some cells during slow wave sleep (Livingstone and Hubel, 1981). This led to the view that information is more faithfully relayed to the cortex during tonic mode firing in the awake state, in contrast to the suppression of information being relayed to cortex when there is increased thalamic bursting activity, such as during sleep, with the effect of the subcortical driver input being attenuated, likely due to TRN activity. In the LGN of the lightly anaesthetised cat, relay cells in burst mode fire arrhythmically when there is no external visual input (Guido et al., 1992). If bursting were to completely supress information transfer, then theoretically any visual input during anaesthesia would not be relayed or would stimulate rhythmic bursting. It was found however that the presentation of a sinusoidal grating visual stimulus caused a bursting response which was time-locked to the stimulus, but with a different firing profile from that evoked in tonic mode (Guido et al., 1992). During burst modes, there is less spontaneous activity than during

tonic modes, which potentially reduces the signal to noise ratio in response to inputs, with a greater ability to detect a stimulus in burst than tonic mode. This has given rise to the hypothesis that relay cells function in tonic mode during awake states to relay sensory information to the cortex, and conversely reduce input during sleep by burst firing. These burst firing states are therefore suited to detecting the onset of a new stimulus, functioning as a 'wake-up call' (Swadlow and Gusev, 2001, Sherman 2001), similar to the searchlight hypothesis of TRN (Crick, 1984).

It is well-established that inhibitory input from the TRN influences the firing of relay neurons (Pinault, 2004; Halassa and Acsády, 2016). TRN neurons release GABA onto both ionotropic $GABA_A$ and metabotropic $GABA_B$ postsynaptic receptors on relay neurons to elicit IPSPs. Compared with relay cells, TRN neurons have both similarities and differences in their physiological properties. They respond similarly to the low threshold Ca^{2+} conductance with burst and tonic firing modes, but have slower T current activation and inactivation kinetics (Huguenard and Prince, 1992). Inactivation is voltage-independent, which increases the duration of the low threshold spike and facilitates burst firing. This causes a sustained inhibition of the target relay neuron, while the reticular neuron is firing. During the subsequent refractory period the reticular neuron is no longer inhibiting the relay neuron, allowing repolarisation. Within the TRN, reticular neurons form gap junctions with each other. They have been shown also to form chemical synapses, but this is likely to be just in juvenile rats and mice (Crabtree, 2018). Activation of $GABA_A$ receptors on the target relay neuron inhibits the cell by opening chloride (Cl^-) channels, increasing the Cl^- conductance, and shunting the membrane potential to around -70 to -75mV, therefore making the cell less susceptible to depolarisation via EPSPs. Activation of $GABA_B$ receptors causes hyperpolarisation by an increase in K^+ conductance. The duration of the $GABA_B$ IPSP is about

10 to 100-fold longer than the $GABA_A$ IPSP. Because of these properties, $GABA_B$ receptor activation is likely to initiate burst firing in relay cells.

Having outlined the key anatomical and physiological properties of thalamocortical projection neurons, in particular motor thalamus, it is important to define the structural and functional organisation of the areas connected by the motor thalamic nuclei. The following sections will describe structural and functional properties of the basal ganglia, cerebellum, and cortex, and how these regions interact with motor thalamus.

1.2 Basal Ganglia

1.2.1 Basal Ganglia Pathways

The basal ganglia are a group of subcortical nuclei involved in movement and movement initiation, action selection, and cognitive processes. They are situated between the forebrain and midbrain in mammals, with homologues in birds and reptiles, and are connected in a reciprocal loop with the cortex and motor thalamus (Parent and Hazrati, 1995; Bolam et al., 2000). The primary input region of the basal ganglia is the striatum, receiving cortical and thalamic input, which comprises the caudate nucleus, putamen (forming the dorsal striatum), and nucleus accumbens (the main part of ventral striatum). GABAergic medium spiny neurons (MSNs) are the principal neurons of the striatum, comprising the majority of striatal neurons. There is also a diverse array of cholinergic and GABAergic interneurons within striatum, some of which are PV-expressing (Kubota et al., 1993; Bolam et al., 2009). The striatum is composed of neurochemically distinct matrix and striosome compartments (Graybiel and Ragsdale, 1978; Gerfen, 1985). The dorsal striatum receives glutamatergic afferent projections of intratelencephalic (IT) and pyramidal tract (PT) neurons from sensory, motor and association cortices, as well as input from the intralaminar thalamus. These axons synapse mostly onto

the dendritic spine heads of MSNs and interneurons, as well as less frequently onto dendritic shafts and somata. The dorsolateral striatum (DLS) is the striatal region through which sensorimotor information passes, being the main recipient of primary motor somatosensory cortical afferents, whereas the ventral regions of striatum, including nucleus accumbens, are involved in limbic circuitry (Parent et al., 1995). Dorsomedial striatum (DMS) and DLS are thought to differ in terms of their function, with DLS involved in sensory-driven stimulus-response behaviours, due to its sensorimotor cortical inputs and innervation from higher order sensory thalamic nuclei, while DMS receives more frontal cortical input, and hence may be more involved with mediating goal-directed behaviour (Alloway et al., 2017). The cortex also directly innervates the subthalamic nucleus (STN), via the hyperdirect pathway. As well as excitatory cortical input, the striatum also receives inhibitory corticostriatal projections. GABAergic corticofugal neurons innervate the basal ganglia (Tomioka et al., 2015), including a small number of PV+ L5 GABAergic neurons from retrosplenial and somatosensory cortex (Jinno and Kosaka, 2004). Inhibitory somatostatin (SST)-positive corticostriatal neurons from mouse motor and auditory cortex directly innervate MSNs, influencing spike timing (Rock et al., 2016). The striatum does not directly innervate the cortex or thalamus. Instead, the main output structures of the basal ganglia, the substantia nigra pars reticulata (SNr) and globus pallidus interna (GPi), innervate motor thalamus (VA and VM in rodents), as well as intralaminar and MD thalamus, which then project to cortex. Output tends to be primarily from SNr in rodents and GPi in primates. There is also a direct projection from GPe to frontal cortex (Saunders et al., 2015). The basal ganglia also influence movement by direct projections to brainstem motor centres and innervate other structures such as the lateral habenular nucleus and superior colliculus.

Classically, there are thought to be two main pathways from the striatum through the basal ganglia: the direct and indirect pathways. The prokinetic direct pathway is formed by direct projections from the D1 receptor-expressing population of MSNs in the striatum to GPi and SNr, as well as innervating GPe. The inhibitory indirect pathway consists of D2 receptor-expressing MSN afferents to GPe, which innervates the output nuclei either directly, or via the glutamatergic STN. The dorsal striatum receives dopaminergic input from the substantia nigra pars compacta (SNc), through the nigrostriatal pathway. These neurons synthesise dopamine by tyrosine hydroxylase (TH), and tend to innervate dendritic shafts, somata and dendritic spines of MSNs and interneurons, modulating the cortical input. Dopamine is essential for movement and is depleted in Parkinson's disease due to degradation of SNc neurons. The SNc also innervates GPe and STN. Dopamine pathways are also important in reward, motivation and decision-making, with the neurons encoding a reward prediction error (Schultz 1998). The raphé nucleus also innervates striatum, releasing 5-hydroxytryptamine (5-HT). The nucleus accumbens receives input from the limbic cortex, hippocampus and ventral tegmental area (VTA).

Historically, there have been two distinct views on how motor-related information is spatially distributed in the basal ganglia-thalamocortical motor circuit: the funnelling model whereby information converges on basal ganglia output nuclei (Kemp and Powell, 1971; Bolam et al., 1993), and the parallel processing or segregated circuit model (Alexander et al., 1986; Alexander and Crutcher, 1990), developed from observations in primate thalamus. More recently, the idea of reinforcement-driven dimensionality reduction has provided a model of how cortical information may be transferred and compressed in the striatum, allowing the basal ganglia to transfer selective information back to cortex (Bar-Gad et al., 2000; 2003).

1.2.2 Basal Ganglia Models

The mechanisms of how the basal ganglia communicate with the motor thalamus to control its activity are still under discussion (Bosch-Bouju et al., 2013; Yin 2016). There are three main models for explaining how this might occur: the gating model, entrainment model and rebound model (Bosch-Bouju et al., 2013).

The gating model, which has been the generally preferred model for circuits in the mammalian brain, suggests that the basal ganglia can control activity in mammalian motor thalamus by a disinhibition mechanism (Deniau and Chevalier 1985; Albin et al., 1989; DeLong, 1990; Chevalier and Deniau, 1990; DeLong and Wichmann, 2009). Basal ganglia output provides a level of tonic inhibition to the thalamus, which is removed when excitatory cortical input to the basal ganglia produces a net suppression of output. This would specifically be the case for the direct pathway, in contrast to the hyperdirect and indirect pathways, which would facilitate an increase in inhibitory output. Due to the number of synapses within each route, the direct pathway theoretically has a latency between that of the other pathways, meaning that the effect of disinhibition would be temporally sandwiched between brief periods of increased inhibition. This would allow excitatory input to the basal ganglia-recipient motor thalamus (initially thought to be cerebellar input, but now known to be primarily cortical) to drive firing.

According to the rebound model, basal ganglia input can trigger spikes in thalamus by rebound low threshold calcium spikes (LTS) following hyperpolarisation of thalamic neurons, functioning as excitatory inputs, and exhibiting driver-like characteristics. This is mainly based on data from the songbird brain, where the GABAergic output from Area X, similar to the mammalian GPi, can drive LTS bursts following initial inhibition in the medial portion of the

dorsolateral thalamic nucleus (DLM), the motor thalamus equivalent, *in vitro* (Luo and Perkel, 1999; Person and Perkel, 2005) and in the anaesthetised bird (Person and Perkel, 2007). Area X forms calyx-like terminals in DLM, and activity in these structures is increased during song learning. The anterior forebrain pathway, which incorporates Area X and DLM, is thought to be analogous to the mammalian basal ganglia motor thalamocortical circuit. In the anaesthetised songbird, there is evidence suggesting that Area X causes firing in DLM by both the entrainment model as well as the gating model, resulting in different firing profiles, and possibly switching between the two mechanisms, depending on state (Kojima and Doupe, 2009).

The entrainment model, also based on avian data, suggests that the basal ganglia temporally controls inhibition of the motor thalamus. A reduction of pallidal inhibition during time windows allows excitatory cortical afferents to cause firing with highly precise timing at a high constant rate within pallidal interspike intervals (ISI) in the awake singing bird, in contrast to the rebound firing seen in the anaesthetised bird (Goldberg et al., 2012; Goldberg and Fee, 2012). The number of thalamic spikes depends linearly on the duration of the ISI, rather than basal ganglia activity leading up to the ISI.

Another model more recently proposed is the 'super-integrator' model (Bosch-Bouju et al., 2013). In this model, both basal ganglia and cerebellum receive L5 cortical input, before sending an integrated signal including motivation, action selection, and proprioception to their respective thalamic territories. The motor thalamus acts as a 'super-integrator', to process these inputs as well as direct cortical information from L5 and L6, sending the processed information back to cortex with a spiralling mechanism.

The gating model is based on assumptions that first order and higher motor thalamocortical pathways are analogous to, and interact in a similar way to, sensory pathways. The driver and modulator concepts are well-suited to describe input to thalamus from sensory regions, but the pathways may be more complex within the motor circuit. More research is required to establish the extent of similarity between sensory and motor thalamocortical pathways, and whether the 'super-integrator' model is a more representative explanation of information transfer. Emerging evidence suggests that motor thalamic nuclei might not be exclusively first order and higher order, but rather contain some elements of both.

1.3 Cerebellum

The cerebellum is important for various aspects of motor function, including coordination, posture and motor planning (Gao et al., 2018). It is involved with movement timing and has recently been shown to be involved with goal-directed movement initiation (Dacre et al., 2019). Sensorimotor cortex innervates pontine nuclei, which then innervate the cerebellar cortex via the medial cerebellar peduncle (Hintzen et al., 2018). Structurally, the cerebellum is formed of the cerebellar cortex and the cerebellar nuclei. Cerebellar cortex has three layers: granular, Purkinje, and molecular (Llinás et al., 2004). The innermost layer, the granular layer, contains numerous small granule cells, which send their glutamatergic axons to the molecular layer and branch into two to form parallel fibres. There are also interneurons, including Golgi cells in this layer. All input to granule cells comes from excitatory mossy fibres, which originate in the pontine nucleus, spinal cord, or vestibular nuclei. Mossy fibres form enlarged terminal structures known as rosettes, which innervate the dendritic claw of granule cells, formed of only four to five dendrites, and also directly innervate the deep cerebellar nuclei. The central layer, the Purkinje layer, is formed by a single layer of large GABAergic Purkinje cells, which

have extensively branched spiny dendrites in the molecular layer and innervate the deep cerebellar nuclei. Within the outermost molecular layer, the parallel fibres innervate Purkinje cell dendrites. Interneurons in the molecular layer, primarily basket cells and stellate cells, innervate the Purkinje cells.

Purkinje cells are also innervated by excitatory climbing fibres from the contralateral inferior olivary nucleus in the brainstem, with each fibre innervating a single Purkinje cell, forming multiple synapses, and sending collaterals to the deep cerebellar nuclei. Purkinje cells are the sole output from the cerebellar cortex to the deep cerebellar nuclei, with one neuron innervating a few nuclear cells, and each cell receiving input from multiple Purkinje cells. The deep cerebellar nuclei lie within the white matter at the core of the cerebellum. These are the fastigial nucleus, the dentate nucleus, and the interpositus nucleus, which consists of the globose and emboliform nuclei. The inhibitory Purkinje cell input is integrated with input from the mossy and climbing fibres. The glutamatergic interpositus and dentate nuclei innervate the ventral thalamic nuclei, as well as the red nucleus, brainstem, and spinal cord. The cerebellum sends signals to the cortex via the cerebellar-thalamocortical pathway (Horne and Butler, 1995). The main thalamic target region of cerebellar fibres from each of the deep cerebellar nuclei is VL, with afferents providing driver input to the thalamus, but there is also some innervation of VM and CL (Sherman and Guillery, 2006; Gornati et al., 2018). Large vGluT2+ cerebellar terminals form synapses on proximal dendrites in VL, and elicit large EPSPs in target neurons, characteristic of driver input (Uno et al., 1970; Shermann and Guillery, 2006; Rovo et al., 2012; Table 1.2).

1.4 Cortex

1.4.1 General Structural Organisation of the Cortex

Different cortical regions have diverse functions and connectivity with different thalamic nuclei and subcortical structures. The mammalian neocortex has a dorsal to ventral laminar organisation, from superficial layer 1 (L1) to L6 at the most ventral part, which reaches a depth of around 1.5mm below the brain surface in mice. Layers can be further subdivided into more superficial and deeper regions, for example L1a and L1b, and vary in thickness between regions. Pyramidal neurons and interneurons are spatially intermingled within layers with the exception of L1, which contains cell bodies and neuropil of interneurons, but not pyramidal neuron somata, only their dendrites. L4 is prominent in somatosensory cortex but has been considered as absent from motor cortex, with motor cortex often described as agranular, as L4 contains spiny stellate neurons rather than pyramidal neurons and so is termed granular cortex. However, a narrow band of Rorb and Necab1 expression suggests that L4 is present in M1, although smaller than in somatosensory cortex. Yamawaki et al. (2014) demonstrated using optogenetics that neurons in L4 of the forelimb area of M1 receive VL input. Horizontally, the cortex is organised into cortical columns encompassing all layers.

1.4.2 Motor Cortex Divisions

In rodents, motor cortex comprises a few regions in frontal cortex. The exact boundary coordinates of these regions as defined in the literature vary, as well as their nomenclature, but for the purposes of the experiments in this thesis the definitions according to the mouse brain atlas of Paxinos et al., 2007 have been followed. The main regions will be briefly outlined here, and some of their connections with thalamus are described in section 1.5.2. Primary motor cortex (M1) is responsible for volitional behaviour and movement in response to

sensory input, as it receives input from both somatosensory thalamic nuclei as well as primary somatosensory cortex (S1). Secondary motor cortex (M2) is medial to M1, adjacent to primary cingulate cortex (Cg1), and begins anterior to M1. For this reason, it is sometimes considered part of medial prefrontal cortex, although it is controverted whether rodent brains have a PFC, as defined in primates. The exact nature of M2 function is unclear, and may comprise a range of functions, including linking sensory cues to motor actions (Barthas and Kwan, 2017). The anterior pole of M2 can also be referred to as anterior lateral motor cortex (ALM) (Guo et al., 2017).

1.4.3 Cortical Pyramidal Neurons

Excitatory pyramidal neurons are the most abundant neuron within the neocortex, forming around 70-80% of total neurons. They are spiny neurons comprising a soma, axon, basal dendrites, and an apical dendrite which extends across layers. Their axon terminals release glutamate, and hence can be detected by vGluT1 expression. They are the major output neuron of the cortex to subcortical regions, as well as projecting ipsilaterally or contralaterally within cortex. Afferents to subcortical regions tend to originate in deeper cortical layers, with superficial neurons generally remaining within the cortex. L2, L3 and L5 contain the somata of pyramidal neurons, which have apical dendrites branching to form tufts in L1. Pyramidal neurons receive afferent input from other cortical pyramidal neurons and inhibitory interneurons, as well as from subcortical sources. They tend to form synapses with dendritic shafts and spines mainly of other pyramidal neurons, with axonal boutons that are either *en passant*, forming a swelling along the axon, or *terminaux*, forming a bulb-like structure at the end of an axon. Spiny pyramidal neurons generally have more connections with other layers

than intralaminar connections (Douglas and Martin, 2004), although there is much intralaminar connectivity within L2/3.

Depending on the location of their axonal targets, pyramidal neurons can be divided into three main interconnected groups: intratelencephalic (IT), pyramidal tract (PT), and corticothalamic (CT) neurons (Shepherd, 2013; Harris and Shepherd, 2015; Fig. 1.2). All projection neurons have collaterals within the cortex. L2/3 neurons tend to deliver information within cortex, ipsilaterally or contralaterally, while L5-6 neurons largely send information to subcortical regions. Different neurons encode information with different firing patterns, for example intracortically projecting L2/3 pyramidal neurons have sparse firing, with low spontaneous and evoked firing rates, while L5 output neurons have faster firing rates, which evidently are suited to their particular roles (Harris and Mrsic-Flogel, 2013).

IT neurons are a heterogeneous group situated throughout L2-6, and innervate the telencephalon, which includes cortex, striatum, and other areas such as amygdala. They are sparse firing and have a hyperpolarised resting membrane potential. They target other IT neurons as well as PT and CT neurons in cortex, and are the only class that sends afferents both ipsilaterally and contralaterally. L4 IT neurons include both pyramidal and spiny stellate neurons, and in somatosensory cortex they receive substantial thalamic input from first order nuclei. They extensively innervate L2/3, L5a, and L5b, but receive significantly less excitatory input from other cortical layers. L2/3 IT neurons innervate PT neurons in L5b, as well as IT neurons in L2/3 and L5, and L2/3 interneurons (Helmstaedter et al., 2009; Harris and Shepherd, 2015).

PT neurons are large pyramidal cells located in L5b. They send output bilaterally to subcortical targets such as brainstem and spinal cord, as well as innervating ipsilateral cortex and basal

ganglia, and provide driver input to thalamus. PT neurons in different cortical areas preferentially target different subcortical regions, for example PT neurons in motor cortex target brainstem and spinal cord. They receive substantial IT input from various layers, as well as thalamocortical inputs at the dendritic level. Their intrinsic physiological properties are different from IT neurons, as they are characterised by having a depolarised resting membrane potential, are non-adapting in their firing, and some can display burst firing.

CT neurons are located exclusively in L6 and project to ipsilateral thalamus as well as branching to L4 and L5a within cortex. They send modulatory afferents to thalamus, typically to the area from which they receive input, but also to higher order nuclei, as well as collaterals to TRN. They receive input from IT and PT neurons, as well as thalamocortical afferents. L5b and L6 contain more than one class of excitatory neuron, but they can be distinguished by differences in expression of molecular markers: IT neurons express SATB2, PT neurons express FEZF2 and CTIP2, and CT neurons express TBR1.

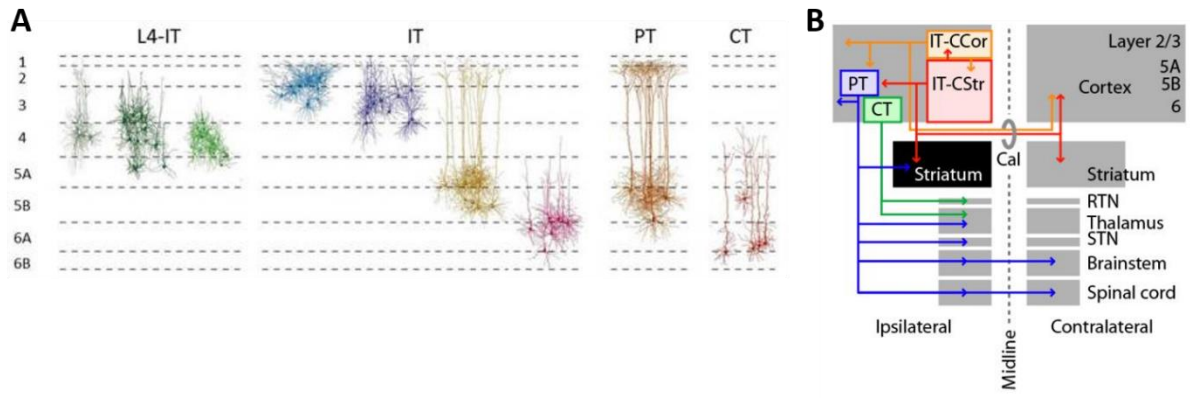


Figure 1.2 Dendritic morphology and long-range axonal projections of cortical excitatory neurons
(A) Dendritic morphology of L2-6 IT neurons, L5B PT neurons and L6 CT neurons in S1 of mouse barrel cortex. L4 contains three types of IT neurons: pyramidal, star pyramidal, and spiny stellate cells. Adapted from Fig. 1, Harris & Shepherd, 2015, and Fig. 2, Oberlaender et al., 2012.
(B) Long-range axonal projections of PT, CT and IT neurons. PT neurons project to ipsilateral striatum, thalamus, STN and many brainstem and spinal cord regions, as well as contralateral brainstem and spinal cord. IT neurons project ipsilaterally and contralaterally via the corpus callosum (Cal) within cortex and to striatum. CT neurons project to ipsilateral thalamus and TRN (RTN). Adapted from Fig. 1, Shepherd 2013.

Cortical pyramidal neurons receive inhibitory input to different regions of the cell. As well as forming synapses onto the soma, axon initial segment, and dendritic shafts, interneurons of multiple types also target dendritic spines of pyramidal neurons. These dendritic spines additionally receive thalamocortical innervation but not excitatory cortical innervation, suggesting that inhibitory cortical afferents selectively gate extracortical inputs but not cortical inputs (Kubota et al., 2007). Input to the distal apical dendrites of cortical pyramidal neurons can exert a strong influence over firing (Larkum et al., 1999; Larkum et al., 2009; Larkum, 2013). Action potentials can arise from the dendrites, developing from dendritic calcium spikes, or from the axon, which can then back-propagate into the dendrites (Stuart and Sakmann, 1994). These back-propagating action potentials facilitate dendritic action potentials. Axonal action potentials can be suppressed by inhibitory input to the dendrites blocking calcium spikes (Larkum et al., 1999), as seen with L1 NDNF+ interneurons inhibiting dendritic spikes in pyramidal neurons of PFC (Anastasiades et al., 2020). Pyramidal neurons can integrate input from all their dendrites, with input to the apical dendrites providing top-down control.

1.4.4 Cortical Interneurons

Cortical GABAergic interneurons provide local inhibition within the cortex, as well as sending some afferents to subcortical regions (Jinno and Kosaka, 2004; Lee et al., 2014; Tomioka et al., 2015). Local interneurons regulate the activity of pyramidal neurons and other interneurons, contributing to the precise control of cortical network activity. Since I will later focus on L1 interneurons in this thesis, I shall provide the context for this here by presenting some general background of cortical interneurons and include a few specific examples. There are multiple types of cortical GABAergic interneurons, which vary in their morphology,

physiology, molecular markers, location, and connectivity (Klausberger and Somogyi, 2008; Rudy et al., 2011; Fishell and Rudy, 2011). A cell type can be defined by the cell-domain and brain area location of presynaptic and postsynaptic contacts, protein expression, intrinsic membrane properties, and *in vivo* temporal firing dynamics (Somogyi and Klausberger, 2005). Interneurons in CA1 hippocampus have been well-characterised (Somogyi and Klausberger, 2005), and there are similarities between these and cortical interneurons. Different interneurons preferentially target different domains of postsynaptic neurons: as well as targeting dendritic spines and shafts, interneurons form synapses with somata and axon initial segments. Electrophysiological firing profiles of pyramidal cells and interneurons can be categorised as fast-spiking, late spiking, regular-spiking, or adapting and bursting (McCormick et al., 1985, Kawaguchi and Kubota, 1997). Other firing types include non-adapting, irregular firing and accelerating (Ascoli et al., 2008). Most interneurons are aspiny, or smooth, in contrast to pyramidal neurons, but may be spiny during development. The most abundant interneuron types include basket cells (Fig. 1.3C), which form basket-like structures with their axons on the dendrites and somata of pyramidal neurons, chandelier or axo-axonic cells (Fig. 1.3C), which are fast-spiking and innervate the axon-initial segment of pyramidal cells, double bouquet cells (Fig. 1.3C), which have vertically oriented dendritic projections above and below their somata, and SST+ Martinotti cells (Fig. 1.3B). Cortical interneurons can be divided into three broad groups, depending on their neurochemical marker expression (Rudy et al., 2011). These are parvalbumin (PV), SST and 5HT3a receptor (5HT3aR)-expressing neurons. PV+ and SST+ interneurons originate in the medial ganglionic eminence (MGE) during development. 5HT3aR+ interneurons mostly originate in the caudal ganglionic eminence (CGE).

PV-expressing neurons are the largest interneuron group, forming about 40% of cortical GABAergic interneurons. These include fast-spiking basket and chandelier cells. Basket cells innervate the soma and proximal dendrites of target neurons, and chandelier cells innervate the axon-initial segment. PV+ neurons are distributed throughout L2-6, with a higher proportion in deeper layers, and none present in L1. In somatosensory cortex, L4 PV+ neurons are the main interneuron recipient of thalamocortical afferents.

SST-expressing neurons account for approximately 30% of cortical interneurons, and are mostly Martinotti cells, which are distributed across all layers, with a preference for deeper over superficial layers. Martinotti cells have axons which terminate in L1 with a wide arborisation and innervate pyramidal neuron apical dendrites as well as innervating the apical and basal dendrites of pyramidal neurons within deeper layers. They have a facilitating response to excitatory input, and as a result have higher activity levels when there is increased pyramidal cell firing. As well as Martinotti cells, SST+ neurons include X94 cells (Ma et al., 2006), which have different electrophysiological properties. Like Martinotti cells, they respond with facilitation to excitatory afferents, but have a lower input resistance and a higher firing frequency. SST+ neurons can also be calretinin (CR)-positive or negative, with differences in dendritic arborisation. SST+/CR- neurons in V1 and S1 receive strong inputs via their dendrites in L2/3 and L4, while SST/CR+ neurons primarily receive input through L2/3 and less in L4.

The 5HT3aR-expressing group also forms around 30% of cortical interneurons and appears to be more diverse than the other two groups. Interneurons expressing 5HT3aR can be broadly divided into vasoactive intestinal peptide (VIP)-expressing (around 40%) and non-VIP-expressing (around 60%) (Lee et al., 2010). 5HT3aR+ interneurons dominate superficial

cortex, comprising the majority of interneurons in L1, about half within L2/3 and significantly fewer in deeper layers. 5HT3aR interneurons all express nicotinic receptors (Lee et al., 2010) and therefore can be modulated by cholinergic as well as glutamatergic and 5-HT input.

All VIP+ neurons in somatosensory cortex express 5HT3aRs and are reelin-. They have a high input resistance, causing them to be more readily excitable than other interneurons. Most innervate the shafts and spines of dendrites of other neurons. VIP+/5HT3aR+ neurons can be further categorised into at least four groups (Miyoshi et al., 2010), the most common of which is the CR+ bipolar or bitufted irregular-spiking (IS) neuron, which is present throughout layers 2-6, particularly in L2/3, and uncommon in L1. These bipolar neurons are vertically oriented, as the name suggests, with superficially located dendrites and an axon reaching deeper layers, which sometimes innervates other interneurons as well as pyramidal neurons. Another VIP+/5HT3aR+ subtype are rapid-adapting or fast-adapting neurons, which fire bursts of action potentials followed by a period of silence. They can be bipolar or tripolar in morphology and are CR-. Other subtypes are bursting non-adapting 2 (bNA2) neurons, which fire a series of action potentials followed by a delay period, and arcade or delayed non-fast spiking (dnFS3) cells. VIP+ basket cells have been observed, but these are uncommon.

Within the VIP-/5HT3aR+ group, 80% of neurons are reelin-expressing. VIP-/SST- neurons include neurogliaform (NGF) cells. These were originally identified by Cajal in the motor cortex and called spiderweb cells due to their morphology of a small soma with multiple thin multipolar radiating dendrites and a short axon (Fig. 1.3B). They were later observed in stratum radiatum and stratum lacunosum moleculare in CA1 of the hippocampus (Lacaille and Schwartzkroin, 1988; Vida et al., 1998; Price et al., 2005) as well as in the striatum (Muñoz-Manchado et al., 2016). Some of the NGF cell population expresses the markers pro-

neuropeptide Y (NPY), reelin, chicken ovalbumin upstream promoter transcription factor 2 (COUPTFII), neuronal nitric oxide synthase (NOS) and α-actinin 2 in varying amounts (Overstreet-Wadiche and McBain, 2015). Cortical NGF cells arise from the CGE and are found throughout cortical areas and in all layers. Hippocampal NOS+ NGF cells originate in the MGE and NOS- NGF cells originate in the CGE, with only CGE-derived NGF cells expressing 5HT3aR, indicating differences in input types (Tricoire et al., 2010). NGF cells have a late-spiking firing pattern and are classified as late-spiking 1 (LS1), with other VIP- 5HT3aR+ cells being either LS1 or LS2. There are also VIP- 5HT3aR+ cells with a bursting non-adapting firing pattern, which are similar to VIP+ bnA cells, except they have a multipolar morphology and tend to be in superficial layers (Rudy et al., 2011). The distance between NGF axon terminals and their postsynaptic dendritic targets is often greater than that for other interneurons, suggesting that the mechanism of transmission is primarily by volume transmission of non-specific GABA release, rather than precise synaptic transmission (Oláh et al., 2009; Overstreet-Wadiche and McBain, 2015). The axons of NGF cells have $GABA_B$ receptors and dense release sites, which release vesicular GABA into the extrasynaptic space, eliciting IPSPs in pyramidal neurons, other interneurons and other NGF cells, thereby linking circuits together. NGF-evoked long-lasting IPSPs have been recorded in human cortical pyramidal cells (Tamás et al., 2003) as well as in human and rat cortical interneurons (Oláh et al., 2007). Postsynaptic targets have both $GABA_A$ and $GABA_B$ receptors, which mediate ionotropic and metabotropic signalling near the release site and extrasynaptically. These properties mean that NGF-mediated transmission can be diffuse and target multiple cells simultaneously within an area, so that it is neither spatially nor temporally precise, with both fast and slow signalling, and synaptic depression due to receptor desensitisation from extracellular GABA (Oláh et al., 2007). Cortical NGF cells also communicate with other NGF cells, interneurons and pyramidal neurons by gap junctions

forming electrical synapses (Simon et al., 2005). Within the somatosensory cortex, NGF cells in L4 suppress PV+ interneuron-mediated feed-forward inhibition but not feed-forward excitation from thalamic input, demonstrating an example of the involvement of NGF cells in a more temporally precise and synapse specific regulation of network activity (Chittajallu et al., 2013). In the rat hippocampus, NGF cells form both chemical and electrical synapses with other NGF cells, with those forming reciprocal electrical synapses showing increased synchrony (Price et al., 2005).

1.4.5 Cortical L1 Interneurons

Layer 1 is unique among cortical layers in that it does not contain the cell bodies of pyramidal cells, but contains the distal tufts of their apical dendrites from deeper layer neurons, as well as somata and processes of interneurons, axons of deeper layer interneurons such as Martinotti cells and dendrites of other interneurons, and thalamocortical axons. There are at least two different types of cortical L1 interneurons: elongated neurogliaform cells (ENGCs, Fig. 1.3A) and VIP+ single bouquet cells (SBC, Fig. 1.3A) or single bouquet-like cells (Jiang et al., 2013; Jiang et al., 2015). Single bouquet cells are horizontally restricted and have a long axon which branches and projects to deeper layers.

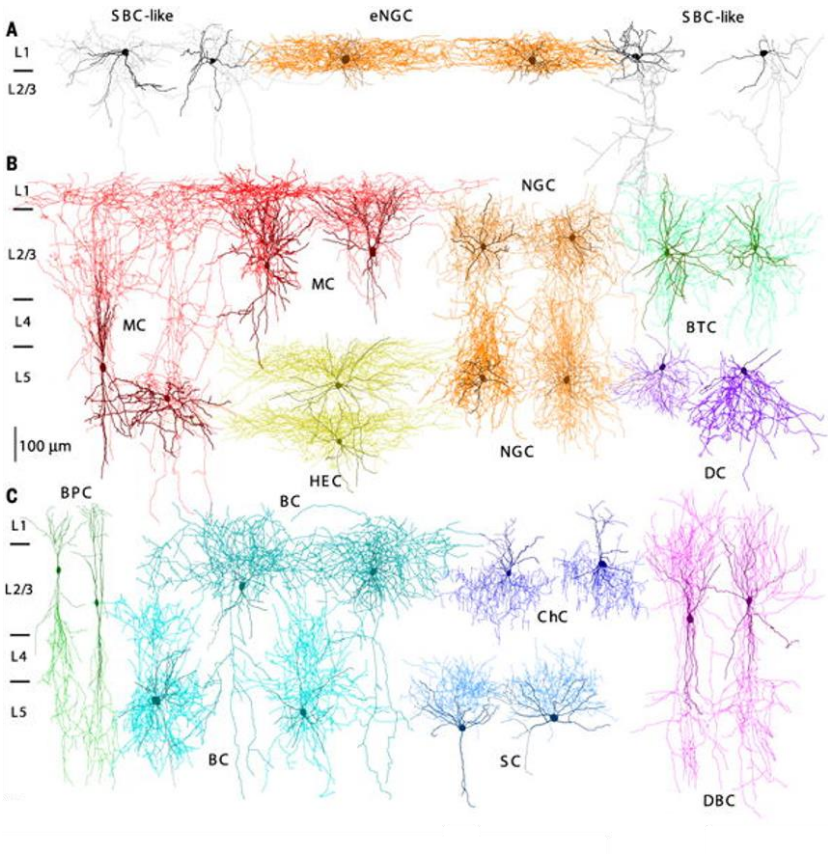


Figure 1.3 Morphology of cortical GABAergic interneurons
GABAergic interneurons in L1, L2/3 and L5 of adult mouse V1, showing two types of morphologically distinct L1 interneurons, seven types of L2/3 interneurons and six types of L5 interneurons. From Fig. 1, Jiang et al., 2015. **(A)** Two types of morphologically distinct L1 interneurons. SBC-like cells (left and right) have their soma and some axonal arborisation in L1, as well as deep-projecting axons (grey), and their dendritic arborisation in L1-3 (dark grey). ENGCs (centre) have the majority of their axonal (orange) and dendritic (brown) arborisations in L1. **(B)** Four Martinotti cells (MC) in both L2/3 and L5; four L2/3 and L5 neurogliaform cells (NGC) (axon in orange and dendrite in brown), two L5 horizontally elongated cells (HEC), two L2/3 bitufted cells (BTC) and two L5 deep-projecting cells (DC). **(C)** Two bipolar cells (BPCs) (axon in lime and dendrite in green), two L2/3 and two L5 basket cells (BCs) (axons in cyan and dendrite in dark cyan), two L2/3 chandelier cells (axon in blue and dendrite in dark blue), two L2/3 double bouquet cells (DBC, axon in magenta and dendrite in purple), and two L5 shrub cells (SC).

ENGCs comprise about 30-40% of L1 neurons (Jiang et al., 2015; Garcia-Munoz & Arbuthnott, 2015). They tend to be located in the more superficial part of L1, L1a, with SBCs localised more in L1b. L1 ENGCs have a similar morphology to NGF cells, with a small soma and dense local axonal arborisation, with the difference that their axons are horizontally elongated and restricted to L1. They do not express NPY, in contrast to some cortical and hippocampal NGF cells. L1 ENGCs are non-adapting and can be divided into late spiking (LS) and non-late spiking

(NLS) but are mostly LS, with slower IPSP kinetics and longer latencies than SBCs (Jiang et al., 2013). Within cortical circuits, ENGCs have been shown in sensorimotor cortical slices to suppress dendritic complex spiking in L5 pyramidal neurons via L2/3 interneurons, whereas SBCs enhance dendritic complex spiking in L5 pyramidal neurons via L2/3 interneurons (Jiang et al., 2013). ENGCs regulate the inhibition of L2/3 and L5 but not L6 pyramidal neurons across multiple cortical columns (Lee et al., 2015). Single-cell RNA sequencing in mouse primary visual cortex and subsequent neural reconstruction and recordings identified the gene for neuropeptide neuron-derived neurotrophic factor (NDNF) in NGF cells in L1 (Tasic et al., 2016), which may be a useful identifying neurochemical marker. Immature L1 also contains Cajal-Retzius cells (Villar-Cervino and Marin, 2012; Ma et al., 2014) which are mainly functional during development and disappear shortly afterwards. Over 90% of L1 interneurons are 5HT3aR+/VIP- and most are reelin+ (Ma et al., 2014).

L1 ENGCs have mainly been studied in vitro, where they are characterised by a late-spiking non-adapting firing pattern (Jiang et al., 2013). Neurogliaform cells in other cortical layers and CA1 of hippocampus are known to form electrical synapses with each other and other interneurons, and can elicit inhibitory responses in postsynaptic neurons via both GABAA and GABAB receptors (Price et al., 2005, Simon et al., 2005, Oláh et al., 2007. In vivo recordings in anaesthetised animals have shown that L1 ENGCs in somatosensory cortex fire short spontaneous action potentials of around 1.6ms duration and respond to somatosensory input from whisker deflection with short latencies (Zhu and Zhu, 2004; Jiang et al., 2013). More recently, spontaneous activity of L1 INs has been measured in vivo in barrel cortex of awake animals, with spontaneous spiking rates of around 3.2Hz (Fan et al., 2020), which is similar to spontaneous firing rates of SOM+ INs and slower than fast-spiking PV+ INs (Zhou and Roper, 2010). ENGCs are temporarily excited and then inhibited in response to whisker stimulation,

during which their spontaneous activity and chance of responding to further inputs is reduced, in barrel cortex of anaesthetised and awake animals (Fan et al., 2020). This response to sensory input, as well as direct optogenetic stimulation of ENGCs, causes lateral inhibition within L1 (Fan et al., 2020).

ENGCs receive a range of cortical and subcortical inputs, including cholinergic input from basal forebrain, and so can be influenced by fear conditioning and likely also by alertness states (Letzkus et al., 2011; Abs et al., 2018). It is not known whether their firing is associated with any particular cortical network oscillations. The spontaneous firing of ENGCs has not yet been measured in motor cortex in vivo in an awake animal, either during a resting state or behaviour, and so the extent to which these observations in other cortical regions translate to motor cortex remains unclear.

Alternatively, L1 interneurons can be divided into four groups based on their morphology, molecular expression profile and physiology (Wozny and Williams, 2011; Schuman et al., 2018). These are NDNF+/NPY- canopy cells, NDNF+/NPY+ NGF cells, NDNF-/VIP+ cells and NDNF-/α7 nAChR+ cells (Schuman et al., 2018). The NGF cells in L1 are similar to those in other layers, with non-adapting late spiking firing patterns, and a dense laterally elongated axonal arbour restricted to L1. Canopy cells have a similar morphology to NGF cells, with a less dense and wider arbour mostly within L1a which is analogous to ENGCs. They display moderately adapting and NLS spike trains, comparable to the morphologically similar and physiologically distinct groups identified by Jiang et al. (2013). Each of the NDNF+ cell types are reciprocally connected. Canopy cells elicit IPSPs in L2 pyramidal cells some of the time, with NGF cells often eliciting IPSPs. Both α7 cells and VIP+ cells are located in L1b, with axons collaterals descending to deeper layers, similar to SBCs. The α7 cells have a large soma and

multipolar dendrites, and VIP+ cells have the smallest L1 soma and bipolar dendrites. These NDNF- cell types are both NLS, with onset spikes at the start of depolarisations. α7 cells display moderate adaptation, an active depolarising hump near the membrane potential threshold, and large hyperpolarisation-activated current (I_h)-mediated hyperpolarising sag, similar to NLS cells in Cruikshank et al. (2012). VIP+ cells are fast-adapting and have a high input resistance.

1.5 Motor thalamocortical circuit

1.5.1 Anatomical connectivity of motor thalamocortical neurons

As described earlier, the different regions of motor thalamus receive their main subcortical input from either the basal ganglia or cerebellum, and preferentially target different cortical layers. Innervation of VA and VM, as well as MD and intralaminar thalamus, by ipsilateral SNr has been demonstrated by anterograde tracing with *Phaseolus vulgaris* leucoagglutinin (PHA-L_4) and biotinylated dextran amine (BDA3k), with ventral SNr targeting VA and dorsal SNr targeting VM in rat (Kuramoto et al., 2011). Similar injections into the deep cerebellar nuclei (DCN) resulted in strong labelling of contralateral VL and weak labelling of VA and VM, as well as weak to moderate labelling of other thalamic regions. These observations were further supported by kainic acid injections into SNr depleting large GAD67+ terminals in the thalamus but not small terminals, and injections into DCN which depleted large vGluT2 terminals in VL (Kuramoto et al., 2011). VA thalamocortical neurons have fewer dendritic processes than VL neurons (Kuramoto et al., 2009).

Although both VA and VM receive basal ganglia input, VM thalamocortical neurons innervate L1 more widely and preferentially than VA thalamocortical neurons (Kuramoto et al., 2015). VM projections to L1 in rat are well-established (Herkenham 1979; Arbuthnott et al., 1990).

VM axons primarily target L1a, but occasionally terminate in L2/3 of motor-associated areas. BZ thalamocortical neurons strongly innervate L1, especially L1a, while EZ neurons prefer L2-5, with much less arborisation in L1 (Kuramoto et al., 2009; 2015; Table 1.1; Fig. 1.1). Kuramoto et al. (2009) anterogradely traced and reconstructed single thalamocortical neurons from these regions to observe their morphology and identify which cortical areas they innervate. Both EZ and IZ neurons innervate primary (M1) and secondary (M2) motor cortex, as well as other areas, including primary somatosensory cortex (S1), forelimb (FL) and hindlimb (HL) areas, frontal association area (FrA), and cingulate cortex (Cg). VA projects to motor and motor-associated areas: M1, M2, FL and HL areas, while VM projects to these areas as well as orbital and cingulate areas. Depending on their cortical targets, VM neurons can be divided into 'motor-preferring' and 'nonmotor-preferring'. Individual neurons can branch to additionally innervate other cortical areas, including S1, S2, and visual areas, but predominantly target motor-associated areas, cingulate and orbital cortex. Both VM and VA innervate striatum, with VA providing more collaterals than VM, and VL has minimal innervation of striatum. VL mainly targets M1 with both direct and indirect connections with pyramidal tract neurons (Aumann, 2002). Cerebellar inputs to VL and VL thalamocortical neurons projecting to motor cortex are topographically organised (Tlamsa and Brumberg, 2010).

L1-projecting thalamocortical neurons are not only found in motor thalamus, but also in sensory, limbic and association thalamic nuclei in the rat, as shown by anterograde and retrograde tracing (Rubio-Garrido et al., 2009). These are matrix, or 'M-type' neurons. Retrogradely labelled thalamic nuclei targeting L1 include VL, VM, AM, Po, dLGN, anterior intralaminar, lateral dorsal nucleus (LD) and MGN. Thalamic nuclei differ in their range of L1 innervation, for example VM, AM and Po target a range of cortical areas, while nuclei such as

dLGN and MD have a more laterally restricted cortical innervation. At the cortical level, axons from individual nuclei converge, and often form arbors within L1a. Additionally, submedius thalamus innervates L1 of medial prefrontal cortex (Arbuthnott et al., 1990), and MD also innervates L1 of cingulate and orbital cortex (Groenewegen 1988).

1.5.2 Thalamocortical and cortical circuits involving L1

Thalamocortical neurons innervate both pyramidal neurons and interneurons and are able to drive dendritic spiking and neuronal firing, which can cause feedforward excitation and inhibition in downstream cortical pathways (Cruikshank et al., 2007; 2010; Harris and Shepherd, 2015). As different classes of interneurons and pyramidal neurons each have distinct electrophysiological properties, they have varying responses to thalamocortical inputs. In this section, examples of thalamocortical and cortical pathways involving interactions with L1 and other layers in sensorimotor, prefrontal and other cortical regions will be covered to help understand general principles, which may be applicable to L1 motor cortex and can help inform predictions of effects of thalamocortical innervation of this region.

Axons from motor thalamocortical neurons terminate in cortical layers 1 to 5 to innervate different somatodendritic regions of L2/3 and L5 pyramidal neurons in motor cortex and other frontal cortical regions. Motor cortex includes primary and secondary motor cortex (M1 and M2), which can be subdivided into different regions based on their peripheral output control, for example, forelimb motor cortex or vibrissal primary motor cortex (vM1), which controls whisker movements in rodents. vM1 and vibrissal sensory cortex (vS1, barrel cortex) are reciprocally connected, as sensory information from whiskers informs their ongoing motor control (Mao et al., 2011). Within vibrissal primary motor cortex (vM1), as in other cortical areas, there is a difference in laminar input from different sources (Hooks et al., 2013). vM1

receives converging excitatory inputs from ipsilateral motor and sensory thalamic nuclei, including AM, VM, VL, and Po, and ipsilateral cortices including M2, primary and secondary somatosensory cortex (S1 and S2), and orbital cortex (OC), as well as from contralateral motor cortex (M2) (Hooks et al., 2013). The strongest ipsilateral input is from ipsilateral thalamus, M2 and OC. Sub-cellular channelrhodopsin2-assisted circuit mapping (sCRACM) (Petreanu et al., 2009; Cruikshank et al., 2010) was used to investigate and map the monosynaptic functional connectivity of long-range excitatory thalamic and cortical inputs to pyramidal neurons within different layers of vM1 (Hooks et al., 2013). Motor thalamic neurons target apical dendrites of L2/3 and L5 pyramidal neurons in L1 of vM1, as shown by anatomical studies, as well as basal dendrites of L2/3 pyramidal neurons and mostly perisomatically innervate L5A neurons, with some input via L1. Cortico-cortical inputs to deeper M1 layers are generally from frontal cortical regions. M2 mainly targets PT neurons perisomatically in L5B of vM1, as well as innervating L5A and L6, while OC targets CT neurons in L6. Upper vM1 layers tend to receive afferents from sensory-related areas: sensory thalamus and primary somatosensory cortex (S1), which innervate L2/3 and L5A pyramidal neurons, with axons in L1 and L5. Local cortical projection neurons transfer information from L2/3 and L5A to L5B, and so sensory input is likely to influence sensorimotor processing and motor output through these circuits.

There may be similarities in thalamocortical circuitry between somatosensory and motor pathways, although there are also substantial differences in cortical organisation between sensory and motor areas, most notably the prominence of L4 in somatosensory cortex, which receives a large amount of innervation from first order somatosensory thalamus (Agmon and Connors, 1991). Multiple interneuron types in mouse somatosensory cortex receive monosynaptic thalamocortical innervation, with PV+, SST+ and VIP+ interneurons all receiving

direct input (Wall et al., 2016). L4 of mouse barrel cortex provides an example of different responses of pyramidal neurons and interneurons to somatosensory thalamocortical input within a cortical area. *In vitro* paired recordings in mouse L4 barrel cortex show that projection neurons from ventrobasal thalamus evoke a greater response in fast-spiking interneurons than in regular-spiking pyramidal neurons, resulting in feedforward inhibition of both pyramidal neurons and interneurons (Cruikshank et al., 2007). This difference in activation appears to be due to the intrinsic synaptic mechanisms of targeted interneurons, as well as a larger convergence of thalamocortical inputs on interneurons than pyramidal neurons, although another *in vitro* study suggests that input to the two groups of neurons are relatively equal (Gabernet et al., 2005). This demonstrates interneuron-mediated feedforward inhibition in L4 somatosensory cortex elicited by thalamocortical input, and that temporal firing responses to thalamocortical input are partially dependent on the postsynaptic cell type.

As well as in L4 somatosensory cortex, feedforward inhibition caused by thalamocortical input to interneurons has been observed in L1 PFC (Cruikshank et al., 2012). In addition to innervating motor cortical areas, VM thalamus targets frontal cortical regions including PFC, where principles of thalamic input pathways to cortical interneurons could be partially applicable to thalamocortical circuitry involving the adjacent motor cortex. Matrix thalamocortical neurons targeting L1 of PFC drive L1 inhibitory interneurons and can cause feedforward inhibition in both L1 interneurons and L2/3 pyramidal neurons via their dendrites in L1 (Cruikshank et al., 2012). The primary thalamocortical L1 target was typically presumed to be pyramidal cell dendrites, but this demonstrates that interneurons are also targeted in PFC. Cruikshank et al. investigated this *in vitro* by optogenetically stimulating thalamocortical terminals in L1 mPFC. These projection neurons were in midline and intralaminar thalamic

nuclei, including VM, VA, submedius, rhomboid, reuniens, CM, PC and interanteromedial nuclei, with terminal arbours mainly located in L1a. The effect of stimulating these afferent fibres caused driving of fast postsynaptic responses mediated by ionotropic glutamate receptors, contrary to the theory that matrix thalamocortical projections mediate slow and diffuse postsynaptic responses, and were larger in LS than NLS cells. These responses were more like those elicited by core projections, which carry temporally precise information. During whole-cell paired recordings of L1 interneurons and L2/3 pyramidal neurons, repeated optogenetic stimulation of thalamocortical input elicited depression in interneurons and facilitation in pyramidal neurons. As in L4 barrel cortex (Cruikshank et al., 2007), L1 PFC interneurons responded to thalamocortical input with larger EPSPs than L2/3 pyramidal neurons. Similar to other studies, late-spiking (LS) interneurons in mPFC were distributed throughout L1 but tended to be denser in L1a, with non-late spiking (NLS) interneurons more numerous in L1b, comparable to the distributions and physiological properties of ENGCs and SBCs. LS interneurons responded more strongly to thalamocortical stimulation than NLS interneurons, which may be due to their location relative to thalamocortical fibre terminals. These L1 LS interneurons formed synapses with other L1 interneurons and L2 pyramidal neurons. NLS interneurons instead showed stronger responses to cortico-cortical input, suggesting a division within L1 interneurons in processing inputs from different areas. This may be one functional distinction between ENGCs and SBCs. It remains to be seen whether thalamocortical innervation of L1 motor cortex firstly targets interneurons, and secondly, if so, elicits feedforward inhibition of pyramidal neurons or interneurons in cortex.

There are reciprocal connections between PFC and the higher order thalamic nuclei VM and MD, with VM and MD innervating the dendrites of L5 pyramidal neurons in L1, and L5 and L6 cortical neurons from the same region feeding back to thalamus. Collins et al. (2018) probed

these circuits with a combination of anatomical tracing, optogenetics and *in vitro* recordings in mice. They found that PFC corticothalamic inputs from both L5 and L6 innervate and drive firing in reciprocally connected thalamocortical neurons in both VM and MD. Most thalamic-projecting neurons were in L6, and neurons from layers 5 and 6 can bifurcate to innervate both thalamic nuclei. These L5 inputs have depressing effects on thalamic neurons on repetitive stimulation consistent with driver input, and L6 inputs have facilitatory effects. L6 inputs to thalamus are modulatory, but more numerous than L5 inputs, and combined L5 and L6 PFC input to VM and MD thalamus is facilitatory, indicating a prominent role of L6 neurons in the reciprocal corticothalamic pathway. L6 neurons also collateralise to TRN, to cause feedforward inhibition in thalamus. Thalamocortical neurons from VM and MD mainly innervate L5 rather than L6 CT neurons in PFC. MD thalamocortical neurons drive L5 cortico-cortical (CC) neurons more strongly than L5 PT neurons, and VM neurons showed no difference in innervation strength. MD neurons drive L2/3 CC neurons more strongly than L5 CC neurons, and VM shows little bias. The strength of MD-evoked EPSPs was much greater than VM-evoked EPSPs, which were unable to evoke action potentials but initiated dendritic calcium spiking, indicating that MD but not VM may provide driver input to PFC. So MD may drive cortical pyramidal neurons while VM input potentially has a more modulatory role in PFC. L2/3 CC neurons that receive MD and VM input innervate L5 PT neurons to complete the circuit.

The same group demonstrated with retrograde rabies viral tracing that within PFC, both L1 NDNF+ and VIP+ interneurons receive monosynaptic input from MD and VM, so that the same thalamic nuclei target both pyramidal neuron dendrites and interneurons within L1 (Anastasiades et al., 2020). VM thalamocortical axons tend to innervate superficial L1a and MD axons terminate in deeper L1a and L1b. MD thalamocortical inputs target VIP+ and NDNF+

interneurons fairly equally in terms of number of contacts, but VM neurons primarily drive NDNF+ cells. Within the superficial cortical circuitry, the two interneuron types are involved in distinct downstream circuits: VIP+ interneurons mainly target SST+ interneurons, while NDNF+ interneurons innervate L2/3 PV+ interneurons and pyramidal neurons but not SST+ interneurons. NDNF+ interneurons can cause disinhibition of pyramidal neurons via L2/3 PV+ interneurons. sCRACM revealed NDNF+ interneurons inhibit action potentials at the level of apical PT dendrites in L1a but not in basal dendrites, and block VM-evoked dendritic calcium spikes in PT apical dendrites. This demonstrates that L1 NDNF+ interneurons are important in regulating VM-evoked firing in cortical output neurons and are themselves directly innervated by VM. Additional research is required to find out whether this is also the case *in vivo*, and if L1 NDNF+ interneurons in motor cortex function in a similar manner to PFC neurons.

As well as L1 NDNF+ interneurons inhibiting VM-evoked firing in pyramidal neurons in PFC (Anastasiades et al., 2020), direct electrical stimulation of L1 ENGCs also suppresses firing in pyramidal neurons (Jiang et al., 2013). In order to find out about the potential difference in roles of L1 SBCs and ENGCs within cortical microcircuits, Jiang et al. recorded from up to eight neurons simultaneously in rat sensorimotor cortex *in vitro* while stimulating with electric current (Jiang et al., 2013). They found that almost all L1 SBCs made unidirectional inhibitory connections with all types of L2/3 interneurons, which inhibited L5 pyramidal neurons in all regions, to cause disinhibition of dendritic complex spikes in these pyramidal neurons within the same cortical column. L1 ENGCs made reciprocal connections with L2/3 interneurons which innervate L5 pyramidal neurons. The differences are that over half of ENGCs recorded formed mutual inhibitory connections with three types of L2/3 interneurons, which targeted distal apical dendrites of L5 pyramidal neurons in the same and adjacent cortical columns, causing inhibition rather than disinhibition. ENGCs also directly innervate the apical dendrites

of L5 pyramidal neurons, but SBCs do not. Similar observations were found from *in vivo* recordings with whisker stimulation. One potential role of ENGCs proposed is to reduce background noise and so enhance the signal to noise ratio (Jiang et al., 2013). A later publication by the same group observed additionally that SBCs and ENGCs targeted L2/3 but not L6 pyramidal neurons via L2/3 interneurons in a similar pattern to L5 pyramidal neurons (Lee et al., 2015). Wozny and Williams (2011) found that within the somatosensory cortex, L1 interneurons receive L2/3 pyramidal input, with the exception of L1 neurogliaform cells, which were shown to strongly inhibit these pyramidal cells. These findings, together with the recordings in PFC, show that L1 ENGCs can effectively inhibit downstream pyramidal neurons and interneurons, and participate in feed-forward inhibition in response to thalamic stimulation.

Further evidence of L1 ENGC control of L2/3 and L5 pyramidal neurons can be found in auditory cortex, suggesting that these interneurons have similar downstream cortical connectivity in different cortical regions. Within mouse auditory cortex, *in vitro* and *in vivo* evidence shows that L1 NDNF+ interneurons provide prolonged inhibitory control to pyramidal neuron dendrites that is distinct from and complementary to SST+ Martinotti cells (Abs et al., 2018). Optogenetic recordings *in vitro* showed a slower and longer-lasting inhibition of L2/3 pyramidal neurons by L1 NDNF+ interneurons than inhibition from Martinotti cells. This shows that L1 ENGCs can inhibit L2/3 as well as L5 pyramidal spiking. There was some mutual inhibition between NDNF+ and SST+ interneurons (Jiang et al., 2013; Jiang et al., 2015), but this appeared to be mostly unidirectional with SST+ interneurons controlling L1 NDNF+ interneurons.

The same group also investigated the intrinsic physiological properties of L1 interneurons in human cortex (Poorthuis et al., 2018). They found expression of NDNF in human L1 interneurons, similar to mouse cortex. In both species, all L1 interneurons expressed nicotinic acetylcholine receptors (nAChRs) and responded rapidly to cholinergic input. The α7 subunit of the nAChR appeared to be responsible for the fast component of the postsynaptic current, and the β7 subunit responsible for the slow current component. The different composition of nAChRs could influence the biphasic response of L1 interneurons. This is consistent with observations that NDNF- α7 cells in L1b are non-late spiking (Schuman et al., 2018). In contrast, not all L1 interneurons respond to 5-HT control, as 5HT3aRs are not found in all L1 interneurons, but are found in VIP+ neurons, which are a group possibly controlled by both cholinergic and serotonergic input. These similarities between human and mouse interneurons indicate a wider relevance for L1 interneuron research in rodents. Although we are primarily interested in glutamatergic thalamic input to L1, it is important to remember there are other input types to L1 that can influence interneuron firing, including ACh and 5-HT. L1 NDNF+ interneurons are found across cortical regions besides motor cortex. As other interneurons have consistent intrinsic properties between different cortical regions, so ENGCs are likely to also have consistent properties, and this is the case so far from published work. However, it remains to be explored how ENGCs influence single unit and LFP activity in motor cortex as part of the basal ganglia-thalamocortical circuit.

1.5.2 Behaviour and motor learning

Different parts of the motor circuit work together to facilitate movement. Both basal ganglia and cerebellar circuits flow through the thalamus to reach the cortex, and so to understand the function of motor thalamus we need to consider the role of the wider circuit. The

respective roles of the basal ganglia and motor cortex in fine motor control and motor learning are not yet fully established, although new information is continuing to emerge (Klaus et al., 2019). The motor cortex has direct outputs to the spinal cord via the pyramidal tract, implying a central role in motor control, but lesion studies have shown that motor cortex is not essential for every type of movement, for example locomotion, which can be controlled by spinal cord central pattern generators (CPGs) (Grillner, 1981).

Motor cortex is however involved in dexterous movement and motor learning (Guo et al., 2015; Papale and Hooks, 2018). A study that endeavoured to dissect the role of motor cortex in learning and executing a skilled movement demonstrated that rats require motor cortex to learn a non-dexterous spatiotemporally precise lever press task but not to execute the previously learnt task, after a lesion (Kawai et al., 2015). This indicates a potential 'tutoring' role of motor cortex to subcortical circuits during learning. Optogenetic inhibition of sensorimotor cortex (centred on M1) in head-fixed mice suppressed previously learnt skilled forelimb reaching for and eating a food pellet, but not similar untrained forelimb movements (Guo et al., 2015). Even in the absence of a cue or pellet, there was a rebound prehension following the end of photoinhibition. In contrast to Kawai et al., optogenetic inhibition suppressed both the dexterous and non-dexterous components of the learnt behaviour. This may be due to the nature of the task requiring reaching to a specific location, or that optogenetic inhibition is faster than a cortical lesion, which would potentially allow other pathways to take over from motor cortex.

Due to the classic view of basal ganglia direct and indirect pathways facilitating and inhibiting movement, it would follow that direct spiny projection neurons (dSPNs) and indirect spiny projection neurons (iSPNs) would respectively excite and inhibit downstream motor cortical

neurons via the thalamus. This is broadly the case, but a minority of iSPN neurons can modulate both an increase and decrease in activity in some M1 neurons (Oldenburg & Sabatini 2015). Surprisingly, cued movement reduces the effect of dSPNs but not iSPNs on motor cortex, with dSPNs modulating activity in M1 neurons that are active during movement.

Motor cortex, in particular anterior lateral motor cortex (ALM), is involved with motor planning along with the thalamus. A series of studies by Svoboda and colleagues used an object detection licking task in head-fixed mice to investigate the role of ALM in movement and motor planning and suggested that this region is homologous to the non-human primate premotor cortex (Guo et al., 2014; Li et al., 2015, Guo et al., 2017). ALM is reciprocally connected with VM and VAL thalamus, as well as other nuclei. VM thalamocortical neurons innervate L5b PT neurons at their apical dendritic tufts in layer 1 of ALM, as well as L2/3 pyramidal neurons, which also target L5 PT neurons, but do not innervate L6 CT neurons projecting back to VM (Guo et al., 2018). Neurons in both the ALM and thalamus showed activity during a delay epoch prior to movement which predicted lick direction (Guo et al., 2017). Optogenetic unilateral inhibition of this delay activity in either ALM or thalamus caused reduced activity in the other structure, and a decrease in performance on contralateral lick trials. This indicates that reciprocally driven activity in motor thalamus and ALM is necessary for motor preparation.

The exact mechanism of interactions between the basal ganglia and ALM in motor preparation and decision making was unknown. The nigro-thalamic pathway contributes to the timing of goal-directed behaviour, with optogenetic stimulation of SNr terminals in VM and VAL thalamus causing an increase in lick omissions and a decrease in impulsive licking, in

a similar task to Guo et al., 2014 (Catanese and Jaeger, 2020). Catanese and Jaeger suggest a model whereby VM/VAL neurons exhibit a ramping activity until a threshold is reached, at which point movement is initiated. If this threshold is reached too early, impulsive licking occurs, and too late then omissions occur. This activity is inhibited by input from the SNr.

The cerebellum is also involved in motor planning along with frontal cortex. Comparable to observations between ALM and thalamus, preparatory activity in frontal cortex is required to maintain cerebellar preparatory activity, and vice versa (Gao et al., 2018). Inhibition of the fastigial nucleus by lesions and optogenetics during the delay phase disrupted the initiation of movement and impaired direction choice but did not affect the execution of movement.

Similar to anatomical studies in rat (Kuramoto et al., 2009, 2015), the activity of thalamocortical neurons targeting different cortical layers differs between basal ganglia and cerebellar-recipient thalamus in mice (Tanaka et al., 2018). Stimulation of SNr resulted in increased activity in more L1 than L3-projecting thalamocortical axons, and stimulation of deep cerebellar nuclei resulted in increased activity in more L3 than L1-projecting thalamocortical axons. They found that stimulation of ChR2 in thalamocortical axons in M1 of awake head-fixed mice induced forelimb movements, and inactivation of thalamocortical axons inhibited motor learning, indicating a thalamic role in both motor learning and execution. Despite this, there are still significant gaps in our knowledge of motor thalamocortical connectivity that need to be addressed to understand the role of these circuits in behaviour.

1.6 Aims

The aims of my DPhil studies as set out in this thesis were to investigate the anatomical and physiological connectivity of the basal ganglia-recipient motor thalamocortical circuit. VM

afferents have been shown to drive ENGC firing in PFC *in vitro* (Cruikshank et al., 2012; Anastasiades et al., 2020), and the downstream effects of ENGC firing on single-unit cortical activity have also been measured in sensorimotor cortex *in vitro*, showing ENGC-mediated inhibition of dendritic complex spiking in L5 pyramidal neurons (Jiang et al., 2013). My goal was to identify whether there is direct thalamic input to ENGCs in L1 motor cortex in mice and to compare it to thalamic innervation of L5 pyramidal neurons. In addition, with the intention of bridging the gap between the increasing number of studies of thalamocortical circuits in mouse and applying them to human thalamocortical circuits, I neurochemically parcellated the macaque thalamus as has been done in rodent thalamus, which could then potentially be extrapolated to human thalamus with which it shares many structural similarities.

Summary of aims:

1) Neurochemically characterise the molecular profile of L1 NDNF+ interneurons in motor cortex.
2) Test the hypothesis that NDNF+ neurons in L1 motor cortex receive monosynaptic input from basal ganglia-recipient motor thalamus.
3) Compare thalamic sources of input to L1 NDNF+ interneurons with thalamic inputs to L5 pyramidal neurons in motor cortex.
4) Neurochemically parcellate the anterior regions of macaque thalamus.
5) Establish the electrophysiological effects *in vivo* of optogenetically stimulating and inhibiting L1 NDNF+ interneurons in motor cortex while stimulating thalamocortical projection neurons.

Experimental summary:

To address these aims, I initially tested a range of neurochemical markers with immunohistochemistry for colocalisation with Cre+ neurons in L1 motor cortex of NDNF-Cre mice, followed by rabies tracing to identify thalamic inputs to these interneurons. In addition, I carried out rabies tracing in RBP4-Cre mice, to identify and compare thalamic innervation of L5 pyramidal neurons in motor cortex. I then attempted to investigate the physiological connectivity of L1 ENGCs within the motor thalamocortical circuit, by *in vivo* awake head-fixed probe recordings in motor cortex and thalamus of NDNF-Cre mice while optogenetically stimulating VM thalamus and inhibiting L1 ENGCs with continuous light stimulation. To complement the neurochemical parcellation of rodent thalamus, I used immunohistochemistry to reveal regions of different intensity in macaque thalamus. The experimental methods and results are described in the following three chapters, with a general discussion at the end.

Chapter 2. Anatomical connectivity of the mouse thalamocortical circuit

2.1 INTRODUCTION

2.1.1 Rodent motor thalamus and thalamocortical connectivity

The motor thalamocortical circuit is instrumental in movement control and motor learning. Basal ganglia and cerebellar circuits influence movement through their connections with brainstem motor centres and motor thalamic nuclei. Thalamocortical projection neurons are important in influencing cortical activity by targeting pyramidal neurons and interneurons within sensorimotor cortex and other cortical areas. Motor cortical regions control execution of movement by output from layer 5 (L5) pyramidal neurons to the brainstem and spinal cord, as well as feeding back to the basal ganglia and thalamus from L5 and L6 (Fig. 2.1A).

Certain thalamic nuclei receive GABAergic afferents from the substantia nigra pars reticulata (SNr), the main output structure of the basal ganglia in rodents, as well as some input from the globus pallidus internus (GPi). These include the intralaminar thalamus, comprising central medial (CM), central lateral (CL) and paracentral (PC) nuclei, mediodorsal (MD), ventral anterior (VA) and ventral medial (VM) thalamic nuclei. VA and VM are part of motor thalamus and are known collectively as the basal ganglia-recipient zone (BZ) (Nakamura et al., 2014). Since basal ganglia efferents are GABAergic, the BZ can be delineated by strong glutamic acid decarboxylase 67 (GAD67) immunostaining which labels these terminals (Kuramoto et al., 2011; Nakamura et al., 2014). The motor thalamus also includes the ventral lateral thalamus (VL), which receives glutamatergic input from the cerebellum, and is thought to be involved more in the refinement of motor execution. The VL is also known as the cerebellar recipient zone (CZ), and as it receives excitatory glutamatergic input from the

cerebellar dentate nucleus it can be identified in rat by strong vesicular glutamate transporter 2 (vGluT2) immunoreactivity in cerebellar terminals and weaker GAD67 immunoreactivity compared with BZ (Nakamura et al., 2014; Kuramoto et al., 2011). VA and VL are often described as a linked complex (VA/VL or VAL) in rodents, due to their proximity to each other and similar cytoarchitecture, with VA situated at rostromedial VA/VL and VL caudolateral to VA. However, as outlined above, VA and VL have distinct input connectivity as well as different output connectivity, and therefore can be regarded as separate structures within motor thalamus. In addition to GAD67 and vGluT2, the distribution of the calcium-binding proteins parvalbumin (PV), calbindin (CB) and calretinin (CR) in somata and neuropil varies across regions of the rat thalamus (Arai et al., 1994), and hence these calcium-binding proteins can also be used to aid in delineation of thalamic regions. For example, in motor thalamus, many VM cell bodies are CB-positive (CB+), but in contrast there is a low density of CB+ cell bodies in VL. Other regions including intralaminar thalamus also have a relatively high density of CB+ neurons. PV cell bodies are particularly dense in TRN, and neuropil in regions including VPM, VPL, ATN and LD (Arai et al., 1994).

Motor thalamus contains a combination of first order and higher order nuclei. BZ thalamus is considered higher order, projecting to superficial cortical layers and receiving driver input from L5 cortex as well as L6 modulatory input, whereas VL is first order, receiving cerebellar driver input and both L5 and L6 cortical input (Bosch-Bouju et al., 2015). In rodents, glutamatergic thalamocortical projection neurons from different motor thalamic nuclei preferentially innervate different cortical layers, as well as having afferents to striatum. VM is known to preferentially innervate layer 1 (L1) of frontal cortex, including motor-associated areas and orbital, cingulate, and prefrontal cortices, involved with cognitive processes involving executive function, in addition to some innervation of striatum (Herkenham 1979;

Arbuthnott et al., 1990), while VA innervates mainly L1 of motor-associated cortical areas and striatum (Fig. 2.1B), and VL innervates L2-5 of motor and motor-associated areas, revealed by single neuron tracing studies in rat (Kuramoto et al., 2009; 2011; 2015). Within L1, BZ thalamus innervates apical tuft dendrites of L2/3 and L5 pyramidal neurons (Fig. 2.1C). Traditionally, these motor thalamocortical projection neurons terminating in L1 have been thought to exclusively innervate pyramidal neurons and not interneurons. However, more recent anatomical and physiological evidence has shown that L1 interneurons in medial prefrontal cortex (prelimbic cortex and cingulate cortex) receive and can be driven by VM input *in vitro* (Cruikshank et al., 2012; Anastasiades et al., 2020; Sieveritz et al., 2020), challenging these previous assumptions. In light of this, it seems reasonable to predict that VM also innervates L1 interneurons in motor cortex, which would significantly change our understanding of the basal ganglia-thalamocortical circuit if this is the case and raise further questions regarding the function of these interneurons within the circuit (Fig. 2.1C).

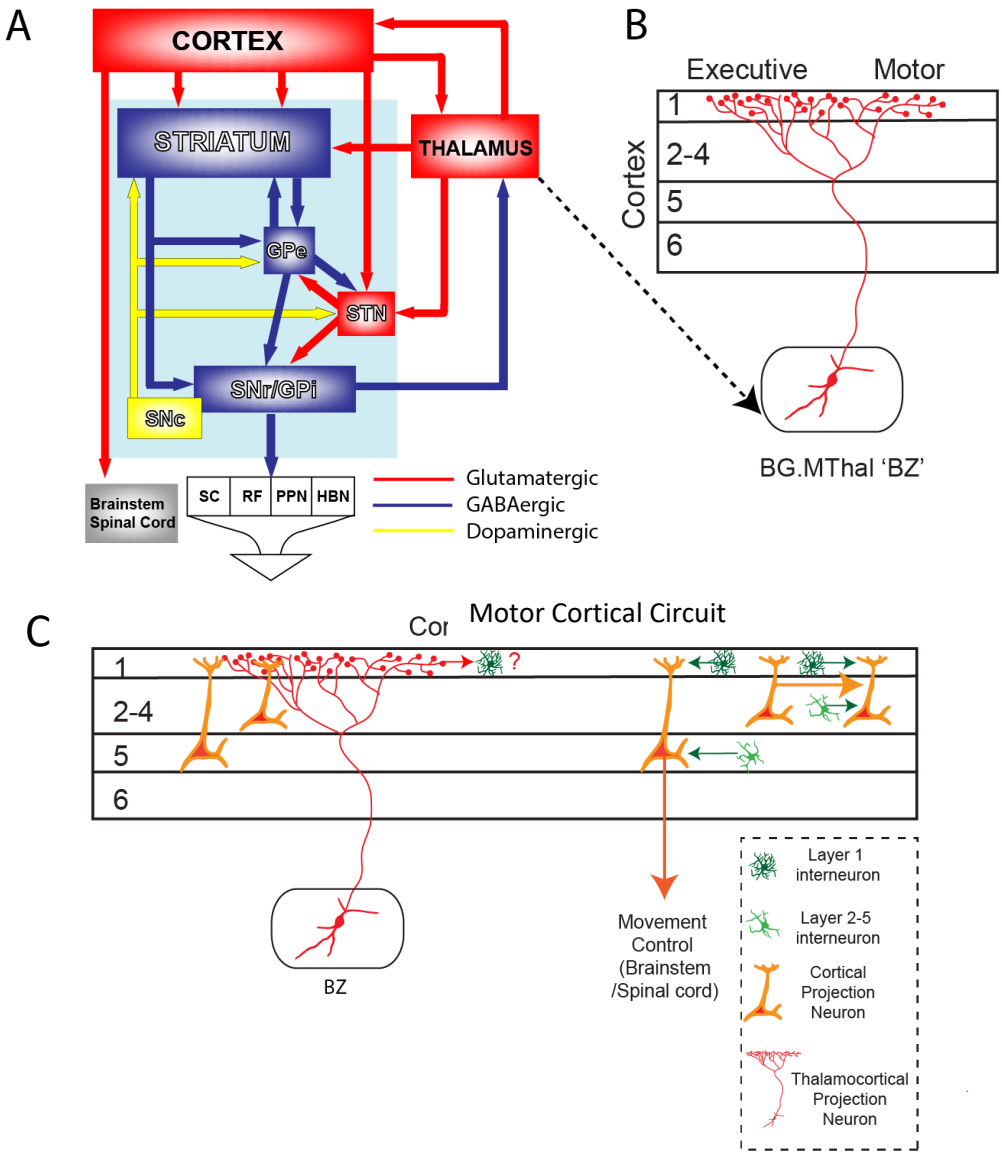


Figure 2.1. Basal ganglia-recipient motor thalamus mainly innervates L1 cortex
(A) Schematic diagram of the cortico-basal ganglia-thalamocortical circuit, adapted from Fig. 1, Bolam et al., 2009. Abbreviations: globus pallidus interna (GPi), globus pallidus externa (GPe), subthalamic nucleus (STN), substantia nigra pars compacta (SNc), substantia nigra pars reticulata (SNr), superior colliculus (SC), reticular formation (RF), pedunculopontine nucleus (PPN), lateral habenular (HBN). **(B)** Basal ganglia- (BG) recipient motor thalamus (BG.MThal/BZ) innervates L1 of cortical regions associated with both motor and executive function. **(C)** Simplified circuit diagram of motor cortex. Left: Thalamocortical projection neurons from BZ synapse on to the apical dendrites of L2/3 and L5 pyramidal neurons within L1 of motor cortex. It is unknown whether or not they also innervate L1 interneurons in motor cortex. Right: Within L1, interneurons are thought to synapse on to the apical dendrites of L2/3 and L5 pyramidal neurons (cortical projection neurons). Interneurons in L2-5 also innervate pyramidal neurons, and pyramidal neurons communicate directly with each other within L2/3. L5 pyramidal neurons project to brainstem and spinal cord, where they are responsible for the control of movement.

2.1.2 Cortical L1 and elongated neurogliaform cells

In L1 cortex of adult mice there are two main types of interneuron as defined by morphology following cell reconstruction: single bouquet cells (SBCs) and extended or elongated neurogliaform cells (ENGCs) (Jiang et al., 2013), although L1 interneurons can also be divided into four groups, taking into account their molecular profile and electrophysiological properties as well as morphology (Wozny and Williams, 2011; Schuman et al., 2018). In addition, L1 can contain Cajal-Retzius cells (Garcia-Munoz & Arbuthnott, 2015; Villar-Cervino & Marín, 2012), which are mainly functional during development and disappear shortly afterwards, although occasionally some remain in adulthood. Neurogliaform (NGF) cells were first described by Cajal (Ramon y Cajal, 1904), and are similar to neuropeptide Y-positive (NPY+) NGF cells found in the hippocampus (Lacaille and Schwartzkroin, 1988). They are found in superficial and deep cortical layers of multiple cortical areas, including frontal cortex (Kawaguchi and Kubota, 1997). ENGCs are similar to NGF cells but are found solely in L1 and have a horizontally elongated axonal arborisation. They have a small cell body, a dense axon confined to L1 and a dense local dendritic arborisation. SBCs do not have such a wide arborisation but instead have a long axon projecting to deeper cortical layers. L1 ENGCs comprise about 30-40% of L1 neurons (Garcia-Munoz & Arbuthnott, 2015) and can be divided by their intrinsic physiological properties into late spiking (LS) and non-late spiking (NLS) neurons (Jiang et al., 2013), but are mostly LS. In contrast to NPY+ hippocampal and other cortical NGF cells, L1 ENGCs are NPY-negative (Overstreet-Wadiche & McBain, 2015).

ENGCs can thus be identified by their laminar position and morphology, as well as having characteristic physiological properties. However, to be able to study their anatomical and physiological connectivity and function on a population level, it is beneficial to be able to genetically target ENGCs, ideally with a neurochemical marker that is expressed in ENGCs but

not in adjacent cells, allowing selective anatomical tracing and physiological manipulation. A single cell transcriptomics study in mouse primary visual cortex found that cell types containing the neuron-derived neurotrophic factor (NDNF) gene corresponded to NGF cells (Tasic et al., 2016). Most NDNF+ cells were identified by this study to co-express reelin as well as some NDNF+ neurons having CR co-expression. All were vasoactive intestinal peptide (VIP)-, PV- and somatostatin (SOM)- negative, and very few were neuronal nitric oxide synthase (NOS)-positive. The study authors subsequently created a Ndnf-IRES2-dgCre-D (NDNF-Cre) mouse line, which preferentially labelled neurons in L1. NDNF is a neurotrophic factor found exclusively in neurons, and is expressed in Cajal-Retzius cells during development which may be involved in cortical lamination, especially in L1 cortex (Soriano and del Rio, 2005; Kuang et al., 2010). L1 ENGCs are NPY-, in contrast to NPY+ NGF hippocampal interneurons. Cortical and hippocampal NGF cells have been shown to express COUP-TFII (Overstreet-Wadiche & McBain, 2015). Reelin+ interneurons have been shown to be the most abundant L1 GABAergic interneuron population (Ma et al., 2014). More recently, NDNF+ L1 cells have been divided into two groups, with the majority (70%) consisting of NPY- 'canopy cells', named due to the shape of their axons in L1a, and the rest NPY+ neurogliaform cells (Schuman et al., 2018). These populations also have distinctions in their electrophysiological properties, such as neurogliaform cells tending to be LS, while canopy cells are non-LS. For the purposes of this project however, all NDNF+ L1 cells are referred to as ENGCs, encompassing both of these subgroups.

If BZ thalamocortical neurons are found to directly innervate L1 interneurons in motor cortex, the role of these interneurons in modulating thalamocortical circuits will depend on how they are embedded in cortical microcircuits. Some useful insight into this comes from *in vitro* recordings, where it is possible to manipulate and record from individual or paired neurons.

In slice preparations of rat sensorimotor cortex, ENGCs have been shown to suppress dendritic complex spiking in L5 pyramidal neurons via L2/3 interneurons, whereas SBCs enhanced dendritic complex spiking in L5 pyramidal neurons via L2/3 interneurons (Jiang et al., 2013). NGF cells signal by volume transmission rather than direct synaptic transmission (Oláh et al., 2009), and ENGCs are electrically coupled. The release of GABA may act as a dampening effect on surrounding pyramidal neurons to regulate motor control. ENGCs can also be reciprocally coupled to other ENGCs and interneurons in deeper layers. They regulate the inhibition of L2/3 and L5 but not L6 pyramidal neurons across multiple cortical columns (Lee et al., 2015).

2.1.3 L5 and cortical output

Long-range cortical output to subcortical regions originates largely in L5 and L6. L5 contains pyramidal output neurons – pyramidal tract (PT) neurons in L5B and intratelencephalic (IT) neurons in L5A and B, as described in the general introduction chapter. Retinol-binding protein 4 (RBP4) is a transport protein for the vitamin A alcohol retinol as well as binding other fatty acids, and its enhanced genetic expression in L5 cortex means it can also be used to identify and target L5 (Blaner 1989; Gray et al., 2017; Perduca et al., 2018). RBP4-Cre mice are selective for both L5 PT and IT neurons throughout L5 (Gerfen et al., 2013; Harris et al., 2014; Jeong et al., 2016), with L5B PT neurons targeting areas including ipsilateral brainstem and spinal cord, with collaterals in cortex, striatum and thalamus, and are therefore involved in directly facilitating movement, while IT neurons target both ipsilateral and contralateral telencephalon (cortex and striatum) (Shepherd, 2013; Harris and Shepherd, 2015). Corticothalamic (CT) neurons are located in L6, providing modulatory input to thalamus. Long range cortical GABAergic projections innervate dorsal striatum (Rock et al., 2016). Cortical

pyramidal neurons receive inputs from a wide array of interneurons with differences in their morphology, expression of neurochemical markers, electrophysiological properties and their target cells and regions of innervation, providing finely tuned control of network activity. As L1 ENGCs innervate these cortical output neurons, it is important to know whether or not they receive direct thalamic innervation in motor cortex to understand how they might fit into the motor thalamocortical circuit.

2.1.4 Aims

1) Neurochemically characterise the molecular profile of L1 NDNF-expressing (NDNF+) interneurons in motor cortex.

2) Test the hypothesis that NDNF+ neurons in L1 motor cortex receive monosynaptic input from basal ganglia-recipient motor thalamus.

3) Compare thalamic sources of input to L1 NDNF+ interneurons with thalamic inputs to L5 pyramidal neurons in motor cortex.

2.2 METHODS

2.2.1 Animals

Experimental procedures were carried out using adult male Ndnf-IRES2-dg-Cre or Tg(Rbp4-cre)KL100Gsat mice (heterozygous on a C57BL/6J background, Jackson Laboratories), or C57BL/6 mice (Charles River) aged 2-12 months old. They were housed with littermates on a 12-hour light-dark cycle, with food and water provided ad libitum. All procedures were carried out according to the Animals (Scientific Procedures) Act, 1986 (UK) and institutional regulations.

2.2.2 Surgery and stereotactic injections

Unilateral injections were made during recovery surgery. Anaesthesia was induced by 4% isoflurane in oxygen and maintained on 1.5-2% isoflurane through a nose mask. The head was shaved while the animal was anaesthetised, and the mouse transferred to the stereotactic frame (David Kopf Instruments). Body temperature was maintained at around 37 ± 0.5°C with a probe and heating pad under the animal. Buprenorphine (Vetergesic, 0.08mg/kg in saline) was administered subcutaneously after induction of anaesthesia to provide analgesia. The head was secured with a bite bar, nose clamp and ear bars. The shaved scalp was cleaned with chlorhexidine and saline before starting the aseptic surgical procedure. Marcain was injected subcutaneously into the scalp to provide local anaesthesia, and the skin was opened with a scalpel incision along the midline. Bregma and lambda were measured to ensure the skull was level and adjusted if necessary. The desired coordinates were measured from Bregma, and a small hole drilled at the location. A prefilled glass injection pipette (internal diameter 15-20µm) was moved to the coordinates and manually lowered to the DV coordinates, then left for 5 minutes for the brain to settle. 400 – 600nl of an AAV5-Ef1a-DIO-YFP virus (Vector Core) was injected manually with a syringe at a rate of 100nl per minute.

The pipette was left in place for at least a further 5 minutes for the virus to diffuse. The pipette was then slowly brought up out of the brain. For L1 superficial injections into motor cortex, instead of a small hole above the target, a craniotomy was made in the right hemisphere posterior to Bregma and anterior to Lambda. A 90° angled pipette holder was used to insert the injection pipette subdurally via the craniotomy at an angle of about 12°, with the end of the pipette over the coordinates AP 1.5, ML 1.3. 550-600nl of virus was injected and left for 5 minutes before removing the pipette. The edges of the skin were brought together to close the scalp, sutured with non-continuous stitches (coated Vicryl suture 5-0) and adhered with Vetbond skin glue (3M). The animal was subcutaneously injected with 0.4ml pre-warmed glucose solution and left to recover in its heated recovery home cage with supplementary food. The animal was monitored post-operatively at least once every 24 hours until it had fully recovered and was within 5% of its original weight. All injections were unilateral in the right hemisphere. Animals were left for at least 2-3 weeks for virus expression prior to perfusion or electrophysiology experiments, with the exception of rabies virus injections.

See supplemental Table S1 for virus information.

2.2.3 Perfusion fixation

Mice were anaesthetised with a terminal dose of pentobarbitone and transcardially perfuse-fixed with saline followed by 4% paraformaldehyde (PFA) in 0.1M phosphate buffered saline (PBS). Brains were removed from the skull and incubated in 4% PFA overnight at 2-8°C, before washing in PBS and storing in PBS with 0.05% sodium azide (PBS-azide) until sectioning.

2.2.4 Histology

Coronal sections were cut at 50 or 60µm using a vibrating microtome and stored in PBS-azide. Free-floating sections were washed 3x 10 minutes in PBS-Triton-azide (PBS-Tx, 0.3% Triton

v/v, 0.5% sodium azide) to permeabilize the tissue. They were then blocked in 20% v/v normal donkey serum (NDS, Vector Laboratories) in PBS-Tx for one hour at room temperature. Following this, the sections were incubated in primary antibody solution, in PBS-Tx with 1% NDS, overnight at room temperature. The sections were then washed 3x 10 minutes in PBS-Tx, and incubated in secondary antibody solution in PBS-Tx with 1% NDS, in the dark for either 4 hours at room temperature, or overnight at 2-8°C. The sections were then washed 3x 10 minutes in PBS, and mounted on glass slides with Vectashield mounting medium (Vector Laboratories), and coverslipped. 4',6-diamidino-2-phenylindole (DAPI) was added at the stage of washing the secondary antibodies, at a concentration of 1:1000 for 30s incubation.

See supplemental Tables S2 and S3 for primary and secondary antibody information.

2.2.5 Microscopy

Multichannel fluorescence images were acquired using a Zeiss Imager.M2 widefield epifluorescence microscope equipped with Plan-Apochromat objective lenses, a Hamamatsu Flash 4.0 LT camera and Colibri LEDs. For whole section or large area images a 5x, 10x or 20x lens was used and tiled images acquired using Stereo Investigator v11.09 (MBF Biosciences). These images were processed offline using Stereo Investigator.

For higher resolution images, a Zeiss LSM880 Axio Imager 2 laser scanning confocal microscope was used. Confocal images of stereological markers and rabies virus-labelled cells were acquired using a 10x Plan-Apochromat air objective lens (NA 0.45) or a 40x oil objective lens (NA 1.4). Zen Black software was used to acquire single image and tile scans with an approximately 10µm optical section, as well as z-stacks. AMCA fluorescence was imaged with excitation from a Diode 405nm laser, Alexa488 fluorescence was imaged with excitation from an Argon 488nm laser, and Cy3 and Alexa647 fluorescence was imaged with excitation from

a HeNe 543nm laser, with MBS-405 and MBS-488/543 beamsplitters. Tiled confocal images were processed and stitched offline using Zen Blue.

2.2.6 Neurochemical characterisation of L1 NDNF+ neurons

To characterise the molecular profile of Cre-expressing neurons in the NDNF-Cre mouse line, three NDNF-Cre mice were injected with 300-600nl AAV5-Ef1a-DIO-hChR2(E123T/T159C)-eYFP into L1 motor cortex (AP 1.5, ML 1.3, DV 0.5) with a vertical injection (see Table S1 for virus details). Mice were perfused 4 weeks after injection, and sections cut at 50µm or 60µm. Starting sections were selected at random, and every 1 in 3 (60µm sections) or 4 serial sections (50µm sections) spanning the whole of motor cortex were incubated in primary antibodies as above, with 11-13 sections of each combination per animal. In each incubation, a primary antibody to GFP was used to enhance the native eYFP fluorescence. Three combinations of antibodies for molecular markers were used (Table 2.1).

Protocol	**Markers and conjugated fluorophores of secondary antibodies**			
A	DAPI	GFP, Alexa488	COUP-TFII, Cy3	Reelin, Alexa647
B	DAPI	GFP, Alexa488	NOS, Cy3	SOM, Alexa647
C	VIP, AMCA	GFP, Alexa488	CR, Cy3	GAD67, Alexa647

Table 2.1: Primary and secondary antibody combinations for each stereology protocol

The superficial motor cortex of each section was imaged using an epifluorescence microscope as above with a 20x objective lens with ApoTome using Stereo Investigator software. Systematic random sampling was carried out using the optical fractionator method (Bjugen and Gundersen, 1993). The probe depth was 8µm, with a 2µm guard zone above the probe and 1µm interval between optical sections. The grid size and counting frame were 350µm x 250µm. Contours were drawn around L1 motor cortex, including both M1 and M2, using DAPI or GAD67 as a guide for the ventral L1 border, and a mouse brain atlas (Paxinos & Franklin, 2001) for a guide to the medial and lateral borders. Only GFP+ neurons indicating Cre-

expressing NDNF+ neurons within L1 motor cortex were counted. Neurons were counted if the point at which the nucleolus (marked by DAPI for protocol A and B) first appeared was within the probe, or the top of the neuron (marked by GFP for protocol C). Cells touching the green inclusion line on the counting frame were included, and those touching the red exclusion line excluded. Numbers of each marker combination were counted, and the proportion as a percentage of total GFP neurons within each protocol for each animal were calculated.

2.2.7 Rabies virus tracing of monosynaptic thalamic input to L1 NDNF+ motor cortical neurons

To identify monosynaptic thalamocortical inputs to L1 NDNF+ and L5 RBP4+ motor cortical neurons, rabies virus tracing was carried out (Wickersham et al., 2007; Wall et al., 2010; Callaway and Luo, 2015). In this method, the retrograde nature of transport of rabies virus (RV) is harnessed and adapted to retrogradely label monosynaptic inputs to a genetically defined population, such as Cre-expressing neurons in a Cre mouse line. The rabies virus, also known as rhabdovirus, is modified to have a glycoprotein (G) necessary for transsynaptic spread deleted and instead replaced with code for EGFP or another fluorescent reporter protein. The glycoprotein is inserted into another virus, referred to as the helper virus. This typically also has a fluorescent reporter protein, such as RFP, or in our case a V5 tag for identification. This helper virus is Cre-dependent, and when it is injected into a brain region, it transfects Cre-expressing cells, and expresses both G and TVA, an avian receptor protein not present in mammals. The modified rabies virus is pseudotyped with the envelope protein ASLV type A (EnvA) which recognises TVA and requires it for entry into cells. In this way, subsequently injected RV into the same area will specifically infect Cre+ cells with TVA. Since

the G protein is supplied by the helper virus in these cells, the RV is able to spread retrogradely, but only monosynaptically as the presynaptic neuron does not contain the G protein, restricting further spread.

Monosynaptic retrograde rabies tracing was performed in NDNF-Cre and RBP4-Cre mice. 550nl of helper virus (AAV5-EF1a-DIO-TVA/V5-2A-RG, Table S1) was injected superficially into L1 motor cortex or into L5 motor cortex as described. Three weeks later, 60nl of G-deleted rabies virus (SAD-DG-GFP[EnvA], Table S1) was injected with a standard vertical injection. Rabies and helper viruses were provided by Konstantinos Meletis (Karolinska Institute, Stockholm, Sweden; Lazaridis et al., 2019; Ährlund-Richter et al., 2019). After injection with the rabies virus, mice were housed individually and handled with caution to prevent potential cross-infection of other animals, according to institutional regulations. Mice were monitored daily for 7 days after the second surgery to ensure there were no adverse effects from the rabies virus including potential weight loss and perfused after 7 days. For tracing inputs to L1, n = 4 NDNF-Cre mice were used. Additional injected NDNF-Cre mice were discarded from further analysis because there were either a negligible number of starter cells, or the tissue was damaged prior to histological analysis. For tracing inputs to L5, n = 5 RBP4-Cre mice were used.

Brains were cut into 50µm coronal sections. Sections from each animal were numbered consecutively, and starting sections were selected at random by using a randomly generated number to avoid bias. Every 1 in 2 cortical sections thereafter spanning the entire rostral-caudal axis of motor cortex were analysed for quantification of starter neurons in NDNF-Cre mice, and every 1 in 4 sections for RBP4-Cre mice as the starter cell labelling was more abundant in these mice. The native fluorescence of GFP-labelled rabies virus neurons was

enhanced with a primary antibody to GFP and an AlexaFluor488-conjugated (Alexa488) secondary antibody, and the V5-tagged TVA helper virus was visualised with an antibody to V5, and a Cy3-conjugated secondary antibody. Cortical layers were delineated using DAPI to mark the L1/L2 boundary and an antibody to Necab1 to delineate L4 for NDNF-Cre mice. In RBP4-Cre mice, cortical layers 4 and 6 were delineated by antibodies to Necab1 and FoxP2. Images of sections were acquired on an epifluorescence microscope with Stereo Investigator for all areas containing V5 labelling. A 10µm stack with an additional 2µm guard zone was acquired for each frame at 20x with Apotome. Contours were drawn manually to demarcate cortical layers and the boundary between motor cortex and adjacent regions. Quantification of starter neurons per subdivision was carried out offline on Stereo Investigator with a similar method to that used for the neurochemical characterisation of L1 NDNF+ neurons. Neurons which expressed both GFP and V5 were designated starter neurons. Starter cells were counted if the top of the cell, as identified by V5, was within the 10µm probe. The grid size and counting frame were 350µm x 250µm. Cells touching the green inclusion line on the counting frame were included, and those touching the red exclusion line excluded.

Rabies-labelled thalamic input neurons were quantified in a similar method to starter neurons. Rabies-labelled neurons were also present in cortex and extra-thalamic subcortical regions, but only the thalamic neurons were quantified. GFP fluorescence from rabies-labelled thalamic neurons was enhanced with a primary antibody to GFP and an Alexa488-conjugated secondary antibody, and the thalamus parcellated by manually drawing contours with the aid of GAD67 and CB immunohistochemistry along with the Paxinos mouse atlas (Franklin and Paxinos, 2008) prior to quantification of rabies-labelled input neurons. GAD67 immunofluorescence was used to delineate basal ganglia-recipient thalamus (Kuramoto et al., 2011). For NDNF-Cre brains, GFP+ neurons were counted offline for each thalamic

subdivision for 1 in 2 sections within a 10µm probe and with a grid size and counting frame of 350µm x 250µm. Neurons were counted if the top, as defined by GFP immunofluorescence, first appeared within the probe, without touching any exclusion lines. As the numbers of starter neurons and hence input neurons were low, input neurons within the whole depth of the section rather than just those within 10 µm were subsequently counted. For RBP4-Cre brains, 1 in 4 thalamic sections were used for sampling with neurons counted within 10µm probes following the same method as described for NDNF-Cre.

To calculate estimated total numbers of starter cells or rabies cells in each layer of motor cortex of thalamic nucleus, the absolute cell counts for starter and rabies cells in RBP4-Cre mice were multiplied by 20, and in NDNF-Cre mice by 10 for starter cells and by 2 for rabies cells (Figs. 2.9D,E; 2.14B,C).

2.3 RESULTS

2.3.1 NDNF-Cre mouse line preferentially labels L1 cortex

The NDNF-Cre mouse line (Tasic et al., 2016) is a knock-in mouse expressing Cre recombinase directed by the endogenous NDNF promoter, with an IRES2 sequence allowing for preserved expression of NDNF. The mouse is designed to be trimethoprim-inducible, but trimethoprim was not used as Cre recombinase activity was reported to be effective in its absence (Tasic et al., 2016)

Using the standard vertical injection protocol to inject an AAV-GFP virus superficially in cortex of the NDNF-Cre mouse, GFP-labelled NDNF-positive (NDNF+) neurons were primarily observed in L1 in contrast to deeper cortical layers (Fig. 2.2 A-B). Somata and neuropil of NDNF+ neurons were present spanning rostral to caudal motor cortex, as well as adjacent

areas such as somatosensory, cingulate, and prefrontal cortices (Fig. 2.2A-C). The morphology of the neurons was similar to that of ENGCs, with a small soma in L1 and dense axonal projections mainly within L1 and spanning multiple cortical columns. The somata tended to be more densely located in L1a than L1b, as with ENGCs (Schuman et al., 2018). Labelling was visible with native GFP fluorescence, but the brightness was increased by incubation with a GFP antibody and a fluorophore-conjugated secondary antibody. Labelled anterograde projections were present in striatum as well as in ipsilateral and contralateral cortex. Due to the technical challenge of injecting virus into L1 cortex, neurons in deeper layers were also labelled at the injection site (Fig. 2.2B). This was because the site of injection was deeper than L1 to allow diffusion of a sufficiently large volume of virus into cortex and minimise reflux. However, adjacent to the injection site, L1 was preferentially labelled. The L1/L2 border could be delineated by the fluorescent nuclear stain DAPI, as the L1 cell density is sparser than in deeper layers. The majority of GFP-labelled neurons were within this region, confirming L1 selectivity (Fig. 2.3A). L1 selectivity was further confirmed by its relative absence from L2/3, as delineated by wolframin (WFS1) immunofluorescence (Shrestha et al., 2015) (Fig. 2.3C), and L1a selectivity by localisation of GFP-labelled neurons within the superficial region of vGluT2 immunofluorescence (Fig. 2.3B), which is more abundant in L1a than L1b and L2 (Kawaguchi, 2017).

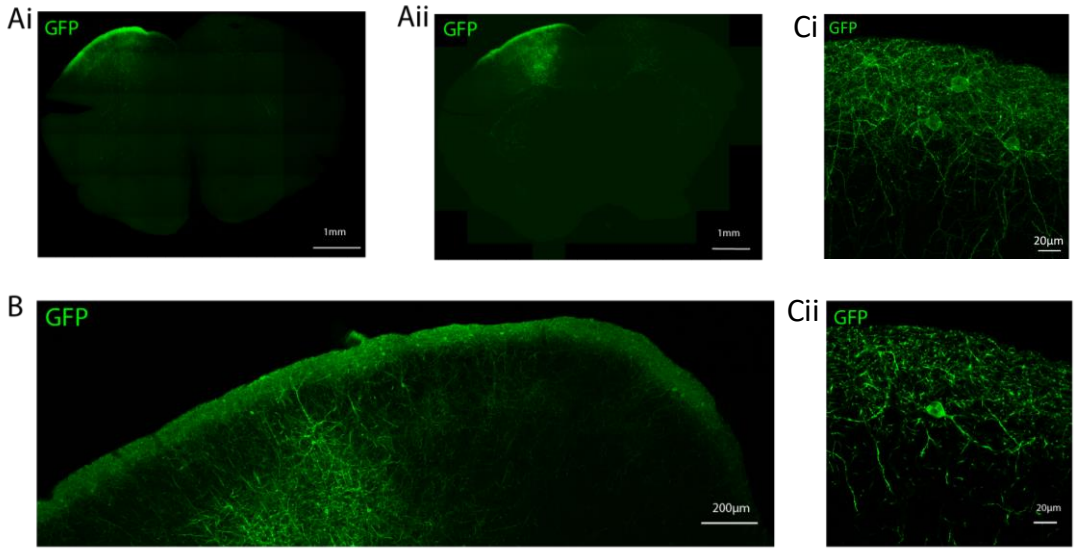


Figure 2.2 NDNF-Cre mouse line allows preferential labelling of L1 cortex
(A) AAV-GFP in L1 of motor cortex of an NDNF-Cre mouse reveals L1 in rostral (Ai) and caudal (Aii) motor cortex. Approximate Bregma coordinates are 2.22 and 0.98mm AP respectively. **(B)** Some neurons in deep layers have also been labelled, but these are relatively restricted compared to L1 labelling which extends bilaterally from the injection site. **(C)** Multiple GFP-labelled neurons in L1 motor cortex (Ci) and a single GFP-labelled NDNF+ neuron along with neuropil from other neurons in L1 motor cortex (Cii).

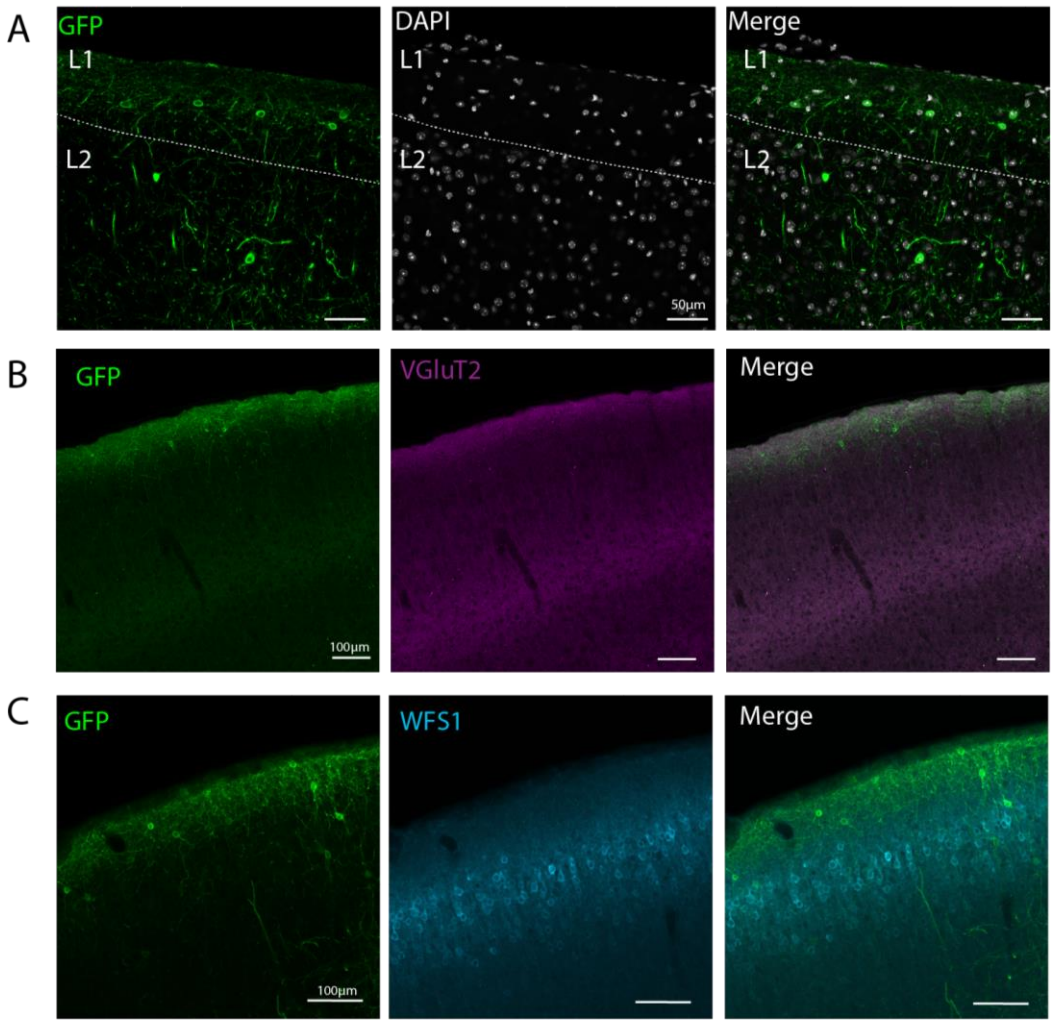


Figure 2.3 Immunohistochemistry showing L1 specificity of NDNF-Cre mouse line
(A) DAPI staining allows demarcation of the L1/L2 border, due to a lower cell density in L1 than L2 (centre panel). NDNF+ (GFP-labelled) cell bodies and fibres are denser in L1 than L2 (left and right panels). **(B)** vGluT2 immunofluorescence overlaps with NDNF+ neurons in L1a cortex. **(C)** NDNF+ neurons are located dorsal to WFS1 immunofluorescence in L2/3.

2.3.2 Neurochemical characterisation of L1 motor cortical NDNF+ neurons

After confirming the L1 preference of Cre-expressing neurons in the NDNF-Cre mouse line, the neurochemical profile of these neurons within motor cortex were tested to ensure they were of a consistent cell type in this regard. This has been done by single-cell RNA sequencing (Tasic et al., 2016) as well as by immunohistochemistry. Since subsequent planned experiments consisted of anatomical tracing, it was important to establish a relative homogeneity of the neurons under investigation using histological methods. The Cre-positive

neurons in L1 motor cortex of the NDNF-Cre mouse line were characterised using immunohistochemistry to identify the presence or absence of common interneuron markers and this was quantified with stereological counting (Table 2.1). Almost all GFP-labelled NDNF+ neurons co-expressed GAD67, consistent with being GABAergic interneurons, apart from two neurons in one animal, which were CR+ (Fig. 2.7A). A few NDNF+ neurons co-expressed CR but not GAD67. These had a distinctive shape of a small oval-shaped cell body with a single horizontal projection, matching the morphology described for Cajal-Retzius cells (Villar-Cervino and Marín, 2012).

The majority of L1 NDNF+ neurons did not express vasoactive intestinal peptide (VIP), neuronal nitric oxide synthase (NOS), somatostatin (SOM) and calretinin (CR) (Figs. 2.5, 2.6, 2.7A,C). All neurons counted were negative for VIP and SOM, and almost all were negative for NOS. Overall, these results demonstrate that L1 NDNF+ neurons in motor cortex are in a different group of interneurons from VIP and SOM interneurons, other common interneuron markers. Out of the NDNF+ neurons tested for chicken ovalbumin upstream transcription factor II (COUP-TFII) and reelin, 79.5% of labelled neurons averaged across three animals expressed both COUP-TFII and reelin, with 11.9% COUP-TFII+/reelin-, and 5.6% COUP-TFII-/reelin+ (Fig. 2.7B). Only 2% were negative for both COUP-TFII and reelin. 85% of NDNF+ neurons in total expressed reelin. Results were similar across all three animals (Fig. 2.7). These findings are in line with a previous study investigating the molecular profile of NDNF positive neurons using transcriptomics (Tasic et al., 2016). The high expression of COUP-TFII in L1 NDNF+ neurons is a novel finding but has been reported in neocortical and hippocampal NGF neurons (Miyoshi et al., 2010; Overstreet-Wadiche et al., 2015). A large proportion of cortical interneurons express parvalbumin (PV), however as PV is completely absent from

interneurons in L1 (Xu et al., 2010) this was not included in stereological characterisation after confirming with trial experiments (data not shown).

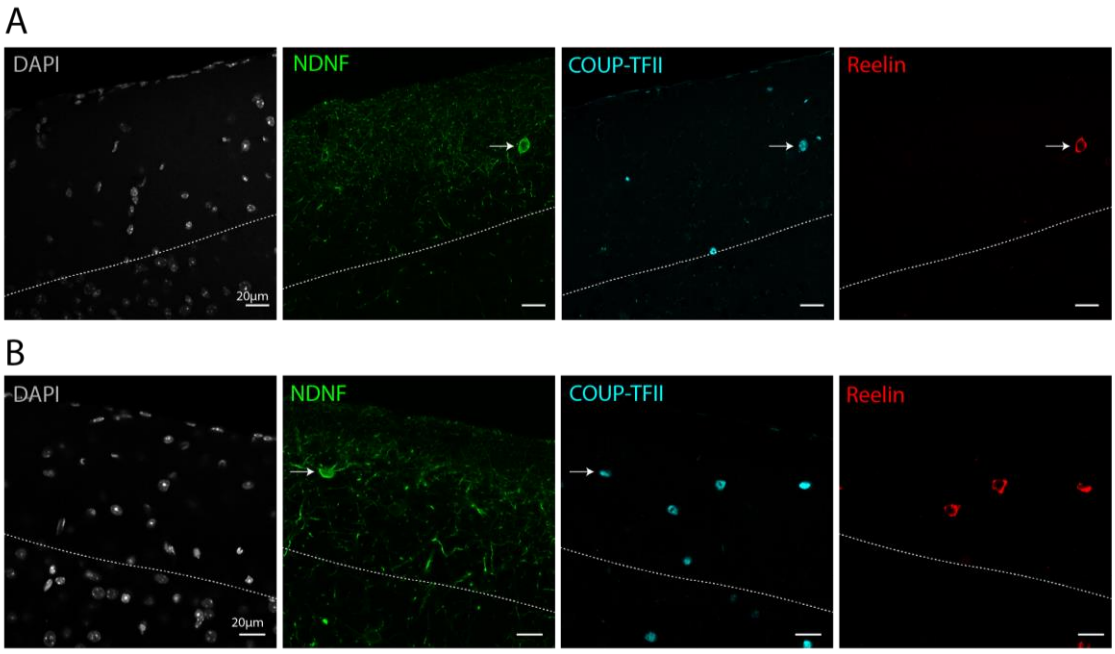


Figure 2.4 NDNF+ neurons in mouse L1 motor cortex mostly co-express COUP-TFII and Reelin
Immunofluorescence signals for DAPI, NDNF, COUP-TFII and Reelin. **(A)** An example of a L1 NDNF+ neuron expressing COUP-TFII and reelin (arrows). **(B)** An example of a L1 NDNF+ neuron expressing COUP-TFII but not reelin (arrows).

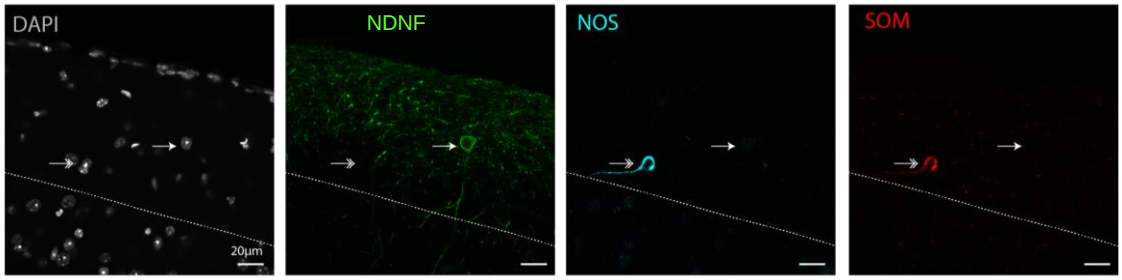


Figure 2.5 Most NDNF+ neurons in mouse L1 motor cortex do not express NOS and SOM.
Immunofluorescence signals for DAPI, NDNF, NOS and SOM. An example of a L1 NDNF+ neuron which is NOS and SOM-negative (single arrowheads). An example of a L1 NDNF- neuron which expresses both NOS and SOM (double arrowheads).

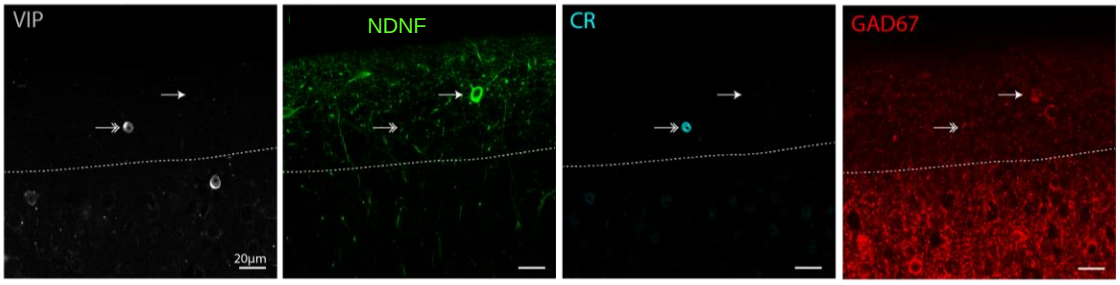


Figure 2.6 NDNF neurons in mouse L1 motor cortex almost exclusively co-express GAD67, but not VIP and CR
Immunofluorescence signals for VIP, NDNF, CR and GAD67. Single arrowheads show GAD67+/NDNF+ neurons, which are CR-VIP-. Double arrowheads show a NDNF-/GAD67+/VIP+/CR+ neuron.

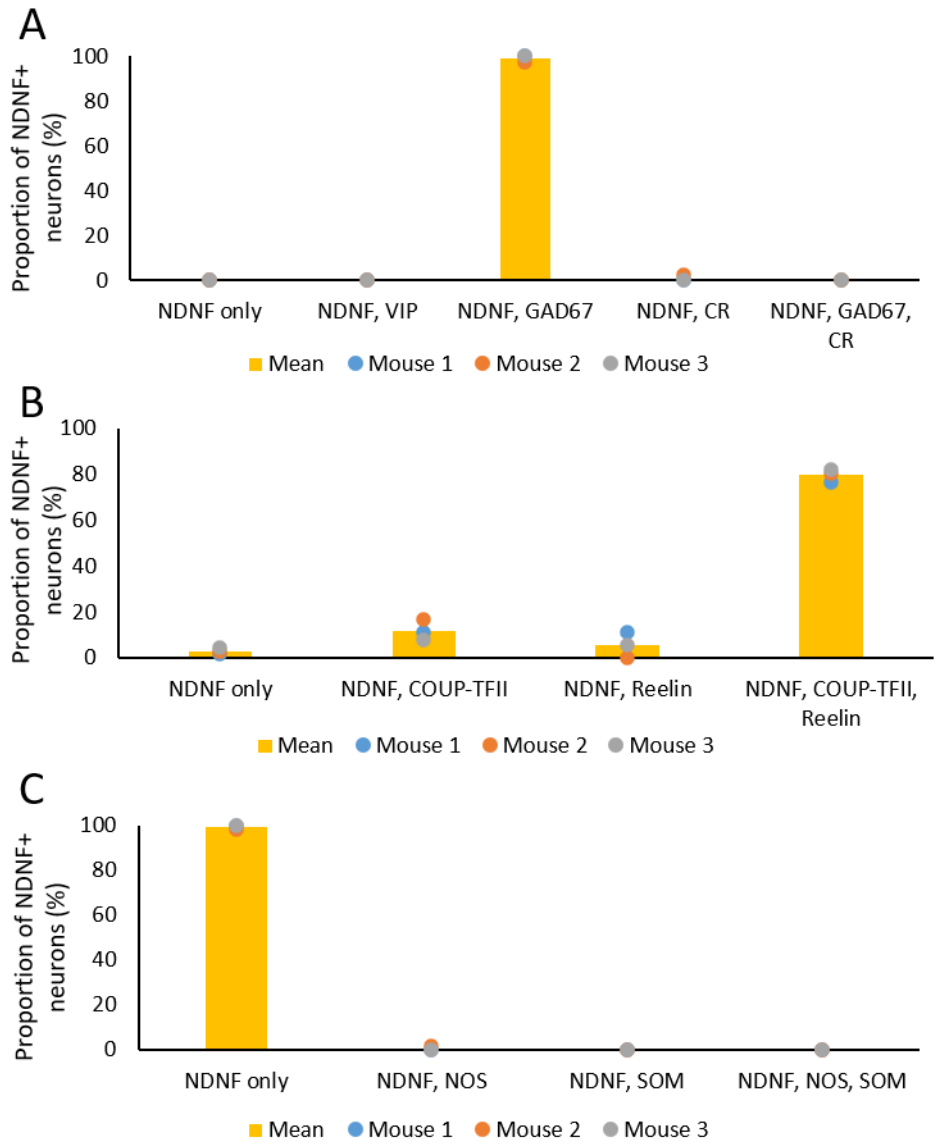


Figure 2.7 Distribution of neurochemical markers in L1 NDNF+ motor cortical neurons
(A) Mean proportion of L1 motor cortical NDNF+ neurons expressing combinations of GAD67, VIP and CR (n = 3). 99% of NDNF+ neurons express GAD67 but not CR or VIP. Total number of counted neurons for each animal: n = 12, 76, 42. **(B)** Mean proportion of NDNF+ neurons expressing combinations of COUP-TFII and Reelin. 79% of neurons express both COUP-TFII and reelin. 12% are COUP-TFII+/reelin-, and 6% are COUP-TFII-/reelin+. 3% of NDNF+ neurons do not express COUP-TFII or reelin. Total number of counted neurons for each animal: n = 63, 102, 88. **(C)** Mean proportion of NDNF+ neurons expressing combinations of NOS and SOM. Almost all neurons (99%) did not express detectable NOS or SOM, with <1% expressing NOS. Total number of counted neurons for each animal: n = 50, 120, 71.

2.3.4 RBP4-Cre mouse line preferentially labels L5 cortex

RBP4-Cre mice were injected with a Cre-dependent AAV-GFP virus, to confirm cortical L5 selectivity. As expected, numerous pyramidal neurons were labelled throughout L5 with apical dendrites terminating in superficial layers (Fig. 2.8).

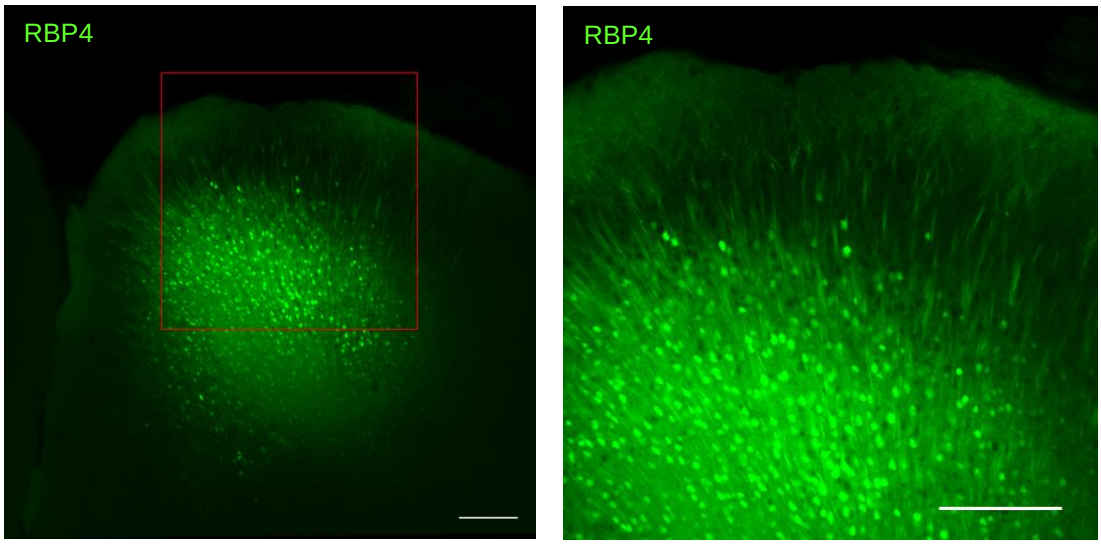


Figure 2.8 RBP4-Cre mouse line allows preferential labelling of L5 cortex
Left: AAV-GFP extensively labels neurons in L5 of RBP4-Cre mouse M2, cingulate and prelimbic cortex. Apical dendrites terminate in superficial layers. Right: Expanded image of outlined region. Scalebars are 200µm.

2.3.5 Different thalamic regions preferentially innervate L1 and L5 motor cortical neurons

In order to identify and compare thalamic inputs to NDNF+ neurons in L1 motor cortex and to RBP4+ neurons in L5 motor cortex, monosynaptic retrograde tracing with rabies virus was carried out. As described in the methods section, four NDNF-Cre mice were injected unilaterally with rabies and helper viruses in L1 of motor cortex, while five RBP4-Cre mice were injected unilaterally with rabies and helper viruses in L5 of motor cortex.

Starter cells in NDNF-Cre mice were mostly (58%) in L1 of motor cortex (Fig. 2.9A,C,D). The rest were in deeper layers, with 19% in L2/3, 4% in L4 and 18% in L5/6. An average of 31.5 starter neurons were counted per animal, within a 10µm stack from every 1 in 2 50µm coronal

sections throughout rostral to caudal motor cortex. An estimated average of 180 starter cells per animal were in L1 (Fig. 2.9D). Most starter cells in RBP4-Cre mice were in L5 (72%) of motor cortex (Fig. 2.9B,C,E). There were few starter cells in L1-3 (2%) and L6 (3%), and a larger proportion in L4 (23%). An average of 264 starter neurons were counted per RBP4-Cre mouse, within a 10μm stack from 1 in 4 50μm motor cortical sections, with an estimated total number of L5 starter neurons of 3780 per animal (Fig. 2.9E).

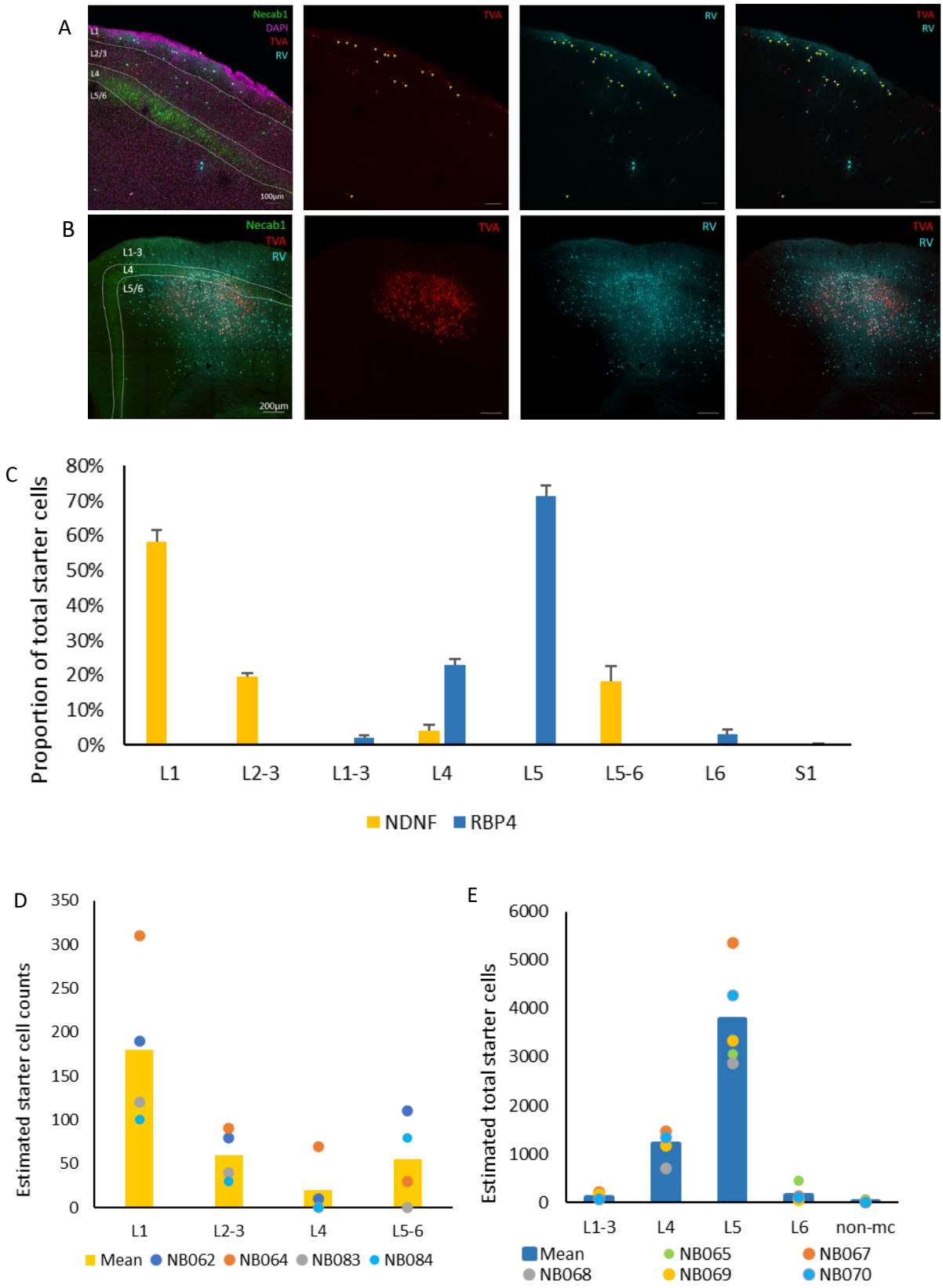


Figure 2.9 Laminar distribution of rabies starter neurons in cortex

(A) Starter neurons in an NDNF-Cre mouse are mainly located in L1. The L1/2 boundary is delineated by DAPI, and L4 is delineated by strong Necab1 immunofluorescence. **(B)** Starter neurons in RBP4-Cre mouse are mainly located in L5. L4 is delineated by Necab1 immunofluorescence. Scalebars in (A) and (B) are 100µm. **(C)**

Proportion of starter cells in each layer of motor cortex in NDNF-Cre (n = 4) and RBP4-Cre (n = 5) mice. Most starter cells were in L1 in NDNF-Cre mice, and in L5 in RBP4-Cre mice. A small number of starter cells were in S1 in one RBP4-Cre mouse. Bars represent mean proportion across animals and error bars represent SEM. **(D)** Mean numbers of starter cells in each layer in NDNF-Cre mice and numbers from individual animals, estimated from cell counts. The mean number of starter cells in L1 was 180 ± 24 (SEM). **(E)** Mean and individual animal numbers of starter cells in each layer in RBP4-Cre mice, estimated from cell counts. The mean number of starter cells in L5 was 3780 ± 464 (SEM).

Retrogradely labelled neurons were present in both cortical and subcortical regions in NDNF-Cre and RBP4-Cre mice. In NDNF-Cre mice, there were mainly ipsilateral and sparse contralateral labelled neurons in cortex. The ipsilateral neurons were mostly in motor and somatosensory cortex, in L1 and deeper layers (Fig. 2.9A). In RBP4-Cre mice, retrogradely labelled cortical neurons were abundant especially in L2/3 and L5 of ipsilateral motor and somatosensory cortex, as well as in contralateral cortex (Fig. 2.9B). The vast majority of subcortical retrogradely labelled neurons in NDNF-Cre and RBP4-Cre mice were ipsilateral. In both NDNF-Cre and RBP4-Cre mice, most subcortical RV neurons were in thalamus, with a few in basal ganglia and other regions.

Rabies-labelled thalamic neurons in NDNF-Cre and RBP4-Cre mice were quantified. For RBP4-Cre mice, this was within a 10µm stack in every 1 in 4 thalamic sections, resulting in an average of 140 neurons (standard deviation (SD) = 55.46) counted per mouse. For NDNF-Cre mice, input neurons within a 10µm stack in every 1 in 2 sections were counted. However, as the numbers of starter cells and input neurons were much lower than in RBP4-Cre mice, neurons in the whole depth of the section in every 1 in 2 sections were counted. This resulted in an average of 37.75 (SD = 30.65) thalamic input neurons counted per mouse. Thalamic regions were delineated by immunohistochemistry and an atlas (Franklin and Paxinos, 2008). Similar to in rat, GAD67 immunofluorescence strongly labelled the neuropil in VM and other regions, but vGluT2 was less effective in demarcating VL as there was not a sufficiently clear difference

in immunofluorescence between VL and surrounding nuclei. Instead, a combination of GAD67 and CB were used to help deduce thalamic nuclei boundaries.

The largest proportion of retrogradely labelled thalamic neurons in NDNF-Cre mice was in ventral medial thalamus (VM) (44%), with an average of 34 estimated total labelled input neurons per animal, which was more than twice as much as any other thalamic region and was consistent across animals (Figs. 2.10 and 2.14A,B). VM and VA together form the basal ganglia-recipient zone or inhibitory zone of motor thalamus (Kuramoto et al., 2009). Interestingly, relatively few VA neurons (2.4%) were labelled compared with VM (Fig. 2.11), suggesting that their output may be more targeted to pyramidal neurons than NDNF+ interneurons in L1 of the injected motor cortical region. As expected, the cerebellar recipient region of motor thalamus, ventral lateral thalamus (VL), sent fewer inputs (8%) than VM to L1 motor cortical NDNF+ interneurons, with an average of 6 estimated input neurons per animal. The intralaminar nuclei, CM, PC and CL, grouped together for the purposes of analysis, contributed 14% of labelled thalamic inputs. The posterior thalamic nucleus (Po) contributed a similar proportion of inputs (15%). Anteromedial thalamus (AM), part of the anterior thalamic nuclei group, contained 12% of thalamic input neurons (Fig. 2.11). Of these main thalamic nuclei, higher order nuclei (VM, Po, CM/PC/CL and MD) contributed a greater proportion of L1 innervation, 73% of thalamic inputs, than first order nuclei (VL, AM, AV, VPL/VPM), which contributed 21% of thalamic inputs. There were a few input neurons in other thalamic nuclei, as well as non-thalamic subcortical regions such as GPi. A caveat to these findings is the location of a large minority of starter cells in deeper layers than L1, despite the targeted injections, so it is impossible to conclude that all rabies-labelled neurons innervate L1 NDNF+ neurons. It is possible that some of the other thalamic nuclei apart from VM project to these deeper layer neurons, along with cortico-cortical neurons.

The distribution of thalamic input neurons to L5 RBP4+ neurons was different from the distribution in NDNF-Cre mice. Whereas VM was the major thalamic source of L1 NDNF+ neuron innervation, VL was the main source of thalamic input to L5 RBP4+ motor cortical neurons (35%, Figs. 2.12 and 2.14). The intralaminar nuclei, CM, PC and CL provided about a quarter (24%) of thalamic inputs (Figs. 2.12 – 2.14). Many of these neurons were close to the border between PC, CL and VL, which was delineated by GAD67 and CB immunofluorescence, and the Paxinos atlas. VM contained 12% of inputs, Po contained 9%, parafascicular nucleus (PF) contained 8%, and AM contained 4%. Medial and lateral ventral posterior nuclei (VPM and VPL) contributed 3% of input neurons (Fig. 2.14). There were also a few neurons in other thalamic nuclei, as well as in extra-thalamic regions, especially GPe and GPi, and including striatum, zona incerta and SNr.

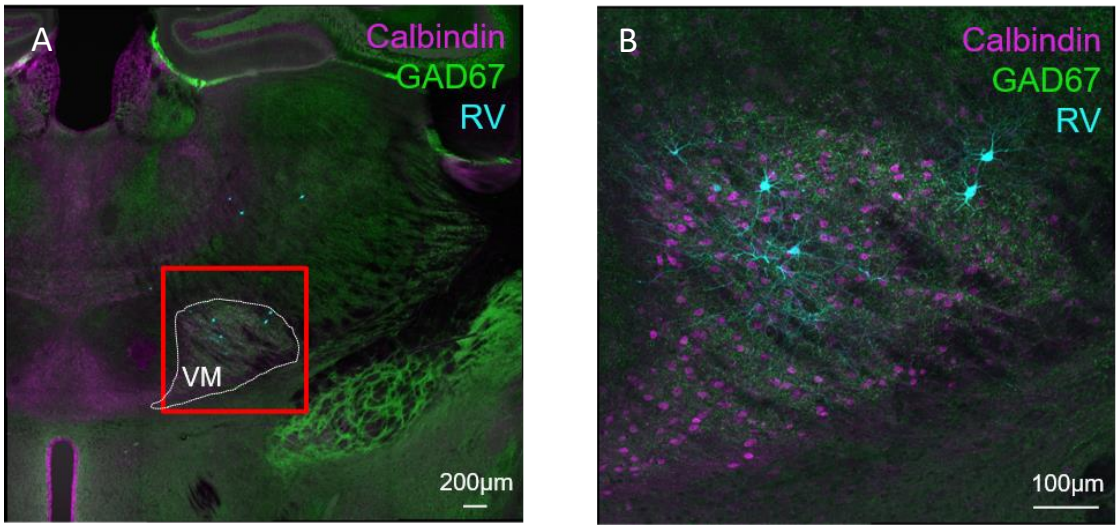


Figure 2.10 VM thalamocortical neurons innervate L1 NDNF+ motor cortical interneurons
(A) Rabies-labelled input neurons in VM of an NDNF-Cre mouse. VM is identified by strong GAD67 and calbindin immunofluorescence. Input neurons are also present in CM/PC/CL, Po and VL thalamus. **(B)** Higher magnification image of highlighted region in (A).

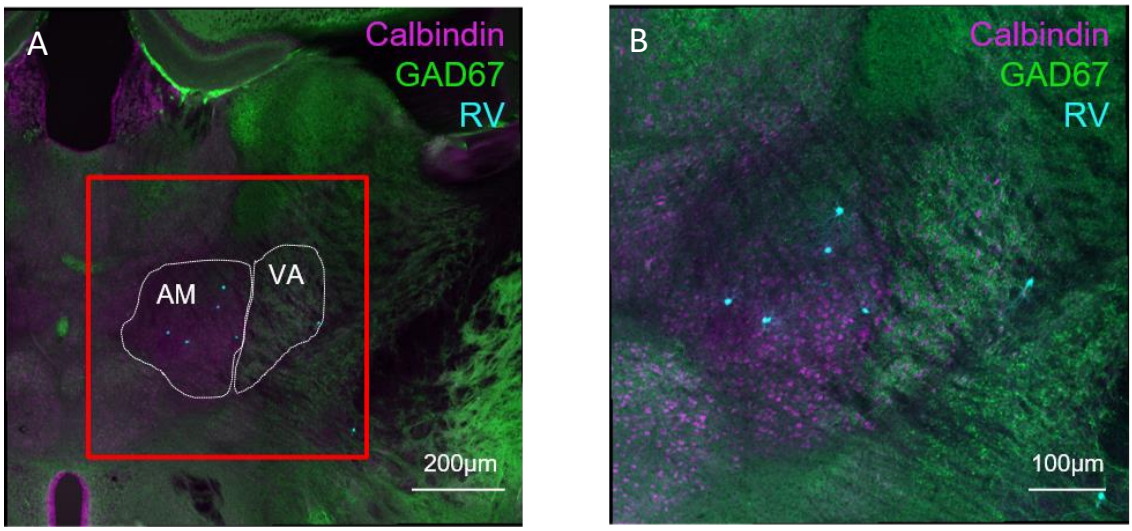


Figure 2.11 AM and VA thalamocortical neurons innervate L1 NDNF+ motor cortical interneurons
(A) Multiple rabies-labelled input neurons in AM and a single input neuron in VA of an NDNF-Cre mouse. AM and VA are identified by weak and strong GAD67 immunofluorescence, respectively. A single input neuron is also present at the border of lateral hypothalamus and internal capsule. **(B)** Higher magnification image of highlighted region in (A).

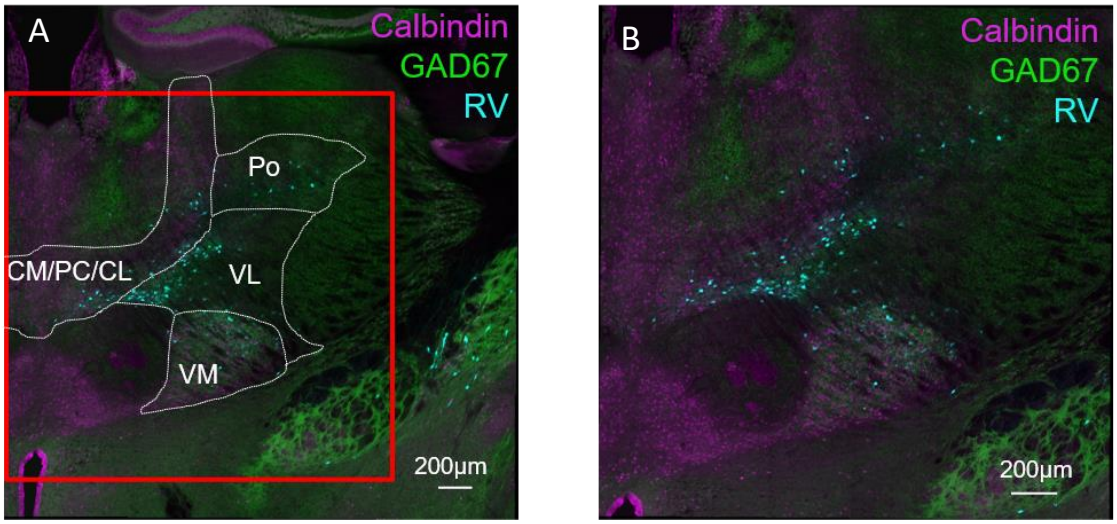


Figure 2.12 VL, CM/PC/CL, VM and Po thalamocortical neurons innervate L5 RBP4+ motor cortical neurons
(A) VL and CM/PC/CL contain multiple input neurons to L5 neurons in an RBP4-Cre mouse. VL is defined by atlas boundaries and a lack of GAD67 immunostaining. There are also input neurons in Po, VM and MD as well as GPe and GPi. **(B)** Higher magnification image of highlighted region in (A).

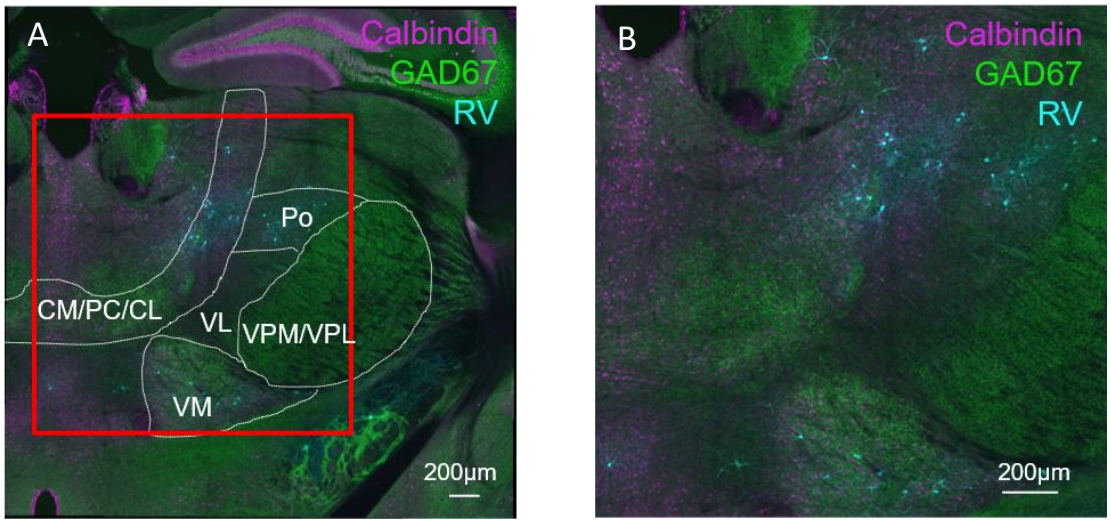


Figure 2.13 CL, Po and VM thalamocortical neurons innervate L5 RBP4+ motor cortical neurons
(A) CL, Po and VM contain input neurons to L5 neurons in an RBP4-Cre mouse. VL is defined by atlas boundaries and a lack of GAD67 immunostaining. There are also individual input neurons in submedius thalamic nucleus and reuniens and in lateral MD and lateral habenula. **(B)** Higher magnification image of highlighted region in (A).

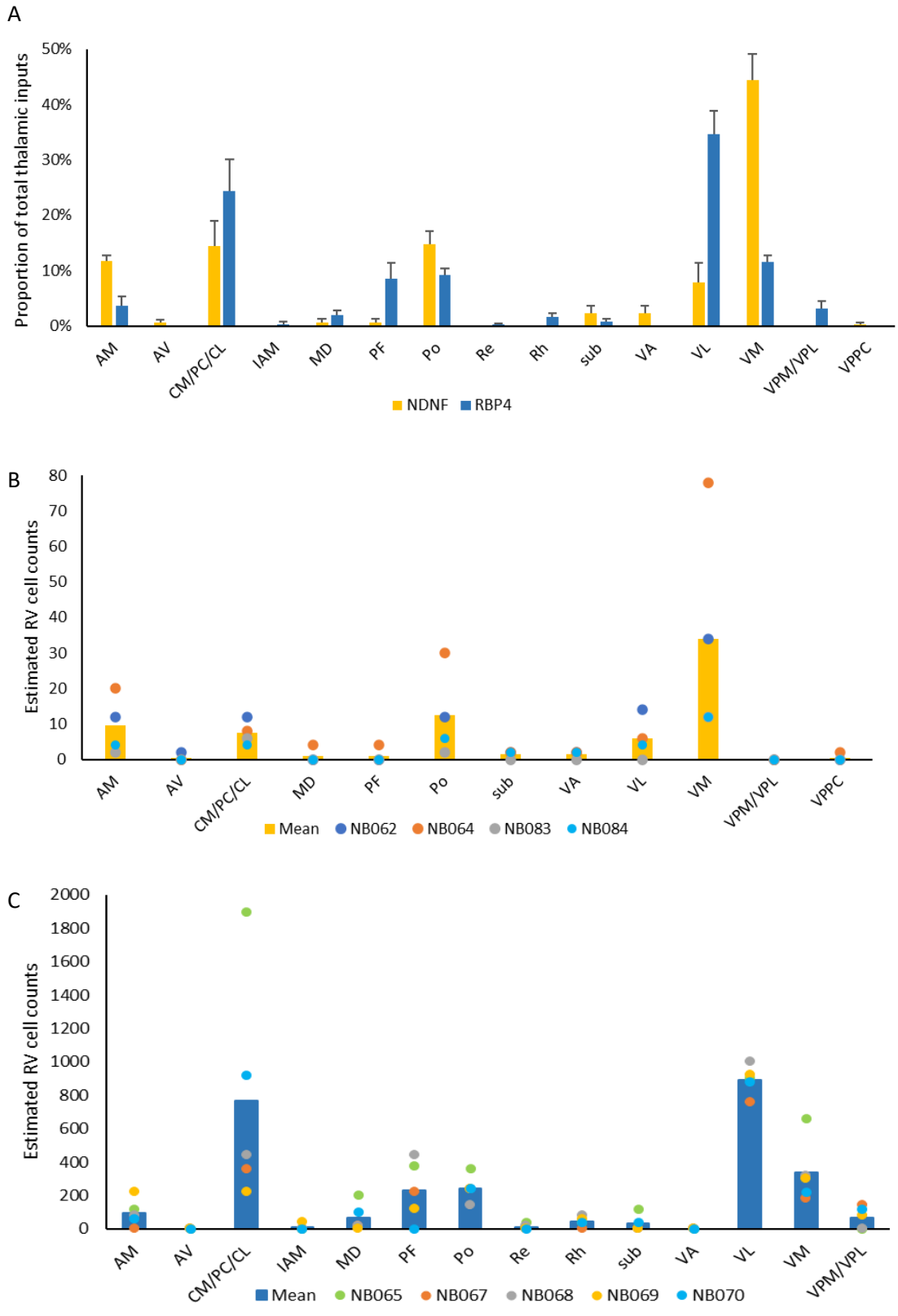


Figure 2.14 Thalamic distribution of monosynaptic inputs to L1 and L5 motor cortical neurons
(A) Proportion of rabies-labelled thalamic input neurons per thalamic region in NDNF-Cre (n = 4) and RBP4-Cre (n = 5) mice. The thalamic nucleus with the largest proportion of input to L1 in NDNF-Cre mice was VM (44%), followed by Po (15%), CM/PC/CL (14%), AM (12%) and VL (8%). In contrast, the thalamic nucleus with the largest proportion of input to L5 in RBP4-Cre mice was VL (35%), followed by CM/PC/CL (24%), VM (12%), Po (9%) and PF (8%). Input neurons to L5 were quantified from stereological counting in 1 in 4 thalamic sections. Input

neurons to L1 were quantified by counting every neuron in 1 in 2 thalamic sections, due to relatively low numbers. Bars represent mean proportion across animals and error bars represent SEM. **(B)** Mean estimated numbers of rabies-labelled thalamic input neurons in NDNF-Cre mice. Mean counts for VM they were 34 ± 16, and for VL they were 6 ± 3. **(C)** Mean estimated numbers of rabies-labelled thalamic input neurons in RBP4-Cre mice. Mean counts for CM/PC/CL were 768 ± 307, for VL they were 892 ± 39, and for VM they were 336 ± 85.

Abbreviations: anterdorsal thalamic nucleus (AD), anteromedial thalamic nucleus (AM), anteroventral thalamic nucleus (AV), central medial thalamic nucleus (CM), centrolateral thalamic nucleus (CL), interanteromedial thalamic nucleus (IAM), mediodorsal thalamic nucleus (MD), parafasicular (PF), posterior thalamic nuclear group (Po), reuniens (Re), rhomboid (Rh), submedius thalamic nucleus (Sub), ventral anterior (VA), ventrolateral (VL), ventromedial (VM), ventral posterolateral thalamic nucleus (VPL), ventral posteromedial thalamic nucleus (VPM).

2.4 DISCUSSION

On the basis of published literature and our observations, it is fair to consider that cortical L1 NDNF+ neurons are elongated neurogliaform cells (ENGCs). The results of these anatomical tracing experiments demonstrate that different thalamic nuclei preferentially innervate L1 NDNF+ interneurons and L5 RBP4+ pyramidal neurons in motor cortex of the mouse. Significantly, this shows for the first time that L1 interneurons in motor cortex receive direct thalamic innervation, in addition to cortical input, and that thalamocortical neurons target interneurons within motor cortical L1 as well as apical pyramidal cell dendrites. These findings refine our knowledge of motor thalamocortical circuitry and stimulate further questions regarding the physiological function of such pathways.

2.4.1 Neurochemical characterisation of L1 NDNF+ motor cortical neurons

To investigate the anatomical thalamic connections to ENGCs, it was necessary to be able to reliably identify and target these neurons. The Ndnf-IRES2-dgCre-D mouse seemed a good candidate for this, as L1 NDNF+ neurons in V1 in this mouse line display molecular, morphological and physiological characteristics of ENGCs (Tasic et al., 2016). More recently, the use of this and another NDNF-Cre line (Schuman et al., 2018) have become more widespread, for example having also been used to target L1 ENGCs in auditory cortex (Abs et

al., 2018) and prefrontal cortex (Anastasiades et al., 2020). L1 selectivity of this mouse line was confirmed by GFP labelling revealing a higher density of NDNF+ neurons and neuropil in L1a than L1b and deeper layers within motor cortex. NDNF+ neurons deeper than L1 may be neurogliaform (NGF) cells rather than ENGCs (Overstreet-Wadiche and McBain, 2015).

Before tracing inputs to L1 NDNF+ cells, it was important to establish whether these neurons belonged to a single interneuron subtype. From the neurochemical characterisation of L1 NDNF+ neurons in motor cortex, these neurons tend to be relatively consistent in their expression of molecular markers, indicating that this is one subtype of GABAergic interneuron. The majority, but not all, of L1 motor cortical NDNF+ neurons expressed both COUP-TFII and reelin (79%), and most were VIP-/CR-/NOS-/SOM-, as well as PV- since this is absent from all L1 neurons. These results were consistent across three animals. All cells were GABAergic apart from two exceptions, which were judged to be non-NGCs, by their morphology. These results reinforce the findings from single cell transcriptomics, which positively correlated NDNF+ cells with the expression of reelin and negatively for VIP, NOS and SOM, with a low CR expression level (Tasic et al., 2016). We have now also shown this at the single cell level in sectioned brain tissue. We also have identified COUP-TFII as being expressed in approximately 97% of NDNF+ L1 neurons. Reelin+, VIP- and SOM- neurons constitute a large majority of GABAergic interneurons in L1 (Rudy et al., 2011). Reelin and VIP are never co-expressed in interneurons arising from the caudal ganglionic eminence, where ENGCs originate (Miyoshi et al., 2010), and we have also observed this lack of co-expression in our labelled neurons. By observation, the size and morphology of NDNF+ neurons appeared consistent. Furthermore, the NDNF+ neurons were all VIP-, whereas the other main L1 interneuron type, SBCs, express VIP (Garcia-Munoz & Arbuthnott, 2015). This would indicate that they are ENGCs rather than SBCs, and that no SBCs express NDNF. By their location in L1,

morphology and molecular characterisation, we therefore propose that these NDNF+ neurons are ENGCs, as defined morphologically. As the main aim was to establish the consistency of the labelled cell type, only NDNF+ neurons identified by GFP were analysed, rather than all L1 neurons. However, it would be useful to find out overall proportions of neurochemical markers in L1 neurons, for example COUP-TFII+/NDNF+ vs COUP-TFII+/NDNF- cells, by crossing the NDNF strain with a reporter mouse and detecting all neurons with NeuN, before immunohistochemistry for selected markers. Using a reporter mouse would also account for the possibility that the AAV may not fully label all NDNF+ neurons in the vicinity of the injection. Still, for each of the antibody markers, there were NDNF- cells observed in L1 which were positive for each marker, confirming firstly that the antibody was effective to in the tissue preparation, and additionally, that NDNF is in a subset of L1 neurons which have different distributions of markers. Although COUPTF-II and reelin are expressed in a large number of ENGCs, they do not appear to be exclusive to ENGCs, and so NDNF is a better marker.

These neurons could have further subdivisions on the basis of their neurochemistry in addition to the markers tested here, for example NPY, which is present in some L1 NDNF+ neurons (Schuman et al., 2018). Abs et al. also observed a strong correlation between NDNF, reelin and NPY in L1, and a weaker correlation between NDNF and NOS by fluorescent *in* situ hybridisation (FISH) of prefrontal and auditory cortices (Abs et al., 2018). They also observed no co-expression of PV, SOM, VIP, and CR with NDNF. It is likely that NDNF+ neurons are 5HT3aR+, as almost all L1 neurons are 5HT3aR+ (Rudy et al., 2011), although this was not tested here. Additionally, there may be variations in electrophysiological properties of individual NDNF+ neurons (Schuman et al., 2018).

2.4.2 Thalamic innervation of L1 NDNF+ motor cortical neurons

Based on research showing that the stimulation of VM thalamocortical afferents can drive L1 interneurons in mouse prefrontal cortex (Cruikshank et al., 2012), our hypothesis was VM thalamocortical projection neurons would directly innervate L1 interneurons in motor cortex. More specifically, that there would be preferential innervation of L1 ENGCs by VA and VM thalamocortical projections compared with VL afferents. It is well established that basal ganglia-recipient thalamus largely targets L1 of motor and motor-associated areas in rodent (Kuramoto et al., 2015; Arbuthnott et al., 1990). The purpose of our retrograde tracing studies was to establish in motor cortex whether L1 interneurons receive direct thalamocortical innervation from BZ, in addition to pyramidal cell dendrites receiving innervation, and the extent to which other areas of thalamus innervate L1 interneurons. Since BZ tends to innervate the superficial part of L1, where ENGCs are more abundant than SBCs, it seemed that ENGCs would be more likely candidates than SBCs to receive BZ innervation, if interneurons were found to be targeted.

In order to identify inputs to ENGCs, we used retrograde rabies tracing as it is a powerful method of tracing monosynaptic inputs to a particular cell type. Starter cells were mostly in L1 motor cortex, in both M1 and M2, although some were deeper than L1 and a few sparse cells were lateral to motor cortex. Retrogradely labelled input neurons were observed in cortex and subcortical structures. Cortical input neurons were observed in L1, which could also be ENGCs or other interneurons, and in deeper cortical layers. These could be L2/3 interneurons, which are known to form reciprocal connections with ENGCs (Jiang et al., 2013). The majority of subcortical retrogradely labelled neurons were found in thalamus. Interestingly, the largest proportion of rabies labelled thalamic neurons were in VM, with few

in VA, the other part of basal ganglia-recipient thalamus (Kuramoto et al., 2009), and fewer in cerebellar-recipient VL than VM. The preference for VM over VA was surprising, since VA targets motor regions more selectively than VM, which innervates orbital and cingulate regions to a larger extent in addition to motor regions. From these results, it appears that VM innervates both pyramidal dendrites and ENGCs in L1 of M1 and M2, while VA primarily targets pyramidal dendrites, so that VM exerts a larger influence over inhibitory control in L1. However, it is possible that this discrepancy may be partially explained by the location of starter neurons. It could be the case that L1 NDNF+ neurons in the injected region at the border of M1 and M2 1.5mm anterior from Bregma might receive more extensive connections from VM than VA, while L1 NDNF+ neurons in adjacent regions could have a different ratio of VM to VA neurons.

As VM, Po and CM/CL/PC, which form a large proportion of the input, are higher order nuclei (Saalmann et al., 2014), ENGCs receive highly processed information. Whether or not they directly form part of a reciprocal circuit from motor cortex back to these nuclei is unknown and would require further investigation to uncover. These findings complement observations in PFC, where VM also preferentially targets L1 NDNF+ interneurons (Cruikshank et al., 2012, Anastasiades et al., 2020). This provides evidence that not only does VM thalamus project to pyramidal cell dendrites in L1 motor cortex, but also directly projects to putative ENGC interneurons. These results show for the first time that VM thalamocortical neurons directly innervate NDNF+ interneurons in L1 motor cortex, aside from a single M2/cingulate-projecting VM neuron (Cruikshank et al., 2012), challenging the assumption that pyramidal neuron dendrites are the only recipient of motor thalamocortical neurons in L1 motor cortex.

Although ENGCs are relatively sparse and restricted to L1, their elongated axonal arbour in the region of numerous pyramidal dendrites and other interneuronal dendrites means they could potentially have a significant influence on coordination of widespread cortical activity. Since ENGCs not only receive cortical input, but also direct thalamic input primarily from VM, it would be interesting to find out what the ENGC-mediated effect of VM thalamocortical input is on physiological cortical activity within motor cortex. Increased ENGC firing due to VM input may inhibit L5 pyramidal cell activity via their apical dendrites, and so decrease PT and IT output. The functional significance of this connection on both L1 NDNF+ interneurons themselves, and downstream cortical circuits, especially L2/3 and L5 pyramidal neurons within motor cortex which receive input to their dendrites from ENGCs within L1, remains to be explored.

2.4.3 Thalamic innervation of L5 RBP4+ motor cortical neurons

The distribution of thalamic innervation of L5 RBP4+ neurons was different from that of thalamic inputs to NDNF+ neurons. Instead of VM, the main thalamic sources of rabies labelled inputs to L5 RPB4+ neurons were VL and intralaminar nuclei (CM/PC/CL). RBP4+ neurons are pyramidal neurons, consisting of both PT and IT neurons. They may receive inputs at different cellular regions, for example the superficial apical dendrites or deeper basal dendrites. This could differ according to the input nucleus, as anterograde tracing shows differences in laminar innervation (Kuramoto et al., 2009). There are still some VM inputs to RBP4+ neurons, presumably innervating their apical dendrites, but this is only around 12% of total labelled thalamic inputs. However, although the proportion differs, the absolute numbers of VM thalamocortical neurons that innervate pyramidal neurons are greater than those innervating ENGCs. The input from VL forms a higher proportion, delivering first order

information from the cerebellum. Overall, the distribution of the type and sources of thalamic input to L1 NDNF+ interneurons and L5 RBP4+ pyramidal neurons within motor cortex differ, although these inputs are not completely segregated as some thalamic nuclei including VM project to both types of neurons. This indicates that interneurons and pyramidal neurons in different layers within the same region of motor cortex receive and process distinct thalamic inputs, with different proportions of afferents from each motor thalamic region, and hence different proportions of inputs from the basal ganglia-thalamocortical circuit and cerebellar-thalamocortical circuit.

Chapter 3 Neurochemical parcellation of the rhesus macaque thalamus

3.1 INTRODUCTION

Traditional atlas boundaries are often defined on the basis of Nissl (cresyl violet) or similar staining. This has been useful for distinguishing areas based on their cytoarchitecture and can be reliably applied to label experimental tissue to help identify areas. However, these methods are limited in that they cannot reveal connectivity to different regions, for which neuronal tracers are required. A complementary method of defining regions is to use immunohistochemistry (IHC) to identify regional expression of molecular markers. This provides an indication of neuronal type by somatic expression as well as the nature of input structures, based on terminal markers in neuropil.

3.1.1 Anatomical and physiological connectivity of primate thalamus

A group of higher order nuclei at the anterior aspect of the thalamus form reciprocal connections with frontal cortical areas and play a particularly important role in memory and cognition. As defined by commonly used stereotaxic atlases, these areas include the mediodorsal, anterior, laterodorsal, and some “motor” nuclei. Although these areas are often defined by their connectivity with cortical areas, their subcortical inputs provide equally important clues as to the function of the circuits in which they are embedded. In both rodents and primates, mediodorsal nuclei (MD) and parts of the motor thalamus (ventromedial and ventral anterior (VM and VA) in rodents, ventral anterior (VA) and ventral oralis (VO) in primates) receive dense input from GABAergic output neurons of the basal ganglia in the ventral pallidum (VP), globus pallidus internal segment (GPi) and substantia nigra pars

reticulata (SNr) (Francois et al., 2002). Subsequent studies in primates have differentiated specific vGluT2 inputs from the basolateral amygdala (BLA) to the MDmc, which then projects to the posterior orbital prefrontal cortex (pOFC), along with directly projecting neurons from BLA to pOFC (Timbie & Barbas 2014; 2015; Timbie et al., 2020). The MDmc to pOFC neurons tend to consist of CB+ matrix neurons projecting to upper cortical layers more than PV+ core neurons. As the ventral nuclei innervate both striatum and cortex, they provide specialised motor-related information. These form reciprocal and non-reciprocal connections between basal ganglia-recipient thalamus and cortical areas, with VA and MD participating in feedback loops, but also in the transfer of information from one cortical area to another (Haber, 2003).

Two other thalamic areas, the anterior thalamic nuclei (ATN), comprising anterodorsal (AD), anteromedial (AM) and anteroventral (AV) nuclei, and laterodorsal nucleus (LD) have similar properties to these established higher order areas (Perry and Mitchell, 2019). The ATN receive substantial inputs from the mammillary bodies (Bubb et al, 2017), while LD receives afferents from subcortical visual areas (Thompson and Robertson, 1987). Both the ATN and the LD are interconnected to different parts of the frontal, cingulate and retrosplenial cortex as well as hippocampus in mammals (Bezdudnaya and Keller, 2008; Perry and Mitchell, 2019).

3.1.2 Macaque atlases and thalamic nomenclature

Regions of the macaque thalamus have a diversity of nomenclature systems employed in a range of published atlases, which are mainly based on location and cytoarchitecture of nuclei. Atlases that are particularly useful for anatomy include Olszewski, 1952: The Thalamus of the Macaca Mulatta: An Atlas for Use with the Stereotaxic Instrument; Ilinsky and Kultas-Ilinsky, 1987: Sagittal cytoarchitectonic maps of the Macaca mulatta thalamus with a revised nomenclature of the motor-related nuclei validated by observations on their connectivity;

Hirai and Jones, 1989: A new parcellation of the human thalamus on the basis of histochemical staining; Ilinsky et al., 2002: Stereotactic Atlas of the Macaca mulatta Thalamus and Adjacent Basal Ganglia Nuclei; Jones, 2007: The thalamus, 2nd ed; Paxinos et al., 2008: The Rhesus Monkey Brain in Stereotaxic Coordinates; Saleem and Logothetis, 2012: A Combined MRI and Histology Atlas of the Rhesus Monkey Brain in Stereotaxic Coordinates. Some of the differences in nomenclature are shown in Table 3.1 below. Between rodents and non-human primates there are also differences in nomenclature, so to allow better comparisons of regions between species the Paxinos macaque atlas (Paxinos et al., 2000; 2008) was developed to be complementary to the Paxinos mouse and rat atlases (Paxinos and Franklin, 2007; Paxinos and Watson, 2009). The boundary regions and nomenclature used in this chapter will be primarily according to the Paxinos atlas, to allow for easier comparison with mouse thalamus, in addition to Ilinsky and Kultas-Ilinsky nomenclature (Ilinsky and Kultas-Ilinsky, 1987; Ilinsky et al. 2002), as this is also widely used (structures and abbreviations in Table 3.2).

Paxinos atlas (2000, 2008)	Ilinsky and Kultas-Ilinsky, 2002	Hirai and Jones, 1989; Jones, 2007	Input structures include
VLM	VL	VLp	Deep cerebellar nuclei and spinal cord
VLL	VL	VLp	Deep cerebellar nuclei and spinal cord
VAM (VA) (nigr)	VAmc		SNr
VAL (VO) (pal)	VAdc, VApc	VA, VLa, VM (VApc equivalent)	GPi
VAMC	VAmc	VAmc	SNr
MDM	MDmc		SNr
MDC	MDpc		Cerebellum, GPi
MDL	MDdc (caudal MDL), MDmf (rostral MDL)		Cerebellum (MDdc), SNr (MDmf), GPi
MDD			
	MDpl		

Table 3.1: Variations in nomenclature of select thalamic nuclei and their input structures, adapted from Kultas-Ilinsky et al., 2011

Abbreviations: dc: densocellular, mc: magnocellular, mf: multiforms, pl: paralamellar, pv: parvocellular

Paxinos atlas (abbreviation)	Paxinos atlas (full name)
AD	Anterodorsal thalamic nucleus
AM	Anteromedial thalamic nucleus
AV	Anteroventral thalamic nucleus
CL	Centrolateral thalamic nucleus
CM	Central medial thalamic nucleus
CMnL	Centromedian thalamic nucleus, lateral part
CMnM	Centromedian thalamic nucleus, medial part
eml	External medullary lamina
IAM	Interanteromedial thalamic nucleus
ic	Internal capsule
IMD	Intermediodorsal thalamic nucleus
LDSF	Lateral dorsal thalamic nucleus, superficial part
MDC	Mediodorsal thalamic nucleus, central part
MDD	Mediodorsal thalamic nucleus, dorsal part
MDL	Mediodorsal thalamic nucleus, lateral part
MDM	Mediodorsal thalamic nucleus, medial part
PC	Paracentral thalamic nucleus
PF	Parafascicular thalamic nucleus
PT	Paratenial thalamic nucleus
PV	Paraventricular thalamic nucleus
Re	Reuniens thalamic nucleus
Rt	Reticular thalamic nucleus
SPF	Subparafascicular thalamic nucleus
SPFPC	Subparafascicular thalamic nucleus, parvicellular part
VAL	Ventral anterior thalamic nucleus, lateral part
VAM	Ventral anterior thalamic nucleus, medial part
VAMC	Ventral anterior thalamic nucleus, magnocellular part
VLL	Ventral lateral thalamic nucleus, lateral part
VLM	Ventral lateral thalamic nucleus, medial part
VPL	Ventral posterolateral thalamic nucleus
VPM	Ventral posteromedial thalamic nucleus
Xi	Xiphoid thalamic nucleus

Table 3.2: Abbreviations of thalamic nuclei according to Paxinos et al., 2000; 2008

3.1.3 Immunohistochemical delineation of motor and MD macaque thalamus

In rodents, advances in anatomical methods have made it possible to define the connectivity of histologically defined areas in unprecedented detail that bring into question the current definition of a thalamic nucleus based on Nissl staining (Hunnicutt et al, 2014). Such approaches, however, require sample sizes that would not be ethically or logistically feasible in primates. An alternative approach is to parcellate the neuropil of thalamic territories using the expression of neurochemical markers that provide proxy information regarding synaptic inputs. In rodents for example, the expression of GAD67 in VA and VM can be used to delineate the thalamic areas that receive dense GABAergic output from the basal ganglia output nuclei (Kuramoto et al, 2009; Nakamura et al, 2014), as described in chapter 2. The neighbouring VL, a first-order nucleus, does not have prominent GAD67-expression, but is enriched with vesicular glutamate transporter 2 (vGluT2) due to the incoming terminals from the cerebellar output nuclei. Other immunohistochemical markers, such as calcium-binding proteins, can provide further delineation by labelling inputs from specific neuronal populations. Although this approach does not provide connectivity information as with anterograde and retrograde labelling, it has the advantage of being able to be readily used to verify the position of recording or stimulation electrodes and optic fibres – an increasingly important part of circuit neuroscience experiments.

Several such immunohistochemical markers have been examined in isolation in primate thalamus. Perhaps most notably, a detailed study by Acsády and colleagues (Rovó et al., 2012) mapped the expression of vesicular glutamate transporter 1 (vGluT1) and vGluT2 across a large area of macaque thalamus, confirming that several higher order nuclei, including the MD, have dense subcortical input. VGluT2 labels subcortical terminals, and vGluT1 tends to

be present in corticocortical and corticothalamic terminals, as well as less commonly in some axons of subcortical origin (Hackett et al., 2011). Rovó et al. (2012) investigated the distribution of vGluT1 and vGluT2 immunoreactivity within *Macaca mulatta* thalamus to identify target regions of subcortical and cortical driver glutamatergic input using a combination of single and double fluorescent immunostaining and electron microscopy. They found that large vGluT2+ and vGluT1+ terminals were mostly segregated, but there was convergence at border regions between first and higher order nuclei, such as between the pulvinar and surrounding nuclei, and MD thalamus. Large vGluT1+ terminals, indicating cortical driver input, were mainly found in MDC but not MDM and MDL, and in anterior, lateral and inferior pulvinar, but not medial pulvinar, demonstrating within-nucleus differences. Large vGluT2+ terminals, indicating subcortical driver input, were observed in regions including the entire VL, consistent with its cerebellar input, and in VPM/VPL and LGN. MDM also contained large vGluT2+ terminals, despite this being a higher order nucleus. Small vGluT1+ terminals were present in medial pulvinar, and both small vGluT1+ and vGluT2+ terminals were observed in LD thalamus. These inter- and intranuclear differences in the distribution of vGluT1 and vGluT2 immunoreactivity reveal variations in cortical versus subcortical glutamatergic afferent targeting and are a useful way of distinguishing between regions.

Calcium-binding proteins are also useful neurochemical markers, able to distinguish between different cell types by soma expression as well as neuropil expression, indicating differences in sources of innervation to target regions. Two calcium binding proteins that can be used to parcellate primate thalamus based on cellular and neuropil immunoreactivity are parvalbumin (PV) and calbindin D-28K (CB), as shown in cynomolgus monkeys (*macaca fascicularis*) and pigtailed monkeys (*macaca nemestrina*) (Jones and Hendry, 1989). They

found that there was no colocalisation of GABA and CB in thalamic cells, indicating that CB+ cells are relay neurons rather than GABAergic interneurons. Jones describes a core and matrix division in the primate thalamus, where PV+ neurons form a 'core' projecting to spatially restricted areas within cortex and CB+ neurons form a 'matrix' of more diffuse cortically-projecting neurons (Jones, 1998). Calcium-binding proteins are therefore useful for differentiating between separate populations of cortically-projecting thalamic relay neurons in close proximity to each other. PV+/GABA+ cells are abundant in TRN, as well as in dLGN and mMGN (Jones and Hendry, 1989). The MDmc (MDM) has numerous PV+ cells and neuropil, with sparse labelling in the rest of MD (Jones and Hendry, 1989). The ventral thalamic nuclei have calcium binding protein labelling of both cell bodies and neuropil, with a different distribution between nuclei.

Inhibitory terminals from basal ganglia have been mapped in the motor thalamic nuclei in primate with glutamic acid decarboxylase, 65kDa (GAD65) immunostaining, but not with GAD67, as with rodent BZ. GAD65 and GAD67 isoforms are both involved with the synthesis of GABA but have distinct functions. GAD65 and GAD67 are located in fibres, terminals and somata. To our knowledge, the majority of studies thus far have used serial sections to describe the distribution of these markers (Kultas-Ilinsky et al, 2011). The general distribution of GAD65 in human thalamus is the same as in rhesus macaque (Kultas-Ilinsky et al, 2011): in human thalamus, both the pallidal and nigral recipient parts of medial VA (VAp and VAn) have strong GAD65 immunoreactivity, as expected, with most of the GAD65 labelling in VAp in fibres rather than somata, similar to GAD67 labelling in rodent thalamus BZ. The calcium-binding proteins CB and PV also label both parts of VA, although PV only labels fibres and punctae within VAp. VL has weaker GAD65 immunoreactivity than VA, consistent with rodent thalamus, which tends to be present in small cells of local GABAergic interneurons rather than

in neuropil of afferent innervating fibres. MD thalamus overall has less dense GAD65 immunoreactivity in patches, with regions of intense immunoreactivity located in MDmc (MDM) and MDmf (MDL), with labelling both of small cell bodies and neuropil. There is lower intensity of GAD65 immunoreactivity in CM. MD also has less dense patchy CB labelling, while CM and VL have no or negligible CB labelling. Immunoreactivity patterns in rhesus macaque are very similar to those described above in human thalamus, although GAD65+ interneuron projections are much less extensive in primate VL than in the human brain.

Here we seek to extend this neurochemical characterisation of the primate thalamus, focusing on the specifics of subcortical differentiation assessed by the expression of vGluT2, GAD67, and calcium-binding proteins. Mapping of these areas in primates has the potential to bridge the transgenic dissection of these thalamocortical circuits in rodents and the need to identify structures based on their synaptic input to investigate their function and dysfunction in humans.

3.1.4 Aims and justification

The aim of this chapter was to create a map complementary to the Paxinos macaque atlas, identifying regions of different IHC staining intensities within the thalamus, with a focus on nuclei in anterior thalamus (MD, ATN and LD, VA and VL) known to contribute to complex cognition and motor control. Having an immunofluorescence-based parcellation of macaque thalamus, enabling the identification of regional antibody colocalisation within the same sections, especially GAD67 and vGluT2, would enhance previous studies. This would thereby provide a comprehensive map of coronal sections for these neurochemical markers, which is useful for greater reliability and accuracy in identifying thalamic regions, for example after implants for electrophysiological recordings or stimulation. Precision of targeting is especially

important in primate experiments, as fewer animals are used than rodents over a longer period and have greater welfare requirements, and therefore the investment of both time and cost per animal is much greater. Ethically, primates are only used in research when there is no other alternative, as they are highly sentient. As primate brains are more similar than rodent brains to human brains, in particular their cognitive processes, their use in medical research can be more relevant to specific aspects of the human brain, such as understanding cognition or disease. For these reasons, the refinement of experiments involving primates is vital.

Aims:

- To carry out a neurochemical-based parcellation of anterior thalamus in a rhesus macaque brain with vGluT2, GAD67 and calcium-binding proteins.
- To immunohistochemically delineate anterior thalamic regions, in particular motor thalamus and mediodorsal thalamus.
- Identify the level of correlation between regions of immunostaining and traditional atlas boundaries.

3.2 METHODS

3.2.1 Surgery and tracer injections

One male adult Old World rhesus macaque monkey (Macaca mulatta) was used in this study. Prior to perfusion, the animal had received a single injection of retrograde tracer cholera toxin subunit B (CTB) into MDmc of the left hemisphere, and retrograde fluorescence tracers fast blue and diamidino yellow into MDpc of the left hemisphere. The surgical approach to target

MDmc and MDpc has been previously published (Chakraborty et al., 2019). The animal was later involved in electrophysiological recording experiments.

3.2.2 Tissue Processing

The monkey was perfused under deep pentobarbital anaesthesia with a 0.1M phosphate buffer (PB) at pH 7.4, followed by 2% paraformaldehyde and 0.1% glutaraldehyde in 0.1M PB. The brain was removed and post-fixed for one week in 4% PFA, and then transferred into a 30% sucrose solution in 0.1M PB at 4°C. Fixed frozen sections were sectioned coronally using a sliding microtome at 50µm. The serial sections were stored at -80°C in a long term cryoprotectant glycine solution until required, then stored at 2-8°C prior to immunostaining.

3.2.3 Immunohistochemistry

For neurochemical parcellation of the thalamus, two main IHC protocols were used: one for calcium-binding proteins and the other for GAD67 and vGluT2 (Table 3.3). The primary antibodies for calcium-binding proteins calretinin (CR), parvalbumin (PV), and calbindin (CB) were revealed with secondary antibodies with conjugated fluorophores AMCA, Alexa488 and Cy3, respectively. GAD67 was revealed with Alexa488 and vGluT2 with Cy3-conjugated secondary antibodies. Every 1 in 10 serial coronal sections spanning the entire rostro-caudal axis of the thalamus were used for each antibody combination, around 24 sections each.

Free-floating sections were permeabilised using 0.3% Triton X-100 (Sigma, Germany) in 0.1M phosphate-buffered saline (PBS) with 0.05% sodium azide, which was used as the base solution (PBS-Tx) for subsequent incubations. Next, they were blocked in 20% normal donkey serum (NDS, Vector Laboratories) for one hour at room temperature. After blocking, the sections were incubated in primary antibody solution with 1% NDS, overnight at room temperature. The sections were then washed for 3x 10 minutes in PBS-Tx to remove the

primary antibody solution, and subsequently incubated in secondary antibody solution with 1% NDS, for either 4 hours at room temperature, or overnight at 2-8°C. Secondary antibodies were all from Jackson ImmunoResearch Laboratories, and were all raised in donkey. After secondary antibody incubation, sections were washed for 3x 10 minutes in PBS, then mounted on glass slides with Vectashield mounting medium (Vector Laboratories).

There was punctate lipofuscin-like autofluorescence in the tissue, which was particularly visible in the 488 channel and masked clear identification of GAD67 terminals. To reduce this autofluorescence in the GAD67 and vGluT2 protocol, we applied copper sulphate ($CuSO_4$) solution after antibody incubation (Schnell et al., 1999). Following the final washes in PBS, sections were incubated in 10mM $CuSO_4$ in 50mM ammonium acetate solution (adjusted to pH5 by acetic acid and ammonium hydroxide) for 30 minutes at room temperature, followed by a further 3x 10 minutes of washing in PBS and mounting on slides.

Antigen	**Species, clonality**	**Dilution**	**Source and code**	**Research Resource Identifier (RRID)**	**Secondary antibody: fluorophore, dilution, code**
Calbindin D28K (C-20) (CB)	Goat, polyclonal	1:500	Santa Cruz, sc-7691	RRID: AB_634520	Cy3, 1:400, 705-165-147
Calretinin (CR)	Rabbit, polyclonal	1:1000	Synaptic Systems, 214102	RRID: AB_2228331	AMCA, 1:250, 711-155-152
Glutamic acid decarboxylase -67 (GAD67)	Mouse, monoclonal	1:500	Chemicon (Merck Millipore), MAB 5406	RRID: AB_2278725	Alexa488, 1:1000, 715-545-150
Parvalbumin (PV)	Guinea Pig, polyclonal	1:500	Synaptic Systems, 195004	RRID: AB_2156476	Alexa488, 1:1000, 706-545-148
Vesicular glutamate transporter 2 (VGluT2)	Rabbit, polyclonal	1:500	MAb-Technologies, VGT2-6	RRID: AB_2315569	Cy3, 1:400, 711-165-152

Table 3.3: Primary and secondary antibodies

3.2.4 Microscopy

Multichannel fluorescence images of whole-brain sections were acquired using a Zeiss Imager.M2 widefield epifluorescence microscope equipped with Plan-Apochromat objective lenses, a Hamamatsu Flash 4.0 LT camera and Colibri LEDs. StereoInvestigator v11.09 (MBF Biosciences) software was used in virtual tissue mode to acquire tiled single-plane images of each stained thalamic section with a 5x objective (NA 0.16).

Higher resolution multichannel confocal images of unilateral thalamus were subsequently acquired from the right hemisphere of every 1 in 2 GAD67 and vGlut2 and CaBP stained sections. These images were obtained using a Zeiss LSM880 Axio Imager 2 laser scanning confocal microscope with a 10x Plan-Apochromat air objective lens (NA 0.45). Zen Black software was used to obtain single-plane tile scans with approximately a 10µm optical section by adjusting the pinhole size for all channels. AMCA fluorescence was imaged with excitation from a Diode 405nm laser, Alexa488 fluorescence was imaged with excitation from an Argon 488nm laser, and Cy3 fluorescence was imaged with excitation from a HeNe 543nm laser. Emission wavelengths were 452nm, 515-526nm and 616-626nm, and were restricted with MBS-405 and MBS-488/543 beamsplitters. Tiled images were processed and stitched offline using Zen Blue.

3.2.5 Fluorescence Intensity Measurements

Fluorescence images were opened on ImageJ (Fiji, v1.53c), and the corresponding Paxinos atlas section (Paxinos et al., 2000) fitted to each image using the BigWarp plugin (Bogovic et al., 2016; Fig. 3.1). This was done by placing landmarks on extrathalamic and thalamic external border regions, but not within the thalamus itself to avoid biasing thalamic nuclei delineations based on immunofluorescence (Gao et al., 2018). The fitted template image was then added

as an overlay with 5% transparency to each channel of the fluorescence image, thalamic regions drawn following the atlas overlay, and the mean fluorescence intensity of each region measured. Measurements from the internal capsule and white matter of the cortex were used as an estimation of background fluorescence, which was subtracted from each measurement to normalise between sections within each antibody series. The deviation from the mean of select subgroups of nuclei within individual sections was calculated. Extreme rostral or caudal sections were excluded from graphs where the template image did not fit well with the fluorescence image due to the shape of the nuclei, or where the total area or number of nuclei within the subgroup was below the average, so affecting the mean fluorescence intensity.

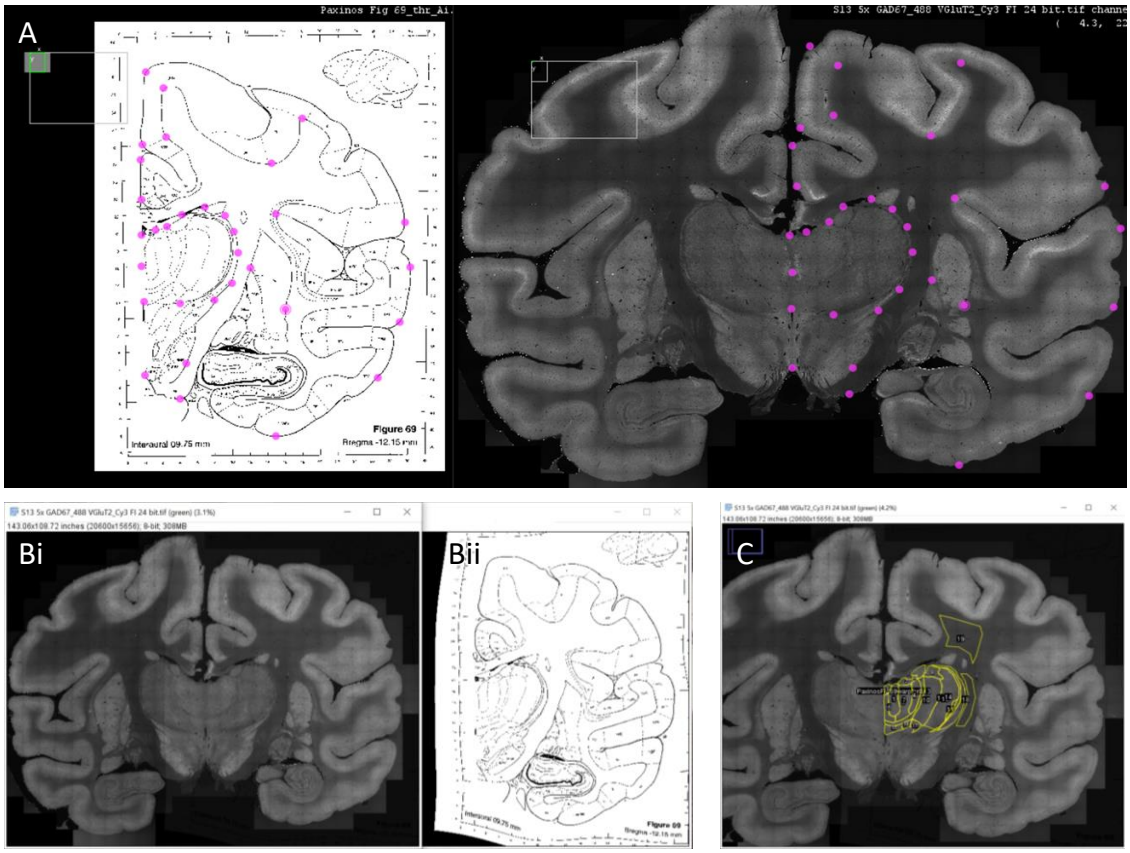


Figure 3.1 Fitting atlas overlay and measuring fluorescence intensity
(A) Using the BigWarp plugin on ImageJ (Fiji), landmarks were manually placed on the fluorescence image (right) and corresponding points on the atlas template image (left). **(B)** The warped atlas image (Bii) was overlaid onto the fluorescence image (Bi). **(C)** Thalamic regions of interest (ROIs) were traced according to the atlas overlay, and the fluorescence intensity measured.

3.3 RESULTS

To identify differences in neurochemistry of the macaque thalamus, the relative levels of fluorescence of GAD67, vGluT2, PV, CB and CR immunoreactivity within each thalamic nucleus were measured, with a particular focus on the more rostral nuclei, especially those involved with motor function. The overall mean fluorescence intensity levels within each nucleus boundary, as defined by Paxinos et al. (2000), are reported, rather than by delineating regions according to their fluorescence staining. This mainly consisted of neuropil for each of the markers. A combination of immunofluorescence in neuropil and somata both contributed to the mean fluorescence intensity for calcium-binding proteins with fluorescence intensity measurements mostly influenced by neuropil. There was also some GAD67 immunoreactivity in cell bodies. Coronal thalamic sections spanning the whole rostrocaudal axis were incubated and imaged, with images and fluorescence measurements from select nuclei, and sections shown in this results section based on notable observations, rather than an exhaustive analysis of each thalamic nucleus. A summary image of the differences in immunofluorescence between neurochemical markers and AP thalamic levels is shown in Figure 3.2.

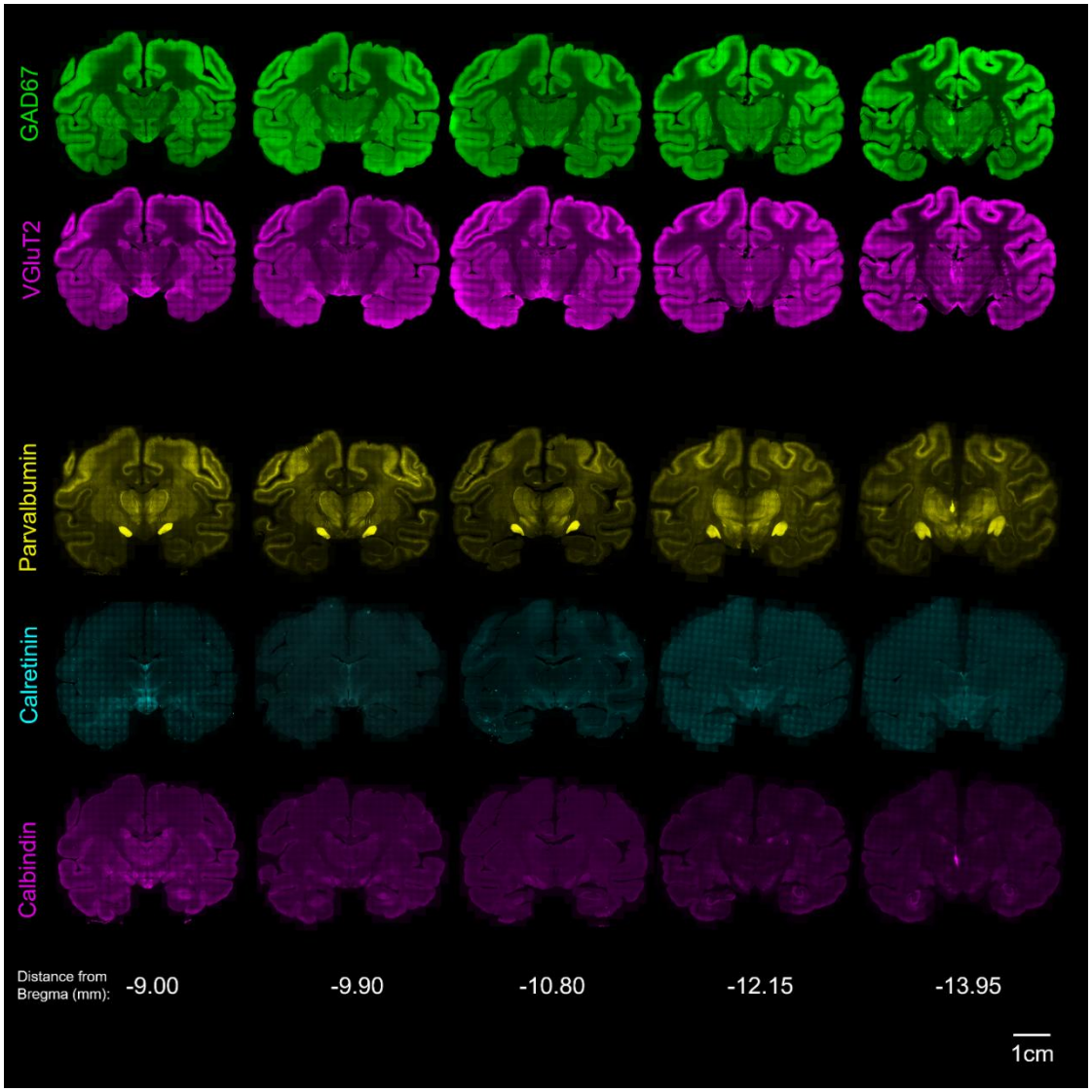


Figure 3.2 Expression profiles of GAD67, vGluT2, PV, CR and CB immunofluorescence at different planes through the rostrocaudal thalamic axis on whole brain coronal sections

3.3.1 Immunofluorescence labelling in MD

There was very dense vGluT2 neuropil staining in the magnocellular or medial subdivision of the MD (MDmc or MDM) (Figs. 3.3A,Dii, 3.4A,Dii, 3.5), forming distinct clusters of large boutons, suggesting potential driver input. This was particularly present in rostral MDM, and was the area of thalamus with the strongest vGluT2 labelling (Fig. 3.5). In contrast, there was a relative paucity of staining in central and lateral MD (MDpc and MDdc). This is similar to observations by Rovo et al. (2012). In caudal MD, all subnuclei had a low level of vGluT2 staining, with no distinction between MDM and more lateral MD subnuclei.

In contrast to vGluT2, there was weak GAD67 neuropil staining in MDM, while there was strong GAD67 immunoreactivity in the central and lateral subdivisions (MDC and MDL). GAD67 was dense in the regions of MD where vGluT2 was sparse, and vice versa (Fig. 3.5). This complementary distribution of GAD67 and vGluT2 suggests targeted innervation of MD regions from distinct sources. There was strong PV neuropil labelling in MDL, with weaker labelling in medial and dorsal MD and moderate labelling in MDC (Figs. 3.4Cii, 3.6). The distribution of PV labelling in MD was similar to that of GAD67, except for in MDM. There was minimal CB and CR labelling in all parts of MD (Figs. 3.3Ci,Ciii, 3.4Ci,Ciii).

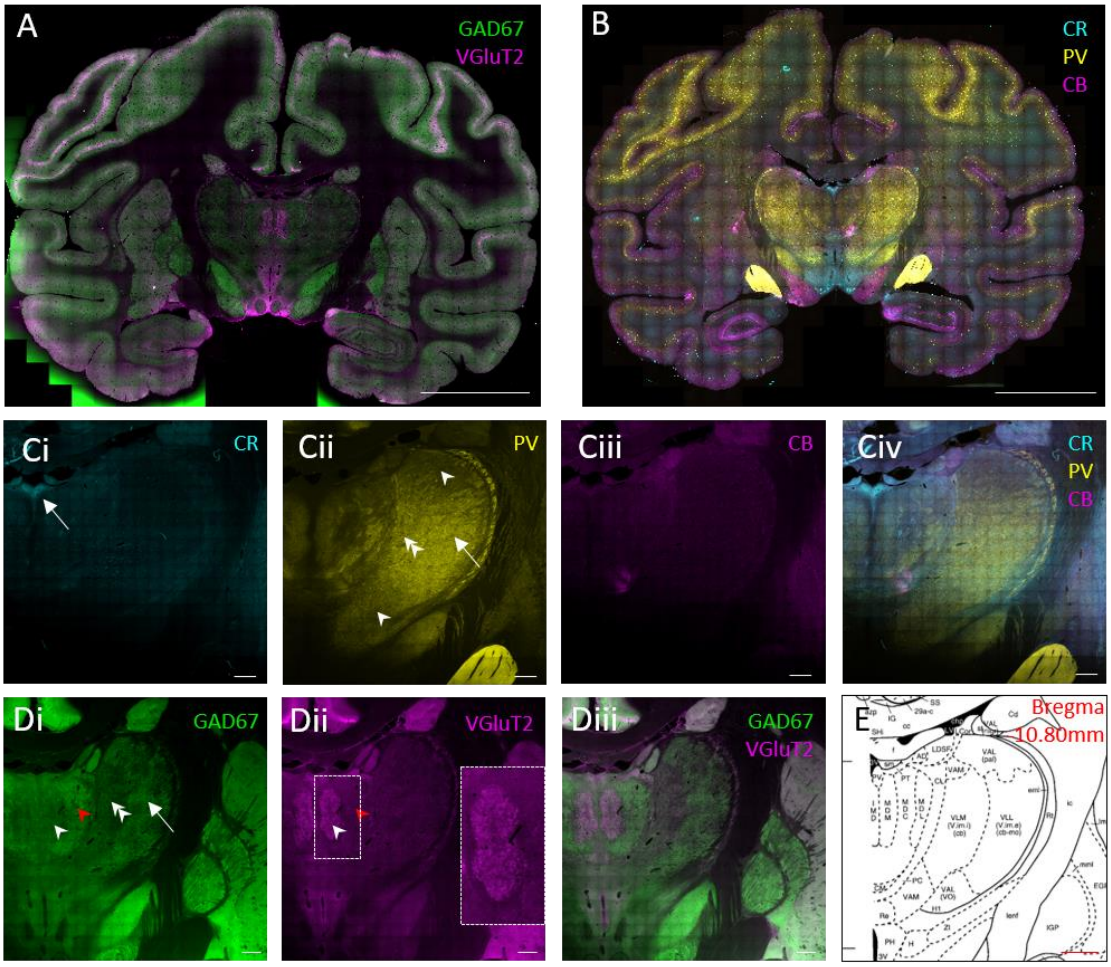


Figure 3.3 The lateral portion of ventral lateral (VL) thalamus has stronger GAD67 immunostaining than medial VL

(A) Low magnification image of GAD67 and vGluT2 immunoreactivity on a whole brain coronal section -10.80mm from Bregma. **(B)** Low magnification image of immunoreactivity for calcium-binding proteins CR, PV, and CB on a whole brain coronal section -11.25mm from Bregma. Scalebars in (A) and (B) are 1cm. **(C)** Higher magnification images of individual fluorescence channels for CR (Ci), PV (Cii), and CB (Ciii) from the same section as (B). CR is dense in the paraventricular nucleus only (Ci, arrow) at this AP thalamic level. PV+ neuropil is dense in medial VL (Cii, double arrowhead) and lateral VL (arrow), more so than in VA (single arrowheads). (Civ) Overlay of CR, PV, and CB. **(D)** Higher magnification single channel images of GAD67 (Di) and vGluT2 (Dii) immunoreactivity in the thalamus from the same section as (A). GAD67 (Di) is stronger in lateral VL (arrow) than medial VL (double arrowhead). Similarly, GAD67 is stronger in the outer portions of MD (MDC and MDL, red arrowhead) than medial MD (MDM, white arrowhead). In contrast, vGluT2 (Dii) is very dense in medial MD (white arrowhead) but weak in MDC and MDL. (Diii) Overlay of GAD67 and vGluT2. Scalebars in (C) and (D) are 1000µm. Overlaid zoomed in panel is of MDM region outlined by the dashed box (Dii). **(E)** Coronal atlas section at -10.80 from Bregma for reference, from Fig. 66 (Paxinos et al., 2000). Scalebar in (E) is 2000µm.

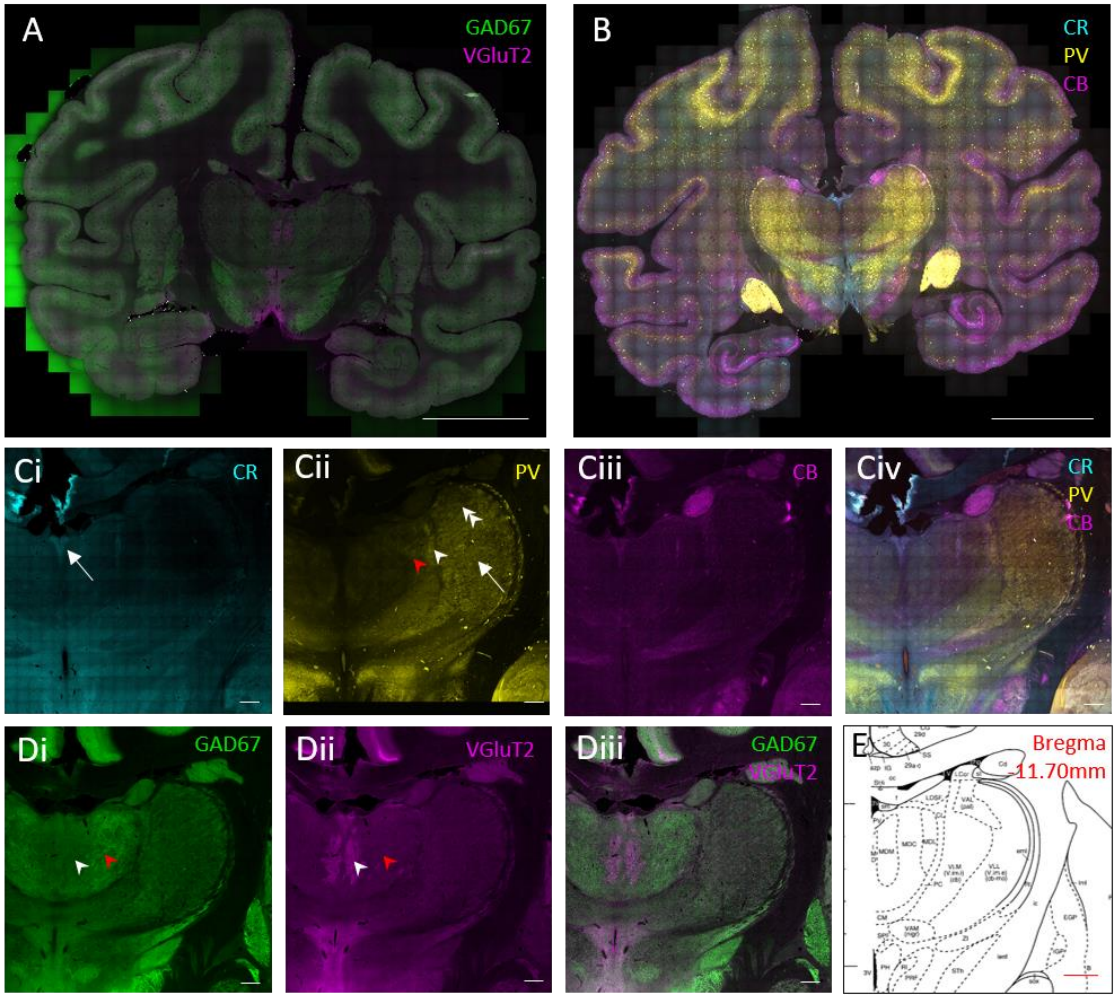


Figure 3.4 MD has distinct regional GABAergic and subcortical glutamatergic innervation
(A) Low magnification image of GAD67 and vGluT2 immunoreactivity on a whole brain coronal section -11.70mm from Bregma. **(B)** Low magnification image of immunoreactivity for calcium-binding proteins CR, PV, and CB on a whole brain coronal section -12.15mm from Bregma. Scalebars in (A) and (B) are 1cm. **(C)** Higher magnification single channel images for CR (Ci), PV (Cii), and CB (Ciii) from the same section as (B). CR is dense in the paraventricular nucleus only (Ci, arrow) at this AP thalamic level. PV neuropil (Cii) is dense in VL (arrow), VA (double arrowhead), intralaminar thalamus (single white arrowhead) and MDL (single red arrowhead). (Civ) Overlay of CR, PV, and CB. **(D)** Higher magnification single channel images of GAD67 (Di) and vGluT2 (Dii) immunoreactivity in the thalamus from the same section as (A). (Di) GAD67 is strongest in MDC and MDL (red arrowhead), and weaker in MDM (white arrowhead). (Dii) vGluT2 is strong in MDM (white arrowhead) but much weaker in MDC and MDL (red arrowhead). (Diii) Overlay of GAD67 and vGluT2. Scalebars in (C) and (D) are 1000µm. **(E)** Coronal atlas section at -11.70 from Bregma for reference, from Fig. 68 (Paxinos et al., 2000). Scalebar in (E) is 2000µm.

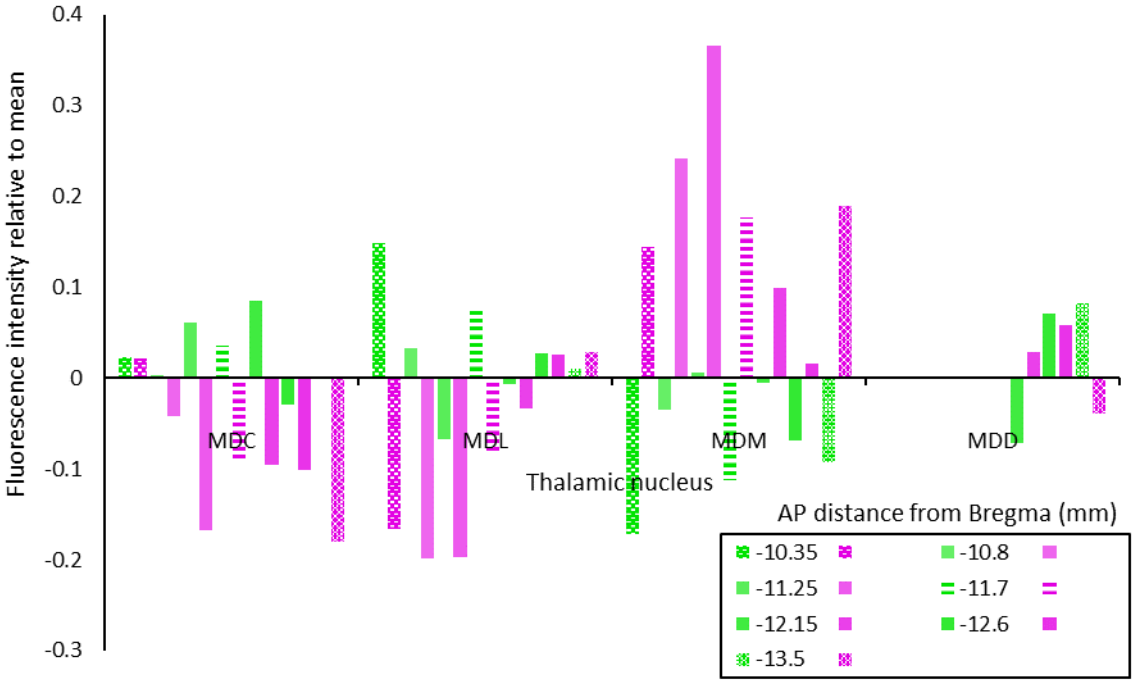


Figure 3.5 MD nuclei have complementary distributions of GAD67 and vGluT2 immunostaining Levels of GAD67 (green) and vGluT2 (magenta) fluorescence intensity of MD subdivisions relative to mean overall MD fluorescence intensity within individual coronal sections at different rostrocaudal levels. Bars represent the proportion of either GAD67 or vGluT2 fluorescence intensity above or below the mean MD fluorescence for different sections, separated according to their distance from Bregma (mm). Note that the most rostral and caudal sections do not contain all four subdivisions, and the area of nuclei varies, therefore the mean fluorescence intensity may differ from adjacent sections. MDC and MDL displayed higher GAD67 immunofluorescence than MDM. Conversely, MDM displayed higher vGluT2 immunofluorescence than MDC and MDL. MDD had a low fluorescence intensity for both GAD67 and vGluT2.

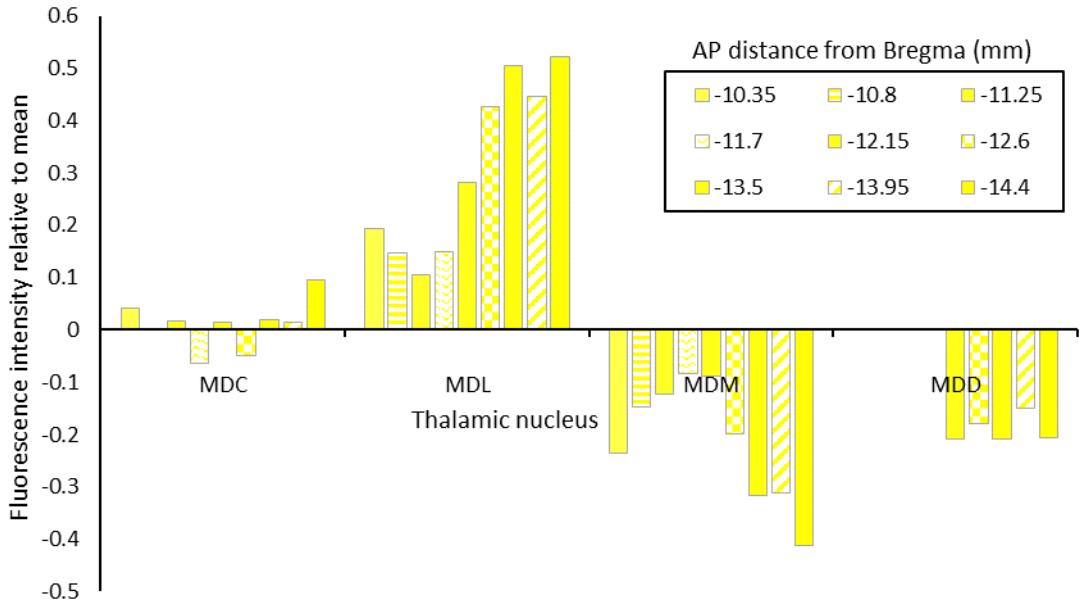


Figure 3.6 MDL has stronger PV immunostaining than other MD nuclei
Levels of PV fluorescence intensity of MD subdivisions relative to mean overall MD fluorescence intensity within individual coronal sections at different rostrocaudal levels. Bars represent the proportion of PV fluorescence intensity above or below the mean MD fluorescence for different sections, indicated by their distance from Bregma (mm). MDL had a higher level of PV immunofluorescence than MDC, MDM and MDD. MDC had a moderate fluorescence intensity, lower than MDL but higher than MDM and MDD.

3.3.2 Immunofluorescence labelling in VA and VL

The rostral motor-associated ventral nuclei, VA and VL, had a low level of vGluT2 immunoreactivity (Fig. 3.9A,C). The more caudal ventral nuclei had a slightly higher level of vGluT2 staining, especially in VLM (Fig. 3.3Dii) and VPL, with less in VPM (not shown). GAD67 immunoreactivity was denser in VAL and VLL than the adjacent VLM (Fig. 3.3Di). GAD67 in the ventral anterior thalamic nucleus, lateral part (VAL) was stronger than in the ventral anterior thalamic nucleus, medial part (VAM) (Figs. 3.7Di, 3.9A,B). Ventral posterior nuclei were also strongly labelled with GAD67 (data not shown). The GAD67 immunoreactivity in these ventral nuclei was consistent with basal ganglia innervation of VA. PV neuropil labelling was particularly dense in the ventral anterior thalamic nucleus, magnocellular part (VAMC) (Figs. 3.7Cii, 3.10). There was also dense PV in VLM and VLL, consisting of mainly neuropil and some sparser but strongly labelled somata (Figs. 3.3Cii, 3.4Cii). In addition, there was PV in the

adjacent VAL which was less dense than in VLM and VLL (Figs. 3.3Cii, 3.4Cii). In contrast to PV, there was weak CR and CB immunoreactivity in the ventral thalamic nuclei (Figs. 3.4-3.8Ci & Cii.

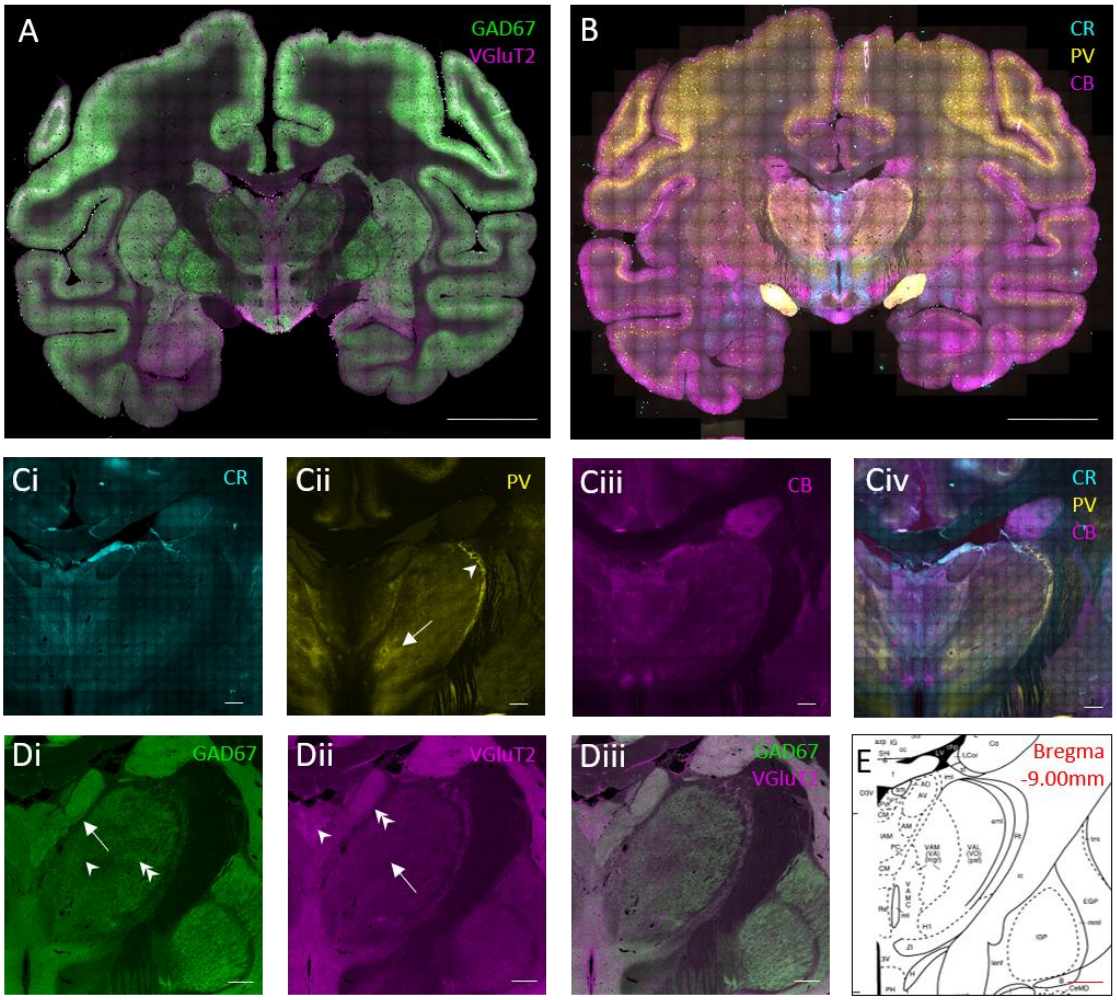


Figure 3.7 Parvalbumin immunostaining is enhanced in the magnocellular portion of ventral anterior thalamus

(A) Low magnification image of GAD67 and vGluT2 immunoreactivity on a whole brain coronal section -9.00mm from Bregma. **(B)** Low magnification image of immunoreactivity for calcium-binding proteins CR, PV, and CB on a whole brain coronal section -9.45mm from Bregma. Scalebars in (A) and (B) are 1cm. **(C)** Higher magnification single channel images of thalamus from the same section as (B) for CR (Ci), PV (Cii), and CB (Ciii). PV is enhanced in VAMC (arrow) and Rt (arrowhead). (Civ) Overlay of CR, PV, and CB. **(D)** Higher magnification single channel images of GAD67 (Di) and vGluT2 (Dii) immunoreactivity in the thalamus from the same section as (A). GAD67 is enhanced in the ATN (arrow), as well as being slightly denser in the lateral part of VA (double arrowhead) than the medial part (single arrowhead). VGluT2 is also enhanced in the ATN (double arrowhead), and weaker in VA (arrow). vGluT2 is dense in the dorsal portion of CM (single arrowhead). (Diii) Overlay of GAD67 and vGluT2. Scalebars in (C) and (D) are 1000µm. **(E)** Coronal atlas section at -9.00 from Bregma for reference, from Fig. 62 (Paxinos et al., 2000). Scalebar in (E) is 2000µm.

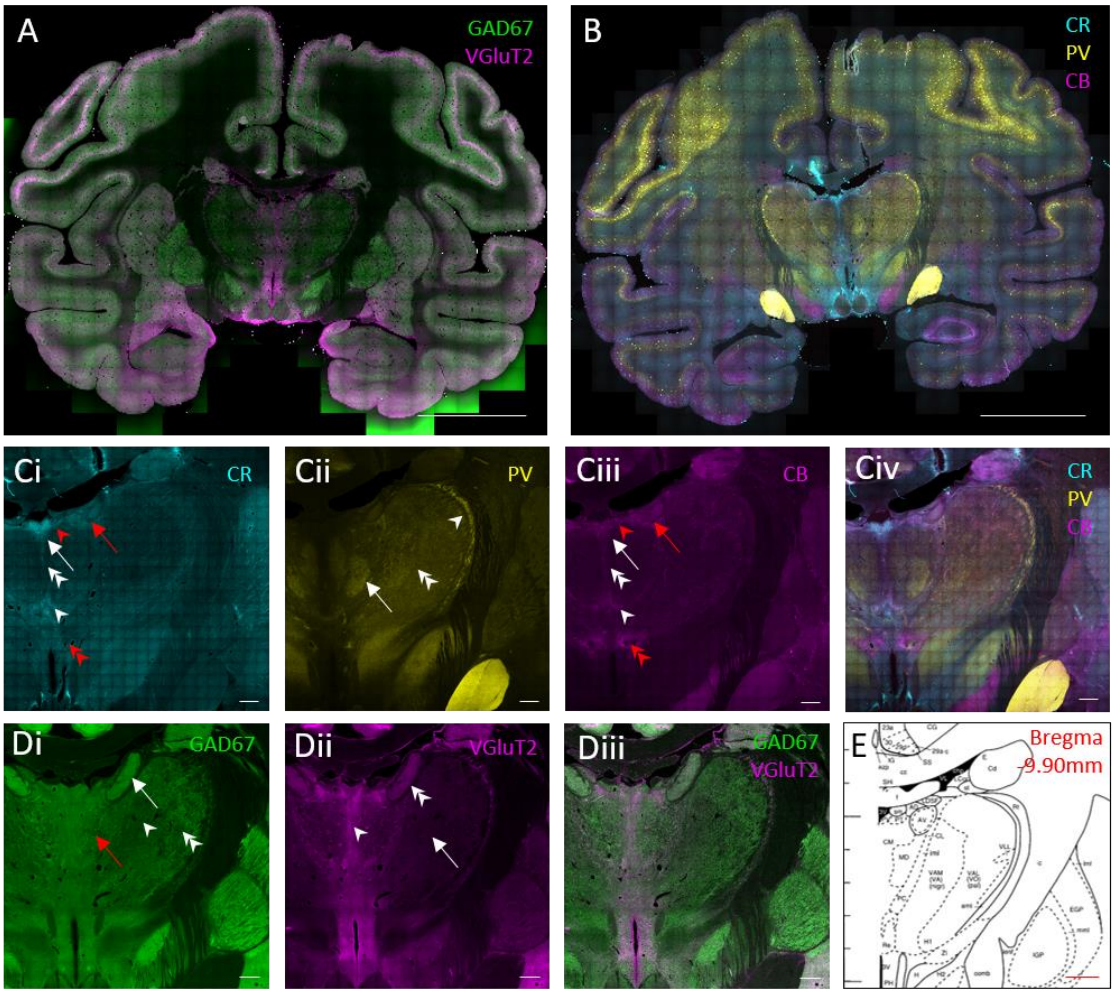


Figure 3.8 GAD67 immunostaining is stronger in the lateral than the medial portion of ventral anterior thalamus

(A) Low magnification image of GAD67 and vGluT2 immunoreactivity on a whole brain coronal section -9.90mm from Bregma. **(B)** Low magnification image of immunoreactivity for calcium-binding proteins CR, PV and CB on a whole brain coronal section -10.35mm from Bregma. Scalebars in (A) and (B) are 1cm. **(C)** Higher magnification single channel images of thalamus from the same section as (B), for CR (Ci), PV (Cii), and CB (Ciii). CR is very dense in the paraventricular nucleus (white arrow), but generally sparser elsewhere at this AP level of thalamus. As well as in paraventricular thalamus (white arrow), both CR and CB are enhanced in other midline nuclei: IMD (double white arrowhead), CM (single white arrowhead), reuniens (double red arrowhead) and paratenial nucleus (single red arrowhead), and in the ATN (red arrow), in contrast to PV. PV (Cii) is expressed in MD thalamus (arrow), as well as VA (double arrowhead) and Rt (single arrowhead). (Civ) Overlay of CR, PV, and CB. **(D)** Higher magnification images of single fluorescence channels showing GAD67 (Di) and vGluT2 (Dii) immunoreactivity in the thalamus from the same section as (A). GAD67 is expressed in MD (red arrow) and VA, with stronger labelling in VAL (double arrowhead) than VAM (single arrowhead). There is strong GAD67 labelling in ATN (Di, white arrow). VGluT2 is also expressed in the ATN (Dii, double arrowhead), and more weakly expressed in VA (arrow). vGluT2 is still strongly expressed in CM, extending down the midline (single arrowhead). (Diii) Overlay of GAD67 and vGluT2. Scalebars in (C) and (D) are 1000µm. **(E)** Coronal atlas section at -9.90 from Bregma for reference, from Fig. 64 (Paxinos et al., 2000). Scalebar in (E) is 2000µm.

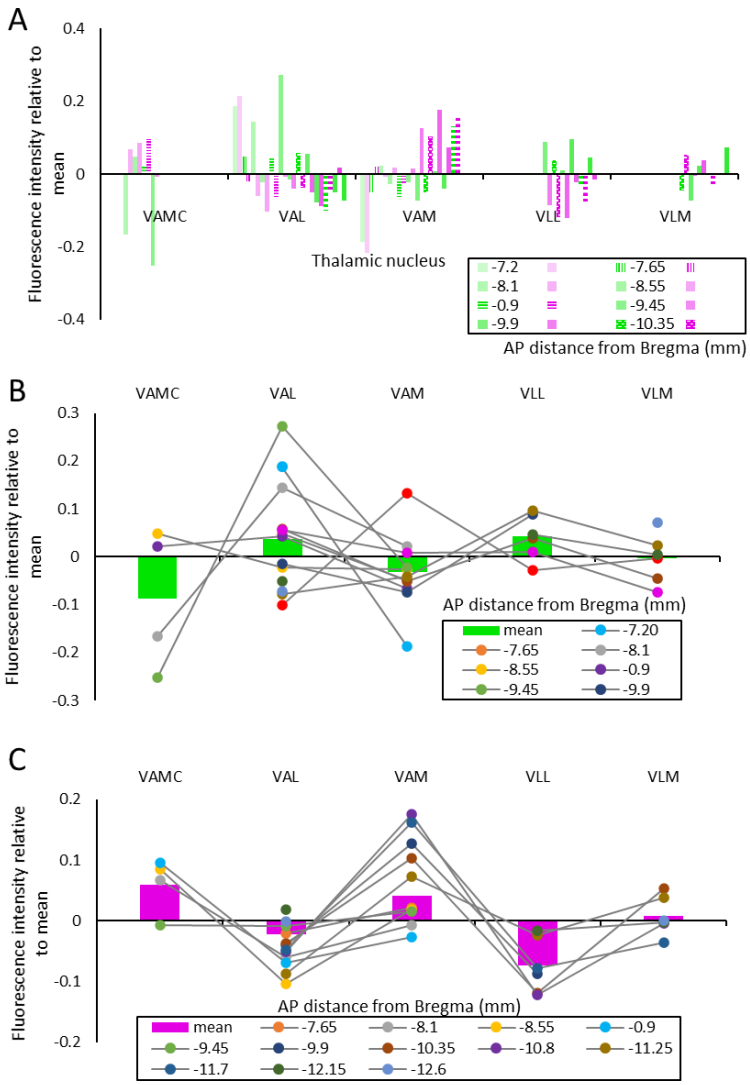


Figure 3.9 VA and VL have different distributions of GAD67 and vGluT2 immunostaining
(A) Levels of GAD67 (green) and vGluT2 (magenta) fluorescence intensity of VA and VL subdivisions relative to mean overall VA and VL fluorescence intensity within individual coronal sections at different rostrocaudal levels. Bars represent the proportion of either GAD67 or vGluT2 fluorescence intensity above or below the mean combined VA and VL fluorescence for different sections, indicated by their distance from Bregma (mm). VA nuclei are rostral to VL, with VL present from -9.9mm onwards in the posterior direction, and VA becoming smaller in area more caudally. GAD67 immunofluorescence was present in all VA and VL nuclei. It was denser in VAL than VAM, and in VLL than VLM. The distribution was reversed for vGluT2, with fluorescence intensity in VAM higher than in VAL, and higher in VLM than VLL. However, these differences were less stark for vGluT2 than GAD67. **(B)** Proportions of mean GAD67 fluorescence intensity (green bars) of VA and VL subdivisions relative to mean overall VA and VL fluorescence intensity within individual coronal sections at different rostrocaudal levels. Individual markers represent relative fluorescence intensity for GAD67, with lines joining values from different nuclei within the same section. **(C)** Proportions of mean vGluT2 fluorescence intensity (magenta bars) of VA and VL subdivisions, relative to mean overall VA and VL fluorescence intensity within individual coronal sections at different rostrocaudal levels.

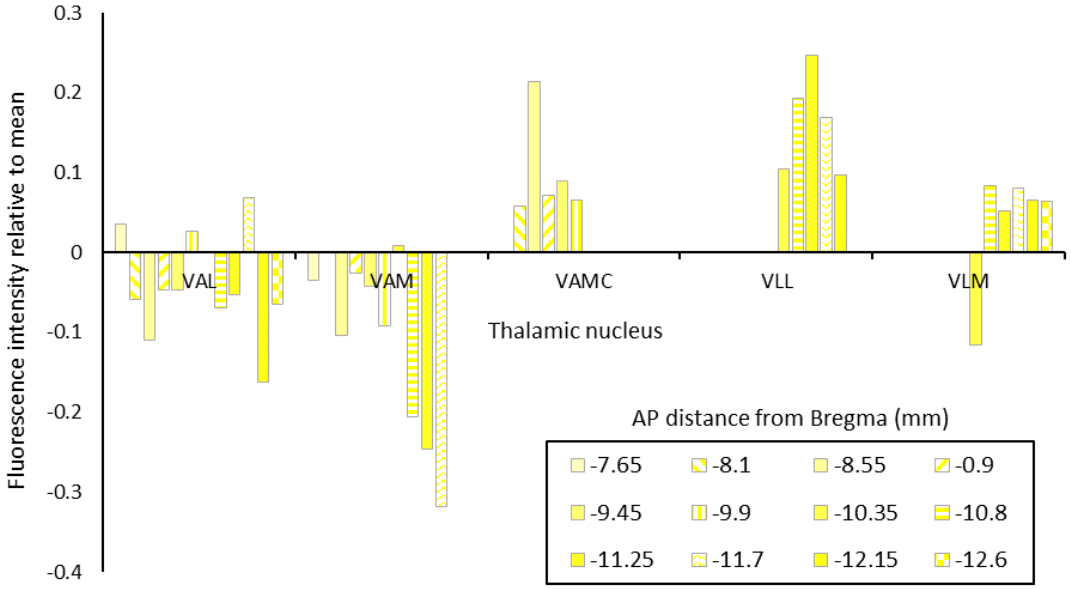


Figure 3.10 VAMC and VL have enhanced PV fluorescence within VA and VL
Levels of PV fluorescence intensity of VA and VL subdivisions relative to mean overall VA and VL fluorescence intensity within individual coronal sections at different rostrocaudal levels. Bars represent the proportion of PV fluorescence intensity above or below the mean combined VA and VL fluorescence for different sections, indicated by their distance from Bregma (mm). VA nuclei are rostral to VL, with VL present from -9.9mm and onwards caudally, and VA becoming smaller in area. PV immunofluorescence was present in all VA and VL nuclei. VAMC had much stronger PV fluorescence intensity than VAL and VAM. VL had a stronger fluorescence intensity than VA in general, with VLL more strongly labelled than VLM.

3.3.3 Immunofluorescence labelling in ATN (AD, AM, AV) and LD

All the ATN subnuclei displayed GAD67 labelling which was stronger in AV than AM and AD (Figs. 3.11, 3.7Di). However, as these nuclei are small, especially AD, it is more difficult to conclude the different levels of fluorescence intensity with the same certainty as for the larger thalamic nuclei. It is possible the immunofluorescence is more evenly distributed than the results suggest. There was fairly strong GAD67 in LD, and relatively weaker vGluT2. AV and AD showed stronger vGluT2 immunoreactivity than AM. The staining in these two subnuclei of the ATN was different from that in the MDM in that there was a more diffuse homogenous labelling compared with dense clusters of large terminals in MDM. There was some sparse CR

and CB labelling distributed across all the ATN subnuclei (Fig. 3.7Ci, Ciii). There was weak PV in AD and AV, but less in AM, and very little or no PV in LD (Fig. 3.7Cii).

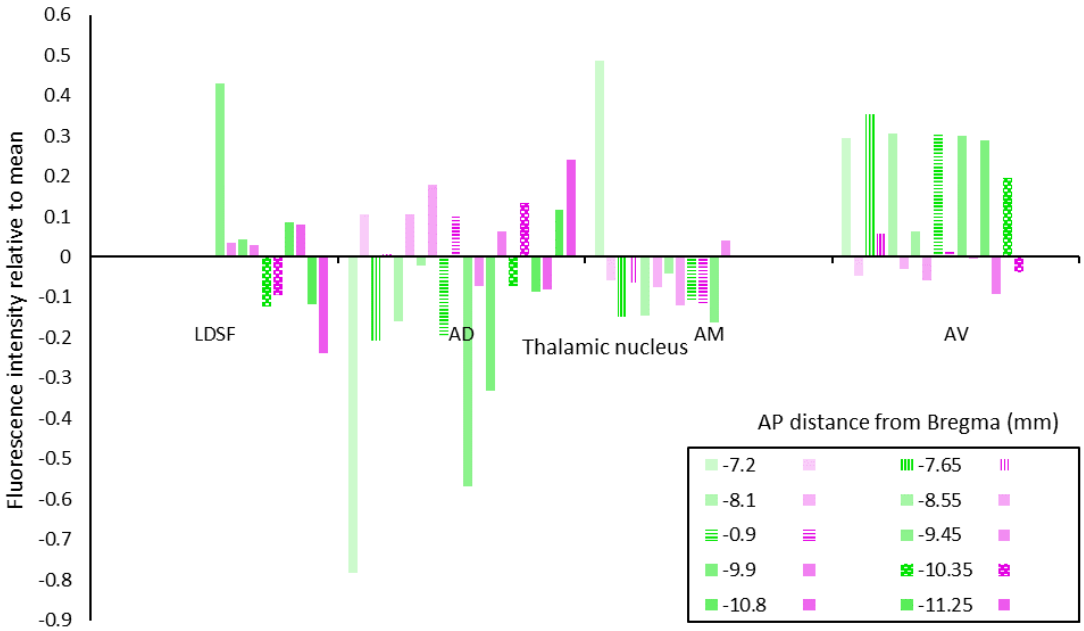


Figure 3.11 Distribution of GAD67 and vGluT2 in ATN and LD
Levels of GAD67 (green) and vGluT2 (magenta) fluorescence intensity of LDSF and ATN subdivisions relative to mean overall LDSF and ATN fluorescence intensity within individual coronal sections at different rostrocaudal levels. Bars represent the proportion of either GAD67 or vGluT2 fluorescence intensity above or below the mean combined LDSF and ATN fluorescence for different sections, indicated by their distance from Bregma (mm). GAD67 staining tended to be stronger in AV than in AD and AM. VGluT2 staining was stronger in AD than in AM and AV and slightly stronger in AV than in AM.

3.3.4 Immunofluorescence labelling in other thalamic nuclei

The intralaminar nuclei, CL, PC and CM, had strong vGluT2 immunofluorescence, particularly at the more anterior thalamic levels (Figs. 3.7Dii, 3.8Dii). There was weak GAD67 immunostaining in the intralaminar thalamic nuclei as well as in IAM and IMD. CR was especially dense in paraventricular thalamus, and slightly weaker in CM (Fig. 3.8Ci). CB was also fairly strong in intralaminar and midline nuclei (IMD, PV, Re, Rh) and LD (Fig. 3.8Ciii), with a similar distribution to CR. In the midline regions between the ATN and MD, there was strong immunoreactivity within the IAM and IMD for vGluT2. In contrast to CR and CB, there was very weak or negligible PV labelling in the IMD, PV, or ventral midline regions (Re and Rh).

There was fairly strong vGluT2 and GAD67 staining and very strong PV staining throughout the reticular thalamus. CB and CR staining was mainly in cell bodies rather than neuropil, although this was not as widespread in the thalamus as expected, since CB is commonly reported in primate thalamus particularly in matrix projection neurons. This may have been due to the antibodies used or the tissue preparation. However, there were a few small areas with noticeable strong staining and CB+ cell bodies on some sections, but not to an extent to be able to distinguish regions of fluorescence intensity as with PV.

3.4 DISCUSSION

This study has highlighted the distinct staining within the MD, motor thalamus, ATN, LD and other thalamic areas of specific markers of neurotransmitters (GAD67, vGluT2) and calcium binding proteins (CB, PV, CR). There were clear variations in staining intensity levels between some nuclei, and also variations within nuclei along the rostrocaudal and medial-lateral axes. These indicate differences in sources, types or strength of input to these regions, in the cases where neuropil is primarily stained. Some nuclei are clearly demarcated by immunostaining, and correlate with atlas boundaries, so immunostaining could be used to aid in delineation of certain regions of primate thalamus, while other nuclei are less distinguishable by the neurochemical markers used here.

3.4.1 MD subdivisions and connectivity

MD was clearly parcellated by vGluT2, GAD67 and PV into its subdivisions, as defined by the Paxinos atlas (Paxinos et al., 2000). Most notably, MDM (MDmc) displayed large, dense, and strongly labelled vGluT2 terminals, in contrast to weaker vGluT2 labelling of surrounding MD nuclei, with this distinction most prominent in rostral MD. This is also complementary to GABAergic innervation: GAD67 is stronger in MDL and MDC, and weaker in MDM. This striking

vGluT2 pattern has been previously observed (Rovó et al., 2012), while strong GAD65 has been observed in MDM and MDL (Kultas-Ilinsky et al., 2011), but this is the first time the difference between GAD67 and vGluT2 has been demonstrated by immunofluorescence in the same tissue section. The size of the vGluT2+ boutons in MDM would suggest that this is driver input. However, immunofluorescence can only reveal the type of input, not its source, which would require further investigation to elucidate, for example anterograde or retrograde tracing or stimulation experiments. One possible source of glutamatergic innervation to MDM is amygdala, as these neurons have recently been shown to innervate MDmc (Timbie et al., 2020). We know from neuroanatomical connectivity that the ventral pallidum goes to MDmc, while the globus pallidus projects to MDpc and lateral MD (Alexander et al., 1986; Haber and Calzavara, 2009). PV neuropil staining is stronger in MDL than more medial MD – this could be from SNr afferents in rostral MD and cerebellar input in caudal MD.

This distribution of immunofluorescence is not present in rodents. This difference could reflect the more complex mediodorsal-frontal cortical networks needed to support the superior cognitive abilities displayed by primates in memory and cognition. Furthermore, this demonstrates the importance of having dedicated immunohistochemical atlas resources for different species.

3.4.2 VA and VL subdivisions and connectivity

As expected, due to differences in input regions to VA and VL motor thalamus from basal ganglia and cerebellum respectively, fluorescence intensity of GAD67 and vGluT2 varied between these nuclei. However, their distributions were not completely equivalent to those in rodent. Like rodents, GAD67 immunoreactivity in macaque was denser in basal ganglia-recipient VA than in cerebellar-recipient VL, with the interesting additional feature of stronger

staining in VAL (pallidal-recipient) than VAM (SNr-recipient). VAdc (VAL) relay neurons and local interneurons form clusters which receive input from multiple branched pallidal fibres, with a high density of innervation of relay neuron somata (Ilinsky et al, 1993). VAmc (VAM) relay neurons and interneurons receive a comparatively lower density of GABAergic innervation from SNr (Ilinsky et al, 1993), which could account for these differences in fluorescence intensity. Some of the GAD67 in VAM and elsewhere is likely to originate in local interneurons in addition to basal

ganglia afferents (Ilinsky and Kultas-Ilinsky, 1990).

Surprisingly, vGluT2 immunofluorescence in both VA and VL was relatively weak compared with MDM, and the distinction was not particularly strong between VA and VL, unlike in rat. This was unexpected, as VL receives glutamatergic cerebellar input, and has been shown to contain more large vGluT2 terminals than VA (Rovó et al., 2012). The more caudal nuclei, VLM and VPL, had stronger vGluT2 staining than VA and VLL. One possible explanation is the copper sulphate methods used to reduce background autofluorescence also reduces antibody signal, and this may have suppressed any subtle differences between VA and VL.

PV had a different distribution from GAD67 and vGluT2. It was particularly strong in VAMC and in VL, which has been previously reported, and may originate from PV+ afferent inputs from GP and deep cerebellar nuclei (Jones and Hendry, 1989) as well as from thalamic reticular nucleus.

3.4.3 Significance

This study has been useful in demonstrating variance in levels of immunostaining between thalamic nuclei in macaque, which is less frequently carried out and utilised than in rodents. Having a reliable reference of regional delineation by a range of neurochemical markers could

help in retrospective identification of thalamic regions for anatomical and physiological experiments in primates. It would allow better comparison between animals and experiments, and greater certainty of accurate targeting. Furthermore, it is a simple and efficient method for confirming injection or stimulation sites. However, additional steps to optimise the staining protocol in comparison to immunohistochemistry in rodents was required for it to work effectively in primate tissue, and CB and CR fluorescence was not as clear as anticipated. Ideally more than one brain would be used to ensure reproducibility, however in the interests of reduction of use of primates just one animal was used, and this was after both tracer injections and electrophysiological recordings, to maximise the data obtained from one animal. Improved targeting of thalamic regions in non-human primates can have translational medical benefits for humans, by aiding the specific thalamic targeting for treatment of conditions such as schizophrenia and Parkinson's (Anticevic et al., 2014, Cury et al., 2017).

Chapter 4 Physiological connectivity of the mouse thalamocortical circuit

4.1 INTRODUCTION

In Chapter 2, rabies tracing experiments revealed the anatomical targeting of L1 NDNF+ ENGCs in motor cortex by thalamocortical neurons, in particular VM projection neurons. This supports published observations of VM thalamocortical neurons which similarly innervate L1 interneurons in other frontal cortical regions of rodents, including cingulate and prelimbic cortices (Cruikshank et al., 2012; Anastasiades et al., 2020; Sieveritz and Arbuthnott 2020). Although the physiological connectivity of L1 ENGCs within the thalamocortical circuit has been investigated in networks involving PFC, this has not been done to the same extent with motor thalamocortical circuits. Therefore, we explored the physiological effects of L1 ENGCs on downstream motor cortical neurons within the VM thalamocortical circuit by measuring single unit firing rates and synchrony in motor cortex in response to optogenetic stimulation of VM neurons and inhibition of motor cortical L1 ENGCs.

4.1.1 VM thalamic input to cortical L1

Thalamocortical neurons from motor thalamus target L2/3 and L5 pyramidal cell apical dendrites in L1 motor cortex, as well as L1 interneurons, which we have demonstrated by rabies tracing. Since the presence of a direct anatomical connection has been established, the next step is to investigate the functional physiological effects of L1 ENGCs within the basal ganglia-recipient motor thalamocortical circuit. As the results of the tracing indicated that VM was the largest contributor of thalamocortical input to L1 ENGCs, we will focus on this thalamic nucleus.

Presynaptic axon terminals of VM thalamocortical projection neurons can excite apical dendrites of L5 PT neurons in L1 of PFC and ALM, along with dendrites of L2/3 pyramidal neurons, to cause dendritic complex spiking (Guo et al., 2018; Collins et al., 2018). VM input to PFC pyramidal neurons evokes EPSPs, but not action potential firing, suggesting a more modulatory than driver role (Collins et al., 2018). Currently, there is limited published data recording the physiological responses and effects of L1 ENGCs in motor cortex within the VM thalamocortical pathway. However, there have been *in vitro* recordings in prefrontal cortical (PFC) regions measuring the downstream effects of modulating VM and L1 ENGC single cell activity, as well as investigating the influence of ENGCs in other cortical areas, which may help to predict the effect of ENGCs in motor cortex. Within L1 of medial PFC, midline, intralaminar and paralaminar thalamic matrix nuclei relay neurons, including VM and AM, preferentially drive late-spiking (LS) L1a interneurons in prelimbic (PrL) and cingulate (Cg) cortex, as well as in Cg/M2 *in vitro*, with evoked EPSPs in L1 interneurons being larger in amplitude than those evoked in L2/3 pyramidal neurons (Cruikshank et al., 2012). These L1 interneurons, which are likely to be ENGCs, have robust responses with short latencies to thalamocortical input, mediated by ionotropic AMPA receptors, suggesting these circuits carry temporally precise information instead of only regulating cortical tone (Cruikshank et al., 2012).

VM thalamocortical neurons innervate a larger number of L5 than L6 cortical output neurons in PFC, driving L5 PT and cortico-cortical neurons with roughly equal strength, and also drive L5 and L2/3 cortico-cortical neurons with little difference (Collins et al., 2018). VM neurons innervate both NDNF+ and VIP+ interneurons in PFC but tend to drive L1a NDNF+ interneurons in preference to VIP+ interneurons (Collins et al., 2018; Anastasiades et al., 2020). Although we are focussing on glutamatergic thalamocortical inputs to L1, there are other sources of L1 innervation, including cholinergic input to all L1 interneurons from basal

forebrain, at least in temporal neocortex, with just VIP+ interneurons responsive to 5-HT input as well as cholinergic input (Poorthuis et al., 2018). Taking this into account, it is beneficial to carry out recordings *in vivo*, as these concurrent inputs will be preserved.

4.1.2 ENGCs in cortical microcircuits

L1 ENGCs innervate a range of postsynaptic cortical neurons, including other ENGCs, interneurons and pyramidal neurons. The downstream effects of L1 interneurons including ENGCs within cortical microcircuits have been investigated independently of thalamic input as well as in response to thalamic input. L1a interneurons in mPFC cause feedforward inhibition in other L1 interneurons and L2/3 pyramidal neurons in response to thalamic input (Cruikshank et al., 2012).

Since L1 ENGCs inhibit spiking in L2/3 and L5 pyramidal neurons in sensorimotor cortex, it seems likely that suppressing L1 ENGC firing would reduce inhibition to downstream pyramidal neurons allowing their firing rates to increase (Jiang et al., 2013; Lee et al., 2015). In rat sensorimotor cortex, ENGCs have reciprocal connections with L2/3 interneurons which innervate L5 pyramidal neurons, to surprisingly have an inhibitory effect on dendritic complex spiking, while L1 SBCs have unidirectional connections with L2/3 interneurons, and overall enhance dendritic complex spiking in L5 pyramidal neurons *in vitro* (Jiang et al., 2013). This overall inhibitory effect can be explained by a mutual inhibitory electric coupling mechanism between ENGCs and L2/3 interneurons to synchronise tonic firing of L2/3 interneurons, which in turn inhibits L5 pyramidal neurons (Jiang et al., 2013).

In PFC, L1 NDNF+ and VIP+ interneurons have distinct preferred interneuronal targets. PFC VIP+ interneurons mostly innervate SST+ interneurons, but NDNF+ interneurons target PV+ interneurons, through which they can additionally cause disinhibition of pyramidal neurons

at the soma level, and not SST+ interneurons (Anastasiades et al., 2020). NDNF+ interneurons also interact with VM-recipient pyramidal neurons to suppress VM-evoked dendritic calcium spikes in PT apical dendrites and inhibit action potentials *in vitro* (Anastasiades et al., 2020).

L1 NDNF+ interneuron firing also elicits IPSPs in other L1 interneurons, L2/3 interneurons and pyramidal neurons in mouse auditory cortex *in vitro*, with the strongest input being to L2/3 pyramidal neurons (Abs et al., 2018). Axons from SST+ Martinotti cells in deeper cortical layers also innervate L2/3 pyramidal neurons at their apical dendrites in L1. These evoked IPSPs in L2/3 pyramidal neurons have a larger amplitude than those evoked in response to input from NDNF+ neurons, but have a lower overall transfer of charge, presumably due to faster kinetics of NDNF+ neurons (Abs et al., 2018). Activation of L1 ENGCs also inhibits dendritic spikes in L5 pyramidal neurons in auditory cortex. L1 NDNF+ neurons do not seem to receive inhibitory input from VIP+ or PV+ interneurons but receive input from SST+ Martinotti cells.

Overall, *in vitro* studies suggest that L1 ENGCs can inhibit dendritic spiking in deeper layer pyramidal neurons as well as PV+ interneurons in a range of cortical regions. They can also participate in feedforward inhibition in response to excitatory input, and disinhibition via targeted interneurons. Since these patterns seem comparable across various cortical regions, motor cortical ENGCs may have some similarities in connectivity.

4.1.3 Experiment summary

Electrophysiological activity in the cortex can be measured at different levels, from widespread network oscillations to single unit activity and domain specific recordings from single neurons, with different recording methods suited to extracting particular kinds of data. For the purposes of this thesis, we will focus primarily on single unit activity since this is comparable to *in vitro* whole-cell recordings in identifying individual cellular responses within

circuits. Extracellular recordings with a probe or tetrode can be used to obtain data from a large number of neurons at once, which can then be processed to identify single or multi units (Buzsaki, 2004). This has the advantage of acquiring a rich dataset allowing analysis of single or multi unit activity, LFP data, and synchrony across units since they are being recorded simultaneously. However, these neurons are not labelled with a dye, so cannot be identified histologically, instead the recording sites can be deduced by physiological characteristics, probe coordinates and probe tracks. Two measures of cortical activity that will be used in this analysis are firing rates and correlation of firing between single units.

Although *in vitro* stimulation and paired recordings are valuable tools in dissecting cortical networks, these circuits can only be fully understood when their activity in the intact brain has also been characterised. To this end, we used linear silicon probes to measure single unit activity from VM thalamus and motor cortex while optogenetically stimulating VM and inhibiting L1 NDNF+ motor cortical interneurons in awake non-behaving head-fixed mice. This methodology has a number of advantages: recording *in vivo* rather than *in vitro* means that the whole neural circuitry is intact and more representative of physiological conditions, especially in non-anaesthetised animals. While single or paired whole-cell recordings are useful for precise targeting of specific neurons and connections, high-yield multi-cell recordings provide an insight into population level responses. Optogenetics combined with multichannel probe recordings allows multiple cells to be modulated and recorded simultaneously. The *in vivo* preparation also has the advantage of being able to target optogenetic stimulation to the soma rather than terminal level due to the spatial separation of structures in the brain, to minimise potential artefacts or cross-activation in cortex. These experiments aim to develop our understanding of L1 ENGCs within the basal ganglia-

thalamocortical circuit beyond anatomical connectivity alone and build on what is currently known about parts of the circuit involving motor cortex and other areas.

4.1.4 Aims

1) Investigate the effect of selective activation of VM thalamocortical neurons on the firing rates of motor cortical neurons in awake mice.

2) Establish the role of L1 NDNF+ interneurons in mediating the effects of this thalamocortical pathway on motor cortical activity.

4.2 METHODS

4.2.1 Animals

Experimental procedures were carried out using adult male Ndnf-IRES2-dg-Cre (heterozygous on a C57BL/6J background, Jackson Laboratories) aged 5-12 months old. They were housed with littermates on a 12-hour light-dark cycle, and singly housed after headpost implantation, with food and water provided ad libitum. All procedures were carried out according to the Animals (Scientific Procedures) Act, 1986 (UK) and institutional regulations.

4.2.2 Surgical procedures

Injections

Unilateral injections were made during recovery surgery, as in chapter 2 methods. Briefly, mice were anaesthetised with 4% isoflurane in oxygen and placed in a stereotactic frame (David Kopf Instruments, California, USA). Buprenorphine (Vetergesic, 0.08mg/kg in saline) was administered subcutaneously after induction of anaesthesia to provide analgesia, and

anaesthesia maintained on 1.5-2% isoflurane through a nose mask. Body temperature was maintained at 37 ± 0.5°C with a probe and heating pad (Harvard Apparatus) under the animal. Injections were either into VM and L1, or L1 alone. The prefilled glass injection pipette (internal diameter 15-20µm) was moved to the coordinates and manually lowered to the DV coordinates, then left for 5 minutes for the brain to settle. 70nl of rAAV5-CAMKIIa-hChR2-mCherry virus was injected manually into VM thalamus (AP -1.4, ML 0.9, DV 4.0) with a syringe at a rate of 100nl per minute (Fig. 4.1A). The pipette was left in place for at least a further 5 minutes for the virus to diffuse. The pipette was then slowly brought up out of the brain. For L1 superficial injections into motor cortex, instead of a small hole above the target, a craniotomy was made in the right hemisphere posterior to Bregma and anterior to Lambda. A 90° angled pipette holder was used to insert the injection pipette subdurally via the craniotomy at an angle of about 12°, with the end of the pipette over the coordinates AP 1.5, ML 1.3. 550-600nl of virus was injected and left for 5 minutes before removing the pipette. Either rAAV5-CAG-FLEX-ArchT-GFP or AAV5-Ef1a-DIO-YFP (as a control) were injected into L1 (Fig. 4.1A). See supplemental tables (Table S1) for virus information. The animal was monitored post-operatively at least once every 24 hours until it had fully recovered and was within 5% of its original weight. All injections were unilateral in the right hemisphere. Mice were left in their home cage for 3 weeks prior to headpost implants.

Headpost implants

Animals were implanted with a titanium custom-made headpost (Get It Made Ltd, London) (internal diameter: 9mm, weight: 1.3g), at least 6 days before starting recordings. Skin was cleared from the skull and the skull was washed with H_20_2 and etched with a scalpel to remove debris and give better adhesion. The edges of the skin were glued to the skull with skin glue

(Vetbond: 3M, Minnesota, USA). The headpost was attached to the skull with superglue (3M) and dental cement (Jet Denture Repair Powder: Lang Dental, Illinois, USA; Meadway Repair Liquid: MR. Dental, Surrey). A reference screw (Precision Technology, East Grinstead) with wire was placed over the cerebellum in one hemisphere, usually ipsilateral to the injection sites. Silicone (Body Double, Smooth-On) was placed over the craniotomy and skull on the injection hemisphere. Animals were singly housed after headpost implants and monitored regularly. The day before recording, a small craniotomy was made during anaesthetised recovery surgery above each recording site and covered with fresh silicone.

4.2.3 *In vivo* optogenetics and probe recordings

Habituation and recordings

In vivo probe recordings were made in awake head-fixed mice that were not trained in any specific behavioural task. Prior to recording, mice were habituated to handling and the recording setup over around 4 - 7 days by head-fixation for increasing time durations until they were able to sit comfortably for an hour. Mice were given sucrose solution periodically via a syringe while head-fixed. The bars of the headpost were fixed into clamps and fastened with thumb screws. The mouse was in a cardboard body tube, supported by a caddy. The entire rig was surrounded by a Faraday cage. Recording sessions were a maximum of 3 hours, as specified in the project licence, up to twice per day, for up to 3 or 4 sessions in total. Sessions were ended earlier if the mouse appeared uncomfortable or restless.

Acute recordings were made with linear silicon probes with 32 channels across four shanks, 100µm between contacts, 200µm between shanks (NeuroNexus, Michigan, USA). Probes were supported by electrode holders and positioned using a stereotactic frame and arms (Kopf). One probe was lowered manually into motor cortex to a maximum depth of between

700µm to 1400µm (A4x8-100-200-177-A32). In experiments involving VM photostimulation, another probe (A4x8-100-200-177-OA32), with an integrated optic fibre on the second shank 200µm above the top contact site (105µm core; connected fibre: 200µm, 0.22NA, Thorlabs, New Jersey, USA), was inserted into VM to a maximum depth of between 3700µm and 4300 µm at an angle of 10° (Fig. 4.1B). Each probe was connected to either a 64 channel (cortical probe) or 32 channel (thalamic probe) headstage (Intan Technologies, California, USA) with an adaptor (Adpt-A32-OM32: Omnetics, Minnesota, USA) and connector (OM32, NeuroNexus). The red fluorescent dye 1,1'-dioctadecyl-3,3,3',3'-tetramethylindocarbocyanine perchlorate (DiI) (Invitrogen, California, USA), in an 80 mg/ml solution (in 50/50% acetone/methanol), was applied to both probes in the last recording session of each animal to mark the probe tracks. The cerebellar reference screw was connected to the cortical headstage, which also had a ground wire attached. A separate optic fibre (100µm, 0.37NA, Thorlabs) was positioned at an angle above the cortical craniotomy, close to but not touching the probe. A piezo vibration sensor (RS Components, Corby) was positioned on the mouse's back to monitor movement periods. Electrophysiological signals were sampled using Spike2 (Cambridge Electronic Design Ltd, Cambridge (CED)) digitised via an RHD2000 USB interface board (Intan Technologies) using the Intan Talker module (v1.4; Intan Technologies) at a rate of 20,000Hz. Recordings were made at least 15 minutes after probe insertion to allow the brain tissue to settle, and the positions adjusted until there were visible cortical units and photostimulation-responsive thalamic units. Cortical probes were initially inserted to a target depth of 800-1000µm, and occasionally moved deeper during the course of a recording session. Optogenetic stimulation was delivered via optic fibres using blue and yellow lasers at wavelengths of 561nm and 473nm (Cobolt, Sweden) controlled by TTL output from Spike2 (v8.14; CED) through a Power1401 Analogue to Digital Converter DAQ

(CED). Custom sequences of either continuous stimulation from one or both lasers were driven using Spike2. Laser power was verified and adjusted prior to each recording session with the help of a power meter interface (PM100USB: Thorlabs) and an integrating sphere photodiode power sensor (S140C: Thorlabs). A camera in front of the mouse was used to monitor the movements and welfare of the animal during recording. Sucrose was hand-delivered orally with a syringe periodically between trials to the mouse. Saline was applied to the craniotomy to ensure it remained moist. The probes were moved to new locations in subsequent recording sessions to avoid re-entering the same tracks. At the end of each session, mice were returned to their home cage.

Stimulation protocols

Three different optogenetic stimulation recording protocols were carried out while recording from both cortex and thalamus: 1) stimulation to activate ChR2 in VM thalamus alone with 473nm blue laser stimulation at 20mW, or 10mW in some of the earliest recordings, 2) inhibition of ArchT-transfected L1 NDNF+ interneurons in frontal cortex with 561nm yellow laser stimulation at 30mW, and 3) both protocols 1 and 2 combined, i.e. stimulation of VM thalamus using ChR2 and inhibition of L1 NDNF+ interneurons using ArchT. Each protocol had 20 repeats of 15s trials or sweeps. For protocols that included ChR2 stimulation, light was delivered continuously for the middle 5 seconds of each sweep (5s-10s). For protocols that included ArchT stimulation, this was applied for the middle 7 seconds of each sweep (4s-11s), and so for protocol 3 the onset and offset of the yellow laser was 1s before and after the blue laser onset and offset.

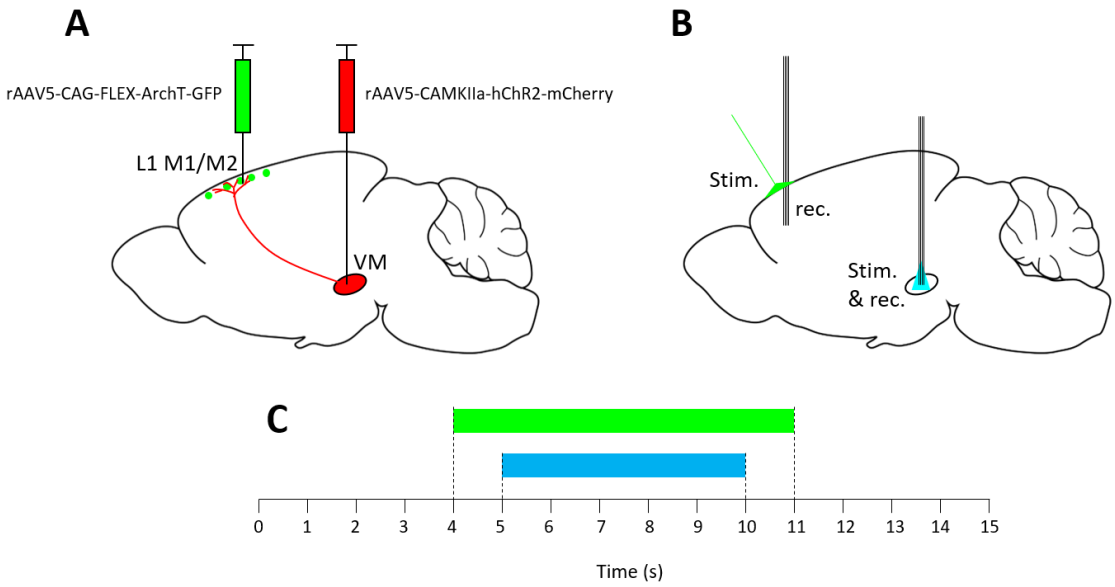


Figure 4.1 Schematic diagrams of injection and recording sites
(A) Injections of ArchT into L1 of M1 and M2, and of ChR2 into VM, in NDNF-Cre mice. **(B)** Experimental recording setup. Light from a 561nm laser was delivered via a single optic fibre above the surface of the brain while recording from motor cortex with a four-shank silicon probe. Blue light from a 473nm laser was delivered to VM thalamus via an integrated fibre attached to a recording probe. **(C)** Time course in each 15s sweep of continuous light from a 561nm laser (green bar, 4s to 11s), and continuous light from a 478nm laser (blue bar, 5s to 10s).

4.2.4 Perfusion fixation and histology

Immediately following the final recording session, mice were anaesthetised with a terminal dose of pentobarbitone and transcardially perfuse-fixed with saline followed by 4% w/v paraformaldehyde (PFA, Sigma, Germany) in 0.1M phosphate buffered saline (PBS). The headpost was removed and brain removed from the skull and incubated in 4% PFA overnight at 2-8°C, before washing in PBS and storing in PBS with 0.05% sodium azide (PBS-azide) until sectioning.

Coronal sections were cut at 50 or 60µm using a vibrating microtome and stored in PBS-azide. For confirmation of injection sites and verification of probe locations, native fluorescence signal was enhanced with antibodies. Free-floating sections were washed 3x 10 minutes in PBS-Triton-azide (PBS-Tx, 0.3% Triton v/v, 0.5% sodium azide) to permeabilize the tissue. They were then blocked in 20% v/v normal donkey serum (NDS: Vector Laboratories, California,

USA) in PBS-Tx for one hour at room temperature. Following this, the sections were incubated in primary antibody solution, in PBS-Tx with 1% NDS, overnight at room temperature. The sections were then washed 3x 10 minutes in PBS-Tx, and incubated in secondary antibody solution in PBS-Tx with 1% NDS, in the dark for either 4 hours at room temperature, or overnight at 2-8°C. The sections were then washed 3x 10 minutes in PBS, mounted on glass slides with Vectashield mounting medium (Vector Laboratories), and coverslipped.

See supplementary table S2 for primary and secondary antibody information.

4.2.5 Microscopy

Multichannel fluorescence images were obtained using a Zeiss Imager.M2 widefield epifluorescence microscope equipped with Plan-Apochromat objective lenses, a Hamamatsu Flash 4.0 LT camera and Colibri LEDs. For whole section or large area images a 5x, 10x or 20x lens was used and tiled images acquired using Stereo Investigator v11.09 (MBF Biosciences, Vermont, USA). These images were processed offline using Stereo Investigator.

4.2.6 Analysis

Spike sorting

Spike2 electrophysiological recording data and protocol event times were imported into MATLAB R2020a (The MathWorks, Natick, MA, USA) using data loading scripts from the sigTOOL toolbox (Lidierth, 2009). A common average referencing (CAR) step was carried out across cortical channels and thalamic channels separately, to remove movement artefacts. Individual Spike2 recordings were concatenated into one cortical and one thalamic binary data file per recording session. These data files were used as the input for the Kilosort2 automated spike sorting algorithm (Pachitariu et al., 2016), obtained from https://github.com/MouseLand/Kilosort, which was run using its default settings.

Kilosort2 output was manually curated using Phy software (developed by Cyril Rossant, https://github.com/cortex-lab/phy). Clusters that had a firing rate of below 0.1Hz throughout the concatenated recordings were excluded by default. Other clusters identified by Kilosort2 were identified as single units 1) if they had an action-potential-like waveform that was restricted to a spatially restricted cluster of channels on the probe, 2) if there was clear evidence of a refractory period in its inter-spike intervals and autocorrelogram, and 3) after merges with other clusters had been considered based on spike waveform similarity and evidence of a refractory period in the cross-correlogram. If there was evidence of contamination of a Kilosort2-identified cluster in the spike waveforms or in the scatterplots of spike features in principal component space, splits were attempted, and accepted if they resulted in clear improvements in the autocorrelogram's refractory period and spike waveform uniformity. Split clusters were then again taken through steps 1-3 above to determine whether they were classified as represented single units.

The spike times for units that passed these criteria were then aligned back to the onset of individual Spike2 protocols and sweeps using custom-written MATLAB scripts.

Inclusion criteria for recording sessions and units

Recording sessions were screened for evidence of an increase in firing rate of thalamic units following ChR2 stimulation to show effective modulation. Only recording sessions with effective optogenetic stimulation of VM thalamus activity were included in the analysis of cortical unit firing rates and cortical unit synchrony. This was defined as either a significant ($p < 0.05$) increase in overall thalamic firing rate (using a Wilcoxon signed-rank test between the firing rates in the baseline window vs. the firing rate in the optogenetic stimulation window

over 20 sweeps), or a significant ($p < 0.05$) increase in firing rate observed in at least 3 of the thalamic units in the recording during VM stimulation in protocol 1.

Cortical units from these sessions were subsequently included in the firing rate and synchrony analysis if they maintained at least a 0.1Hz firing rate during each of the three protocols, as a measure of minimum firing activity. Some recording sessions had more than one version of each protocol at different probe depths. To avoid duplicating any single units, sets of recordings from one probe depth with the highest number of active cortical units were selected for inclusion in analysis from each recording session.

Firing rate analysis

Baseline measures for each 15s sweep were taken from the 4 second time window before any optogenetic stimulation (0s-4s). Measures of optogenetic manipulation were taken from a 4 second window during which both optogenetic manipulations could be active, from 5.1s-9.1s in each protocol. This avoided the first 100ms after ChR2-onset that induced some transient artefacts that were not removed during spike sorting.

The firing rate of each unit was obtained by counting the number of spikes in the target time window, and dividing by the number of seconds in that window, to obtain firing rate in spikes/s. To determine whether the firing rate of an individual unit was significantly affected by the optogenetic stimulation, its firing rate in the baseline window and optogenetic stimulation window were determined for each individual recording sweep. Baseline and optogenetic firing rates were then compared using the paired, non-parametric Wilcoxon signed-rank test. Conducting a paired test minimised the additional variance introduced by any overall fluctuations in unit activity over the course of the recording as each optogenetic firing rate was effectively compared to the corresponding baseline window immediately

preceding it. A non-parametric test was used as firing rates were not normally distributed and not free to vary below 0 – this was relevant as many units (especially in cortex) had firing rates of close to 0 in several of the 4 second time windows.

Overall thalamic firing rate was obtained in a similar manner, except the spiking activity of all identified units in thalamus was pooled together. To test whether the change in overall firing rate was significant, the firing rates in the baseline window for each sweep and the firing rates in the target window for each sweep were compared using the Wilcoxon signed-rank test.

Measuring synchronised spiking between cortical units

Spike events for each unit for each recording sweep were converted to spike counts with a temporal resolution of 10ms. For each recording sweep, the binned spike counts for units were cross-correlated using MATLAB's xcorr function, with a maximum allowed lag on either side of 1 bin (i.e. 10ms). The resulting cross-correlations were normalised to generate a cross-correlation coefficient between -1 and 1 for each possible pair of units. These correlation coefficients were averaged across all sweeps to generate a mean cross-correlation coefficient for each pair. The 'coupling score' for each unit was then defined as the mean of its cross-correlation coefficients with all other units.

Statistical comparisons of unit firing rates and coupling scores

Unit firing rates and coupling scores were compared between the baseline and target window using the Wilcoxon signed-rank test. Secondly, to control for possible increases in coupling score that could be explained by either overall changes in firing rate or a general firing rate profile following optogenetic stimulation onset, the differences in unit coupling scores between baseline and optogenetic windows were compared to the differences in unit

coupling scores obtained from shuffled data. Shuffled data were generated by randomly re-ordering the sweeps for each unit, such that the data for one unit for a particular sweep would be cross-correlated with other units' data from randomly selected sweeps from the same session – breaking any instantaneous temporal correlations but preserving any overall firing rate and response profile effects in the optogenetic window. A unit's shuffled coupling score would be generated from its averaged coupling score from 10 such random shuffles.

4.3 RESULTS

After selection for thalamic and cortical firing criteria, there were a total of 89 single cortical units from 9 recording sessions across 6 animals, out of an original dataset from 18 sessions across 7 animals. Three animals each had two recording sessions included in the analysis. All 9 recording sessions contained single unit data from protocol 1, stimulation of ChR2 in VM, but two sessions did not have data for either protocol 2 or protocol 3, inhibition of L1 NDNF+ interneurons (IN) by ArchT, with and without VM stimulation. Cortical single units that were present in more than one protocol were matched across the protocols.

4.3.1 Sustained photostimulation causes modulation of VM thalamic single unit firing rates

In order to selectively stimulate VM thalamocortical neurons, we used an optrode to deliver 5s continuous stimulation with a blue laser (473nm) to the soma region of ChR2-transfected neurons within VM. Some thalamic single units, recorded by the 32-channel probe, responded to blue light stimulation. Within most recording sessions, there was a combination of non-modulated, positively modulated and negatively modulated units (Fig. 4.2). Positively modulated units were time-locked to the laser stimulation and displayed an increase in firing rate compared with baseline rates over the duration of the stimulation period (Fig. 4.2). Since

it has been well-established that VM projection neurons innervate L1 motor cortex (Herkenham, 1979; Arbuthnott et al., 1990), we presumed that these thalamic recorded neurons would have terminals in L1. We found this to be the case with our injected mice, where injections of hChR2-mCherry resulted in labelled neuropil in L1a (Fig. 4.20B). Although not all thalamic neurons responded strongly to blue light stimulation, this may have been due to a lack of opsin expression or distance from the laser. Conversely, there may have been optogenetically modulated thalamic neurons that were not detected by the probe due to their location, but nevertheless innervated L1 motor cortex. However, to ensure that all cortical units were from recording sessions with optogenetic stimulation of thalamus and that any effect in cortex was not masked due to redundant inclusion of data with no thalamic stimulation, only sessions with positive modulation of thalamic firing rates were analysed.

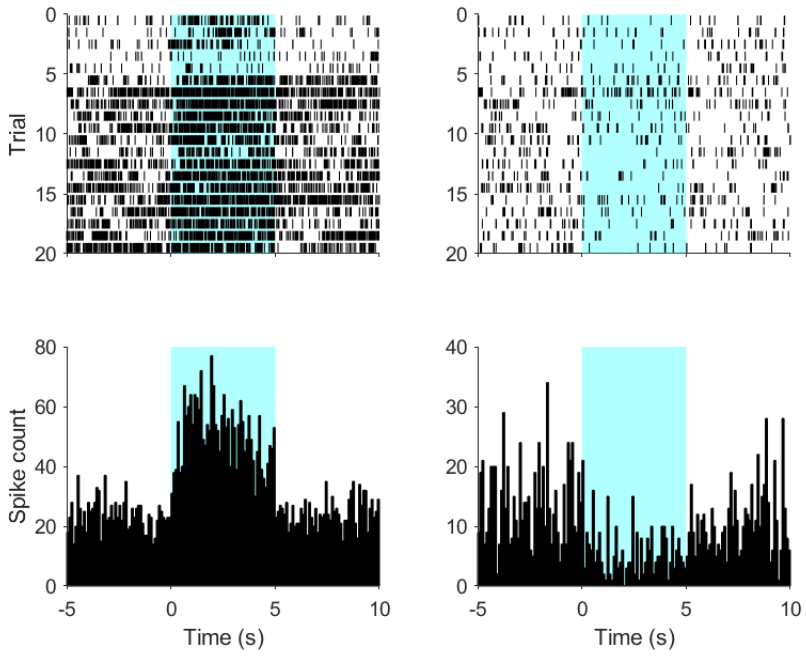


Figure 4.2 Two example thalamic units with optogenetic stimulation of VM
The top row shows raster plots of two single units from one recording session across 20 consecutive trials with continuous blue laser stimulation between 0 and 5s, showing an increase (left) and decrease (right) in firing rate in response to stimulation. The bottom row shows the corresponding peri-stimulus time histograms (PSTHs) of total spike counts over 20 consecutive trials with continuous blue laser stimulation between 5 and 10s. Blue bars represent the time period with the laser on.

From the recording sessions that passed the selection criteria of a minimum of three positively modulated thalamic units or a statistically significant overall increase in firing rate in response to optogenetic stimulation, a subset of thalamic single units showed a strong increase in firing rate during optogenetic stimulation (Fig. 4.3Aii). There was a clear increase in mean firing rates during VM stimulation only over all thalamic units combined (n = 315), which decreased slightly while the light was delivered and returned to baseline levels after the light offset, and few negatively modulated units (Fig. 4.3Ai). There was also an increase in thalamic unit firing rates during VM stimulation and light delivery to cortical L1 NDNF+ interneurons (Figs. 4.3B, n = 279), which remained fairly constant during the stimulation window before returning to baseline levels. Like the responses to VM stimulation alone, there were also few negatively modulated units.

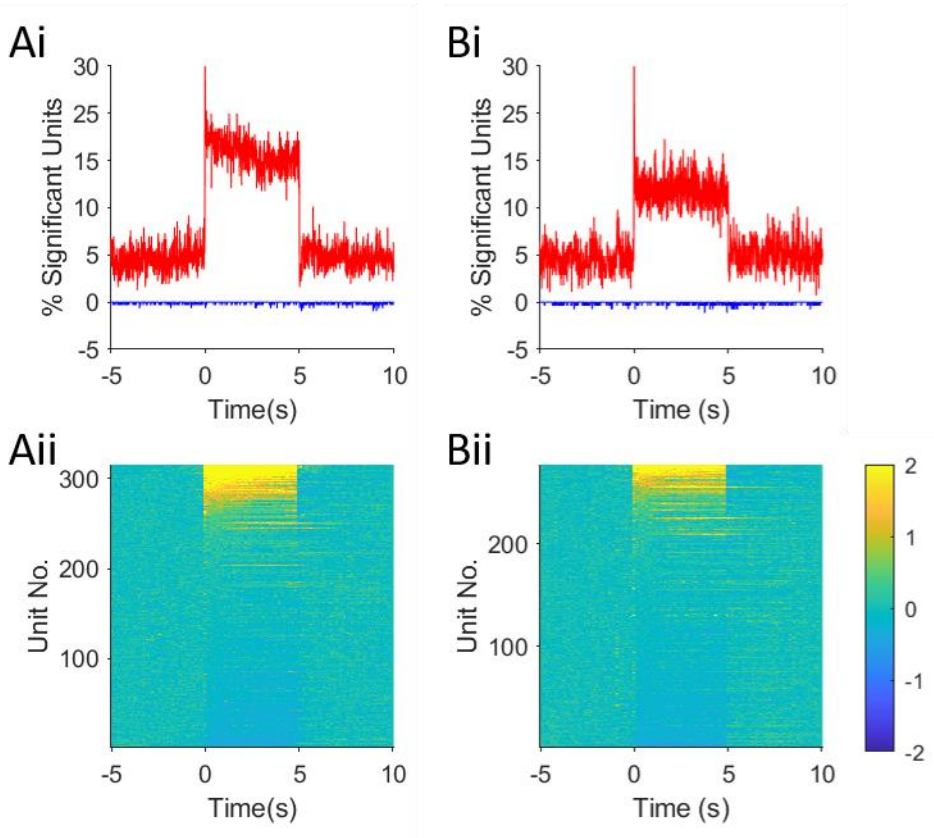


Figure 4.3 Modulation of the firing rates of thalamic single units in response to VM stimulation with and without inhibition of cortical L1 NDNF+ neurons

(Ai) Percentage of thalamic single units (n = 315) that have a significant increase (z-score value > 2, red trace) in firing rate compared to the pre-stimulation baseline window, and a significant decrease (z-score value < -2, negative scale, blue trace) in firing rate in response to VM stimulation, in 10ms bins. Continuous blue laser stimulation was delivered between 0s and 5s. **(Aii)** Heatmap showing the z-scored firing rate per unit (n = 315) relative to the pre-stimulation baseline window, with blue light stimulation of VM between 0s and 5s, in 10ms bins, normalised to the baseline window. **(Bi)** Percentage of thalamic single units (n = 279) that have a significant increase (z-score value > 2, red trace) in firing rate compared to the pre-stimulation baseline window, and a significant decrease (z-score value < -2, negative scale, blue trace) in firing rate in response to VM stimulation with simultaneous delivery of yellow light to cortex. Continuous blue laser stimulation was delivered between 0s and 5s, and yellow laser between -1s and 6s. **(Bii)** Heatmap showing the z-scored firing rate per unit (n = 279) relative to the pre-stimulation baseline window, with blue light stimulation of VM between 0s and 5s and yellow light between -1s and -6s.

4.3.2 VM stimulation has little effect on motor cortical single unit firing rates

We analysed data from a total of 9 sessions from 6 animals for single motor cortical units with a minimum baseline activity of 0.1Hz across the three protocol conditions of VM photostimulation alone, L1 NDNF+ IN inhibition alone, and simultaneous VM stimulation

and L1 NDNF+ IN inhibition, in which sessions met the inclusion criteria of positive thalamic modulation in response to activation of ChR2. This yielded a total of 89 single motor cortical units, which were biased towards deeper layers.

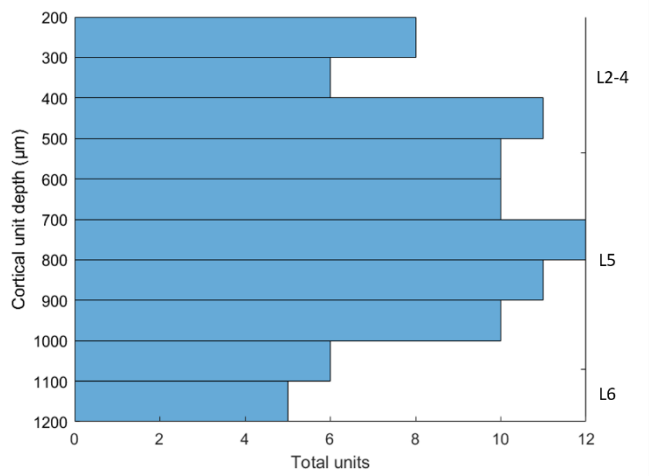


Figure 4.4 Depths of motor cortical units
Distance from the pia of all recorded motor cortical single units included in this analysis (n = 89) based on the probe depth and position of contacts on the probe. Most units that passed the selection criteria were in L2-5, with more units in L5 than L2-4.

Analysis of this data did not support our hypothesis, as continuous optogenetic stimulation of VM had little effect on the firing rate of single units in motor cortex (Figs. 4.5, 4.6, 4.8). Most single cortical units from an example session showed no significant change in firing rates in response to VM stimulation (n = 14, Figs. 4.5, 4.6). There was no overall change in mean firing rate of all cortical units between the baseline 'light off' period compared with the 'light on' period (Fig. 4.8D). 3% of all single units were significantly negatively modulated by the light ($p < 0.05$, Wilcoxon signed-rank test) and under 1% were positively modulated (Fig. 4.8B,C). There was also little change in firing rates over the duration of the stimulation period (Figs. 4.6, 4.7, 4.8A).

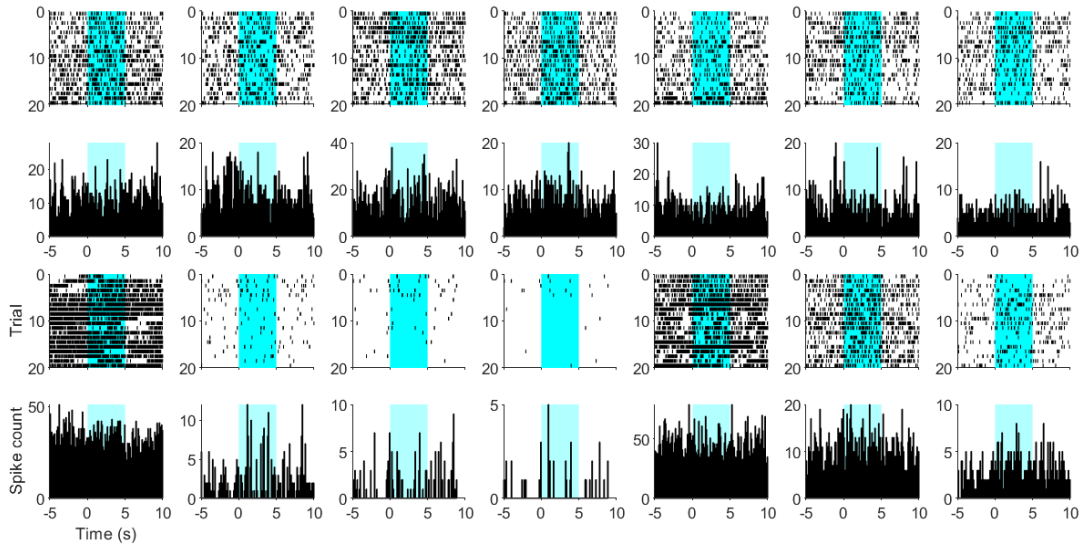


Figure 4.5 Firing rates of single cortical units in one recording session show little response to VM stimulation.

Top and third rows: Raster plots of spikes per trial (20 trials, 15s sweeps) for each single cortical unit that passed the selection criteria (n = 14) in one recording session, with VM stimulation. Blue bars represent the period of continuous laser stimulation between 0 and 5s. Second and bottom rows: PSTHs of total spike counts for the same units in the raster plots over 20 consecutive trials with continuous blue laser stimulation between 0 and 5s. Blue bars represent the time period with the laser on. There was variation in the firing rates between the cortical units, which did not change much in response to optogenetic stimulation.

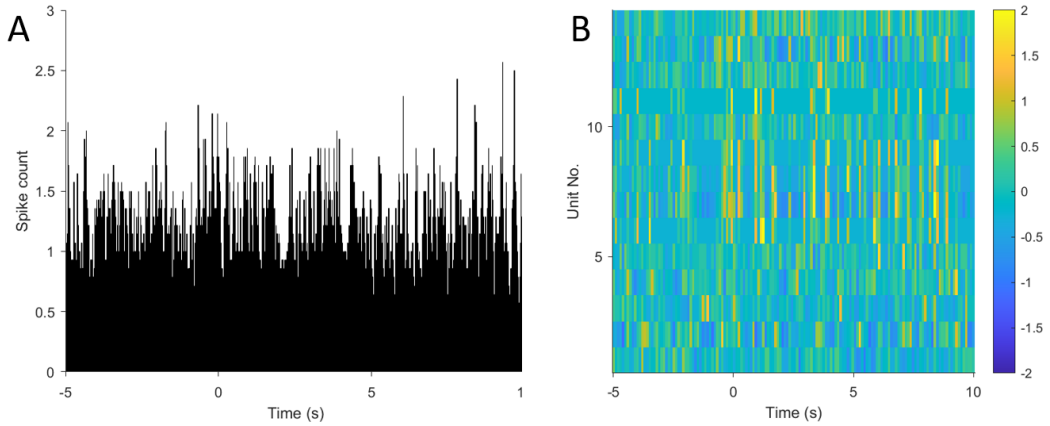


Figure 4.6 Mean firing rates of all cortical units in an example session during VM stimulation

(A) PSTH showing the mean firing rates of all cortical single units (n = 14) during one recording session (Fig. 4.5) with VM stimulation (laser on continuously between 0s and 5s). **(B)** Heatmap showing the z-scored firing rates per unit (n = 14) for the single session in Fig. 4.5 relative to the pre-stimulation baseline window, with blue light stimulation of VM between 0s and 5s, in 10ms bins, normalised to the baseline window.

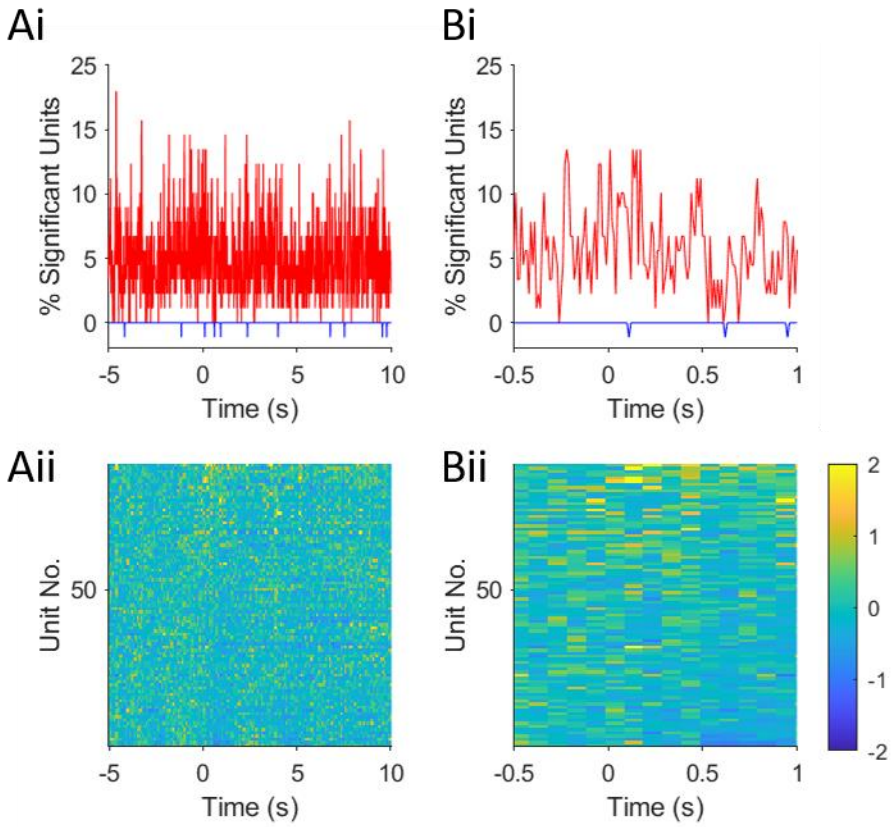


Figure 4.7 Modulation of firing rates of cortical single units in response to VM stimulation
(Ai) Percentage of cortical single units (n = 89) that have a significant increase (z-score value > 2, red trace) in firing rate compared to the mean firing rate during the pre-stimulation baseline window (-5s to -1s), and a significant decrease (z-score value < -2, negative scale, blue trace) in firing rate in response to VM stimulation, in 10ms bins, over a 15s sweep. Continuous blue laser stimulation was delivered between 0s and 5s. There was little change in the proportions of units with a significant increase in firing rate during the stimulation compared with the baseline window. Very few units had a significant decrease in firing rate. **(Aii)** Heatmap showing the z-scored firing rate per unit (n = 89) relative to the pre-stimulation baseline window, with blue light stimulation of VM between 0s and 5s, in 10ms bins, normalised to the baseline window. **(Bi)** Same as in (Ai), for the time window between -0.5s and 1s, around the onset of the laser stimulation. **(Bii)** Same as in (Bii), for the time window between -0.5s and 1s, around the onset of the laser stimulation.

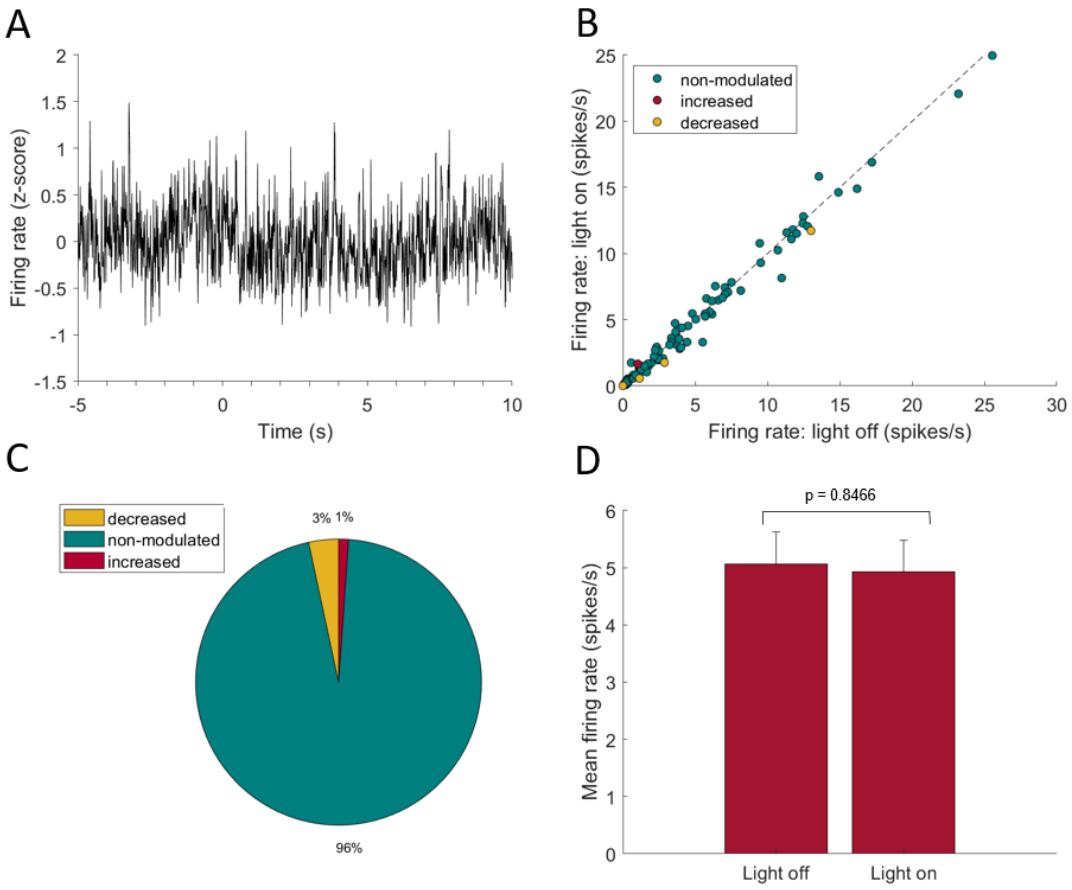


Figure 4.8 Relative firing rates of cortical units in response to optogenetic stimulation of VM
(A) Plot of mean z-scored firing rates of cortical single units across all sessions with VM stimulation (0s to 5s) shows no overall change in firing rates compared with the pre-stimulation period baseline window (-5s to -1s). **(B)** Mean firing rates per cortical single unit (n = 89) during the 'light off' baseline window (0 to 4s) and during the 'light on' target period (0.1 to 4.1s). **(C)** Proportions of positively modulated, negatively modulated and non-modulated cortical single units. Most units (96%) were not modulated, with 3% significantly suppressed and 1% significantly increased in response to VM stimulation ($p < 0.05$, two-sided Wilcoxon rank sum test). **(D)** Mean firing rate of cortical units during the 'light off' baseline window (-5s to -1s) and mean firing rate of cortical units during the 'light on' target period (0.1 to 4.1s). Mean firing rate with the light off was 5.07 ± 0.56 spikes/s, and 4.93 ± 0.55 spikes/s with the light on. Error bars are SEM. There is no significant difference between firing rates in the presence or absence of optogenetic stimulation ($p = 0.847$, two-sided Wilcoxon rank sum test).

4.3.3 Optogenetic inhibition of L1 NDNF+ neurons partially suppresses motor cortical single unit firing rates with and without VM stimulation

To investigate the influence of motor cortical L1 NDNF+ ENGCs on the downstream cortical circuitry with the basal ganglia-thalamocortical circuit, we first inhibited ArchT-transfected L1 NDNF+ neurons in motor cortex with yellow light from a 561nm laser delivered via an optic

fibre above the cortical surface while measuring cortical single unit spiking activity, between 4-11s of each 15s sweep, represented as between 0-7s on the graphs below (Figs. 4.9, 4.10, 4.11, 4.12). This was then followed by simultaneously inhibiting L1 NDNF+ neurons by activating ArchT, and stimulating VM by activating ChR2 as previously, while measuring both motor cortical and VM thalamic single unit activity (Figs. 4.14, 4.15, 4.16, 4.17).

Overall, optogenetic inhibition of L1 motor cortical NDNF+ neurons caused a decrease in firing rate of motor cortical neurons (Fig. 4.12). Around 75% of recorded single units were not modulated, 8% increased their firing rate and 17% decreased their firing rate in response to photoinhibition (Fig. 4.12B,C). This was unexpected, as suppression of L1 ENGC activity would theoretically remove this inhibitory input to downstream cortical neurons. Some single units demonstrated a marked increase or decrease in firing rate (Figs. 4.9, 4.10B). These effects did not appear to be localised to a particular cortical depth (data not shown).

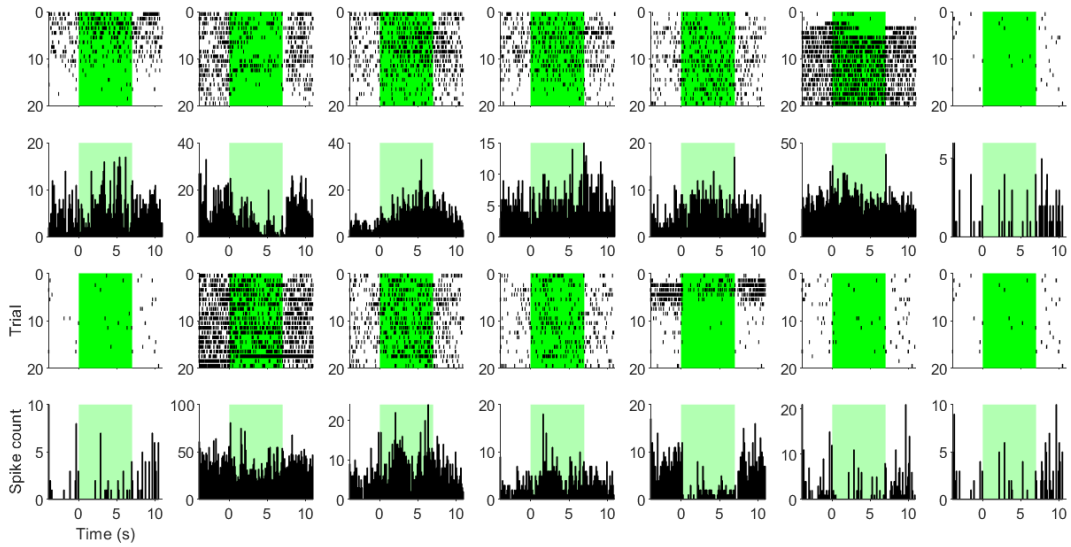


Figure 4.9 Firing rates of single cortical units display no significant overall change in response to L1 cortical interneuron inhibition

Top and third rows: Raster plots of spikes per trial from one recording session (20 trials, 15s sweeps) for each single cortical unit that passed the selection criteria (n = 14) in one recording session, with continuous optogenetic inhibition of L1 NDNF+ neurons in frontal cortex. Green bars represent the period of continuous laser stimulation between 0 and 7s. Second and bottom rows: PSTHs of total spike counts for the same units in the raster plots over 20 consecutive trials with continuous yellow laser inhibition between 0s and 7s. Green bars represent the time period with the laser on. Some single units had no significant change in firing rate in response to optogenetic inhibition of L1 interneurons compared with pre-inhibition baseline firing rates, while others had a significant increase or decrease.

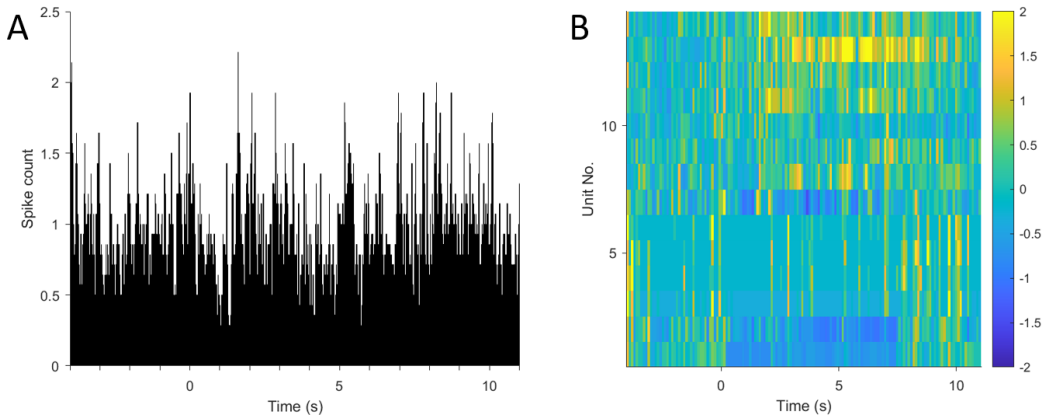


Figure 4.10 Mean firing rates of all cortical units in an example session during L1 inhibition

(A) PSTH of mean firing rates of all cortical single units (n = 14) during one recording session (Fig. 4.9) in response to continuous light delivery from a 561nm laser to L1 of frontal cortex between 0s and 7s. **(B)** Heatmap showing the z-scored firing rate per unit (n = 14) for the single session in Fig. 4.9 relative to the pre-stimulation baseline window, with yellow light stimulation of cortex between 0s and 7s, in 10ms bins, normalised to the baseline window.

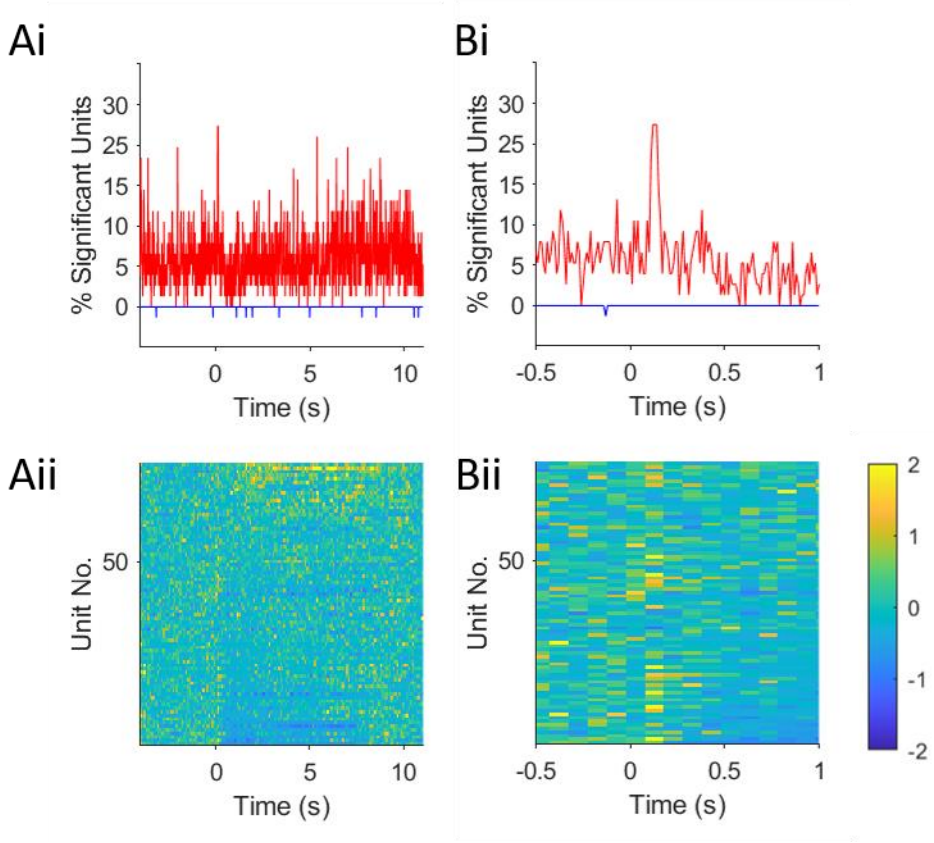


Figure 4.11 Modulation of firing rates of cortical single units in response to L1 NDNF+ neurons inhibition

(Ai) Percentage of cortical single units (n = 76 units, 8 sessions) that have a significant increase (z-score value > 2, red trace) in firing rate compared to the mean firing rate during the baseline window prior to photoinhibition (-4s to 0s), and a significant decrease (z-score value < -2, negative scale, blue trace) in firing rate in response to cortical L1 NDNF+ neuron inhibition, in 10ms bins, over a 15s sweep. Continuous yellow laser stimulation was delivered between 0s and 7s. There was little change in the proportions of units with a significant increase in firing rate during the stimulation compared with the baseline window. Very few units had a significant decrease (z-score value < -2) in firing rate within these sub-second time bins. **(Aii)** Heatmap showing the z-scored firing rate per unit (n = 76) relative to the pre-stimulation baseline window, with green light stimulation of cortex between 0s and 7s, in 10ms bins, normalised to the baseline window. **(Bi)** Same as in (Ai), for the time window between -0.5s and 1s, around the onset of the laser inhibition. **(Bii)** Same as in (Aii), for the time window between -0.5s and 1s, around the onset of the laser inhibition.

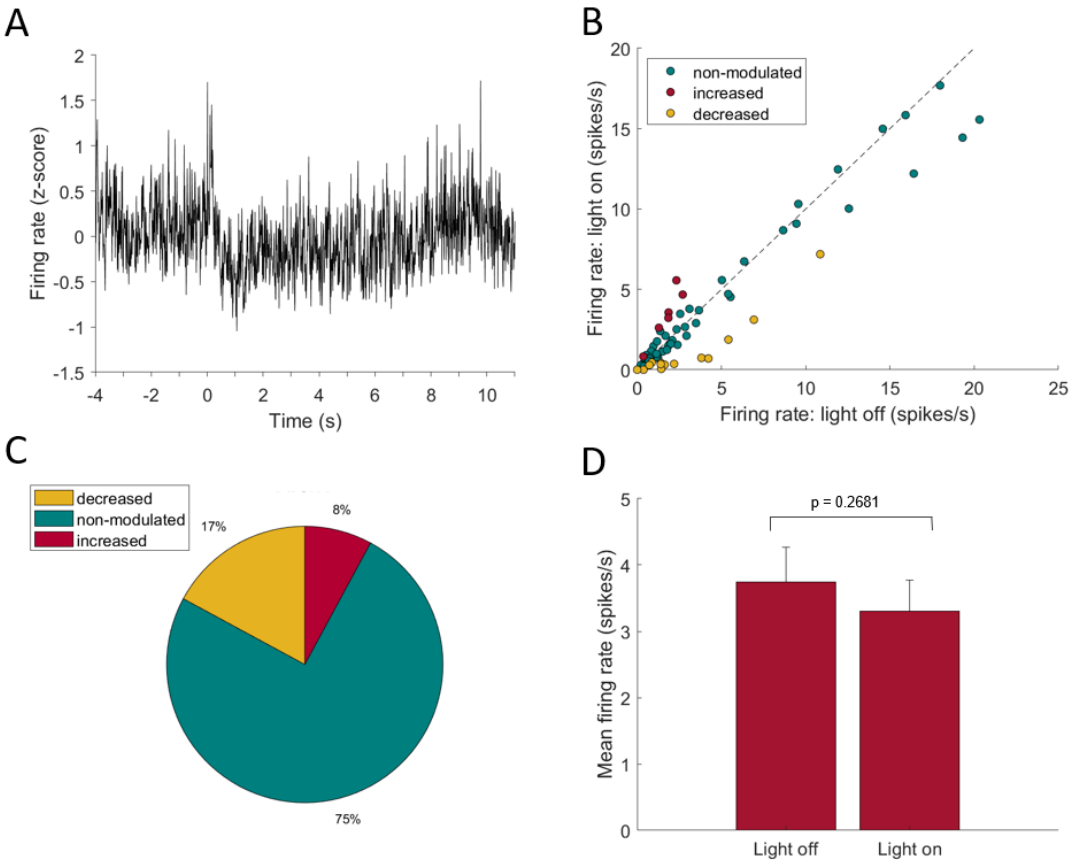


Figure 4.12 Relative firing rates of cortical units in response to optogenetic inhibition of L1 NDNF+ ArchT-transfected neurons

(A) Plot of mean z-scored cortical firing rates of cortical single units (n = 76) across all sessions (n = 8) shows a decrease in firing rates with L1 NDNF+ neuron inhibition (0s to 7s). **(B)** Mean firing rates per cortical single unit (n = 76) during the 'light off' baseline window (-4s to 0s) and during the 'light on' target period (1.1 to 5.1s). Large stimulation artefacts were removed manually for aesthetic purposes by replacing z-score values over 2 with the mean of values on either side. **(C)** Proportions of positively modulated, negatively modulated and non-modulated cortical single units. Most units (75%) were not modulated, with 17% significantly suppressed and 8% significantly increased in response to VM stimulation ($p < 0.05$, two-sided Wilcoxon rank sum test). **(D)** Mean firing rate of cortical units during the 'light off' baseline window (-0.4 to 0s) and mean firing rate of cortical units during the 'light on' target period (1.1 to 5.1s). Mean firing rate with the light off was 3.74 ± 0.52 spikes/s, and 3.31 ± 0.47 spikes/s with the light on, with no significant difference between firing rates in the presence or absence of optogenetic stimulation ($p = 0.847$, two-sided Wilcoxon rank sum test).

As a control for cortical inhibition, NDNF-Cre mice (n = 2 mice, 4 sessions) with injected AAV-GFP instead of ArchT underwent the same L1 inhibition experiments with protocol 2. A total of 67% of units were not modulated, 23% were suppressed and 11% increased their firing rates during the laser on period compared with baseline firing rates (Fig. 4.13A,B). There was

a non-significant reduction in overall mean firing rates between baseline and laser conditions (Fig. 4.13C). These grouped data effects were similar to those seen with L1 inhibition in mice with ArchT (Fig. 4.12), indicating that any apparent effect of suppression of firing was not necessarily dependent on opsin-mediated laser inhibition of ArchT-transfected NDNF+ neurons, and may be explained by heating effects of the laser.

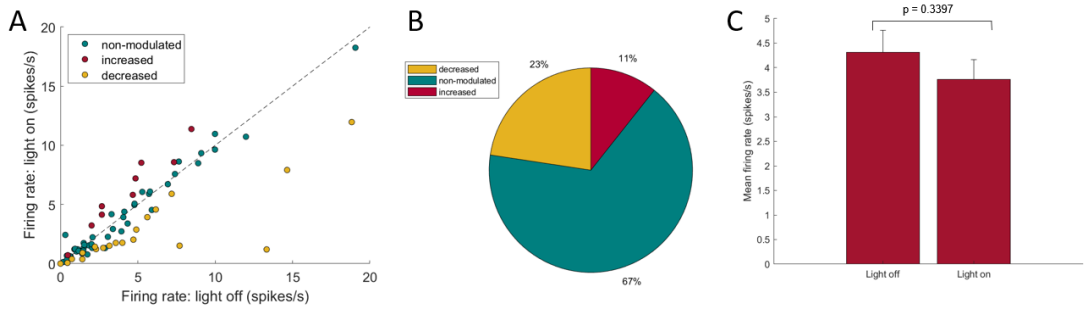


Figure 4.13 Relative firing rates of cortical units in response to light delivery to opsin-negative GFP-control L1 NDNF+ neurons

(A) Plot of mean z-scored cortical firing rates of cortical single units (n = 75) across all sessions (n = 4, 2 animals) shows a decrease in firing rates with L1 NDNF+ neuron inhibition with a 561nm laser (0s to 7s). **(B)** Mean firing rates per cortical single unit (n = 75) during the 'light off' baseline window (-4s to 0s) and during the 'light on' target period (1.1 to 5.1s). **(C)** Proportions of positively modulated, negatively modulated, and non-modulated cortical single units. Most units (67%) were not modulated, with 23% significantly suppressed and 11% significantly increased in response to VM stimulation ($p < 0.05$, two-sided Wilcoxon rank sum test). **(D)** Mean firing rate of cortical units during the 'light off' baseline window (-0.4 to 0s) and mean firing rate of cortical units during the 'light on' target period (1.1 to 5.1s). Mean firing rate with the light off was 4.32± 0.44 spikes/s, and 3.77 ± 0.39 spikes/s with the light on, with no significant difference between firing rates in the presence or absence of optogenetic stimulation ($p = 0.3397$, two-sided Wilcoxon rank sum test).

Finally, for protocol 3 ('ChR2 and ArchT'), we looked at the effects on cortical single unit firing rates in response to VM stimulation and L1 NDNF+ neuron inhibition (Figs. 4.14, 4.15, 4.16, 4.17). The effect on firing rates appeared similar to that seen with L1 inhibition alone, with an overall non-significant reduction in firing rate during simultaneous delivery of both blue and yellow light, in comparison to baseline rates (Fig. 4.17D). 73% of analysed units were non-modulated, 23% were significantly suppressed, and 4% had a significant increase in firing rates (Fig. 4.17B,C). Single units (n = 14) from one recording session showed a range of units with

no modulation or an increase or decrease in firing rate during optogenetic stimulation and inhibition (Figs. 4.14, 4.15B), some of which displayed similar responses to those seen in the same units with L1 inhibition alone (Fig. 4.9). Overall, there was confirmed positive thalamic modulation, but no significant change in firing rates of cortical units for any of the three protocols.

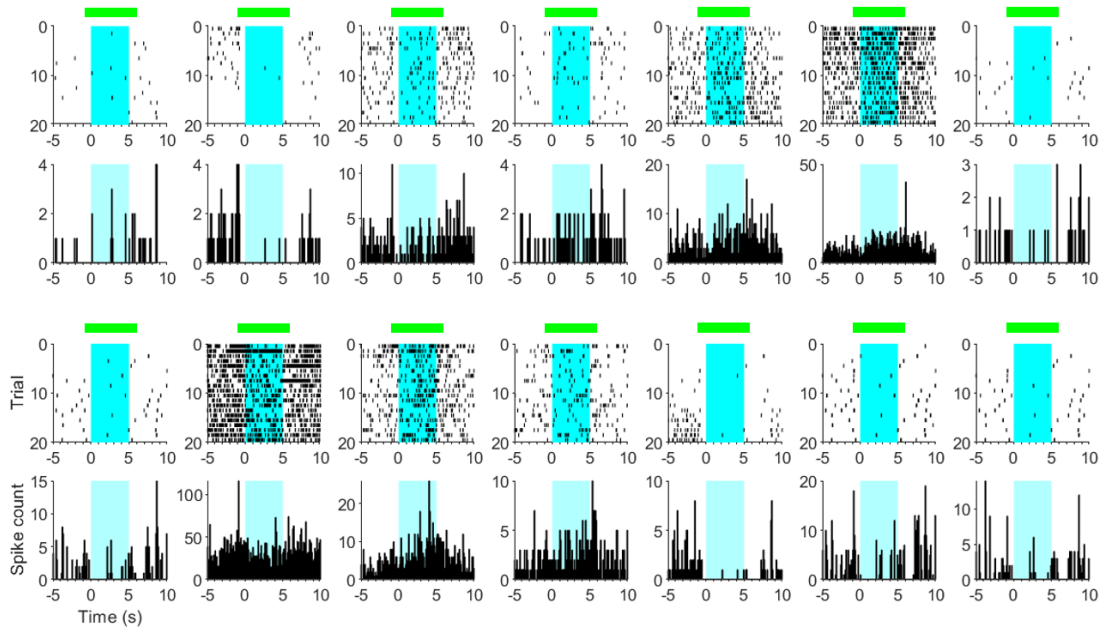


Figure 4.14 Firing rates of single cortical units in one recording session during optogenetic stimulation of VM and inhibition of L1 cortical NDNF+ neurons

Top and third rows: Raster plots of spikes per trial (20 trials, 15s sweeps) for each single cortical unit that passed the selection criteria (n = 14) in one recording session, with VM stimulation between 0s and 5 and L1 inhibition between -1s and 6s. Blue bars represent the period of continuous blue laser stimulation and green bars represent the period of continuous yellow laser inhibition. Second and bottom rows: PSTHs of total spike counts for the same units in the raster plots over 20 consecutive trials with continuous blue laser stimulation between 0 and 5s and L1 inhibition between -1s and 6s. Some single units had no significant change in firing rate in response to optogenetic inhibition of L1 interneurons compared with pre-inhibition baseline firing rates, while others had a significant increase or decrease.

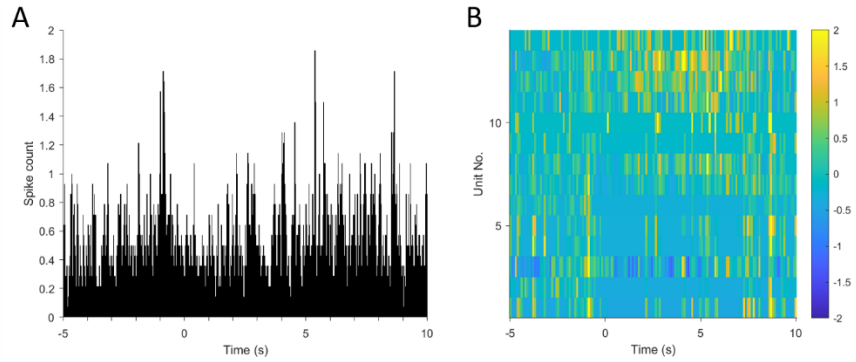


Figure 4.15 Mean firing rates of all cortical units in an example session during VM stimulation and L1 NDNF+ IN inhibition

(A) PSTH of mean firing rates of all cortical single units (n = 14) during a single recording sessions (Fig. 4.14) in response to VM stimulation between 0s and 5s and inhibition of L1 NDNF+ frontal cortical neurons between -1s and 6s. **(B)** Heatmap showing the z-scored firing rate per unit (n = 14) from the single session in Fig. 4.14 relative to the pre-stimulation baseline window, with blue light stimulation of VM between 0s and 5s, and continuous yellow laser stimulation delivered between -1s and 6s. Bins are 10ms, with z-scored firing rates normalised to the baseline window (-5s to -1s).

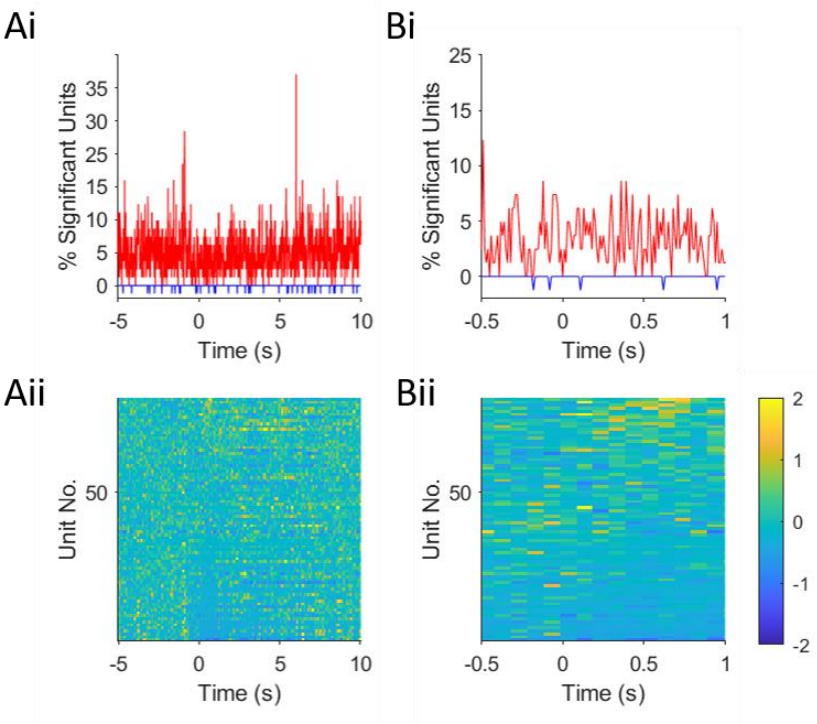


Figure 4.16 Modulation of firing rates of cortical single units in response to VM stimulation and L1 inhibition

(Ai) Percentage of cortical single units (n = 81 units, 8 sessions) that have a significant increase (z-score value > 2, red trace) in firing rate compared to the mean firing rate during the pre-stimulation baseline window (-5s to -1s), and a significant decrease (z-score value < -2, negative scale, blue trace) in firing rate in response to VM stimulation and L1 NDNF+ neuron inhibition, in 10ms bins, over a 15s sweep. Continuous blue laser stimulation was delivered between 0s and 5s, and continuous yellow laser stimulation was delivered between -1s and 6s. There was a slight decrease in the proportions of units with a significant increase in normalised firing rate during the stimulation compared with the baseline window. Very few units had a significant decrease in firing rate. **(Aii)** Heatmap showing the z-scored firing rate per unit (n = 81) relative to the pre-stimulation baseline window, with blue light stimulation of VM between 0s and 5s, and continuous yellow laser stimulation delivered between -1s and 6s. Bins are 10ms, with z-scored firing rates normalised to the baseline window (-5s to -1s). **(Bi)** Same as in (Ai), for the time window between -0.5s and 1s, around the onset of the laser stimulation. **(Bii)** Same as in (Aii), for the time window between -0.5s and 1s, around the onset of the laser stimulation.

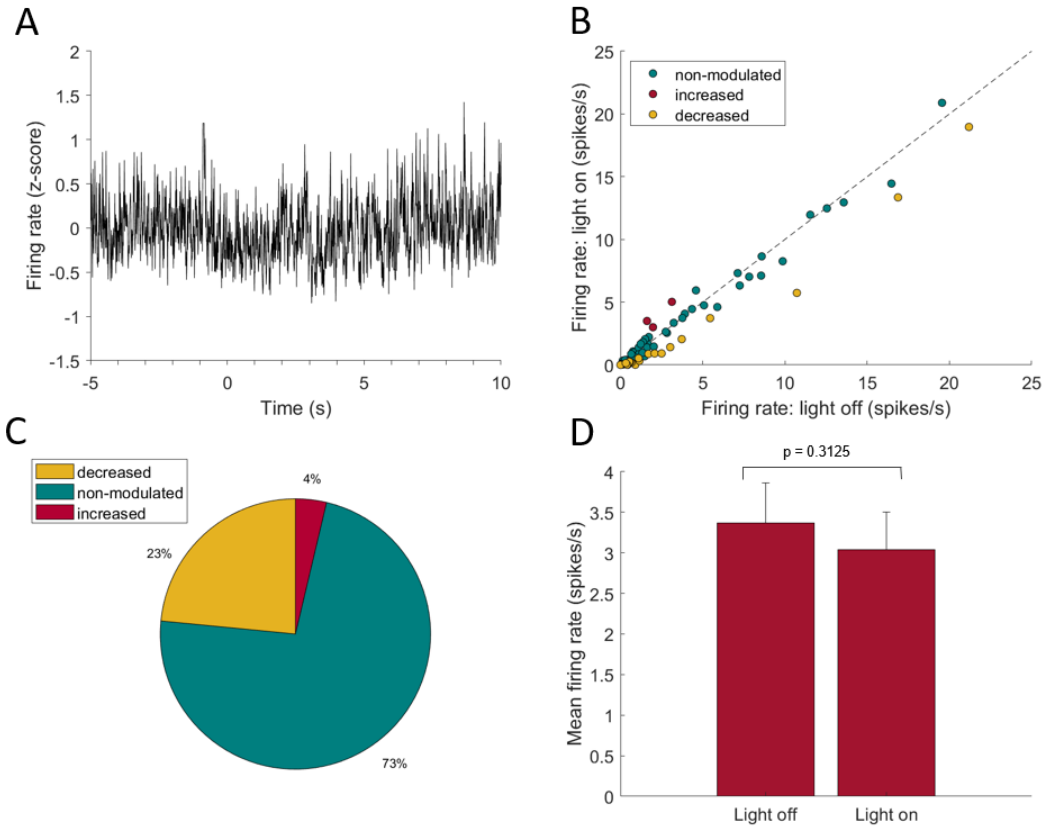


Figure 4.17 Relative firing rates of cortical units in response to optogenetic stimulation of VM and inhibition of L1 NDNF+ neurons

(A) Plot of mean z-scored cortical firing rates of cortical single units across all sessions with VM stimulation (0s to 5s) and inhibition of L1 NDNF+ neurons (-1s to 6s) shows a slight decrease in firing rates compared with the prestimulation baseline window. Large stimulation artefacts were removed manually for aesthetic purposes by replacing z-score values over 2 with the mean of values on either side. **(B)** Mean firing rates per cortical single unit (n = 81) during the 'light off' baseline window (0 to 4s) and during the 'light on' target period where both lasers were on simultaneously (0.1 to 4.1s). **(C)** Proportions of positively modulated, negatively modulated and non-modulated cortical single units. Most units (73%) were not modulated, with 23% significantly suppressed and 4% significantly increased in response to VM stimulation ($p < 0.05$, two-sided Wilcoxon rank sum test). **(D)** Mean firing rate of cortical units during the 'light off' baseline window (-5s to -1s) and mean firing rate of cortical units during the 'light on' target period (0.1 to 4.1s). Mean firing rate with the light off was 3.37 ± 0.50 spikes/s, and 3.04 ± 0.46 spikes/s with the light on. Error bars are SEM. There is no significant difference between firing rates in the presence or absence of optogenetic stimulation ($p = 0.313$, two-sided Wilcoxon rank sum test).

4.3.4 Effects of VM stimulation and inhibition of L1 NDNF+ neurons on cortical single unit synchrony

Since there was no significant change in motor cortical single unit firing rates between baseline and optogenetic conditions, we decided to explore whether there was a change in

the synchrony between these units in response to optogenetic modulation of thalamic and cortical neurons. Each cortical single unit (n = 89) was cross-correlated with all other units in the same recording session to generate correlation coefficients for the baseline and optogenetic conditions as a measure of coupling (Figs 4.18C,D,F,G, 4.19A), and a delta coupling coefficient calculated from the difference between baseline and optogenetic correlation coefficients (Figs. 4.18E,H, 4.19B). Coupling scores from shuffled trials were used as a control. For protocol 1, with blue light stimulation of ChR2 in VM with alone, there was no significant change in cortical synchrony ($p = 0.171$ for the difference between baseline and optogenetic correlation scores, and $p = 0.195$ for the difference between the delta coupling coefficients of matched and shuffled trials). For protocol 2, with yellow light inhibition of L1 NDNF+ neurons with ArchT alone, there was no significant change in cortical synchrony for the difference between baseline and optogenetic correlation scores ($p = 0.07$, Fig. 4.19A) but a significant difference between the delta coupling coefficients of matched and shuffled trials and ($p = 0.003$). For protocol 3 with simultaneous stimulation of VM and yellow light inhibition of L1 NDNF+ neurons, there was a significant change in cortical synchrony for the difference between baseline and optogenetic correlation scores ($p < 0.001$, Fig. 4.19A) and a significant difference between the delta coupling coefficients of matched and shuffled trials and ($p < 0.001$). This increase in synchrony when both lasers are active is demonstrated by an example recording session, with a clear increase in paired correlation between cortical single units during optogenetic modulation (n = 14 units) (Fig. 4.18).

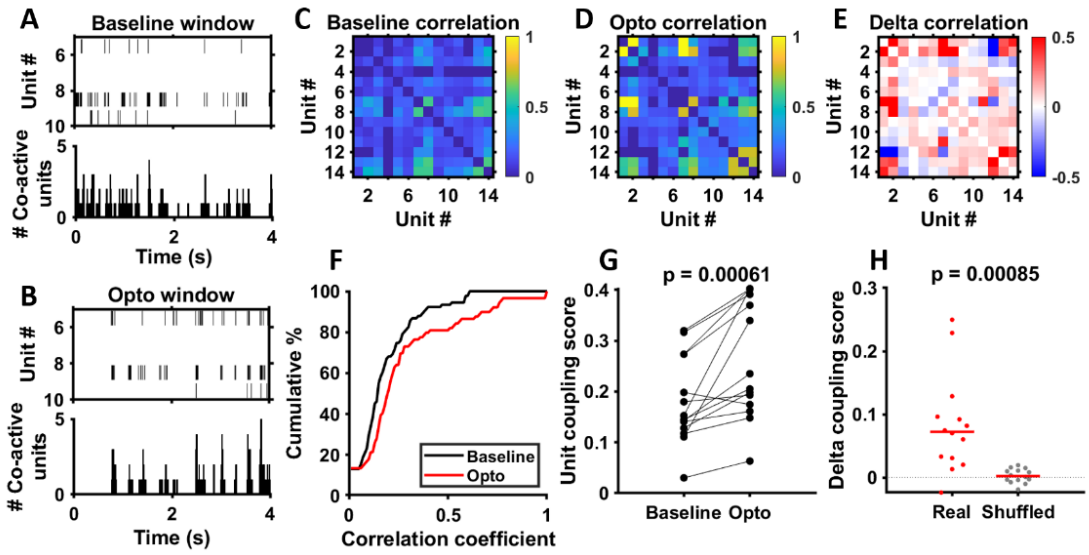


Figure 4.18 Synchrony of motor cortical single units in response to optogenetic stimulation of VM and inhibition of cortical L1 NDNF+ neurons

Correlation measures of motor cortical single units (n = 14) from a single recording session, comparing synchrony in the absence and presence of optogenetic stimulation of VM and inhibition of cortical L1 NDNF+ neurons. **(A)** Top: Spike trains of three example units from one trial during a single session during the 4s baseline pre-stimulation window. Bottom: Number of co-active units from a single trial during the 4s baseline pre-stimulation window. Bars represent the number of concurrently active units, within the same 10ms bin or one bin on either side. **(B)** Top: Spike trains of three example units from one trial during a single session during the beginning 4s of the optogenetic stimulation window, from 0.1s after the onset of blue laser stimulation of VM and 1.1s after the onset of yellow laser inhibition of L1 NDNF+ neurons. Bottom: Number of co-active units during the same 4s optogenetic stimulation window. Bars represent the number of concurrently active units, within the same 10ms bin or one bin on either side. **(C)** Pairwise correlations between units (n = 14) in the 4s baseline window, averaged across 20 trials. **(D)** Pairwise correlations between units (n = 14) in the 4s optogenetic stimulation window, averaged across 20 trials. There are more pairs of units with higher correlation compared with baseline pairwise correlations. There was a negative correlation between units 1,2 and 12 not shown by the colour scale. **(E)** Matrix showing the differences in pairwise correlations between the baseline and optogenetic stimulation windows. **(F)** Cumulative distribution of pairwise correlations corresponding to the baseline correlation matrix (black line) and the optogenetic stimulation correlation matrix (red line) showing a clear rightward shift. **(G)** Unit coupling scores, representing the average of all pairwise correlations for each individual unit (n = 14) during the baseline and optogenetic stimulation windows. Most units show a higher unit coupling score during the opto period than baseline (p = 0.00061). **(H)** The unit coupling scores in (G) were used to calculate a delta coupling score of the difference in pairwise correlations between the baseline and opto periods for paired trials for each unit (real, red markers). Delta coupling scores were also calculated with the difference between baseline and opto pairwise correlations calculated using shuffled trials for each unit (shuffled, grey markers). There was a significant difference in unit coupling score between the real and shuffled trials (p = 0.00085).

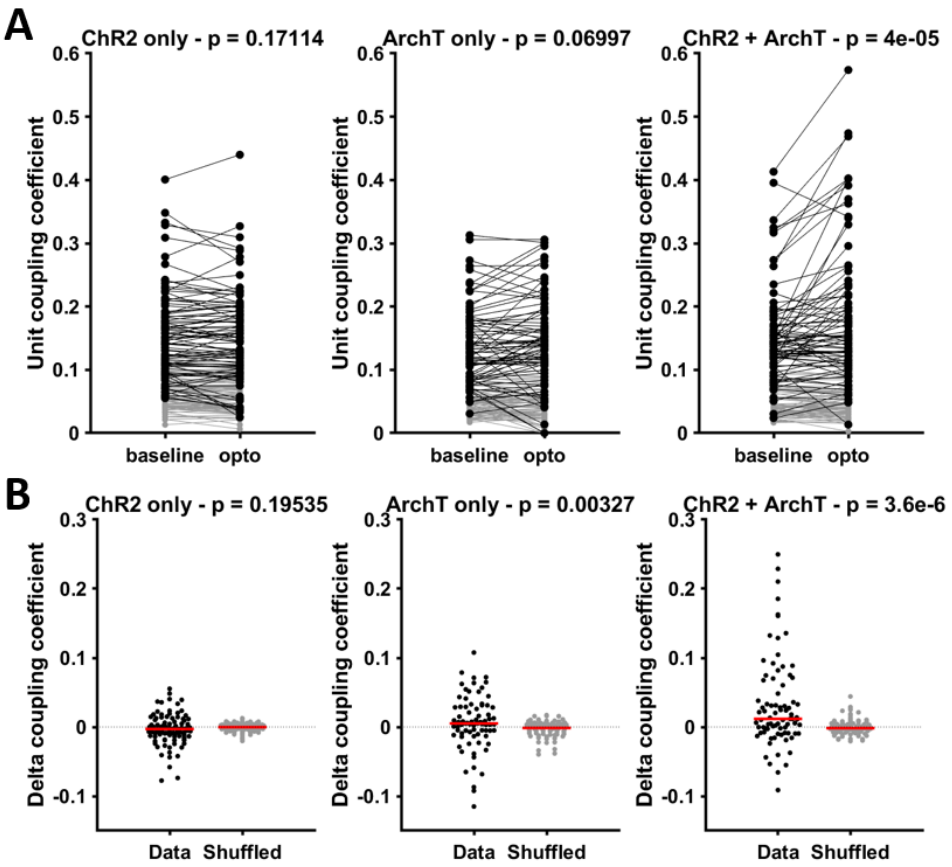


Figure 4.19 Unit coupling scores for each optogenetic protocol

(A) Left: Unit coupling scores for each unit (n = 89) during the 'ChR2 only' protocol representing the average of all pairwise correlations of each unit during the baseline window (-5 to -1s before laser onset) and optogenetic VM stimulation window (0.1 to 4.1s of laser onset). There was no significant difference between the baseline and stimulation window coupling scores (p = 0.171). Centre: Unit coupling scores for each unit (n = 76) representing the average of all pairwise correlations of each unit during the 'ArchT only' protocol with optogenetic inhibition of L1 NDNF+ neurons. The baseline window was -4 to 0s before laser onset and the optogenetic inhibition window was at 1.1 to 5.1s from laser onset. There was no significant difference between the baseline and stimulation window coupling scores (p = 0.070). Right: Unit coupling scores for each unit (n = 81) representing the average of all pairwise correlations of each unit during the 'ChR2 and ArchT' protocol with optogenetic stimulation of VM and inhibition of L1 NDNF+ neurons. The baseline window was -5 to -1s before VM stimulation and -4 to 0s before L1 inhibition and the optogenetic stimulation window was at 0.1 to 4.1s from the blue laser onset. The optogenetic window scores were significantly higher than the baseline scores for the matched trial ($p = 4 \times 10^{-5}$). Coupling scores from matched trials are represented by black markers and lines, shuffled trials are in grey. **(B)** The unit coupling scores in (A) were used to calculate a delta coupling score of the difference in pairwise correlations between the baseline and opto periods for paired trials for each unit (data, black markers). Delta coupling scores were also calculated with the difference between baseline and opto pairwise correlations calculated using shuffled trials for each unit (shuffled, grey markers). The ChR2 only scores showed no significant difference between paired data trials and shuffled trials (p = 0.195), whereas both ArchT only and ChR2 and ArchT combined showed a significant difference between the data delta coupling coefficient and shuffled delta coupling coefficient (p = 0.003, and 3.6×10^{-6}, respectively).

4.3.4 Histological verification of injection and probe recording sites

The cortical and thalamic injection and probe recording sites were verified after the final recording sessions by histology (Fig. 4.20). The accuracy of the targeted injection of ChR2-mCherry into VM was verified in a non-recorded animal by colocalization of rAAV5-CAMKII-hChR2-mCherry with GAD67 immunofluorescence (Fig. 4.20A). mCherry-labelled neuropil was seen in L1a motor cortex ipsilateral to the thalamic injection site, confirming the presence of projections in L1 (Fig. 4.20B). Cortical L1 NDNF+ neurons in a recorded animal show GFP labelling, indicative of ChR2 expression (Fig. 4.20C), and a probe track labelled by DiI shows the recording site in motor cortex (Fig. 4.20Cii). There was tissue damage in both probe locations after recordings.

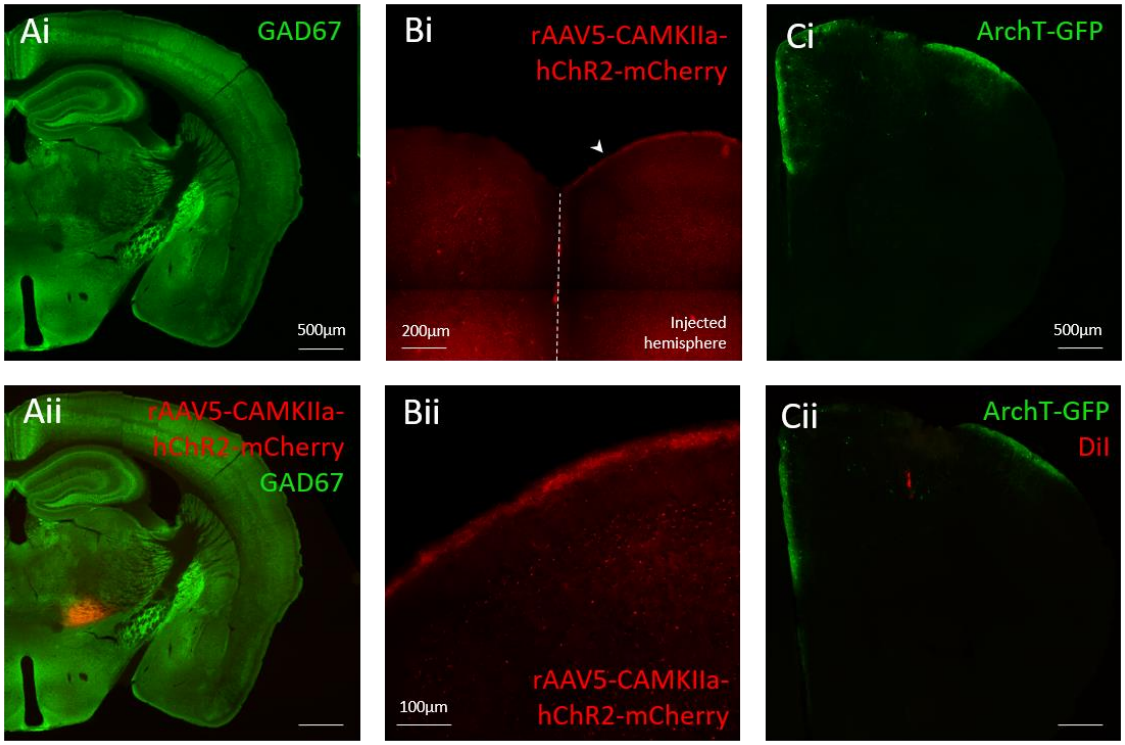


Figure 4.20 Injection and probe sites in cortex and VM thalamus
(Ai) GAD67 immunostaining reveals VM thalamus in a region of enhanced fluorescence. **(Aii)** Injection site of rAAV5-CAMKIIa-hChR2-mCherry (red) into VM thalamus shows colocalization with VM thalamus as identified by GAD67 immunofluorescence (green). **(Bi)** rAAV5-CAMKIIa-hChR2-mCherry injected into VM labels ipsilateral cortical L1a (arrowhead). **(Bii)** Higher magnification of (Bi), showing rAAV-CAMKIIa-hChR2-mCherry labelling in L1a motor cortex. **(Ci)** Injection site of AAV5-CAG-FLEX-ArchT-GFP into L1 motor cortex of an NDNF-Cre mouse. **(Cii)** A single probe track labelled by DiI after recording from an NDNF-Cre mouse.

4.4 DISCUSSION

4.4.1 Firing rates

To examine the response in cortex to VM thalamocortical input, we first needed to delineate the effects of ChR2 mediated optogenetic stimulation in VM. This generally led to an increase in thalamic activity, demonstrated by sustained increases in firing rates of single thalamic units in VM in response to optogenetic stimulation. Overall, optogenetic stimulation of VM did not appear to significantly alter the firing rates of motor cortical neurons aside from a brief initial increase in firing rate in some motor cortical single units. This may have been due to a number of reasons, including insufficient numbers of VM neurons stimulated by the light, or the stimulated VM neurons terminating in a different cortical location from the recorded cortical region. There may also have been inhibitory effects in thalamus and cortex resulting from optogenetic stimulation, such as TRN afferents inhibiting firing in some VM neurons, which could explain single thalamic units with a reduction in firing rate, or activated VM-recipient L1 ENGCs suppressing cortical firing by feedforward inhibition.

Optogenetic inhibition of L1 NDNF+ interneurons through ArchT appeared to strongly suppress firing rates in some cortical single units, both with and without VM stimulation. This could have been by suppressing a disinhibitory pathway through ENGCs and their target interneurons. Overall, there was a non-significant trend of reduction of firing rates in response to optogenetic inhibition. However, similar effects were seen in control experiments using GFP instead of ArchT in NDNF+ neurons, indicating that this might not be an effect mediated by the opsin in L1 NDNF+ interneurons, but possibly a result of heating from the laser, especially as we were using continuous rather than pulsed stimulation in these experiments. In future experiments, we could use a lower laser power, but initially we wanted

to ensure we did not miss any effects due to insufficient laser power. Despite this, it does not rule out some opsin-mediated effect, but it is currently not possible to separate out the opsin and heat-based effects.

For these analyses, we did not segregate units into groups based on depth, waveform properties or inter-spike interval, to look at general cortical responses, and so these units may be a combination of pyramidal neurons and interneurons. However, in future analyses and with more data it would be beneficial to separate out different cortical units which may reveal characteristic effects on different neural populations. We used different recording sessions from the same animals to contribute to the included n = 9 sessions, rather than n = 6 animals, because the probes were moved to different sites between each acute recording session and would therefore be unlikely to detect the same single units.

4.4.2 Cortical synchrony

As well as measuring changes in cortical unit firing rates in response to optogenetic stimulation and inhibition, we looked at the effects of VM stimulation and L1 NDNF+ IN inhibition on cortical synchrony by measuring the pairwise correlations of cortical single units (Fig. 4.19). There was no significant change in pairwise correlations of recorded cortical units between baseline and optogenetic 4s windows in response to stimulation of VM only (protocol 1), or between delta coupling coefficients of matched and shuffled data trials. There was also no significant difference in pairwise correlations between cortical units with and without optogenetic inhibition of L1 NDNF+ INs, but there was a significantly higher delta coupling coefficient between matched trials compared with shuffled data trials. For recording trials with both stimulation of VM and inhibition of L1 NDNF+ INs, there was a more robust increase in synchrony during the time window when both lasers were active compared with

the baseline window, with a significant increase in both the pairwise unit coupling coefficients and the delta coupling coefficients for matched versus shuffled trials. Again, it is possible that light-induced heating by the yellow laser may have caused or contributed to the increase in cortical synchrony seen in protocols 2 and 3. However, as there was a stronger increase in synchrony in protocol 3 than protocol 2, with simultaneous light delivery to VM and L1, and no change in synchrony with VM stimulation alone, this may be at least partially an opsin-driven effect. We do not yet have the equivalent control experiments to confirm whether this is the case. Since overall firing rates decreased in protocols 2 and 3, this may have impacted the synchrony, although this would probably be more likely if there had been an increase in firing rates. Overall, heat-induced changes are a potential confound of the synchronous effects seen in cortex but may be combined with a genuine opsin-mediated effect.

Taking these findings at face value would therefore suggest that a function of L1 NDNF+ neurons may be to regulate VM-driven motor cortical synchrony. There was no detectable increase in cortical synchrony with VM stimulation alone, which could be due to the inhibitory activity of NDNF+ INs, especially as they also receive excitatory input from VM, or any increase may have been too weak for detection or obscured by units from a mixture of cortical neurons. Thalamocortical inputs from other higher order thalamic nuclei, including pulvinar, medial thalamic nuclei and intralaminar thalamus, are known to cause an increase in synchrony in their cortical regions of innervation, which may serve to modulate synchrony between cortical areas according to behavioural requirements (Saalmann et al., 2012; Saalmann, 2014). L1 NDNF+ INs are well situated to be able to do this due to their unique position in L1a, directly innervating multiple pyramidal neurons, as well as indirectly by feedforward inhibition and disinhibition, and receiving primarily higher order thalamocortical input, as shown by rabies tracing, cortical input from sensorimotor cortices, and cholinergic

input. L1 NDNF+ neurons in PFC have already been shown to modulate VM input to L2/3 pyramidal neurons and L5 PT neurons by suppressing dendritic spiking *in vitro* (Anastasiades et al., 2020), which may be the mechanism by which this regulation of synchrony is achieved. As PT neurons send driver input back to motor thalamus, as well as to striatum and brainstem and spinal cord, it appears that ENGCs may play an important role in regulating synchronous activity at the cortical level of higher order motor thalamocortical circuits, and influence motor output. It is not yet known whether motor cortical ENGCs provide more of a long-lasting blanket inhibition or more tightly temporally coupled feedforward inhibition in response to thalamic inputs, but there is evidence that both may in fact be the case. For example, L1 NDNF+ INs in auditory cortex exert a sustained inhibition on pyramidal dendrites (Abs et al., 2018), while L1 INs in PFC can respond to thalamic input with a high level of temporal precision via ionotropic glutamate receptors (Cruikshank et al., 2012).

In future analysis and experiments, it would be of interest to look in more detail at the timing of unit spike correlations, and to establish the modulatory effects of L1 NDNF+ INs on oscillatory VM stimulation, as well as finding out whether synchrony is increased in both motor cortex and PFC simultaneously, as they both receive VM innervation.

From these optogenetic experiments, we saw that the suppression of ENGC firing led to an increase in cortical synchrony, which was mainly in putative pyramidal neurons. This was somewhat surprising, since if the main influence of ENGCs on pyramidal neuronal synchrony were via direct inhibition of their apical dendrites this would presumably increase synchrony, and therefore inhibition of ENGCs would decrease synchrony, which did not appear to be the case. Other components of the cortical circuitry, such as other interneurons, are known to be involved in mediating changes in cortical synchrony. Cortical synchrony has been most

commonly investigated in relation to oscillations, for example at gamma frequency (30-80Hz) which is prominent during active states. Although we did not study oscillatory synchrony, the correlation between single units was detected using 10ms bins, which is comparable to high-frequency gamma cycle lengths. Sufficient levels of synchrony are believed to be required for successful communication between neuronal groups by creating temporal communication windows, according to the communication through coherence hypothesis (Fries, 2005). However, excessive synchrony at lower frequencies is correlated with pathological states, such as increased beta oscillations in Parkinson's disease.

To interpret the circuit mechanisms that could underlie the influence of ENGCs on cortical synchrony, it is important to consider other cortical cell types through which this could be mediated. PV+ interneurons maintain synchronous activity in pyramidal neurons in both hippocampus (Ellender et al., 2014; Antonoudiou et al., 2020) and a range of cortical areas, particularly in the gamma frequency band (Sohal et al., 2009; Cardin et al., 2009; Carlén et al., 2012; Chen et al., 2017), and regulate excitation and inhibition balance in PFC (Ferguson and Gao, 2018). PV+ INs are generally fast-spiking and are abundant in cortex, apart from L1, and hippocampus, where they perisomatically innervate pyramidal neurons or at the axon-initial segment and can hence control spike timing. Optogenetically inhibiting cortical PV+ INs in vivo reduces gamma oscillations in infralimbic and prelimbic cortex, while conversely stimulating PV+ INs can produce gamma rhythmicity in infralimbic and prelimbic cortex (Sohal et al., 2009), and similarly in barrel cortex (Cardin et al., 2009). This property appears to be unique to PV+ INs, since SOM+ INs sustain beta band oscillations (5 – 30Hz) in visual cortex (Chen et al., 2017). The exact mechanisms by which PV+ INs and pyramidal neurons interact to sustain gamma oscillations are not yet fully clear but are known to occur via NMDA receptors (Carlén et al., 2012) and $GABA_A$Rs (Sohal et al., 2009). Since L1 ENGCs directly inhibit L2/3 PV+ INs in

prefrontal cortex (Anastasiades et al., 2020), consistent with similar observations in sensorimotor and auditory cortices (Wozny and Williams, 2011; Letzkus et al., 2011; Jiang et al., 2013;), through this disinhibitory pathway ENGCs may thereby contribute to reducing cortical synchrony. Cortico-cortical and subcortical inputs to L1 could influence PV-mediated synchrony through ENGCs. Additionally, ENGC suppression of dendritic spikes in pyramidal neurons could act to reduce excitatory input to PV+ INs. However, as ENGCs can inhibit neurons by volume transmission of GABA to inhibit both $GABA_A$ and $GABA_B$ postsynaptic receptors, the potential slower and longer lasting timescale combined with their target innervation region of pyramidal apical dendrites would make them less well suited than PV+ INs in regulating spike timing and therefore synchrony.

In conclusion, I predict that ENGCs suppress cortical synchrony primarily via their inhibition of L2/3 PV+ INs, as these interneurons are known to mediate network oscillations and are downstream of ENGCs. To test this theory, we could investigate the interaction between ENGCs and PVs in vitro or in vivo by inhibiting PV+ INs, as will be suggested in the following chapter.

4.4.3 Cortical microcircuits and outputs

Since L1 ENGCs inhibit spiking in L2/3 and L5 pyramidal neurons in both sensorimotor and auditory cortex, it seems likely that suppressing L1 ENGC firing in motor cortex would reduce inhibition to downstream pyramidal output neurons allowing their firing rates to increase (Jiang et al., 2013; Lee et al., 2015, Abs et al., 2018), although there may also be the removal of disinhibition via L2/3 PV+ interneurons. In PFC, L1 NDNF+ neurons mediate inhibition of VM-evoked dendritic spikes in pyramidal neurons (Anastasiades et al., 2020), which may also be the case in motor cortex, so that the suppression of ENGC activity in the presence of VM

stimulation might elicit an increase in pyramidal neuron spiking from background levels. If this is the case, there may be an increase in L5 activity since stimulation of L5 can cause recurrent excitatory activity, in contrast to L2/3 (Beltramo et al., 2013; Harris and Mrsic-Flogel, 2013). Since L1 ENGCs simultaneously innervate pyramidal neurons across cortical columns and throughout cortical layers, they could also potentially affect coherence.

4.4.4 Potential function of L1 NDNF+ neurons

The role of L1 NDNF+ ENGCs in motor cortical circuits is currently unclear. However, some observations and theories regarding the function of NDNF+ interneurons in other circuits may be indicative of parallel functions in motor cortex. ENGCs innervate both L2/3 and L5 pyramidal cells in mouse auditory cortex and PFC (Abs et al., 2018; Anastasiades et al., 2020) and L5 pyramidal neurons in rat sensorimotor cortex (Jiang et al., 2013), putting them in a unique position of being able to influence both intracortical principal neurons and subcortically projecting neurons. We observed some rabies-labelled neurons in L1 motor cortex of RBP4-Cre mice, which may be ENGCs, indicating direct innervation. One theory is that ENGC-mediated inhibition of L5 pyramidal cells along with SBC-involved circuits may serve to augment signal to noise ratio, allowing the selection of salient information from higher order thalamic and other inputs by coincidence detection (Jiang et al., 2013).

In auditory cortex, L1 NDNF+ neurons provide a source of inhibition to distal pyramidal neuron dendrites that is distinct from L1-projecting Martinotti interneurons and is highly plastic (Abs et al., 2018). Disinhibition of L2/3 pyramidal neurons by both NDNF+ and VIP+ L1 interneurons via L2/3 PV+ interneurons in auditory cortex has been associated with associative fear learning and memory, particularly in response to cholinergic input, with L1 neurons able to encode reinforcement (Letzkus et al., 2011, Abs et al., 2018). Since distal dendritic inhibition

can occur independently of somatic membrane potential changes (Palmer et al., 2012), one theory is that L1 NDNF+ interneurons may function in controlling dendritic spikes while allowing stimulus representation at the somatic level, possibly to suppress the induction of additional plasticity after the completion of memory formation to preserve memories (Abs et al., 2018). Interneurons with distinct temporal activity (in response to different network states) can influence pyramidal cell activity by innervating different regions of pyramidal neurons in hippocampal CA1 (Somogyi et al., 2013). L1 interneurons are also responsible for mediating cross-modality interactions in primary visual cortex (V1) (Ibrahim et al., 2016). L1 interneurons are not the only interneurons involved in thalamocortical circuits, as higher order thalamic inputs to S1 gate plasticity by disinhibition of L2/3 pyramidal neurons via non-L1 VIP+ and SST+ interneurons (Williams and Holtmaat, 2019).

ENGCs in motor cortex may therefore likewise enable the integration of multimodal inputs from sensorimotor cortical and thalamic inputs, as well as executive signals, which can then be transferred within and out of cortex, either to motor-related subcortical regions to update information, or to motor output signals to the peripheral nervous system. This fits with our observations of higher order thalamic innervation of L1 motor cortical NDNF+ INs from VM as well as somatosensory thalamic nuclei, such as Po, and with the apparent ENGC modulated control of VM mediated cortical synchrony in motor cortex. As NDNF+ neurons have been associated with learning and plasticity in other cortices, they may also play a role in learning and plasticity in the motor cortex, whether in the formation of new motor skills or helping to preserve existing pathways.

Chapter 5 General Discussion

5.1 Overview

The anatomical and physiological connectivity of the rodent basal ganglia thalamocortical circuit has become an increasingly popular area of study in recent years. Advances in methodologies such as rabies tracing and optogenetics have enabled experiments which examine the connectivity of this circuit in more detail. The secrets of the 'crowning mystery' of L1 (Hubel, 1982) are beginning to be unearthed. Much of the research so far into L1 ENGCs in frontal cortical circuits and frontal thalamocortical circuits has been carried out *in vitro*, allowing detailed investigation into interactions of these interneurons at the single cellular level. However, as these connections do not occur in isolation in the brain, it is valuable to understand how L1 ENGCs influence the basal ganglia thalamocortical circuit physiologically *in vivo* in an awake animal, especially in cortical neurons, as this takes into account other physiological factors present. Furthermore, to our knowledge these circuits have not yet been explored in motor cortex. Simultaneous extracellular recording of multiple neurons with multi-channel probes allows the acquisition of population data from which a range of information can be extracted, including firing rates of single and multi-units, LFP data and synchrony. In this thesis, I tried to establish whether motor cortical L1 ENGCs receive direct thalamocortical innervation, and if so, how the anatomical distribution of inputs from thalamic nuclei compares with the thalamic sources of afferents to L5 pyramidal neurons. After observing retrogradely labelled VM neurons presynaptic to L1 NDNF+ INs, I then investigated the function of L1 NDNF+ INs within this circuit by measuring the effects on cortical single unit firing rate and synchrony in motor cortex while modulating the activity of VM and L1 NDNF+ INs.

To complement existing neurochemical parcellation of the thalamus in rodents, we parcellated macaque anterior thalamus with neurochemical markers. As it is not possible to do comparable experiments in macaques to rodents, where invasive techniques and a high throughput of animals are standard, methods of accurately verifying anatomical locations are especially useful.

The main findings of this thesis are summarised below:

- L1 NDNF+ neurons in motor cortex of Ndnf-IRES2-dg-Cre mice are GABAergic, and mostly (79%) co-express reelin and COUP-TFII, as verified by immunohistochemistry.
- L1 NDNF+ interneurons in mouse motor cortex receive direct innervation from ipsilateral thalamus, in particular from VM and other higher order regions.
- L5 RBP4+ pyramidal neurons in mouse motor cortex receive direct innervation from a range of thalamic nuclei, especially from VL and intralaminar thalamus.
- Sustained optogenetic stimulation of VM thalamocortical neurons *in vivo* elicits no overall change in firing rate of motor cortical single units.
- Sustained optogenetic stimulation of VM thalamocortical neurons *in vivo* with simultaneous suppression of L1 NDNF+ neurons causes greater synchrony of single units in motor cortex.
- Macaque MD has a complementary pattern of GABAergic and subcortical glutamatergic innervation in its subnuclei, as revealed by GAD67 and vGluT2 immunostaining.

These results show for the first time direct thalamic innervation of L1 NDNF+ interneurons in motor cortex, which has significant implications for understanding motor thalamocortical

circuitry. Additionally, we have shown that inhibition of L1 NDNF+ INs can increase VM-mediated synchrony in motor cortex, indicating an important role of these interneurons in the basal ganglia-thalamocortical circuit.

5.2 Technical limitations

While some of the findings presented in this thesis are novel, there are technical limitations which need to be considered when interpreting the results. Several of these limitations are due to the superficial location of L1 cortex, which makes it challenging to work with compared with deeper brain structures.

Stereotactic viral injections into L1 cortex are difficult to execute successfully, as shallow injections can result in viral reflux with little penetration of the tissue. However, deeper injections to counteract this compromise the laminar specificity by transfecting neurons in neurons deeper than L1. Other methods which involve leaving the area above L1 exposed with a large craniotomy over a period of time would potentially risk mechanical damage to the surface tissue, especially in mice where the dura is thin. To seek to improve L1 targeting of injections, we developed a method whereby the virus injection pipette was inserted subdurally via a craniotomy posterior to the desired injection site in motor cortex at a shallow angle. Although this caused some tissue damage at the insertion site, there was relatively less tissue damage in motor cortex. This technique improved the L1 specificity compared with regular horizontal injections, although transfected neurons were not exclusively in L1. Having labelled neurons in additional layers poses a problem in interpreting the L1 NDNF-Cre rabies tracing results, as ideally all starter cells would have been in L1 or motor cortex, but in reality, around 58% of starter cells were in L1 with the rest in L2-6, where NDNF is expressed in what are presumably NGF cells in addition to L1 ENGCs. Consequently, rabies-labelled thalamic

input neurons partly represent monosynaptic input to NDNF+ neurons in these deeper layers in addition to L1 ENGCs. So, although it is likely that the majority of rabies-labelled neurons including VM thalamocortical neurons do innervate L1, some of the identified thalamic inputs may be biased towards these deeper layers. Additionally, starter cells in RBP4-Cre mice were not all in L5, although this was a higher proportion (72%), with most of the other neurons in the L4/5 border region assigned to L4. Another potential limitation of the rabies tracing experiments is the extent of transfection of starter cells and presynaptic input neurons by the viruses, which may not be 100%, and is also affected by titre. We tried to maximise the proportion of neurons transfected by using a high titre virus (Ählund-Richter et al., 2019). Rabies virus is also toxic to neurons, so there may be some cell death.

Awake *in vivo* head-fixed recordings enable the acquisition of valuable datasets. However, experiments on awake animals have particular limitations. Although the mice were head-fixed, there was still some noise due to movement. We tried to minimise this by habituating the animals to the head-fix set up so that they would not be restless during experiments. A piezo sensor was positioned on the animal's body to monitor any large movements, for potential identification in future analyses. We also carried out recordings in a Faraday cage and grounded the cortical probe. Common-average referencing was used to remove any noise artefact that was present across multiple channels.

A restriction of these acute *in vivo* recordings is the requirement for repeated re-entry of the silicon probes into the brain for each recording session, as opposed to a chronic implant, which causes tissue damage, especially with the optrode. The exposed surface of L1 motor cortex also makes it susceptible to tissue damage over repeated sessions. To try to account for this, the cortical probe was inserted into fresh tissue with different coordinates in each

session, and the position of the thalamic probe was also adjusted slightly. Each animal generally had up to 3 recording sessions before the tissue quality deteriorated to yield significantly fewer cortical single units or light-responsive thalamic units. Due to the nature of head-fixed recordings, the sessions could be up to a maximum of 3 hours, for the well-being of the animals, in contrast to potentially longer sessions with anaesthetised animals. These constraints limited the total recording time and hence amount of data obtained per animal. To maximise the consistency of data obtained across animals, a limited number of short recording protocols were carried out each time, with 20 laser sweeps per protocol to give sufficient repeats of the same condition for analysis.

With optogenetics, there is often some tissue heating along with light delivery, which can influence firing in opsin-negative animals (Stujenske et al., 2015; Owen al., 2019). The laser power we used may have caused heating, especially with continuous stimulation, contributing to false positive inhibitory effects in cortex. Thus, to validate our findings, in the future we first plan to repeat experiments in control animals with lower laser powers to ensure there are no effects in opsin-negative animals, before continuing with experiments.

These extracellular multi-channel probe recordings are advantageous in yielding a rich dataset of a high number of single and multi units as well as LFP data. However, unlike single cell juxtacellular or *in vitro* patch clamp recordings, individual neurons cannot be labelled to identify histologically.

With the neurochemical parcellation of macaque thalamus, there were issues of background lipofuscin-like autofluorescence to overcome, with the aid of $CuSO_4$, but may have been there in CaBP immunohistochemistry incubations. It would be good to have had an n larger than

one, but there were other factors to consider in the experiment design such as reduction and refinement.

5.3 Function of L1 interneurons in higher order motor thalamocortical circuits

Currently, the prevailing theory is that BZ and VL form segregated higher order and first order pathways delivering motor-related information to cortex (Sherman and Guillery, 2006), but it has been posited that they may also have some degree of integration at the thalamic level (Bosch-Bouju et al., 2015). The higher order and first order and driver and modulator models work well in describing somatosensory pathways, but it remains to be fully explored to what extent they are representative of motor pathways, or whether the levels of segregation differ. For the purposes of this study, the generally accepted designations of higher and first order thalamic nuclei have been adopted, in the absence of further compelling evidence to the contrary.

Since VM thalamocortical neurons target L1 ENGCs in prefrontal cortex (Cruikshank et al., 2012), and BZ also innervates L1 motor cortex (Herkenham et al., 1979; Kuramoto et al., 2009), we hypothesised that BZ neurons would innervate L1 ENGCs in motor cortex in addition to pyramidal neurons. Rabies tracing from L1 motor cortical NDNF+ neurons confirmed this by revealing preferential innervation from VM and other higher order nuclei, but comparatively little from VA. There was also some innervation from first order VL, but proportionally less than to L5 RBP4+ neurons in the same cortical area. Motor thalamus may serve as an integrator of basal ganglia and cerebellar inputs (Bosch-Bouju et al., 2015), but integration also occurs at the cortical level, with differences in motor thalamic nuclei inputs

to neuronal types and layers, potentially allowing signals from these different sources to update higher level targets with specific information which can be separately controlled depending on behavioural states. What could be the function of these L1 INs within the basal ganglia-thalamocortical circuit, and would they have any effect on modulating thalamocortical input? Our probe recordings showed no overall change in firing rates of cortical neurons in response to VM stimulation, and a small but non-significant decrease in response to L1 NDNF+ IN photoinhibition with and without VM stimulation. The effect of stimulating VM on cortical firing rates contrasts with *in vitro* recordings stimulating VM terminals in cortex, which could be for a number of reasons including feedforward inhibition through cortical interneurons or due to reciprocal inhibition of VM from TRN. The inhibitory effect of L1 NDNF+ IN inhibition could be partly heat-related, as it was seen in control experiments. Any real opsin-mediated effect could be due to disinhibition of L2/3 pyramidal interneurons. A disadvantage of *in vivo* optogenetic recordings is that it is more complicated to disentangle and identify exact pathways through which effects are mediated, compared with *in vitro* experiments. However, broadly speaking, the findings may be more representative of normal physiological function. It is hard to draw any definitive conclusions from the effects on cortical firing rates at this stage, if only to say that stimulation of VM does not necessarily translate into a directly linked increase in cortical neuron firing rates, neither does inhibiting L1 NDNF+ INs (as presumed) appear to remove blanket inhibition to elicit a net increase in cortical firing rates. Interestingly, stimulation of VM along with L1 NDNF+ IN inhibition produced an increase in synchrony in cortical single unit firing, which was not seen with VM stimulation alone, and was also the case with L1 NDNF+ IN inhibition, but with less robust of an effect.

As suppressing L1 NDNF+ IN firing concurrently with enhancing VM firing has an effect of increasing temporal correlation in cortical single unit spiking, and from knowledge that VM thalamocortical input can enhance dendritic spiking in L5 pyramidal neurons of PFC (Collins et al., 2018), we reason that L1 ENGCs may play a role in regulating VM-evoked synchrony in motor cortex. This in turn could be in response to simultaneous input to L1 ENGCs from VM, or other cortical inputs, as well as their intrinsic activity.

As well as VM, there are other inputs to L1 motor cortex, as mentioned in previous chapters. There are other sources of excitatory inputs from motor and sensory thalamic nuclei to L1 motor cortex, including VA (Kuramoto et al., 2009) and other higher order thalamic nuclei such as Po and intralaminar thalamus, as well as some first order nuclei such as VL, which directly innervate L1 NDNF+ INs, as revealed by our rabies tracing. Additionally, L1 INs have nAChRs which mediate responses to ACh, from basal forebrain (Poorthuis et al., 2018). There are also cortical inputs to L1, from motor and somatosensory cortical regions. Inhibitory cortical input to L1 also arises from SST+ Martinotti cells, and within L1 ENGCs have reciprocal innervation. VIP+ L1 SBCs cells, with their deeper projecting axons, presumably contribute little to L1 innervation. As well as established cortico-cortical connections from S1 to M1, there also exists a trans-thalamic pathway from S1 to M1 through higher order Po (Mo and Sherman, 2019). More research is required to know how these diverse inputs interact in motor cortical L1 to influence both IN and pyramidal firing during different behavioural states.

There is more burst firing in higher order than first order relays, which may serve to increase the increase of stimulus detection by higher order nuclei, and relay information from one cortical area to another more effectively (Ramcharan et al., 2005). Characteristic of higher order nuclei, VM innervates cortex and receives reciprocal L5 driver input over multiple

iterations, allowing for finely tuned transfer and modification of information between thalamus, cortical areas including prefrontal and motor cortex, basal ganglia, and connected structures. In this way, cognitive and motor processing can be continuously updated and inform one another. The participation of L1 ENGCs in these loops potentially allows for more nuanced control of such information transfer and may be important in regulating plasticity during motor learning.

We endeavoured to maintain normal physiological states as far as possible within experimental constraints by performing experiments in awake mice. However, continuous optogenetic stimulation and inhibition produced activity that would not occur naturally, as both effects will be abnormally synchronised. Nevertheless, such stimulation provides a useful first sense of neuronal responses to activation or inhibition of a given population of neurons on their targets. Oscillatory stimulation, which we also performed in VM but have yet to analyse due to time constraints and technical difficulties of artefact removal, is likely to be more representative. This also may provide different responses, as in sensory thalamocortical circuits (Kirchgessner et al., 2020).

5.4 Neurochemical parcellation as a method of nucleus delineation

Neurochemical parcellation is a simple and effective way of delineating regions in the brain such as thalamic nuclei and cortical layers (Nakamura et al., 2014), and we have demonstrated this in both mouse cortex and thalamus and NHP thalamus. Expression of neurochemical markers aids the identification and classification into neuronal types of single neurons or neural populations, such as NDNF expression of ENGCs, and other markers can also be used to help verify cell types, such as reelin and COUP-TFII. These can then be genetically exploited for anatomical tracing or optogenetics, to target a specific group. Neurochemical

characterisation alone however does not reveal connectivity, but neurotransmitter-related markers can indicate the nature of innervation, as with vGluT2+ terminals in macaque MD.

5.5 Translational applications

The research presented in this thesis is a combination of rodent and non-human primate (NHP) data. To what extent is research using these species necessary or interchangeable when looking at the connectivity of the thalamocortical circuit in the ways presented here, and are there any applications in human medicine? Although rodents and NHPs are both mammalian, there are major differences in the structure and function of their brains, for example a larger and more complex cortex in NHPs, especially PFC, with more white matter tracts, and differences in structural organisation and connectivity of the thalamus between species. These inter-species differences therefore require separate brain atlases and lines of research for rodents and NHPs, although information from each can be used to inform the other, and to develop hypotheses and models. Rat and mouse brains are quite similar in their structural organisation and connectivity but have some minor differences.

NHP research is especially useful for clinical research applications, due to closer homology between brain structures than rodents and humans. Being able to more accurately identify and target structures is of great benefit, such as deep brain stimulation for essential tremor, Parkinson's disease and obsessive-compulsive disorder (Benabid et al., 1993; Haber et al., 2020). Mouse and human ENGCs share similar anatomical and physiological properties, such as the expression of NDNF, presence of nAChRs, and late-spiking physiology (Poorthuis et al., 2018), indicating that our research involving NDNF+ interneurons is likely of relevance to humans, and will be able to help guide future research while taking into account new knowledge about the motor thalamocortical circuitry. Manipulation of L1 ENGCs in human

motor cortex may have future clinical applications in treatments for motor related disorders, such as Parkinson's disease or essential tremor.

5.5 Outlook

These anatomical and electrophysiological experiments have focussed on investigating basal ganglia-recipient thalamocortical connectivity with L1 motor cortical NDNF+ ENGCs. To find out the extent to which these observations are specific to VM and L1 ENGCs, it would be beneficial to repeat the rabies-tracing and head-fixed recording experiments in VIP-Cre mice as a comparison. To understand the effect of motor cortical ENGCs on the motor thalamocortical circuit as a whole, especially on cortical output neurons, the recording experiments could be carried out while stimulating VL instead of VM and inhibiting ENGCs. Although VL provides less direct innervation of motor cortical ENGCs than VM, the ENGCs likely inhibit VL-recipient pyramidal neurons at the apical dendrite level, and it would be interesting to know their effect on firing rate and synchrony of these neurons while they receive VL input. These additional experiments would provide an insight into the function of L1 interneurons within the motor thalamocortical circuit as a whole.

Due to external circumstances, it was not possible to carry out controls for thalamic stimulation in the absence of an opsin, but it is intended to do this shortly. Since the control experiments in L1 with GFP instead of ArchT suggested there was heat-induced inhibition in the absence of opsin, it would also be worth repeating the experiments with a lower laser power.

The analysis of electrophysiological data presented here builds a picture of what is occurring in motor cortex in response to VM thalamocortical stimulation and L1 ENGC inhibition in

terms of single unit firing rates and synchrony, but there is still more information to extract from this dataset, such as looking at changes in multiunit firing and LFPs. There are also experiments not yet analysed with oscillatory laser stimulation of VM in combination with continuous ArchT-inhibition of L1 ENGCs, as well as cortical-only recordings with ChR2-stimulation of L1 ENGCs. It is possible that the oscillatory stimulation elicits a different effect on cortical neuron firing rates or synchrony, especially as the VM-mediated initial increase in cortical single unit firing rates was not sustained over the duration of the continuous laser stimulation pulse. With the dataset presented here, it would also be of interest to segregate cortical units on the basis of depth as well as location in M1 or M2, and to segregate pyramidal neurons from interneurons based on the peak to trough ratio of waveforms or interspike intervals. A greater number of experiments would help to make these targeted analyses more robust.

The single unit correlation results indicated that a decrease in ENGC firing causes an increase in cortical single unit synchrony in motor cortex and I would therefore predict conversely that an increase in ENGC firing would reduce cortical synchrony. First of all, to confirm this, we can repeat a modified version of protocol 2 of the optogenetic experiment in Chapter 4, to directly stimulate ChR2-transfected ENGCs in L1 of motor cortex with blue light, with the expectation that cortical synchrony would be suppressed during the optogenetic window.

Next, to test the theory that ENGCs suppress cortical synchrony via PV+ INs, we can adapt this experiment to simultaneously modulate ENGCs and PV+ INs and observe the effects on cortical synchrony. Because of the role of in PV+ INs in contributing to gamma oscillations, one type of cortical synchrony, we surmise that they may be important in mediating the cortical synchrony we saw in motor cortex. To first establish that PV+ INs and pyramidal

neurons maintain gamma oscillations in motor cortex, it would be beneficial to reproduce optogenetic experiments to directly inhibit or stimulate PV+ INs in motor cortex to confirm that there are similar mechanisms here to other cortical areas (Sohal et al., 2009).

After confirming this, we could investigate the interactions between ENGCs and PV+ INs more directly in vitro and in vivo by stimulating ENGCs and either acutely or chronically inhibiting PV+ INs, and vice versa. We could optogenetically inhibit ENGCs and measure PV+ IN or pyramidal neuron activity in vivo with calcium imaging (Packer et al., 2015; Stamatakis et al., 2018). It could also be possible to stimulate ENGCs in vitro while inhibiting PV+ INs pharmacologically with DREADDs, and calcium imaging of pyramidal neurons. If these predictions are correct, we would expect to see an increase in synchrony when ENGCs alone are inhibited, a decrease when they are stimulated, and no change when they are stimulated and PV+ INs are concurrently inhibited.

Further modifications of the electrophysiological experiments include simultaneous probe recordings from PFC and motor cortex while stimulating VM, since this innervates both areas, although this would be technically challenging. Since the basal ganglia-thalamocortical circuit is not a unidirectional pathway, but rather a loop involving VM and motor cortex, another idea to trace the transmission of information from motor cortex to VM and back again is to deliver a unique pattern of oscillatory stimulation to motor cortex, and trace its movement and preservation throughout the circuit.

As we are looking at the motor circuit, it would be insightful to find out the function of L1 NDNF+ INs on learning and execution of behavioural tasks or non-learned movement, such as incorporating locomotion on a treadmill, lever press or reaching tasks.

5.6 Concluding remarks

The experiments presented in this thesis have explored the anatomical and physiological connectivity of the basal ganglia-recipient motor thalamus, complementing an increasing body of research into this fascinating area. We have confirmed anatomically direct innervation of L1 ENGCs in motor cortex by VM and other higher order thalamocortical neurons and found that these ENGCs may play a role in modulating VM-evoked synchrony *in vivo*. This has provided novel insights into higher order thalamocortical motor circuits and stimulated many possible future avenues of exploration.

Supplementary Tables

Virus	Source	Titre	Injection site(s)	Coordinates	Volume (nl)
AAV5-Ef1a-DIO-hChR2(E123T/T159C)-eYFP	Vector Core, University of North Carolina (UNC), Chapel Hill, NC, USA	4.9 - 6.2x10^{12} vg/ml	Motor cortex	AP 1.5, ML 1.3, DV 0.0	550nl
AAV5-Ef1a-DIO-YFP	Vector Core, UNC	6.5x10^{12} vg/ml	L1 and L5 motor cortex, VM thalamus	AP 1.5, ML 1.3, DV 0.0 and DV 0.8, AP -1.3, ML 0.8, DV 3.9	400nl, 60nl
AAV5-DIO-TVA/V5-2A-RG	Dr. Konstantinos Meletis, Karolinska Institutet, Stockholm, Sweden	2x10^{12}pp/ml	L1 and L5 motor cortex	AP 1.5, ML 1.3, DV 0.0 and DV 0.8	400nl
SAD-DG-GFP[EnvA]	Dr. Konstantinos Meletis, Karolinska Institutet, Stockholm, Sweden	1 × 10^{10} infection units/ml	L1 and L5 motor cortex	AP 1.5, ML 1.3, DV 0.5 and DV 0.8	60nl
rAAV5-CAMKIIa-hChR2-mCherry	Dr Karl Deisseroth; Vector Core, UNC	1 × 10^{10} infection units/ml	VM thalamus	AP -1.4, ML 0.9, DV 4.0	70nl
rAAV5-CAG-FLEX-ArchT-GFP	Vector Core, UNC	8.5x10^{12} vg/ml	Motor cortex	AP 1.5, ML 1.3, DV 0.0	550nl

Table S1: Viruses

Antigen	Species, clonality	Dilution	Company	Catalogue No.	Research Resource Identifier (RRID)
Calbindin D28K (C-20) (CB)	Goat, polyclonal	1:300	Frontier Institute	Go-Af1040	RRID: AB_2571569
Calbindin D28K (C-20) (CB)	Goat, polyclonal	1:500	Santa Cruz	sc-7691	RRID: AB_634520
Calretinin (CR)	Goat polyclonal	1:500	Swant	CG1	RRID: AB_10000342
Calretinin (CR)	Rabbit, polyclonal	1:1000	Synaptic Systems	214102	RRID: AB_2228331
COUP transcription factor 2 (COUP-TFII)	Mouse, monoclonal	1:500	Perseus Proteomics	PP-H7147-00	RRID: AB_2314222
Forkhead box protein P2 (N-16) (FoxP2)	Goat, polyclonal	1:500	Santa Cruz	Sc-21069	RRID: AB_2107124)
Glutamic acid decarboxylase-67 (GAD67)	Mouse, monoclonal	1:500	Chemicon	MAB 5406	RRID: AB_2278725
Green fluorescent protein (GFP)	Rat, monoclonal	1:1000	Nacalal Tesque	04404-84	RRID: AB_10013361
N-Terminal EF-Hand Calcium Binding Protein 1 (Necab1)	Rabbit, polyclonal	1:1000	Life Technologies – Thermo Fisher	PA5-54849	RRID: AB_2644587
Neuronal nitric oxide synthase (nNOS)	Goat, polyclonal	1:1000	Abcam	Ab1376	RRID: AB_300614
Parvalbumin (PV)	Guinea Pig, polyclonal	1:500	Synaptic Systems	195004	RRID: AB_2156476
Reelin	Goat, polyclonal	1:1000	R&D Bio-Techne	AF3820-SP	RRID: AB_2253745
Somatostatin (SOM)	Rabbit, polyclonal	1:500	BMA Biomed, Peninsula Laboratories	T-4103	RRID: AB_518614
Vasoactive intestinal peptide (VIP)	Rabbit, polyclonal	1:1000	Immunostar	20077	RRID: AB_572270
Vesicular glutamate transporter 2 (vGluT2)	Rabbit, polyclonal	1:500	Synaptic Systems	135-403	RRID: AB_887883
Vesicular glutamate transporter 2 (vGluT2)	Rabbit, polyclonal	1:500	MAb-Technologies, VGT2-6	VGT2	RRID: AB_2315569

V5	Chicken, polyclonal	1:2000	Abcam	ab9113	RRID: AB_307022
Wolframin (WFS1)	Rabbit, polyclonal	1:500	Proteintech	11558-1-AP	RRID: AB_2216046

Table S2: Primary antibodies

Fluorophore	**Species reactivity**	**Dilution**	**Company**	**Catalogue No.**	**Research Resource Identifier (RRID)**
AMCA	Rabbit	1:250	Jackson ImmunoResearch (JIR)	711-155-152	RRID:AB_2340602
Brilliant violet	Goat	1:250	JIR	705-675-147	RRID:AB_2651102
Brilliant violet	Rabbit	1:250	BioLegend	406410	RRID:AB_10897810
Alexa Fluor 488	Mouse	1:1000	JIR	715-545-151	RRID:AB_2341099
Alexa Fluor 488	Rat	1:1000	JIR	712-545-153	RRID:AB_2340684
Cy3	Chicken	1:400	JIR	703-165-155	RRID:AB_2340363
Cy3	Mouse	1:400	JIR	715-165-151	RRID:AB_2315777
Cy3	Rabbit	1:400	JIR	711-165-152	RRID:AB_2307443
Alexa Fluor 647	Rabbit	1:250	JIR	711-605-152	RRID:AB_2492288
Red Nissl		1:200	Life Technologies	N21483	RRID:AB_2572212

Table S3: Fluorescent antibodies. All secondary antibodies are raised in donkey.

References

Abs, E., R. B. Poorthuis, D. Apelblat, K. Muhammad, M. B. Pardi, L. Enke, D. Kushinsky, D. L. Pu, M. F. Eizinger, K. K. Conzelmann, I. Spiegel and J. J. Letzkus (2018). "Learning-Related Plasticity in Dendrite-Targeting Layer 1 Interneurons." Neuron 100(3): 684-699.e686.

Agmon, A. and B. W. Connors (1991). "Thalamocortical responses of mouse somatosensory (barrel) cortex in vitro." Neuroscience 41(2-3): 365-379.

Ährlund-Richter, S., Y. Xuan, J. A. van Lunteren, H. Kim, C. Ortiz, I. Pollak Dorocic, K. Meletis and M. Carlén (2019). "A whole-brain atlas of monosynaptic input targeting four different cell types in the medial prefrontal cortex of the mouse." Nat Neurosci 22(4): 657-668.

Albin, R. L., A. B. Young and J. B. Penney (1989). "The functional anatomy of basal ganglia disorders." Trends Neurosci 12(10): 366-375.

Alexander, G. E., M. D. Crutcher and M. R. DeLong (1990). "Basal ganglia-thalamocortical circuits: parallel substrates for motor, oculomotor, "prefrontal" and "limbic" functions." Prog Brain Res 85: 119-146.

Alexander, G. E., M. R. DeLong and P. L. Strick (1986). "Parallel organization of functionally segregated circuits linking basal ganglia and cortex." Annu Rev Neurosci 9: 357-381.

Alloway, K. D., J. B. Smith, T. M. Mowery and G. D. R. Watson (2017). "Sensory Processing in the Dorsolateral Striatum: The Contribution of Thalamostriatal Pathways." Frontiers in systems neuroscience 11: 53-53.

Anastasiades, P. G., D. P. Collins and A. G. Carter (2020). "Mediodorsal and ventromedial thalamus engage distinct L1 circuits in the prefrontal cortex." bioRxiv: 2020.2001.2008.898817.

Anticevic, A., M. W. Cole, G. Repovs, J. D. Murray, M. S. Brumbaugh, A. M. Winkler, A. Savic, J. H. Krystal, G. D. Pearlson and D. C. Glahn (2014). "Characterizing thalamo-cortical disturbances in schizophrenia and bipolar illness." Cereb Cortex 24(12): 3116-3130.

Antonoudiou, P., Y. L. Tan, G. Kontou, A. L. Upton and E. O. Mann (2020). "Parvalbumin and Somatostatin Interneurons Contribute to the Generation of Hippocampal Gamma Oscillations." The Journal of Neuroscience 40(40): 7668-7687.

Arai, R., D. M. Jacobowitz and S. Deura (1994). "Distribution of calretinin, calbindin-D28k, and parvalbumin in the rat thalamus." Brain Res Bull 33(5): 595-614.

Arbuthnott, G. W., N. K. MacLeod, D. J. Maxwell and A. K. Wright (1990). "Distribution and synaptic contacts of the cortical terminals arising from neurons in the rat ventromedial thalamic nucleus." Neuroscience 38(1): 47-60.

Ascoli, G. A., L. Alonso-Nanclares, S. A. Anderson, G. Barrionuevo, R. Benavides-Piccione, A. Burkhalter, G. Buzsaki, B. Cauli, J. Defelipe, A. Fairen, D. Feldmeyer, G. Fishell, Y. Fregnac, T. F. Freund, D. Gardner, E. P. Gardner, J. H. Goldberg, M. Helmstaedter, S. Hestrin, F. Karube, Z. F. Kisvarday, B. Lambolez, D. A. Lewis, O. Marin, H. Markram, A. Munoz, A. Packer, C. C. Petersen, K. S. Rockland, J. Rossier, B. Rudy, P. Somogyi, J. F. Staiger, G. Tamas, A. M. Thomson, M. Toledo-Rodriguez, Y. Wang, D. C. West and R. Yuste (2008). "Petilla terminology: nomenclature of features of GABAergic interneurons of the cerebral cortex." Nat Rev Neurosci 9(7): 557-568.

Aumann, T. D. (2002). "Cerebello-thalamic synapses and motor adaptation." The Cerebellum 1(1): 69.

Bar-Gad, I., G. Havazelet-Heimer, J. A. Goldberg, E. Ruppin and H. Bergman (2000). "Reinforcement-driven dimensionality reduction--a model for information processing in the basal ganglia." J Basic Clin Physiol Pharmacol 11(4): 305-320.

Bar-Gad, I., G. Morris and H. Bergman (2003). "Information processing, dimensionality reduction and reinforcement learning in the basal ganglia." Prog Neurobiol 71(6): 439-473.

Barthas, F. and A. C. Kwan (2017). "Secondary Motor Cortex: Where 'Sensory' Meets 'Motor' in the Rodent Frontal Cortex." Trends in neurosciences 40(3): 181-193.

Beltramo, R., G. D'Urso, M. Dal Maschio, P. Farisello, S. Bovetti, Y. Clovis, G. Lassi, V. Tucci, D. De Pietri Tonelli and T. Fellin (2013). "Layer-specific excitatory circuits differentially control recurrent network dynamics in the neocortex." Nature Neuroscience 16(2): 227-234.

Benabid, A. L., P. Pollak, E. Seigneuret, D. Hoffmann, E. Gay and J. Perret (1993). "Chronic VIM thalamic stimulation in Parkinson's disease, essential tremor and extra-pyramidal dyskinesias." Acta Neurochir Suppl (Wien) 58: 39-44.

Bezdudnaya, T. and A. Keller (2008). "Laterodorsal nucleus of the thalamus: A processor of somatosensory inputs." The Journal of comparative neurology 507(6): 1979-1989.

Bjugn, R. and H. J. Gundersen (1993). "Estimate of the total number of neurons and glial and endothelial cells in the rat spinal cord by means of the optical disector." J Comp Neurol 328(3): 406-414.

Blaner, W. S. (1989). "Retinol-Binding Protein: The Serum Transport Protein for Vitamin A*." Endocrine Reviews 10(3): 308-316.

Bolam, J., M. Brown, J. Moss and P. Magill (2009). "Basal Ganglia: Internal Organization." Encyclopedia of Neuroscience.

Bolam, J. P., Y. Smith, C. A. Ingham, M. von Krosigk and A. D. Smith (1993). "Convergence of synaptic terminals from the striatum and the globus pallidus onto single neurones in the substantia nigra and the entopeduncular nucleus." Prog Brain Res 99: 73-88.

Bosch-Bouju, C., B. I. Hyland and L. C. Parr-Brownlie (2013). "Motor thalamus integration of cortical, cerebellar and basal ganglia information: implications for normal and parkinsonian conditions." Front Comput Neurosci 7: 163.

Bubb, E. J., L. Kinnavane and J. P. Aggleton (2017). "Hippocampal - diencephalic - cingulate networks for memory and emotion: An anatomical guide." Brain and neuroscience advances 1(1): 2398212817723443.

Buzsáki, G. (2004). "Large-scale recording of neuronal ensembles." Nature Neuroscience 7: 446.

Callaway, E. M. and L. Luo (2015). "Monosynaptic Circuit Tracing with Glycoprotein-Deleted Rabies Viruses." J Neurosci 35(24): 8979-8985.

Cardin, J. A., M. Carlén, K. Meletis, U. Knoblich, F. Zhang, K. Deisseroth, L. H. Tsai and C. I. Moore (2009). "Driving fast-spiking cells induces gamma rhythm and controls sensory responses." Nature 459(7247): 663-667.

Carlén, M., K. Meletis, J. H. Siegle, J. A. Cardin, K. Futai, D. Vierling-Claassen, C. Rühlmann, S. R. Jones, K. Deisseroth, M. Sheng, C. I. Moore and L. H. Tsai (2012). "A critical role for NMDA receptors in parvalbumin interneurons for gamma rhythm induction and behavior." Mol Psychiatry 17(5): 537-548.

Catanese, J. and D. Jaeger (2020). "Nigro-Thalamic Projection Controls Timing of Action Initiation." bioRxiv: 2020.2001.2012.903500.

Chakraborty, S., Z. Ouhaz, S. Mason and A. S. Mitchell (2019). "Macaque parvocellular mediodorsal thalamus: Dissociable contributions to learning and adaptive decision-making." European Journal of Neuroscience 49(8): 1041-1054.

Chen, G., Y. Zhang, X. Li, X. Zhao, Q. Ye, Y. Lin, H. W. Tao, M. J. Rasch and X. Zhang (2017). "Distinct Inhibitory Circuits Orchestrate Cortical beta and gamma Band Oscillations." Neuron 96(6): 1403-1418.e1406.

Chevalier, G. and J. M. Deniau (1990). "Disinhibition as a basic process in the expression of striatal functions." Trends Neurosci 13(7): 277-280.

Chittajallu, R., K. A. Pelkey and C. J. McBain (2013). "Neurogliaform cells dynamically regulate somatosensory integration via synapse-specific modulation." Nat Neurosci 16(1): 13-15.

Collins, D. P., P. G. Anastasiades, J. J. Marlin and A. G. Carter (2018). "Reciprocal Circuits Linking the Prefrontal Cortex with Dorsal and Ventral Thalamic Nuclei." Neuron 98(2): 366-379.e364.

Crick, F. (1984). "Function of the thalamic reticular complex: the searchlight hypothesis." Proceedings of the National Academy of Sciences 81(14): 4586-4590.

Cruikshank, S. J., O. J. Ahmed, T. R. Stevens, S. L. Patrick, A. N. Gonzalez, M. Elmaleh and B. W. Connors (2012). "Thalamic control of layer 1 circuits in prefrontal cortex." J Neurosci 32(49): 17813-17823.

Cruikshank, S. J., T. J. Lewis and B. W. Connors (2007). "Synaptic basis for intense thalamocortical activation of feedforward inhibitory cells in neocortex." Nat Neurosci 10(4): 462-468.

Cruikshank, S. J., H. Urabe, A. V. Nurmikko and B. W. Connors (2010). "Pathway-specific feedforward circuits between thalamus and neocortex revealed by selective optical stimulation of axons." Neuron 65(2): 230-245.

Cury, R. G., V. Fraix, A. Castrioto, M. A. Pérez Fernández, P. Krack, S. Chabardes, E. Seigneuret, E. J. L. Alho, A. L. Benabid and E. Moro (2017). "Thalamic deep brain stimulation for tremor in Parkinson disease, essential tremor, and dystonia." Neurology 89(13): 1416-1423.

Dacre, J., M. Colligan, J. Ammer, J. Schiemann, T. Clarke, V. Chamosa-Pino, F. Claudi, J. A. Harston, C. Eleftheriou, J. M. P. Pakan, C.-C. Huang, A. Hantman, N. L. Rochefort and I. Duguid (2019). "Cerebellar-recipient motor thalamus drives behavioral context-specific movement initiation." bioRxiv: 802124.

DeLong, M. and T. Wichmann (2009). "Update on models of basal ganglia function and dysfunction." Parkinsonism & related disorders 15 Suppl 3(0 3): S237-S240.

DeLong, M. R. (1990). "Primate models of movement disorders of basal ganglia origin." Trends Neurosci 13(7): 281-285.

Deniau, J. M. and G. Chevalier (1985). "Disinhibition as a basic process in the expression of striatal functions. II. The striato-nigral influence on thalamocortical cells of the ventromedial thalamic nucleus." Brain Res 334(2): 227-233.

Douglas, R. J. and K. A. Martin (2004). "Neuronal circuits of the neocortex." Annu Rev Neurosci 27: 419-451.

Ellender, T. J., J. V. Raimondo, A. Irkle, K. P. Lamsa and C. J. Akerman (2014). "Excitatory effects of parvalbumin-expressing interneurons maintain hippocampal epileptiform activity via synchronous afterdischarges." J Neurosci 34(46): 15208-15222.

Fan, L. Z., S. Kheifets, U. L. Böhm, H. Wu, K. D. Piatkevich, M. E. Xie, V. Parot, Y. Ha, K. E. Evans, E. S. Boyden, A. E. Takesian and A. E. Cohen (2020). "All-Optical Electrophysiology Reveals the Role of Lateral Inhibition in Sensory Processing in Cortical Layer 1." Cell 180(3): 521-535.e518.

Ferguson, B. R. and W.-J. Gao (2018). "PV Interneurons: Critical Regulators of E/I Balance for Prefrontal Cortex-Dependent Behavior and Psychiatric Disorders." Frontiers in neural circuits 12: 37-37.

Fishell, G. and B. Rudy (2011). "Mechanisms of inhibition within the telencephalon: "where the wild things are"." Annu Rev Neurosci 34: 535-567.

Francois, C., D. Tande, J. Yelnik and E. C. Hirsch (2002). "Distribution and morphology of nigral axons projecting to the thalamus in primates." J Comp Neurol 447(3): 249-260.

Fries, P. (2005). "A mechanism for cognitive dynamics: neuronal communication through neuronal coherence." Trends Cogn Sci 9(10): 474-480.

Gabernet, L., S. P. Jadhav, D. E. Feldman, M. Carandini and M. Scanziani (2005). "Somatosensory integration controlled by dynamic thalamocortical feed-forward inhibition." Neuron 48(2): 315-327.

Gao, Z., C. Davis, A. M. Thomas, M. N. Economo, A. M. Abrego, K. Svoboda, C. I. De Zeeuw and N. Li (2018). "A cortico-cerebellar loop for motor planning." Nature.

Garcia-Munoz, M. and G. W. Arbuthnott (2015). "Basal ganglia—thalamus and the “crowning enigma”." Frontiers in Neural Circuits 9: 71.

Gerfen, C. R. (1985). "The neostriatal mosaic. I. Compartmental organization of projections from the striatum to the substantia nigra in the rat." J Comp Neurol 236(4): 454-476.

Gerfen, C. R., R. Paletzki and N. Heintz (2013). "GENSAT BAC cre-recombinase driver lines to study the functional organization of cerebral cortical and basal ganglia circuits." Neuron 80(6): 1368-1383.

Goldberg, J. H. and M. S. Fee (2012). "A cortical motor nucleus drives the basal ganglia-recipient thalamus in singing birds." Nat Neurosci 15(4): 620-627.

Gornati, S. V., C. B. Schafer, O. H. J. Eelkman Rooda, A. L. Nigg, C. I. De Zeeuw and F. E. Hoebeek (2018). "Differentiating Cerebellar Impact on Thalamic Nuclei." Cell Rep 23(9): 2690-2704.

Gray, L. T., Z. Yao, T. N. Nguyen, T. K. Kim, H. Zeng and B. Tasic (2017). "Layer-specific chromatin accessibility landscapes reveal regulatory networks in adult mouse visual cortex." Elife 6.

Graybiel, A. M. and C. W. Ragsdale, Jr. (1978). "Histochemically distinct compartments in the striatum of human, monkeys, and cat demonstrated by acetylthiocholinesterase staining." Proc Natl Acad Sci U S A 75(11): 5723-5726.

Grillner, S. (1981). Control of locomotion in bipeds, tetrapods, and fish In: Brooks VB (ed) Handbook of physiology-the nervous system, II, Waverly Press, Baltimore.

Groenewegen, H. J. (1988). "Organization of the afferent connections of the mediodorsal thalamic nucleus in the rat, related to the mediodorsal-prefrontal topography." Neuroscience 24(2): 379-431.

Groenewegen, H. J. and H. W. Berendse (1994). "The specificity of the 'nonspecific' midline and intralaminar thalamic nuclei." Trends Neurosci 17(2): 52-57.

Guido, W., S. M. Lu and S. M. Sherman (1992). "Relative contributions of burst and tonic responses to the receptive field properties of lateral geniculate neurons in the cat." J Neurophysiol 68(6): 2199-2211.

Guillery, R. W. (1995). "Anatomical evidence concerning the role of the thalamus in corticocortical communication: a brief review." J Anat 187 (Pt 3)(Pt 3): 583-592.

Guo, J.-Z., A. R. Graves, W. W. Guo, J. Zheng, A. Lee, J. Rodríguez-González, N. Li, J. J. Macklin, J. W. Phillips, B. D. Mensh, K. Branson and A. W. Hantman (2015). "Cortex commands the performance of skilled movement." eLife 4: e10774.

Guo, K., N. Yamawaki, K. Svoboda and G. M. G. Shepherd (2018). "Anterolateral Motor Cortex Connects with a Medial Subdivision of Ventromedial Thalamus through Cell Type-Specific Circuits, Forming an

Excitatory Thalamo-Cortico-Thalamic Loop via Layer 1 Apical Tuft Dendrites of Layer 5B Pyramidal Tract Type Neurons." J Neurosci 38(41): 8787-8797.

Guo, Z. V., H. K. Inagaki, K. Daie, S. Druckmann, C. R. Gerfen and K. Svoboda (2017). "Maintenance of persistent activity in a frontal thalamocortical loop." Nature 545(7653): 181-186.

Guo, Z. V., N. Li, D. Huber, E. Ophir, D. Gutnisky, J. T. Ting, G. Feng and K. Svoboda (2014). "Flow of cortical activity underlying a tactile decision in mice." Neuron 81(1): 179-194.

Haber, S. N. (2003). "The primate basal ganglia: parallel and integrative networks." Journal of Chemical Neuroanatomy 26(4): 317-330.

Haber, S. N. and R. Calzavara (2009). "The cortico-basal ganglia integrative network: the role of the thalamus." Brain Res Bull 78(2-3): 69-74.

Haber, S. N., A. Yendiki and S. Jbabdi (2020). "Four Deep Brain Stimulation Targets for Obsessive-Compulsive Disorder: Are They Different?" Biol Psychiatry.

Hackett, T. A., T. Takahata and P. Balaram (2011). "VGLUT1 and VGLUT2 mRNA expression in the primate auditory pathway." Hear Res 274(1-2): 129-141.

Halassa, M. M. and L. Acsady (2016). "Thalamic Inhibition: Diverse Sources, Diverse Scales." Trends Neurosci 39(10): 680-693.

Harris, J. A., K. E. Hirokawa, S. A. Sorensen, H. Gu, M. Mills, L. L. Ng, P. Bohn, M. Mortrud, B. Ouellette, J. Kidney, K. A. Smith, C. Dang, S. Sunkin, A. Bernard, S. W. Oh, L. Madisen and H. Zeng (2014). "Anatomical characterization of Cre driver mice for neural circuit mapping and manipulation." Frontiers in Neural Circuits 8: 76.

Harris, K. D. and T. D. Mrsic-Flogel (2013). "Cortical connectivity and sensory coding." Nature 503(7474): 51-58.

Harris, K. D. and G. M. G. Shepherd (2015). "The neocortical circuit: themes and variations." Nature neuroscience 18(2): 170-181.

Helmstaedter, M., B. Sakmann and D. Feldmeyer (2009). "L2/3 interneuron groups defined by multiparameter analysis of axonal projection, dendritic geometry, and electrical excitability." Cereb Cortex 19(4): 951-962.

Herkenham, M. (1979). "The afferent and efferent connections of the ventromedial thalamic nucleus in the rat." J Comp Neurol 183(3): 487-517.

Hintzen, A., E. A. Pelzer and M. Tittgemeyer (2018). "Thalamic interactions of cerebellum and basal ganglia." Brain Struct Funct 223(2): 569-587.

Hirai, T. and E. G. Jones (1989). "A new parcellation of the human thalamus on the basis of histochemical staining." Brain Res Brain Res Rev 14(1): 1-34.

Hooks, B. M., T. Mao, D. A. Gutnisky, N. Yamawaki, K. Svoboda and G. M. G. Shepherd (2013). "Organization of cortical and thalamic input to pyramidal neurons in mouse motor cortex." The Journal of neuroscience : the official journal of the Society for Neuroscience 33(2): 748-760.

Horne, M. K. and E. G. Butler (1995). "The role of the cerebello-thalamo-cortical pathway in skilled movement." Prog Neurobiol 46(2-3): 199-213.

Hubel, D. H. (1982). "Cortical Neurobiology: A Slanted Historical Perspective." Annual Review of Neuroscience 5(1): 363-370.

Huguenard, J. R. and D. A. Prince (1992). "A novel T-type current underlies prolonged Ca(2+)-dependent burst firing in GABAergic neurons of rat thalamic reticular nucleus." J Neurosci 12(10): 3804-3817.

Hunnicutt, B. J., B. R. Long, D. Kusefoglu, K. J. Gertz, H. Zhong and T. Mao (2014). "A comprehensive thalamocortical projection map at the mesoscopic level." Nat Neurosci 17(9): 1276-1285.

Ibrahim, L. A., L. Mesik, X. Y. Ji, Q. Fang, H. F. Li, Y. T. Li, B. Zingg, L. I. Zhang and H. W. Tao (2016). "Cross-Modality Sharpening of Visual Cortical Processing through Layer-1-Mediated Inhibition and Disinhibition." Neuron 89(5): 1031-1045.

Ilinsky, I., K. Kultas-Ilinsky and B. Knosp (2002). "Stereotactic Atlas of the Macaca mulatta Thalamus and Adjacent Basal Ganglia Nuclei."

Ilinsky, I. A. and K. Kultas-Ilinsky (1987). "Sagittal cytoarchitectonic maps of the Macaca mulatta thalamus with a revised nomenclature of the motor-related nuclei validated by observations on their connectivity." Journal of Comparative Neurology 262(3): 331-364.

Ilinsky, I. A. and K. Kultas-ilinsky (1990). "Fine structure of the magnocellular subdivision of the ventral anterior thalamic nucleus (V Amc) of Macaca mulatta: I. Cell types and synaptology." Journal of Comparative Neurology 294(3): 455-478.

Ilinsky, I. A., W. G. Tourtellotte and K. Kultas-Ilinsky (1993). "Anatomical distinctions between the two basal ganglia afferent territories in the primate motor thalamus." Stereotact Funct Neurosurg 60(1-3): 62-69.

Jeong, M., Y. Kim, J. Kim, D. D. Ferrante, P. P. Mitra, P. Osten and D. Kim (2016). "Comparative three-dimensional connectome map of motor cortical projections in the mouse brain." Sci Rep 6: 20072.

Jiang, X., S. Shen, C. R. Cadwell, P. Berens, F. Sinz, A. S. Ecker, S. Patel and A. S. Tolias (2015). "Principles of connectivity among morphologically defined cell types in adult neocortex." Science 350(6264): aac9462.

Jiang, X., G. Wang, A. J. Lee, R. L. Stornetta and J. J. Zhu (2013). "The organization of two new cortical interneuronal circuits." Nat Neurosci 16(2): 210-218.

Jinno, S. and T. Kosaka (2004). "Parvalbumin is expressed in glutamatergic and GABAergic corticostriatal pathway in mice." J Comp Neurol 477(2): 188-201.

Jones, E. G. (1975). "Some aspects of the organization of the thalamic reticular complex." J Comp Neurol 162(3): 285-308.

Jones, E. G. (1998). "Viewpoint: the core and matrix of thalamic organization." Neuroscience 85(2): 331-345.

Jones, E. G. (2007). The Thalamus, Cambridge University Press.

Jones, E. G. and S. H. Hendry (1989). "Differential Calcium Binding Protein Immunoreactivity Distinguishes Classes of Relay Neurons in Monkey Thalamic Nuclei." Eur J Neurosci 1(3): 222-246.

Kawaguchi, Y. (2017). "Pyramidal Cell Subtypes and Their Synaptic Connections in Layer 5 of Rat Frontal Cortex." Cerebral Cortex 27(12): 5755-5771.

Kawaguchi, Y. and Y. Kubota (1997). "GABAergic cell subtypes and their synaptic connections in rat frontal cortex." Cereb Cortex 7(6): 476-486.

Kawai, R., T. Markman, R. Poddar, R. Ko, Antoniu L. Fantana, Ashesh K. Dhawale, Adam R. Kampff and Bence P. Ölveczky (2015). "Motor Cortex Is Required for Learning but Not for Executing a Motor Skill." Neuron 86(3): 800-812.

Kemp, J. M. and T. P. Powell (1971). "The connexions of the striatum and globus pallidus: synthesis and speculation." Philos Trans R Soc Lond B Biol Sci 262(845): 441-457.

Kirchgessner, M. A., A. D. Franklin and E. M. Callaway (2020). "Context-dependent and dynamic functional influence of corticothalamic pathways to first- and higher-order visual thalamus." Proceedings of the National Academy of Sciences 117(23): 13066-13077.

Klaus, A., J. A. d. Silva and R. M. Costa (2019). "What, If, and When to Move: Basal Ganglia Circuits and Self-Paced Action Initiation." Annual Review of Neuroscience 42(1): 459-483.

Klausberger, T. and P. Somogyi (2008). "Neuronal diversity and temporal dynamics: the unity of hippocampal circuit operations." Science 321(5885): 53-57.

Kojima, S. and A. J. Doupe (2009). "Activity propagation in an avian basal ganglia-thalamocortical circuit essential for vocal learning." The Journal of neuroscience : the official journal of the Society for Neuroscience 29(15): 4782-4793.

Kuang, X.-L., X.-M. Zhao, H.-F. Xu, Y.-Y. Shi, J.-B. Deng and G.-T. Sun (2010). "Spatio-temporal expression of a novel neuron-derived neurotrophic factor (NDNF) in mouse brains during development." BMC neuroscience 11: 137-137.

Kubota, Y. and Y. Kawaguchi (1993). "Spatial distributions of chemically identified intrinsic neurons in relation to patch and matrix compartments of rat neostriatum." Journal of Comparative Neurology 332(4): 499-513.

Kultas-ilinsky, K. and I. A. Ilinsky (1990). "Fine structure of the magnocellular subdivision of the ventral anterior thalamic nucleus (V Amc) of Macaca mulatta: II. Organization of nigrothalamic afferents as revealed with EM autoradiography." Journal of Comparative Neurology 294(3): 479-489.

Kultas-Ilinsky, K., I. A. Ilinsky and C. Verney (2011). "Glutamic acid decarboxylase isoform 65 immunoreactivity in the motor thalamus of humans and monkeys: gamma-aminobutyric acidergic connections and nuclear delineations." J Comp Neurol 519(14): 2811-2837.

Kuramoto, E., F. Fujiyama, K. C. Nakamura, Y. Tanaka, H. Hioki and T. Kaneko (2011). "Complementary distribution of glutamatergic cerebellar and GABAergic basal ganglia afferents to the rat motor thalamic nuclei." Eur J Neurosci 33(1): 95-109.

Kuramoto, E., T. Furuta, K. C. Nakamura, T. Unzai, H. Hioki and T. Kaneko (2009). "Two types of thalamocortical projections from the motor thalamic nuclei of the rat: a single neuron-tracing study using viral vectors." Cereb Cortex 19(9): 2065-2077.

Kuramoto, E., S. Ohno, T. Furuta, T. Unzai, Y. R. Tanaka, H. Hioki and T. Kaneko (2015). "Ventral medial nucleus neurons send thalamocortical afferents more widely and more preferentially to layer 1 than neurons of the ventral anterior-ventral lateral nuclear complex in the rat." Cereb Cortex 25(1): 221-235.

Lacaille, J. C. and P. A. Schwartzkroin (1988). "Stratum lacunosum-moleculare interneurons of hippocampal CA1 region. II. Intrasomatic and intradendritic recordings of local circuit synaptic interactions." J Neurosci 8(4): 1411-1424.

Lacey, C. J., J. P. Bolam and P. J. Magill (2007). "Novel and distinct operational principles of intralaminar thalamic neurons and their striatal projections." J Neurosci 27(16): 4374-4384.

Larkum, M. (2013). "A cellular mechanism for cortical associations: an organizing principle for the cerebral cortex." Trends Neurosci 36(3): 141-151.

Larkum, M. E., T. Nevian, M. Sandler, A. Polsky and J. Schiller (2009). "Synaptic integration in tuft dendrites of layer 5 pyramidal neurons: a new unifying principle." Science 325(5941): 756-760.

Larkum, M. E., J. J. Zhu and B. Sakmann (1999). "A new cellular mechanism for coupling inputs arriving at different cortical layers." Nature 398(6725): 338-341.

Lazaridis, I., O. Tzortzi, M. Weglage, A. Märtin, Y. Xuan, M. Parent, Y. Johansson, J. Fuzik, D. Fürth, L. E. Fenno, C. Ramakrishnan, G. Silberberg, K. Deisseroth, M. Carlén and K. Meletis (2019). "A hypothalamus-habenula circuit controls aversion." Molecular Psychiatry 24(9): 1351-1368.

Lee, A. J., G. Wang, X. Jiang, S. M. Johnson, E. T. Hoang, F. Lanté, R. L. Stornetta, M. P. Beenhakker, Y. Shen and J. Julius Zhu (2015). "Canonical Organization of Layer 1 Neuron-Led Cortical Inhibitory and Disinhibitory Interneuronal Circuits." Cerebral Cortex (New York, NY) 25(8): 2114-2126.

Lee, A. T., D. Vogt, J. L. Rubenstein and V. S. Sohal (2014). "A Class of GABAergic Neurons in the Prefrontal Cortex Sends Long-Range Projections to the Nucleus Accumbens and Elicits Acute Avoidance Behavior." The Journal of Neuroscience 34(35): 11519-11525.

Lee, S., J. Hjerling-Leffler, E. Zagha, G. Fishell and B. Rudy (2010). "The largest group of superficial neocortical GABAergic interneurons expresses ionotropic serotonin receptors." J Neurosci 30(50): 16796-16808.

Letzkus, J. J., S. B. E. Wolff, E. M. M. Meyer, P. Tovote, J. Courtin, C. Herry and A. Lüthi (2011). "A disinhibitory microcircuit for associative fear learning in the auditory cortex." Nature 480(7377): 331-335.

Lidierth, M. (2009). "sigTOOL: A MATLAB-based environment for sharing laboratory-developed software to analyze biological signals." J Neurosci Methods 178(1): 188-196.

Livingstone, M. S. and D. H. Hubel (1981). "Effects of sleep and arousal on the processing of visual information in the cat." Nature 291(5816): 554-561.

Llinás, R., K. Walton and E. Lang (2004). The synaptic organization of the brain, Oxford Univ Press, New York.

Luo, M. and D. J. Perkel (1999). "A GABAergic, Strongly Inhibitory Projection to a Thalamic Nucleus in the Zebra Finch Song System." The Journal of Neuroscience 19(15): 6700-6711.

Ma, J., X.-H. Yao, Y. Fu and Y.-C. Yu (2014). "Development of Layer 1 Neurons in the Mouse Neocortex." Cerebral Cortex 24(10): 2604-2618.

Ma, Y., H. Hu, A. S. Berrebi, P. H. Mathers and A. Agmon (2006). "Distinct Subtypes of Somatostatin-Containing Neocortical Interneurons Revealed in Transgenic Mice." The Journal of Neuroscience 26(19): 5069-5082.

Mao, T., D. Kusefoglu, B. M. Hooks, D. Huber, L. Petreanu and K. Svoboda (2011). "Long-range neuronal circuits underlying the interaction between sensory and motor cortex." Neuron 72(1): 111-123.

McCormick, D. A., B. W. Connors, J. W. Lighthall and D. A. Prince (1985). "Comparative electrophysiology of pyramidal and sparsely spiny stellate neurons of the neocortex." J Neurophysiol 54(4): 782-806.

Miyoshi, G., J. Hjerling-Leffler, T. Karayannis, V. H. Sousa, S. J. Butt, J. Battiste, J. E. Johnson, R. P. Machold and G. Fishell (2010). "Genetic fate mapping reveals that the caudal ganglionic eminence produces a large and diverse population of superficial cortical interneurons." J Neurosci 30(5): 1582-1594.

Mo, C. and S. M. Sherman (2019). "A Sensorimotor Pathway via Higher-Order Thalamus." The Journal of Neuroscience 39(4): 692-704.

Munoz-Manchado, A. B., C. Foldi, S. Szydlowski, L. Sjulson, M. Farries, C. Wilson, G. Silberberg and J. Hjerling-Leffler (2016). "Novel Striatal GABAergic Interneuron Populations Labeled in the 5HT3a(EGFP) Mouse." Cereb Cortex 26(1): 96-105.

Nakamura, K. C., A. Sharott and P. J. Magill (2014). "Temporal coupling with cortex distinguishes spontaneous neuronal activities in identified basal ganglia-recipient and cerebellar-recipient zones of the motor thalamus." Cereb Cortex 24(1): 81-97.

Oláh, S., M. Füle, G. Komlósi, C. Varga, R. Báldi, P. Barzó and G. Tamás (2009). "Regulation of cortical microcircuits by unitary GABAergic volume transmission." Nature 461(7268): 1278-1281.

Olah, S., G. Komlosi, J. Szabadics, C. Varga, E. Toth, P. Barzo and G. Tamas (2007). "Output of neurogliaform cells to various neuron types in the human and rat cerebral cortex." Front Neural Circuits 1: 4.

Oldenburg, I. A. and B. L. Sabatini (2015). "Antagonistic but Not Symmetric Regulation of Primary Motor Cortex by Basal Ganglia Direct and Indirect Pathways." Neuron 86(5): 1174-1181.

Olszewski, J. (1954). "The thalamus of the Macaca Mulatta. By J. Olszewski. Basel and New York, S. Karger. 1952. 93 Pages, no price. (Reviewed by L. V. Amador.)." Journal of Comparative Neurology 100(3): 757-757.

Overstreet-Wadiche, L. and C. J. McBain (2015). "Neurogliaform cells in cortical circuits." Nat Rev Neurosci 16(8): 458-468.

Owen, S. F., M. H. Liu and A. C. Kreitzer (2019). "Thermal constraints on in vivo optogenetic manipulations." Nature Neuroscience.

Pachitariu, M., N. Steinmetz, S. Kadir, M. Carandini and H. Kenneth D. (2016). "Kilosort: realtime spike-sorting for extracellular electrophysiology with hundreds of channels." bioRxiv: 061481.

Packer, A. M., L. E. Russell, H. W. P. Dalgleish and M. Häusser (2015). "Simultaneous all-optical manipulation and recording of neural circuit activity with cellular resolution in vivo." Nature Methods 12(2): 140-146.

Palmer, L. M., J. M. Schulz, S. C. Murphy, D. Ledergerber, M. Murayama and M. E. Larkum (2012). "The Cellular Basis of GABA_B-Mediated Interhemispheric Inhibition." Science 335(6071): 989-993.

Papale, A. E. and B. M. Hooks (2018). "Circuit Changes in Motor Cortex During Motor Skill Learning." Neuroscience 368: 283-297.

Parent, A. and L.-N. Hazrati (1995). "Functional anatomy of the basal ganglia. I. The cortico-basal ganglia-thalamo-cortical loop." Brain Research Reviews 20(1): 91-127.

Paxinos, G., X. F. Huang and A. W. Toga (2000). The Rhesus Monkey Brain in Stereotaxic Coordinates, Academic Press.

Paxinos, G. and M. Keith B. J. Franklin (2007). The Mouse Brain in Stereotaxic Coordinates, Elsevier Science.

Paxinos, G., M. Petrides, X. F. Huang and A. W. Toga (2008). The Rhesus Monkey Brain in Stereotaxic Coordinates, Elsevier Science.

Paxinos, G. and C. Watson (2009). The Rat Brain in Stereotaxic Coordinates, Elsevier/Academic.

Perduca, M., S. Nicolis, B. Mannucci, M. Galliano and H. L. Monaco (2018). "Human plasma retinol-binding protein (RBP4) is also a fatty acid-binding protein." Biochimica et Biophysica Acta (BBA) - Molecular and Cell Biology of Lipids 1863(4): 458-466.

Perry, B. A. L. and A. S. Mitchell (2019). "Considering the Evidence for Anterior and Laterodorsal Thalamic Nuclei as Higher Order Relays to Cortex." Front Mol Neurosci 12: 167.

Person, A. L. and D. J. Perkel (2005). "Unitary IPSPs drive precise thalamic spiking in a circuit required for learning." Neuron 46(1): 129-140.

Person, A. L. and D. J. Perkel (2007). "Pallidal Neuron Activity Increases during Sensory Relay through Thalamus in a Songbird Circuit Essential for Learning." The Journal of Neuroscience 27(32): 8687-8698.

Petreanu, L., T. Mao, S. M. Sternson and K. Svoboda (2009). "The subcellular organization of neocortical excitatory connections." Nature 457(7233): 1142-1145.

Pinault, D. (2004). "The thalamic reticular nucleus: structure, function and concept." Brain Res Brain Res Rev 46(1): 1-31.

Pinault, D., J. Bourassa and M. Deschênes (1995). "The Axonal Arborization of Single Thalamic Reticular Neurons in the Somatosensory Thalamus of the Rat." European Journal of Neuroscience 7(1): 31-40.

Poorthuis, R. B., K. Muhammad, M. Wang, M. B. Verhoog, S. Junek, A. Wrana, H. D. Mansvelder and J. J. Letzkus (2018). "Rapid Neuromodulation of Layer 1 Interneurons in Human Neocortex." Cell Reports 23(4): 951-958.

Price, C. J., B. Cauli, E. R. Kovacs, A. Kulik, B. Lambolez, R. Shigemoto and M. Capogna (2005). "Neurogliaform neurons form a novel inhibitory network in the hippocampal CA1 area." J Neurosci 25(29): 6775-6786.

Ramcharan, E. J., J. W. Gnadt and S. M. Sherman (2005). "Higher-order thalamic relays burst more than first-order relays." Proceedings of the National Academy of Sciences of the United States of America 102(34): 12236-12241.

Rock, C., H. Zurita, C. Wilson and A. J. Apicella (2016). "An inhibitory corticostriatal pathway." Elife 5.

Rovo, Z., I. Ulbert and L. Acsady (2012). "Drivers of the primate thalamus." J Neurosci 32(49): 17894-17908.

Rubio-Garrido, P., F. Pérez-de-Manzo, C. Porrero, M. J. Galazo and F. Clascá (2009). "Thalamic input to distal apical dendrites in neocortical layer 1 is massive and highly convergent." Cereb Cortex 19(10): 2380-2395.

Rudy, B., G. Fishell, S. Lee and J. Hjerling-Leffler (2011). "Three Groups of Interneurons Account for Nearly 100% of Neocortical GABAergic Neurons." Developmental neurobiology 71(1): 45-61.

Saalmann, Y. B. (2014). "Intralaminar and medial thalamic influence on cortical synchrony, information transmission and cognition." Frontiers in systems neuroscience 8: 83-83.

Saalmann, Y. B., M. A. Pinsk, L. Wang, X. Li and S. Kastner (2012). "The pulvinar regulates information transmission between cortical areas based on attention demands." Science 337(6095): 753-756.

Saleem, K. and N. Logothetis (2012). A combined MRI and Histology Atlas of the Rhesus Monkey Brain in Stereotaxic Coordinates. 2nd edition with Horizontal, Coronal, and Sagittal Series. Elsevier/Academic Press.

Saunders, A., I. A. Oldenburg, V. K. Berezovskii, C. A. Johnson, N. D. Kingery, H. L. Elliott, T. Xie, C. R. Gerfen and B. L. Sabatini (2015). "A direct GABAergic output from the basal ganglia to frontal cortex." Nature 521(7550): 85-89.

Schultz, W. (1998). "Predictive reward signal of dopamine neurons." J Neurophysiol 80(1): 1-27.

Schuman, B., R. Machold, Y. Hashikawa, J. Fuzik, G. Fishell and B. Rudy (2018). "Four unique interneuron populations reside in neocortical layer 1." The Journal of Neuroscience.

Shepherd, G. M. (2013). "Corticostriatal connectivity and its role in disease." Nat Rev Neurosci 14(4): 278-291.

Sherman, S. M. (2001). "A wake-up call from the thalamus." Nature Neuroscience 4(4): 344-346.

Sherman, S. M. and R. W. Guillery (1996). "Functional organization of thalamocortical relays." J Neurophysiol 76(3): 1367-1395.

Sherman, S. M. and R. W. Guillery (2002). "The role of the thalamus in the flow of information to the cortex." Philos Trans R Soc Lond B Biol Sci 357(1428): 1695-1708.

Sherman, S. M. and R. W. Guillery (2006). Exploring the thalamus and its role in cortical function, 2nd ed. Cambridge, MA, US, MIT Press.

Shrestha, P., A. Mousa and N. Heintz (2015). "Layer 2/3 pyramidal cells in the medial prefrontal cortex moderate stress induced depressive behaviors." eLife 4: e08752.

Sieveritz, B. and G. W. Arbuthnott (2020). "Prelimbic cortical targets of ventromedial thalamic projections include inhibitory interneurons and corticostriatal pyramidal neurons in the rat." Brain Structure and Function.

Simon, A., S. Oláh, G. Molnár, J. Szabadics and G. Tamás (2005). "Gap-Junctional Coupling between Neurogliaform Cells and Various Interneuron Types in the Neocortex." The Journal of Neuroscience 25(27): 6278-6285.

Smith, Y., A. Galvan, T. J. Ellender, N. Doig, R. M. Villalba, I. Huerta-Ocampo, T. Wichmann and J. P. Bolam (2014). "The thalamostriatal system in normal and diseased states." Front Syst Neurosci 8: 5.

Smith, Y., D. V. Raju, J. F. Pare and M. Sidibe (2004). "The thalamostriatal system: a highly specific network of the basal ganglia circuitry." Trends Neurosci 27(9): 520-527.

Sohal, V. S., F. Zhang, O. Yizhar and K. Deisseroth (2009). "Parvalbumin neurons and gamma rhythms enhance cortical circuit performance." Nature 459(7247): 698-702.

Somogyi, P., L. Katona, T. Klausberger, B. Lasztóczi and T. J. Viney (2013). "Temporal redistribution of inhibition over neuronal subcellular domains underlies state-dependent rhythmic change of excitability in the hippocampus." Philosophical transactions of the Royal Society of London. Series B, Biological sciences 369(1635): 20120518-20120518.

Somogyi, P. and T. Klausberger (2005). "Defined types of cortical interneurone structure space and spike timing in the hippocampus." J Physiol 562(Pt 1): 9-26.

Soriano, E. and J. A. Del Río (2005). "The cells of cajal-retzius: still a mystery one century after." Neuron 46(3): 389-394.

Stamatakis, A. M., M. J. Schachter, S. Gulati, K. T. Zitelli, S. Malanowski, A. Tajik, C. Fritz, M. Trulson and S. L. Otte (2018). "Simultaneous Optogenetics and Cellular Resolution Calcium Imaging During Active Behavior Using a Miniaturized Microscope." Frontiers in Neuroscience 12(496).

Stuart, G. J. and B. Sakmann (1994). "Active propagation of somatic action potentials into neocortical pyramidal cell dendrites." Nature 367(6458): 69-72.

Stujenske, Joseph M., T. Spellman and Joshua A. Gordon (2015). "Modeling the Spatiotemporal Dynamics of Light and Heat Propagation for In Vivo Optogenetics." Cell Reports 12(3): 525-534.

Swadlow, H. A. and A. G. Gusev (2001). "The impact of 'bursting' thalamic impulses at a neocortical synapse." Nat Neurosci 4(4): 402-408.

Tamas, G., A. Lorincz, A. Simon and J. Szabadics (2003). "Identified sources and targets of slow inhibition in the neocortex." Science 299(5614): 1902-1905.

Tanaka, Y. H., Y. R. Tanaka, M. Kondo, S.-I. Terada, Y. Kawaguchi and M. Matsuzaki (2018). "Thalamocortical Axonal Activity in Motor Cortex Exhibits Layer-Specific Dynamics during Motor Learning." Neuron 100(1): 244-258.e212.

Tasic, B., V. Menon, T. N. Nguyen, T. K. Kim, T. Jarsky, Z. Yao, B. Levi, L. T. Gray, S. A. Sorensen, T. Dolbeare, D. Bertagnolli, J. Goldy, N. Shapovalova, S. Parry, C. Lee, K. Smith, A. Bernard, L. Madisen, S. M. Sunkin, M. Hawrylycz, C. Koch and H. Zeng (2016). "Adult mouse cortical cell taxonomy revealed by single cell transcriptomics." Nat Neurosci 19(2): 335-346.

Thompson, S. M. and R. T. Robertson (1987). "Organization of subcortical pathways for sensory projections to the limbic cortex. I. Subcortical projections to the medial limbic cortex in the rat." J Comp Neurol 265(2): 175-188.

Timbie, C. and H. Barbas (2014). "Specialized pathways from the primate amygdala to posterior orbitofrontal cortex." J Neurosci 34(24): 8106-8118.

Timbie, C. and H. Barbas (2015). "Pathways for Emotions: Specializations in the Amygdalar, Mediodorsal Thalamic, and Posterior Orbitofrontal Network." J Neurosci 35(34): 11976-11987.

Timbie, C., M. García-Cabezas, B. Zikopoulos and H. Barbas (2020). "Organization of primate amygdalar-thalamic pathways for emotions." PLoS Biol 18(2): e3000639.

Tlamsa, A. P. and J. C. Brumberg (2010). "Organization and morphology of thalamocortical neurons of mouse ventral lateral thalamus." Somatosensory & motor research 27(1): 34-43.

Tomioka, R., K. Sakimura and Y. Yanagawa (2015). "Corticofugal GABAergic projection neurons in the mouse frontal cortex." Frontiers in Neuroanatomy 9(133).

Tricoire, L., K. A. Pelkey, M. I. Daw, V. H. Sousa, G. Miyoshi, B. Jeffries, B. Cauli, G. Fishell and C. J. McBain (2010). "Common Origins of Hippocampal Ivy and Nitric Oxide Synthase Expressing Neurogliaform Cells." The Journal of Neuroscience 30(6): 2165-2176.

Uno, M., M. Yoshida and I. Hirota (1970). "The mode of cerebello-thalamic relay transmission investigated with intracellular recording from cells of the ventrolateral nucleus of cat's thalamus." Experimental Brain Research 10(2): 121-139.

Vida, I., K. Halasy, C. Szinyei, P. Somogyi and E. H. Buhl (1998). "Unitary IPSPs evoked by interneurons at the stratum radiatum-stratum lacunosum-moleculare border in the CA1 area of the rat hippocampus in vitro." The Journal of physiology 506 (Pt 3)(Pt 3): 755-773.

Villar-Cervino, V. and O. Marin (2012). "Cajal-Retzius cells." Curr Biol 22(6): R179.

Wall, N. R., M. De La Parra, J. M. Sorokin, H. Taniguchi, Z. J. Huang and E. M. Callaway (2016). "Brain-Wide Maps of Synaptic Input to Cortical Interneurons." The Journal of Neuroscience 36(14): 4000-4009.

Wall, N. R., I. R. Wickersham, A. Cetin, M. De La Parra and E. M. Callaway (2010). "Monosynaptic circuit tracing in vivo through Cre-dependent targeting and complementation of modified rabies virus." Proceedings of the National Academy of Sciences of the United States of America 107(50): 21848-21853.

Wickersham, I. R., D. C. Lyon, R. J. O. Barnard, T. Mori, S. Finke, K.-K. Conzelmann, J. A. T. Young and E. M. Callaway (2007). "Monosynaptic Restriction of Transsynaptic Tracing from Single, Genetically Targeted Neurons." Neuron 53(5): 639-647.

Williams, L. E. and A. Holtmaat (2019). "Higher-Order Thalamocortical Inputs Gate Synaptic Long-Term Potentiation via Disinhibition." Neuron 101(1): 91-102.e104.

Wozny, C. and S. R. Williams (2011). "Specificity of Synaptic Connectivity between Layer 1 Inhibitory Interneurons and Layer 2/3 Pyramidal Neurons in the Rat Neocortex." Cerebral Cortex (New York, NY) 21(8): 1818-1826.

Xu, X., K. D. Roby and E. M. Callaway (2010). "Immunochemical characterization of inhibitory mouse cortical neurons: three chemically distinct classes of inhibitory cells." J Comp Neurol 518(3): 389-404.

Yamawaki, N., K. Borges, B. A. Suter, K. D. Harris and G. M. Shepherd (2014). "A genuine layer 4 in motor cortex with prototypical synaptic circuit connectivity." Elife 3: e05422.

Yin, H. H. (2016). "The role of opponent basal ganglia outputs in behavior." Future Neurology 11(2): 149-169.

Zhou, F.-W. and S. N. Roper (2010). "Altered Firing Rates and Patterns in Interneurons in Experimental Cortical Dysplasia." Cerebral Cortex 21(7): 1645-1658.

Zhu, Y. and J. J. Zhu (2004). "Rapid arrival and integration of ascending sensory information in layer 1 nonpyramidal neurons and tuft dendrites of layer 5 pyramidal neurons of the neocortex." J Neurosci 24(6): 1272-1279.